

# Multiscale investigation and characterization of nanoparticle reinforced plastics

- toward a circular plastics economy -



Ivanna Lins Colijn

## *Propositions*

1. For plastics, a united vision on a future circular economy is lacking.  
(this thesis)
2. Nanoparticle dispersion is key to functional nanocomposite design.  
(this thesis)
3. Within technical sciences, female role models need to be put in the spotlights more frequently.
4. Seeing the PhD experience as the freshman year(s) of academics eases the burden.
5. Society determines circularity.
6. For cheap products, mitigating unsustainable practices starts by introspection rather than of blaming others.

Propositions belonging to the thesis, entitled

Multiscale investigation and characterization of nanoparticle reinforced plastics  
– toward a circular plastics economy –

Ivanna Lins Colijn

Wageningen, 20th of January 2023

Multiscale investigation and characterization  
of nanoparticle reinforced plastics  
- toward a circular plastics economy -

Ivanna Lins Colijn

# Thesis committee

## **Promotor**

Prof. Dr C.G.P.H Schroën,

Personal chair at the Laboratory of Food Process Engineering

Wageningen University & Research,

University of Twente, Enschede

## **Other members**

Prof. Dr C.J.A.M. Termeer, Wageningen University & Research

Prof. Dr J.H.B. Sprakel, Wageningen University & Research

Prof. Dr K.U. Loos, University of Groningen, Groningen

Dr W. van den Berg, The Compound Company, Geleen

This research was conducted under the auspices of Graduate School VLAG (Advanced Studies in Food Technology, Agrobiotechnology, Nutrition and Health Sciences).

Multiscale investigation and characterization  
of nanoparticle reinforced plastics  
- toward a circular plastics economy -

Ivanna Lins Colijn

**Thesis**

Submitted in the fulfilment of requirements for the degree of doctor  
at Wageningen University

By the authority of the Rector Magnificus

Prof. Dr. A.P.J. Mol,

in the presence of the

Thesis Committee appointed by the Academic Board

to be defended in public

on Friday 20 January 2023

at 4 p.m. in the Omnia Auditorium.

Ivanna Lins Colijn

Multiscale investigation and characterization of nanoparticle reinforced plastics  
- toward a circular plastics economy -

230 pages

PhD thesis, Wageningen University, Wageningen, the Netherlands (2023)

With references and summary in English

ISBN: 978-94-6447-508-1

DOI: <https://doi.org/10.18174/582002>

# Contents

<b>Chapter 1</b>	General introduction and thesis outline	7
	<b>Part I: Model systems</b>	21
<b>Chapter 2</b>	Thermoplastic bio-nanocomposites: from measurement of fundamental properties to practical application	23
<b>Chapter 3</b>	Nanoparticle – polymer interactions drive nanoparticle dispersion and thus nanocomposite design – a molecular dynamics study	53
<b>Chapter 4</b>	Particle dispersion drives nano to bulk dynamics required for nanocomposite design	77
	<b>Part II: Biobased systems</b>	93
<b>Chapter 5</b>	Quantification of energy input required for chitin nanocrystal aggregate size reduction through ultrasound	95
<b>Chapter 6</b>	Chitin nanocrystal hydrophobicity adjustment by fatty acid esterification for improved polylactic acid nanocomposites	115
	<b>Part III: Plastic products and society</b>	139
<b>Chapter 7</b>	Science and media framing of the future of plastics in relation to transitioning to a circular economy	141
<b>Chapter 8</b>	General discussion - from fundamental insights toward the rational design of (bio)nanocomposites in a circular plastics economy	165
<b>References</b>		191
<b>Summary</b>		211
<b>Acknowledgements</b>		217
<b>About the Author</b>		223
<b>Publications</b>		225
<b>Training activities</b>		227
<b>About the cover</b>		229



---

# 1

## Introduction and thesis outline

---

# Introduction

In terms of sustainability, we are running a race against time with disastrous consequences if lost. The plastics industry is often pinpointed as an important industry that requires urgent transition toward a more circular approach. This thesis has taken this as inspiration and revolves around the development of advanced materials – thermoplastic nanocomposites – that fit within the idea of a circular economy. It is the result of a multidisciplinary study and touches on fundamental, technical, and societal challenges surrounding the topic.

We start our introduction with a historical perspective on plastic materials. Thereafter, we discuss the challenges that bioplastics need to meet, and how the addition of nanoparticles can expand their applications. Lastly, we pinpoint how bioplastic nanocomposites can be developed and what limits the rational design of these systems.

## 1.1 The history of plastics – from exceptional material properties to great concerns

Materials have always played a key role in human's lives, and even many time periods have been named after them, e.g., the stone, bronze, and iron ages. In the last 100 years, plastics have revolutionized our society and today plastics can be found for all kinds of applications including packaging, building construction products, textiles, and many more. Although plastic-like materials such as natural rubber, nails, horn, and tortoise shell have always existed, it is good to point out that the term '*plastic*' is most often used for polymers that are at least partly synthetic.

&lt; 1850

Natural materials

Looking at the world through today's eyes, it is hard to imagine a world without plastic. The first plastics developed were biobased and only partly synthetic, and initially intended as a replacement for valuable expensive materials such as ivory. In 1856, the first thermoplastic was discovered by Alexander Parkes, who made '*Parkesine*' from nitrocellulose [1]. Initially, Parkesine was promoted as an inexpensive replacement for rubber, but it appeared moldable, transparent, and maintained its shape after cooling. These unique material properties caught the attention of different scientists, and Parkes' invention was soon followed by '*Galalith*', a milk based bioplastic, and '*Celluloid*' and '*Rayon*' both cellulose based plastics [1,2]. In 1907, the first fully synthetic polymer was invented, namely '*Bakelite*'. Its resistance to high temperatures and stress impressed consumers and manufacturers. Consequently, Bakelite gathered popularity in everyday household products, like clocks, jewellery, and telephones.

1850 - 1930

The first plastics

Theoretical frameworks covering the physics, synthesis, and structure of polymers started to get shape in the early '30; this scientific progress accelerated the synthesis of new types of polymers such as polyethylene, nylon, polystyrene, and polypropylene. Additionally, the low prices and processability of petroleum made the production of fossil-based plastics

1930 - 1960

The glory years of plastics

economically interesting [3]. Due to continuous development and the unique properties of plastics, they started to replace other materials such as wood or glass [2,3]. For the first time in history, humans were not dependent on natural resources (excluding oil from this comparison). Interestingly, this initiated a certain excitement in regard to what a future world would look like. This is nicely illustrated by the following quote from philosopher Roland Barthes:

*“The hierarchy of substances is abolished: a single one replaces them all: the whole world can be plasticized ...”* [4].

Since the Second World War, the demand and production of fossil-based plastics have only been increasing and are still increasing as we speak [3,5]. The market for plastics has grown very progressively. In 2019, nearly 370 million tons of plastic were produced globally. Focussing on the European market, 58 tonnes of plastic were produced [5], providing jobs for over 1.5 million people, and generating over 350 billion euros in turnover in 2019. Consequently, the European plastics industry ranks 7<sup>th</sup> in Europe in industrial value-added contribution. This is comparable to the pharmaceutical and chemical industry [5]. These numbers illustrate that there is a clear demand for plastic-like products.

However, the fact that we are dealing with non-biodegradable materials in combination with our consumption/disposal pattern has become an increasingly toxic path that we travel. Since the '60, concerns about the effect of plastic pollution on human health and marine life have grown. Since the beginning of the 21<sup>st</sup> century, the scientific world started to show interest in (micro/nano)plastic pollution and its effect on marine life, human life, and the environment [5,6]. Simultaneously, the continuously increasing demand for plastics contributes to the increasing demand for fossil fuels and their corresponding negative implications for the environment and climate change. Currently, it is estimated that plastic production emits 13.4 million tons of CO<sub>2</sub> per year, and thus contributes

1960 - today  
Increasing concerns

to 20% of the chemical industry emissions EU-wide (mentioned in [7], from database [8]). In terms of meeting one of the biggest challenges of our times, i.e., limiting global temperature increase to  $< 2$  °C [9], it is therefore crucial to redesign our current plastics industry to such an extent that greenhouse emissions are limited as much as possible. Since 2018, strategies are being developed to transform toward a more circular plastic economy at the national [10], European [11], and global level [12]. There is a clear need for new materials with comparable properties to plastics, while having a lower footprint and contributing to the aim of a circular economy. We therefore need to question ourselves what these novel materials should look like, and what their role is within a future circular economy.

## 1.2 Bioplastics – advantages and challenges

Bioplastics are often proposed as alternatives to their fossil-based counterparts. The term ‘bioplastics’ is commonly defined as plastics that are either biobased and/or biodegradable or compostable [13,14]. Biodegradable plastics, sometimes referred to as ‘bio-decomposable plastics’, can be degraded into CO<sub>2</sub> and/or methane by micro-organisms. It is good to point out that this term can cause confusion, especially because environmental conditions such as temperature, water or oxygen availability, and micro-organism type and count, highly impact the degradation kinetics [13]. Compostable plastics on the other hand meet the requirements of the international EN13432 standard [15]; this demands a material to be fully degraded under commercial composting conditions within 12 weeks [13].

### 1.2.1 Bioplastics – PLA

Currently, different bioplastics are produced on a (semi-) industrial scale such as polylactic acid (PLA), polybutylene succinate (PBS), polyhydroxyalkanoates (PHAs), or polybutylene adipate terephthalate (PBAT) [16]. Among these, PLA is often promoted as the most promising one because its:

- Mechanical properties are comparable to PET (e.g., tensile strength, tensile modulus, and elongation at break) [17].

- Price is at a competitive level compared to fossil-based plastics; in fact, the use of bioplastics including PLA could become economically favourable considering the current fluctuating and increasing petroleum prices.
- Excellent environmental footprint as biobased sources can be used for L-lactide (the monomeric unit of PLA) production, e.g., corn, potatoes, or cane sugar, depending on the local availability near the PLA production facility [13].
- Circularity because PLA can be composted [13,17], or chemically/mechanically recycled [18,19].
- Availability/processability as PLA is available in different molecular weights and grades enabling a wide range of processing methods, e.g., extrusion or injection moulding.

These properties are a consequence of PLA's chemical nature, and to a lesser extent of the processing conditions used. This thermoplastic polyester consists of  $(C_3H_2O_2)_n$  monomeric units and is commonly prepared via ring-opening polymerisation of pure L-lactide [17], i.e., the cyclic dimer of the basic repeating unit (**Figure 1.1**). PLA is a fully biobased thermoplastic made through fermentation at industrial scale. It is good to point out that L-lactide can also be produced via chemical synthesis but this often leads to a lower yield and a higher formation of by-products [17,20].

To derive high molecular weight PLA, ring opening polymerization of pure L-lactide is most efficient. Lactic acid can be present in two chiral forms: L-lactide and D-lactide and the properties of the produced PLA depend on the ratio of these two in the polymer backbone. Generally speaking, a high L-lactide content results in a polymer with a higher crystallinity accompanied by a higher glass transition and melting temperature. A higher D-lactic acid

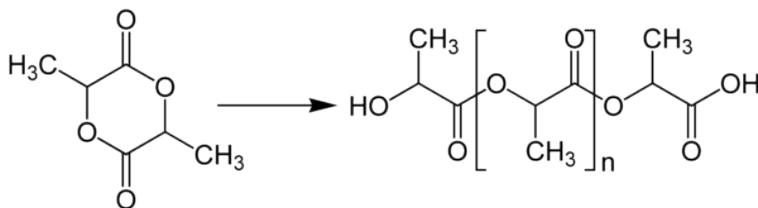


**Figure 1.1:** Ring opening polymerization of L-lactide (left) is commonly the preferred reaction to produce polylactic acid (right).

content results in a more amorphous polymer with a lower glass transition and melting temperature. Most of commercially available PLA consist of 85 – 99% L-lactic acid and 15 - 1% D-lactic acid [13]. When more than 10% of the PLA consists of D-lactic acid, the material becomes fully amorphous.

### 1.2.2 Limitations of bioplastics – an industry in its infancy

Despite the interesting properties of PLA and other bioplastics, the current global bioplastic production is nearly 1% of the total [21]. The use of bioplastics for packaging is still a niche, and this is related to the costs, availability, processability, and performance of these materials that, in general, underperform those of fossil plastics [22–24].

In terms of functionality, commonly mentioned limitations are poor barrier properties, the hydrophilic character, the non-transparency, and insufficient mechanical properties of bioplastic materials [22]. Depending on the application, certain characteristics should be changed. For instance for the food industry, the relatively high water vapour transmission limits the application of bioplastics for products that need high water barrier protection such as cookies or meat (**Figure 1.2**), whereas a high water vapour transmission rate is advantageous for products that need to ‘breathe’ such as fruits or vegetables.

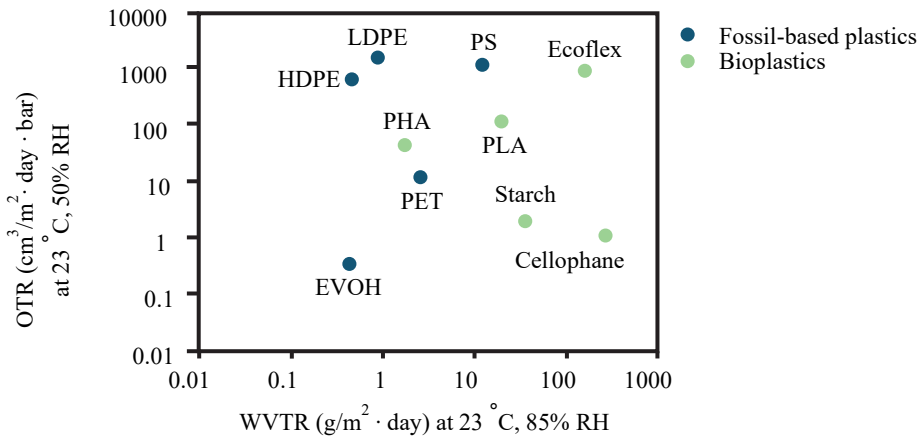


**Figure 1.2:** Barrier properties of various fossil-based (blue) and biobased (green) plastics used in the packaging industry without the use of additional barrier coating. Adapted from [25,26].

Obviously, petroleum-based plastics are the result of years of innovation, while bioplastics are still in their infancy, and various options for improvement are considered. These options relate both to the material as such, as well as the processes that are used and need to be tuned to make bioplastics that meet specific requirements. Previously water vapour permeability was discussed as a point of improvement, but in terms of oxygen transfer, bioplastic may already outperform fossil-based plastics; this is highly relevant for the suppression of oxidation reactions that lead to considerable reductions in shelf-life of food products, and food waste.

### 1.2.3 Techniques to alter bioplastic properties?

To arrive at a new generation of plastic products that fit within a circular economy, we need to be in a position to fine-tune and alter bioplastic properties at will. **Table 1.1** summarizes the pros and cons of potential routes to do so. In light of a transition toward a circular economy, it is important to design materials that are:

- biodegradable/compostable and/or recyclable.
- meet the required material properties for its envisioned purpose.

This can be challenging when considering multi-layered bioplastic films or by blending different bioplastics together given the limited biobased plastics that are currently available. Alternatively, the available biopolymers can be modified (e.g., chemical grafting [27]), or plasticizers and/or micro/nanoparticles can be added [28]. The latter route offers opportunities to create materials with additional functionality through the micro/nanoparticles of choice. Toyota was the first to patent a polymeric nanocomposite (nylon-6 composite 5% nano-clay polyamide [29]), which resulted in a significantly higher tensile strength and resistance to heat distortion. Interestingly, nanocomposites are widely applied in the aviation and automotive industry. Also in food packaging, they have been shown to lead to improved mechanical strength, barrier properties, and altered thermal profile [30–35]. Additionally, depending on the selected materials, nanocomposites even possess added functionality related to antioxidant/antimicrobial effects [26,36–39]. Despite this wealth of evidence, the potential to use nanoparticles in bioplastic applications is highly underexplored and therefore the focus of this thesis.

**Table 1.1:** Advantages and disadvantages of techniques to alter material properties of (bio)plastics.

Technique	Advantages	Disadvantages
Plasticisers, e.g., lactide or PEG [40]	<ul style="list-style-type: none"> <li>+ Increases ductility and improves processability</li> <li>+ Small quantities required</li> <li>+ Increases flexibility/reduces brittleness</li> <li>+ Approved for application with food</li> </ul>	<ul style="list-style-type: none"> <li>- Depending on molecular weight fast migration; fast changes in material properties upon time [40]</li> <li>- Lowers the glass transition temperature</li> <li>- Toxicology concerns upon migration [41]</li> <li>- Often fossil-based</li> </ul>
Impact modifiers, e.g., Biomax Strong, or Sukano [42,43]	<ul style="list-style-type: none"> <li>+ Often decreases brittleness while remaining strength [44,45] and transparency [45]</li> </ul>	<ul style="list-style-type: none"> <li>- High concentrations are required, often minimum 10 v/v % [40]</li> <li>- Often non-biodegradable</li> <li>- Not always approved for application in food [40]</li> </ul>
Polymer blends [46,47]	<ul style="list-style-type: none"> <li>+ Effectively alters material properties depending on the compatibility between two polymers</li> <li>+ Relatively cheap solution</li> </ul>	<ul style="list-style-type: none"> <li>- Mixing can be challenging depending on polymer compatibility</li> <li>- Properties depend on (bio)plastics available (limited choice)</li> <li>- More difficult to recycle</li> </ul>
Micro/nanocomposites, e.g., carbon nanotubes, talc, or montmorillonite [48,49]	<ul style="list-style-type: none"> <li>+ Small amounts required to induce changes</li> <li>+ Effectively increases mechanical strength, and sometimes barrier properties</li> <li>+ If nanoparticle possesses certain activity (e.g., antimicrobial), the plastic could potentially possess that functionality as well</li> </ul>	<ul style="list-style-type: none"> <li>- Induces high stiffness</li> <li>- Difficult to prevent nanoparticle aggregation</li> <li>- Difficult to recycle</li> </ul>

### 1.3 Chitin nanocrystals as fillers for bio-nanocomposites

As was clear from the previous section, using nanoparticles can be advantageous, and to date, most research was done with inorganic nanoparticles in petroleum-based plastics [50]. For bioplastics, the particle of choice should be of the same category, and nanoparticles from polysaccharides and in particular chitin nanocrystals have gathered a lot of attention [51].

Chitin is the second most abundant polysaccharide next to cellulose and present in exoskeletons of arthropods (shrimps and crabs [51–53]), in insects, fungi, and algae.

Although currently considered waste from the fish industry, chitin and especially chitin nanocrystal production could become a high-added value activity. Chitin nanocrystals can be produced via a simple acid hydrolysis step which results in needle like nanoparticles with a typical length between 200 – 400 nm and a diameter between 10 – 15 nm (**Figure 1.3**). During acid hydrolysis, the disordered amorphous regions within the chitin are hydrolyzed, while the highly crystalline domains remain intact [52,53]. The remaining nanocrystals are therefore highly crystalline, i.e., 57 – 93%, which is believed to provide these crystals their high strength. To be complete, it is good to point out that these chitin nanocrystal properties can slightly differ depending on the reaction procedure and the chitin nanocrystal source [53]. Additionally, the surface can be modified or functionalized at will as the presence of hydroxyl and amine groups allow surface modification, as elaborated on in **Chapter 6**.

These chitin nanocrystals possess properties that could make them of special interest to the food industry. Depending on the degree of acetylation, these crystals exhibit antioxidant and antimicrobial functionality. Additionally, due to their needle shape morphology, they are supposed to have superior barrier properties compared to sphere shaped nanoparticles as an increased torturous diffusion path is created [51], although this may be questionable given the low amounts of particles that are generally used.

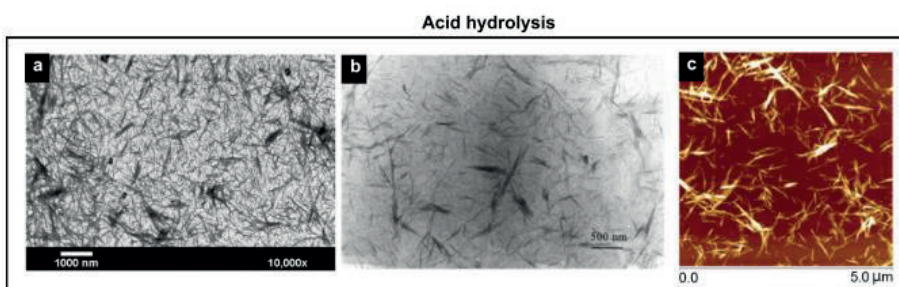


**Figure 1.3:** Needle shaped chitin nanocrystals produced via acid hydrolysis and observed with (A) transmission electron microscopy, (B) electron microscopy, and (C) atomic force microscopy. Modified from [53].

The main challenge is how to produce bio-nanocomposites with homogeneously dispersed nanocrystals. First, chitin nanocrystals have a high tendency to self-aggregate into microscale agglomerates, due to the abundant hydroxyl groups which form strong hydrogen bonds between the nanocrystals [54]. Second, the poor compatibility between relatively hydrophilic chitin nanocrystals and relatively hydrophobic PLA drives the nanocrystals together once they are added to a biodegradable plastic matrix [55], as described in detail in **Chapter 2**.

#### 1.4 Nanocomposites – how to rationally design them?

According to the generally accepted hypothesis, superior nanocomposite properties are the consequence of nanoparticle – polymer interactions resulting in altered polymer dynamics. It is therefore believed that the desired nanocomposite properties can be fine-tuned by:

- Polymer selection, such as degree of polymerization, chemistry, or architecture.
- Nanoparticle selection, such as size, shape, and surface chemistry.
- Nanocomposite design, such as nanoparticle loading, nanoparticle – polymer interaction, or processing method.

In practice, the design of nanocomposites is far from trivial, mainly because phenomena governing nanocomposite behaviour are not that well understood. Polymer melts – and nanocomposites specifically – show processes rich in dynamics, that take place at multiple time- and length scales, and are interrelated (**Chapter 3**, **Chapter 4**, and [56]). For instance, it is well known that mechanical properties such as stiffness, strength, and stress relaxation are highly impacted by the polymer's segmental relaxations [56,57]. Nanoparticle – polymer interactions alter these segmental relaxations, but how these translate through to the nanocomposite's bulk scale is largely unravelled.

The limited knowledge of the effect of nanoparticles on nanocomposite dynamics is not the only obstacle to the rational design of nanocomposites. Nanoparticle aggregation is generally considered the biggest challenge within the field. To prevent this issue, phenomena governing nanocomposite formation need to be understood much better. We address this from a theoretical perspective in relation to available experimental techniques in **Chapter 2**. In short, for the rational design of nanocomposites, it is important to relate nanoparticle – polymer properties and interactions, to nanocomposite structure and dynamics. In **Chapter 3** we used molecular dynamics simulations to investigate the structure at the interface and

beyond. This knowledge can be used to understand how nanocomposite structure affects interphasial dynamics and ultimately nanocomposite properties experienced by humans, which we started in **Chapter 4**.

## 1.5 Outline of this thesis

From the previous sections, it becomes clear that the addition of nanoparticles can expand the application of bioplastics to fit within a circular economy. To facilitate the rational design of fully biobased nanocomposites we need to understand the links between nanoparticle - polymer interactions, nanocomposite structure and morphology, nanocomposite dynamics, and consequently nanocomposite properties. This thesis aims to characterize the multiscale physical and chemical properties of nanoparticle reinforced plastics that are needed for a transition toward a circular economy; a schematic overview is shown in **Figure 1.4**.

The thesis is divided into three main parts. In **Part I**, we aim to understand nanocomposite behaviour on different length and time scales. In **Part II**, we focus on the design of nanocomposites made of chitin nanocrystals and polylactic acid as a polymeric matrix, and in **Part III** we focus on the societal relevance.

The order of the chapters is therefore divided as follows. In **Chapter 2** we review different theoretical frameworks available to help the design of nanocomposites and discuss different techniques to investigate nanocomposite systems. In **Chapter 3**, we use a coarse-grained molecular dynamics simulation to understand the relation between nanoparticle-polymer interactions and nanocomposite structure. We do this for a wide temperature range, as temperature plays a key role during processing but also during nanocomposite use. In **Chapter 4**, we investigate the effect of polymer chain length and nanoparticle – polymer interaction on nanocomposite dynamics at the interphasial region and bulk scale in a polymer melt; a multiscale approach is presented as a crucial link between nano-/microscale phenomena and bulk scale behaviour.

In **Part II**, we focus on the design of nanocomposites made of chitin nanocrystals with polylactic acid as a polymeric matrix. In **Chapter 5** we analyze how much (sonication) energy input is needed to break chitin nanocrystal aggregates up, since they are not desired for nano-composite production. In **Chapter 6** we propose a way to modify chitin nanocrystals

via a direct Steglich esterification reaction, and we investigate the effect of this modification on altered material properties.

**Part III** of the thesis starts with **Chapter 7** in which we focus on the societal responses toward the plastic transition; we investigate the envisioned role of plastics in a circular economy and what the role of different plastics types will be within this economy. In **Chapter 8**, all topics mentioned in the chapters will be revisited and put into perspective in this general discussion. We discuss how model systems can be used for the design of bio-nanocomposites and how this can result in valuable plastic materials for a circular economy.

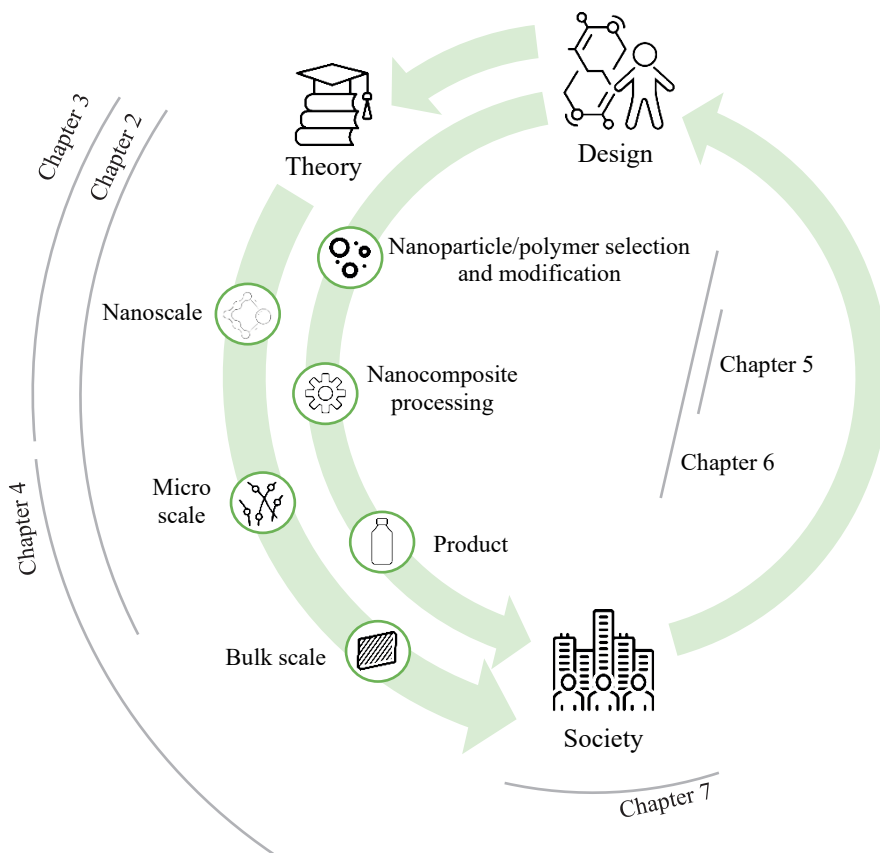


**Figure 1.4:** Schematic overview of the thesis outline.



**P**art I  
Model systems



---

# 2

## Thermoplastic bio-nanocomposites: From measurement of fundamental properties to practical application

---

*Published as “Ivanna Colijn and Karin Schroën. 2021. Thermoplastic Bio-Nanocomposites: From Measurement of Fundamental Properties to Practical Application. Advances in Colloid and Interface Science 292: 102419.”*

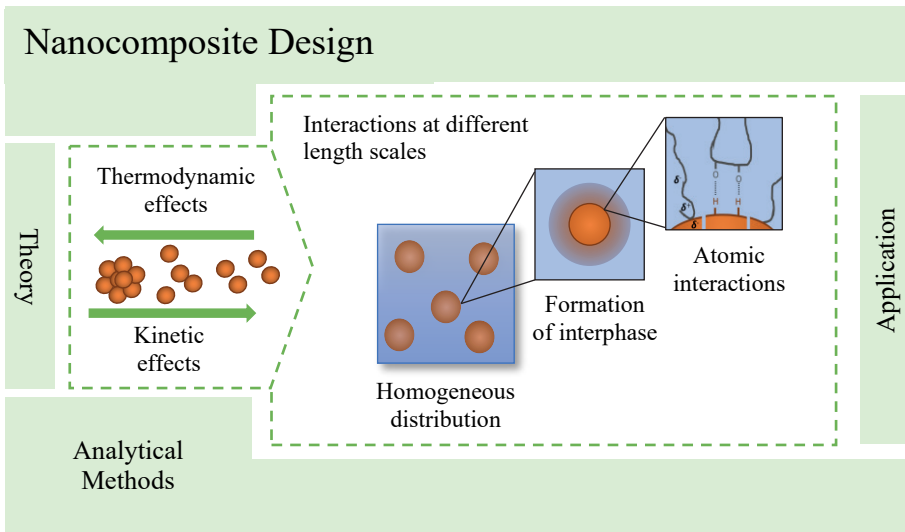
## 2.1 Abstract

Although the discovery of plastic has revolutionized materials used in many industries and by consumers, their non-biodegradable nature has led to one of the greatest problems of our times: plastic waste in the environment. Bioplastics which are biobased and biodegradable, have been suggested as alternatives to their fossil-based counterparts, but their properties often do not meet the requirements that standard plastics would, and are in clear need of improvement.

One way to do so is by the addition of nanoparticles which, when homogeneously dispersed, have been reported to result in great improvements. However, in practice, homogenous distribution of nanoparticles is not that trivial due to their tendency to aggregate, also after adding to the polymer matrix. Although theoretical frameworks to prevent this process are available, we feel that the options explored in practice are often rather trial-and-error in nature. For that reason, we review the theories available, aiming to facilitate the design of nanocomposites for a sustainable future.

We first discuss thermodynamic frameworks which revolve around nanoparticle aggregation. To minimize nanoparticle aggregation, the nanoparticle and polymer can be selected in such a way that they have similar polar and dispersive surface energies. The second part is dedicated to nanocomposite processing, where kinetic effects act on the nanocomposite material therewith influencing its final morphology, although it is good to point out that other factors such as reaggregation also affect the final nanocomposite morphology. The third section is dedicated to how nanoparticles affect the polymer matrix to which they are added. We describe how interactions at an atomic scale, result in the formation of an interphasial region which ultimately leads to changed bulk material properties.

From these three sections, we conclude that three parameters are often overlooked when designing nanocomposites, namely the surface energies of the nanoparticles and polymers, the aggregation bond energy or strength, and the interphasial region. Therefore, in the fourth section, we provide an overview of techniques to identify these three parameters. We finish with a summary and outlook for the design of bio-nanocomposites, where we bring all insights from the previous four sections together.



*Graphical abstract*

## 2.2 Introduction

For the production of the first plastics, natural materials were used that were eventually modified to reach improved functionality, and in a later stage evolved into completely synthetic polymers that showed remarkable properties in terms of, e.g., strength per weight of material used. Currently, synthetic polymers are subject to scrutiny for their environmental impact related to the use of fossil fuels for their production, and low biodegradability. Biodegradable polymers are therefore gaining more and more interest, although it should also be pointed out that the functionality of these polymers can be rather low compared to their synthetic counterparts. Further functionalization is therefore needed, and in this chapter we focus on the use of nanoparticles to do so.

The addition of nanoparticles to polymer matrixes has led to extraordinary material properties compared to the base-polymer, such as increased mechanical strength, increased thermal stability, and increased barrier properties [31–35,58,59]. In the early days, the focus laid mainly on the automotive and aviation industry, which resulted in the use of nanocomposites in, for example, tires or conveyor belts. Besides tuning macroscopic polymer properties, it has been suggested that extra functionality, e.g., antioxidant or antimicrobial, can be created

if the nanoparticle possesses that functionality [38,39,60–62]. These latter two aspects are especially of interest for packaging materials for food, or medical applications.

The enhanced properties of nanocomposites are related to the high surface area of the nanoparticles, which facilitates interaction with the base polymer. However, not all combinations are successful, in fact, huge differences in final material properties have been reported even when similar starting materials were used. Besides, the properties of the polymer and the particles need to be matched: one of the main challenges is to achieve a homogeneous dispersion of nanoparticles throughout the polymer matrix. This is only possible if particle aggregation, a process driven by fundamental properties of the polymer and the particle, is prevented. Besides that, we feel that clear material – process – structure – property relationships are missing, and that design of a nanocomposite mostly relies on trial-and-error approaches, also due to the complexity of the processes at hand. In short, designing a nanocomposite with desired properties is far from trivial.

Investigating nanocomposite systems is a challenge in itself due to the small size of the nanoparticles which asks for advanced techniques. Still, a lot of knowledge is available, which we try to compile in this review. The first section is dedicated to particle and polymer properties, and revolves around thermodynamic arguments. In the second section, we highlight process-related aspects that revolve around kinetic effects that play a role, e.g., in aggregation. In the third section, we focus on how nanoparticle – polymer interactions affect material properties on different length scales. The fourth section is dedicated to techniques to quantify several design parameters as identified in the earlier three sections. We will wrap up with a section in which we bring the insights presented in the previous sections together as an outlook for the design of bio-nanocomposites.

### **2.3 Nanoparticle and polymer selection**

Nanoparticle and polymer selection is a crucial step in nanocomposite design because nanoparticles can significantly change material properties. To maximize their effect on the polymer matrix, one should achieve a homogeneous dispersion, which is generally considered the main challenge in nanocomposite development and design.

For homogeneous dispersion given equilibrium conditions, the interfacial compatibility between the filler and the polymer plays a crucial role. From a thermodynamic point of view, the free energy can be used to determine whether a process may take place. For nanocomposites, the free energy of immersion ( $\Delta G_i$ ), can be used to quantify whether the dispersed state is favoured over the non-dispersed state [63] (**Figure 2.1**).

$$\Delta G_i = \gamma_{pf} - \gamma_{ff} \quad (2-1)$$

where  $\gamma_{pf}$  is the interfacial energy in  $\text{J/m}^2$  between the polymer and the filler and  $\gamma_{ff}$  is the surface energy of the filler alone in  $\text{J/m}^2$ . When  $\Delta G_i$  is  $< 0$ , the dispersed state is favoured and when  $\Delta G_i > 0$  the non-dispersed phase is favoured.

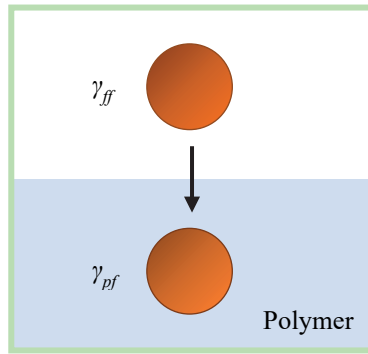


**Figure 2.1:** Schematic representation of the free energy of immersion.

The  $\gamma_{pf}$ -part of the equation can be calculated using the surface energies of the filler and polymer (which is also related to the contact angle, see **section 2.8.1**). The total surface energy of a compound is the product of a dispersive component ( $\gamma^d$ ) and a polar component ( $\gamma^p$ ). The dispersive component represents interactions due to London's dispersive forces whereas the polar component represents the polar functional groups such as the hydroxyl or amino moieties. The total surface energy can be described as:

$$\gamma = \gamma^d + \gamma^p \quad (2-2)$$

Implementing equation (2-2) in equation (2-1) gives the following relationship between the free energy of immersion as function of the dispersive and polar components of the filler and the polymer, respectively [13]:

$$\Delta G_i = \gamma_p - 2(\sqrt{\gamma_f^d \gamma_p^d} + \sqrt{\gamma_f^p \gamma_p^p}) \quad (2-3)$$

where  $\gamma_f^d$  and  $\gamma_p^p$  are the dispersive components of filler and polymer, respectively, and  $\gamma_f^p$  and  $\gamma_p^d$  the polar components. Equation (2-3) indicates that the polar and dispersive components of the filler and the polymer should be similar in order to allow spontaneous dispersion of the filler in the polymer matrix.

Stöckelhuber et al. [63] used this approach for rubbers in combination with different fillers including silica and nanoclays. Most  $\Delta G_i$ 's were strongly negative, and could be correlated to the free energy of immersion and different dispersibility behaviours, although there are some doubts about the actual values that were obtained. Tang et al. [64] modified attapulgite to improve its compatibility with EPDM (ethylene-propylene-diene monomer). Although a decline in the free energy of immersion did not directly lead to a decreased aggregate size, it could be correlated to an increased tensile strength, i.e., improved mechanical properties.

Alternatively, the work of adhesion between filler-filler and filler-polymer has been suggested by Natarajan, Li et al. [65] who showed that the ratio between the work of adhesion of the filler-polymer ( $W_{FP}$ ) needs to be higher than the work of adhesion between the filler particles ( $W_{FF}$ ). Similarly to the free energy of immersion,  $W_{FP}/W_{FF}$  can be calculated using the dispersive and polar components equation (2-4).

$$\frac{W_{FP}}{W_{FF}} = \frac{2(\sqrt{\gamma_f^d \gamma_p^d} + \sqrt{\gamma_f^p \gamma_p^p})}{2\gamma_f} \quad (2-4)$$

Natarajan, Li et al. [65] found consistent relationships between  $W_{FP}/W_{FF}$  and the dispersion of different silica nanoparticles in polystyrene, poly(methyl methacrylate), poly(ethyl methacrylate), and poly(2-vinylpyridine). Khoshkava & Kamal [66] used the same approach to investigate modified cellulose nanocrystals in polylactic acid and polypropylene. Also here an increased  $W_{FP}/W_{FF}$  was indicative of improved dispersibility, although this could not be related to aggregate size. Interestingly, these results correspond well to molecular dynamic simulations which show that the interaction strength of filler-polymer and filler-filler were the dominant enthalpic factors for dispersion of nanoparticles in a polymer melt [67].

Whether one uses  $\Delta G_i$ ,  $W_{FP}/W_{FF}$ , or another comparable approach, generally having a similar polar and dispersive component in nanoparticle and matrix is a good approach to improve nanoparticle dispersion [68–70]. Obviously, this limits the combinations that can be considered greatly, therefore modification of either the particle or the polymer is a viable way to extend the options for nanocomposite production. For example, Zhang et al. [68] modified carbon black nanoparticles and found improved dispersion when the surface energies were similar to polylactic acid, and Gan et al. [70] tuned surface acetylation of cellulose nanocrystals to match poly(3-hydroxybutyrate-co-4-hydroxybutyrate). These are only a couple of examples; many papers discuss possible modification routes, for instance [71–74].

## 2.4 Nanocomposite processing

In the previous section, we presented a theoretical framework for (modified) nanoparticle selection based on thermodynamic arguments. However, in practice this may not be the determining factor to achieve a homogeneous dispersion of nanoparticles in the polymer matrix. Nanoparticles may get physically trapped in a solidified polymer, thus leading to a kinetically arrested system that has not reached thermodynamic equilibrium [75]. Which of the aspects contributes most to the actual product also depends on the production method, and those are elaborated on in this section.

In general, three different production methods can be distinguished, i.e., solvent casting, melt mixing, and in situ polymerization. During solvent casting, the nanoparticles and polymer are added to a solvent after which the mixture is ‘poured’ into a mould. As it takes some time until all solvent is evaporated, both thermodynamic and kinetic arguments are expected to be relevant, depending on the removal rate of the solvent. During in situ polymerization, the nanoparticles are either added to a solution with the monomer or to the monomer itself. The polymerization process starts at the surface of the particles triggered by a catalyst, which can be an external initiator, heat, or radiation [76,77]. In contrast to the solvent casting and melt mixing process, a covalent bond is formed. This has been shown to improve the dispersibility in the polymer matrix [78,79], as potential nanoparticle aggregates were torn apart during the reaction [80]. For the product made, both the (modified) thermodynamic, and kinetic considerations are of importance. During melt mixing, nanoparticles are added to a polymer melt under high shear forces. Often a twin-screw extruder is used to promote dispersion of

fillers [81]. Compared to in situ polymerization and solvent casting, kinetics is expected to play the biggest role in melt mixing as the material is directly solidified after production. In industry, melt mixing is by far the most used processing method because it is relatively environmentally friendly, cost-effective, and industrially viable [77]. For that reason, we mainly consider melt mixing based on extrusion in the next section.

The relevant processes in an extruder can be sub-divided into different phases as presented in **Figure 2.2**, during which:

1. Nanoparticles are added to the polymer melt.
2. The nanoparticle surface is wetted by the matrix and depending on the interfacial compatibility, the polymer may infiltrate the aggregates. The latter process is sometimes referred to as intercalation.
3. Nanoparticle aggregates break up and are ‘homogeneously’ dispersed in the matrix.
4. Depending on the interfacial compatibility and the solidification time, reaggregation may occur.

### 2.4.1 Filler addition

In general, there is a continuous competition between thermodynamics driving the particles together and kinetics breaking the aggregates up, which leads to a certain aggregate size [82]. Móczó & Pukánszky [83] described this mathematically:

$$\frac{F_a}{F_h} = k \frac{W_{AB}}{\eta \dot{\gamma} R} \quad (2-5)$$

where  $F_a/F_h$  is the ratio between the adhesive forces and hydrodynamic forces acting on a nanoparticle aggregate,  $W_{AB}$  is the reversible work of adhesion between particles in an aggregate,  $\dot{\gamma}$  is the shear rate,  $\eta$  is the melt viscosity, and  $R$  is the aggregate radius or in ideal cases the radius of the individual nanoparticles. Separating  $R$  gives:

$$R = k \frac{W_{AB}}{\eta \dot{\gamma}} \frac{F_h}{F_a} \quad (2-6)$$

Equation (2-6) basically suggests that the final morphology of a nanocomposite depends on the kinetic and adhesive forces acting, rather than the initial state of the nanoparticles, e.g., a

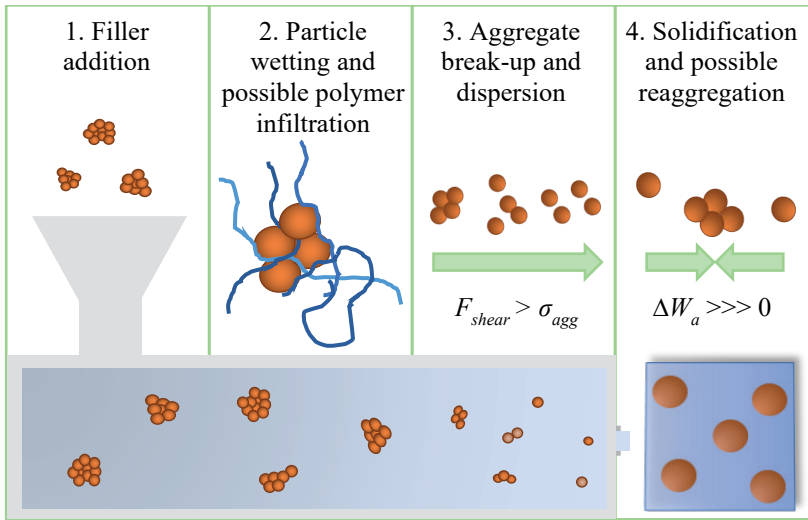


**Figure 2.2:** Different processes occurring in an extruder where (1) nanoparticle addition (2) particle wetting and the surrounding polymer infiltrating the nanoparticle aggregates (3) nanoparticle aggregate break-up provided that the applied shear forces are higher than the cohesive shear forces (4) solidification and possible reaggregation when the difference in the work of adhesion is much larger than 0.

powder or dispersion. Experimentally this has been confirmed by Gaspar et al. [84] who investigated the morphology of different fullerene C<sub>60</sub> formulations along the axis of a twin-screw extruder. The final morphology was mainly driven by thermodynamics and flow conditions, and particle pre-treatment was less important.

However, in practice the equilibrium size is seldomly reached, considering the commonly applied shear rates and short residence times in an extruder. To improve dispersion, it is expected that interfacial compatibility is the most important design parameter, that is, in combination with certain process conditions. Nevertheless, the actual preparation of the nanoparticle may play a role as pointed out by for instance, Khoshkava & Kamal [85], who found a smaller aggregate size in polypropylene nanocomposites when the cellulose nanocrystals were spray dried instead of freeze dried, which is expected to have influenced the porosity of the particles [85–87]. Obviously, starting from a smaller initial aggregate size is beneficial, as this is closer to the final desired morphology. Furthermore, it was found that dispersibility improved by increasing the porosity of the nanoparticle aggregates [87,88] as also discussed in the next section.

### 2.4.2 Particle wetting and polymer infiltration

The nanoparticle surface can be wetted by the polymer melt provided that the interfacial compatibility is beneficial. Whether this is the case is determined by the contact angle ( $\theta$ ), which is  $0^\circ$  in the case of complete wetting, but has a finite value in most practical systems. The contact angle can be calculated from the surface energies of the filler and polymer [89,90]:

$$\cos \theta = -1 + 2 \frac{\sqrt{\gamma_P^d \gamma_F^d}}{\gamma_F} + 2 \frac{\sqrt{\gamma_P^p \gamma_F^p}}{\gamma_F} = -1 + 2 \frac{W_{PF}}{W_{FF}} \quad (2-7)$$

$$\cos \theta = \begin{cases} -1 + 2 \frac{W_{PF}}{W_{FF}} & \frac{W_{PF}}{W_{FF}} < 1 \\ 1 & \frac{W_{PF}}{W_{FF}} \geq 1 \end{cases}$$

Please note that the interfacial properties discussed in the thermodynamics section co-determine the contact angle. A contact angle of  $\sim 0^\circ$  implies better particle dispersibility.

Whether polymer infiltration due to capillary effects plays an important role, depends on nanoparticle and polymer properties. Generally, capillary rise can be described by the Lucas-Washburn equation:

$$H(t) = \sqrt{\frac{\gamma_p r t \cos \theta}{2\eta}} \quad (2-8)$$

where  $H$  is the rise of a fluid (in our case a molten polymer),  $r$  is the pore radius of the nanoparticle aggregate,  $\theta$  is the contact angle between the meniscus and the wall,  $\eta$  is the viscosity of the fluid (in our case a molten polymer) and  $t$  is the wetting time.

Depending on the properties of the nanoparticle and polymer, capillary forces may be very significant, or not at all important. To illustrate this, we consider magnesium carbonate nanoparticles with an aggregate size of 30 nm leading to pore sizes between 1 – 10 nm [91]. When completely wetted ( $\theta = 0^\circ$ ) and added to a polymer melt with a viscosity of 600 Pa·s,

the capillary rise  $H = 3 \mu\text{m}$  after 60 seconds, which implies that the polymer can penetrate the whole nanoaggregate. This also illustrates the size of aggregates that are expected to be affected by polymer intrusion, and which ones are not or hardly. We are aware that capillary forces are sometimes mentioned, but in most cases they play a minor role because of the high viscosity of the polymer melt in combination with small pore sizes and the short times available for intrusion to take place. Still, in some applications, for instance, carbon nanotubes, capillary forces are relevant, and are sometimes even used in the production of nanocomposites [92].

To be complete, we would like to mention that the suitability of the Lucas-Washburn equation for effects occurring at nanoscale has been questioned by some [93,94], although molecular dynamics studies [92,95], and experimental studies [96] have found good agreement between the Lucas-Washburn equation and capillary forces on nanoscale.

### 2.4.3 Aggregate break-up and distribution

Since nanoparticle aggregates are often the starting point for nanocomposite production, both dispersion and distribution of nanoparticles through the polymer melt are of importance. The molten polymer is transported through the extruder at high shear [81], which in turn leads to nanocomposite dispersion.

Obviously, the higher the shear forces the higher the probability an aggregate will break up. The dimensionless number Prob has been used to describe this [97–99]. A general expression for this probability can be written as:

$$\text{Prob} = e^{\frac{-\sigma_{agg}}{\tau}} \quad (2-9)$$

where  $\sigma_{agg}$  is the cohesive strength of the aggregate and  $\tau$  is the shear stress of the medium. The cohesive strength of the aggregate is dependent on for example the size of the particles as well as the cohesive forces including van der Waals or hydrophobic forces [97]. Unfortunately,  $\sigma_{agg}$  is not often quantified, yet could provide much insight because the extrusion process can be tailored in such a way that the shear forces are higher than that.

The shear stress is the product of the polymer viscosity  $\eta_p$  and the medium strain rate  $\gamma$ .

$$\tau = \eta_p \gamma \quad (2-10)$$

The medium strain rate depends on the geometry of the extruder. For a concentric cylinder the relationship between geometry and medium strain rate is as follows:

$$\gamma = R\omega/h \quad (2-11)$$

where  $R$  is the radius of the housing,  $\omega$  is the rotational speed of the mixing blade (rad/s) and  $h$  is the spacing between the inner wall of the housing and the edge of the mixer blade. Relationships as shown in equation (2-9), can also be described in terms of energy input ( $E_{in}$ ) required to overcome the bond energies within an aggregate ( $E_{agg}$ ):

$$Prob = e^{\frac{-E_{agg}}{E_{in}}} \quad (2-12)$$

For extrusion processing,  $E_{in}$  is commonly described in terms of the specific mechanical energy (SME) that is used to compare the impact of different processing conditions on the nanocomposite material. The SME (in kWh) can be calculated using:

$$SME = \frac{P_{motor}}{\tau_{max}N_{max}} \cdot \frac{\tau N}{Q} \quad (2-13)$$

where  $\tau$  is the drive motor torque,  $N$  is the screw rotation speed, and  $Q$  is the flow rate. Although  $\sigma_{agg}$  or  $E_{agg}$  are rarely determined, qualitatively it is well known that a certain energy barrier needs to be overcome before dispersion occurs, and many large-scale experiments have found a decreasing aggregate size upon increasing SME [100–104]. However, finding experimental proof can be rather unpractical, especially for newly developed materials for which the amount of nanoparticles may be limited in relation to what would be needed for a typical extrusion experiment, and for which the production process would also not be optimized.

To get an impression of whether full dispersion is possible it is recommended to determine  $E_{agg}$  or  $\sigma_{agg}$  using a small scale. Recently, we have developed such a method, which is further discussed in **section 2.8.2** [54]. We found an  $E_{agg}$  of  $\sim 370$  kJ/g chitin nanocrystal aggregates. Van der Waals interactions and hydrogen bonds are believed to be the most important interactions within a chitin nanocrystal aggregate. In addition, we could also quantify a

critical energy barrier of  $\sim 100$  kJ/g chitin nanocrystals, which can be determined as the minimum energy needed before disintegration occurs. Commonly about 0.17 – 0.27 kWh/kg is applied during extrusion. Considering a filler content of 5 wt. % and a maximum residence time of 10 minutes, a maximum  $E_{in}$  of  $\sim 1$  kJ/g material can be achieved. This means that about  $\sim 50$  J/g chitin nanocrystals is available for aggregate breakdown, assuming that the energy is distributed equally. This value is a factor 2000 lower than the critical energy barrier we identified before. We believe that this is one of the reasons why it remains difficult to achieve a homogeneous dispersion of chitin nanocrystals through a polymer matrix without surface modification. Still, one should be cautious in translating these results to larger scale given that the processes taking place in an extruder are very complex. For example, it is well known that the screw configuration can tailor the amount of mechanical mixing, the residence time, and pressure levels, and these are only partly considered in the SME approach [105,106].

#### 2.4.4 Reagglomeration during solidification or annealing

Besides all previously mentioned arguments, it is good to point out that there is a continuous thermodynamic force driving the nanoparticles to re-agglomerate both in (aqueous) dispersions and in polymer melts [82,87,107,108]. This is nicely demonstrated by Vilaverde et al. [108] who investigated the dispersion and re-agglomeration of graphite nanoplatelets in polypropylene melts (**Figure 2.3**). During the extrusion process, the feed stream passes through different extrusion chambers. Early on in the extrusion process (denoted as channel 0 – 5 in **Figure 2.3**), a decreasing particle size was observed. However, once the material entered the relaxation chamber where no kinetic force was applied, the particle size rapidly increased to its original size, emphasizing that continuous force needs to be applied to maintain homogenous dispersion in a polymer melt. Interestingly, in the same work, the particle size decreased faster in chambers 6 - 10, compared to the initial dispersion phase, which is indicative of easier re-dispersion.

After extrusion, the nanocomposite material is solidified, which may also include time to anneal if the time for reaggregation is smaller than for solidification. According to Wang & Keddie [109], the tendency of two particles to reaggregate can be described by the difference in the work of adhesion ( $\Delta W_a$ ). Similarly to the Gibbs free energy ( $\Delta G_i$ ) or

$W_{FP}/W_{FF}$  of equation (2-4), these calculations are based on the dispersive and polar components of the filler and polymer:

$$\Delta W_a = 2 \left( \sqrt{\gamma_F^d - \gamma_P^d} \right)^2 + 2 \left( \sqrt{\gamma_F^P - \gamma_P^P} \right)^2 \quad (2-14)$$

A  $\Delta W_a \approx 0$  has been associated with homogenous dispersion, and a high  $\Delta W_a$  with a large driving force of reagglomeration [65]. In practice,  $\Delta W_a$  is always positive, because it is very unlikely that the polar and dispersive component of the nanoparticle and polymer completely match. This implies that all nanoparticles will eventually form agglomerates given sufficiently long time. It is good to point out that  $\Delta W_a$  is no indicator for the aggregate size, as that is also determined by the mobility of the aggregates as a consequence of their size and medium viscosity.

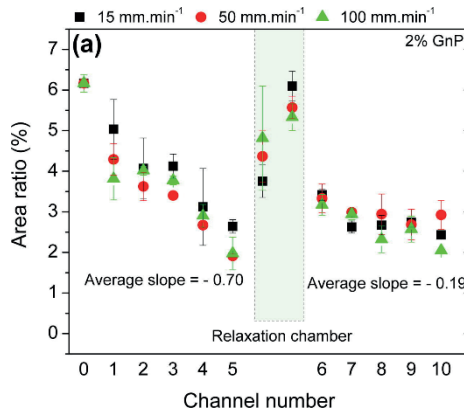


**Figure 2.3:** The evolution of particle size (area ratio (%)) for nanocomposites containing 2 wt. % graphene nanoplates prepared at different speeds. The area ratio of the fillers was determined with image analysis of transmission electron microscopy pictures. Retrieved from [108].

## 2.5 How to combine thermodynamic and kinetic effects?

To summarize, the final structure of a nanocomposite is the result of thermodynamic and kinetic events, and thus both should be considered when designing a nanocomposite material. Hassinger et al. [102] made a first step toward a quantitative tool for predicting dispersion of nanocomposites under non-equilibrium conditions. They tried to describe the final dispersion state of the nanoparticles by the interfacial compatibility between the nanoparticles and

polymer ( $W_{FP}/W_{FF}$ ) and the applied mixing energy in J/s. As hypothesized, their results indicate that the dispersion quality was dependent on both parameters, though a stronger dependency of compatibility between polymer and particle was found. Using data mining techniques, these authors tried to develop a mathematical expression which could predict the final morphology of a nanocomposite based on its compatibility and the applied energy. However, they found that another parameter needed to be included as well, i.e.,  $f(matrix)$ , which describes the mobility and crystallinity of the polymer matrix. The first step toward a predictive tool is very valuable but also emphasizes the complexity of the development of nanocomposite materials.

## 2.6 Effect of nanoparticles on polymer

In the previous two sections, we have presented different ways to look at the dispersibility of nanoparticles in the polymer matrix, i.e., using thermodynamic and kinetic arguments. In this section, we will focus on nanoparticle – polymer interactions and how this affects the material properties at micro and bulk scale (**Figure 2.4**).

## 2.7 Nanoparticle-polymer interfacial interactions

Nanoparticles and polymers can interact in different ways with covalent interactions, hydrogen bonding, and van der Waals interactions considered to be the most important for nanocomposites. To determine the dominating interaction in a certain nanocomposite, the functional groups of the nanoparticles and the matrix of choice need to be considered.

Covalent interactions (formed during in situ polymerization or crosslinking) have proven to effectively improve nanocomposite properties, e.g., mechanical strength [78,79]. Two main reasons could be ascribed to this. First, covalent bonds are very strong (up to  $200 k_B T$ ) especially compared to hydrogen bonds or van der Waals interactions that amount to  $\sim 10$  and  $\sim 1 k_B T$ , respectively [110]. Second, improved nanoparticle dispersibility has been observed because potential aggregates could be torn apart during the reaction [78–80]. Thus for these systems, it is likely that covalent bonds are the most dominant interfacial interactions, and drive product improvement, though hydrogen bonds and van der Waals interactions could contribute as well. For example, Shen et al. [111] added silver graphene oxide nanoparticles to a polylactic acid matrix. Nanocomposites prepared via in situ

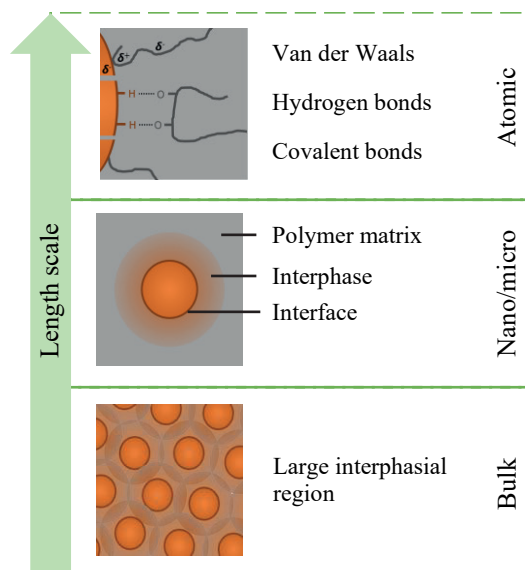


**Figure 2.4:** Schematic overview of nanoparticle interactions at different length scales. Van der Waals interactions, hydrogen bonds, and covalent interactions occur at an atomic level, which results in the formation of an interphase with different properties compared to the nanoparticles and polymers alone. When homogeneously dispersed, this leads to a large interphasial region, with changed bulk properties.

polymerization showed better mechanical and antibacterial properties compared to melt blending, while both techniques resulted in better properties compared to the neat polylactic acid. Luong et al. [112] added graphene sheets to polyimide matrix via in situ polymerization. The Young's modulus increased by approximately 30% at only 0.38 wt. % filler addition.

Though hydrogen bonds and van der Waals interactions are weaker compared to covalent bonds, significant improvements can also be found in nanocomposites if these interactions dominate. The addition of 1 wt. % chitin nanocrystals increased the tensile strength of maize starch films from 1.64 MPa to 3.69 MPa [113]. Also in polyurethane silica nanocomposites, the enhanced thermal and mechanical properties were related to hydrogen bond formation between silanol groups on nanoparticles and the ester and carbonyl groups in the soft segments [114–118]. Obviously, if hydrogen bonds are dominant, both the nanoparticles and the polymers should have functional groups which can either accept or donate protons. The number and nature of the hydrogen bonds seem to be of importance for the

reinforcement [118]. Even nanocomposites of which the reinforcement is entirely dependent on van der Waals interactions have been described in literature. A great example are unfunctionalized carbon nanotubes added via melt blending. Experimental [119] and modelling studies [120,121] showed these systems solely rely on van der Waals interactions [122–126].

Please note that in contrast to most colloidal systems, ionic interactions are not considered for most nanocomposite systems. The conductivity of most plastic polymers is extremely low, and for that reason it is not likely that ionic interactions play a significant role if any. However, ionic interactions could play an important role during the production of nanocomposites, especially if water is present [125,126].

### 2.7.1 Formation of an interphase region

It is widely accepted that the mobility of the interfacial polymer changes as a consequence of the previously discussed interfacial interactions, which ultimately change bulk properties. For this, the strength of the interfacial forces is also of importance, as it influences to which extent the interfacial polymer is restricted [65,83,127–129].

The region at which one single nanoparticle has an influence on the polymer matrix is called the interphase (**Figure 2.4**), and here the properties of the material are different than that of the polymer or the nanoparticles. To date, atomic force microscopy (AFM) is the only way to directly visualize and quantify the length of the interphase region. One example is the study of Pakzad et al. [118] where they investigated the effect of cellulose nanocrystals crosslinked to a polyvinyl alcohol matrix via polyacrylic acid (**Figure 2.5**). By using the peak force tapping mode, the adhesion force between the AFM tip and the nanocomposite was related to the polymer, the nanoparticles, and the interphasial region. It was found that the thickness of the interphase varied between 4 and 35 nm, depending on the particle diameter. This was explained by an increased surface area which can give rise to a thicker interphase [118,130,131]. This effect was also observed with molecular dynamic simulations, however Phys et al. [132] found that the thickness of the interphasial region is only sensitive to the nanoparticle size when the interfacial interactions are strong.

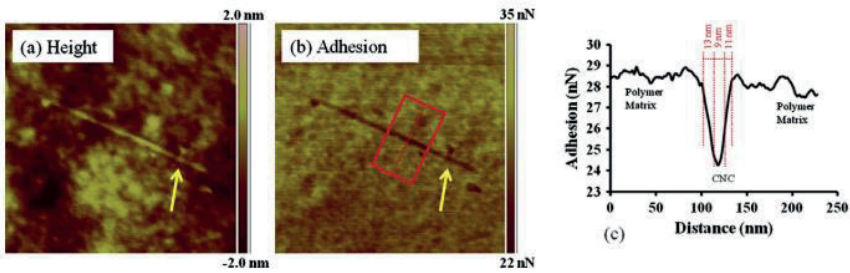


**Figure 2.5:** (A) Height and (B) adhesion maps showing a single cellulose nanocrystal (marked with yellow arrows) (C) Average adhesion profile of the area shown by the red rectangle in the adhesion map in b. Using this profile, CNC diameter (9 nm) and average interphase thickness were measured. Retrieved from [118].

Also others used atomic force microscopy to quantify the interphase: Houssat et al. [133] for polyimide silicon nitride nanocomposite with particles with a size of 20 – 40 nm which resulted in an interphase thickness of 27.25 nm, and Hui Huang et al. [134] found that the interphase of 40 nm sized silica particles could reach 55 – 70 nm in a poly(ethyl methacrylate) and poly(isobutyl methacrylate) matrix. Depending on the particle and polymer properties, the size of the interphase can vary from nanometres to around a micrometre in a heterogeneous gradient system [118,135–138].

### 2.7.2 Change in bulk properties

Though the region of the interphase is relatively small (several nanometres up to  $\sim 1 \mu\text{m}$ ), it is important to realize that the effects that occur in this region are responsible for improvements at bulk scale. Considering the small size of nanoparticles, and high specific surface area, a significant volume of nanoparticle – polymer interphase is created. This implies that even at low particle loadings much of the bulk material could be considered an interphasial region, leading to bulk properties being dominated by the material properties in this region. In fact, there are even indications that the enhancement of stiffness increases by 5% at the midpoint of two interphasial regions, suggesting these effects may be additive [138].

Keeping this in mind, it is logical that bulk properties change, and this has been extensively reported for many different types of particles [31–35,58,59]. Commonly reported enhancements include increased mechanical strength and improved barrier properties

[30-34,51,58,59]. To stress the importance of the interphasial region, it is important to mention that in different numerical, mathematical, and simulation models the interphasial region is used to predict product properties, for instance in the intensity model of Lewis [139], or the multi-core model of Tanaka [140], although many more exist [141–147].

To prevent any confusion, it is good to point out that the degree of crystallinity ( $X\%$ ) is an indicator for polymer mobility at bulk scale. However, increased interphasial region stiffness does not necessarily lead to increased crystallinity; this could be the result of a nucleating effect as reported for among others cellulose nanocrystals [148], carbon nanotubes, and nanoclays [149–151]. When homogeneously dispersed, nanoparticles provide nucleation sites which accelerate polymer crystallization.

Natarajan, Li et al. [65] proposed an experimental approach to predict whether a nanoparticle – polymer combination results in improved properties. They based their method on the hypothesis that for a polymer to spread spontaneously on the filler surface, the relative attraction of the monomeric units needs to be higher than the cohesive attraction in the bulk [152]. This could be described by the ratio between the work of adhesion between the filler-polymer and the polymer-polymer, i.e., the work of spreading  $W_s$ :

$$W_s = 2 \left( \sqrt{\gamma_P^d \gamma_F^d} + \sqrt{\gamma_P^p \gamma_F^p} \right) - 2 (\gamma_P^d + \gamma_P^p) \quad (2-15)$$

A  $W_s$  of  $\geq 0$  suggests an attractive interaction between polymer and filler and should therefore result in a decrease in polymer mobility. When  $W_s$  is  $\leq 0$ , the polymer – polymer interaction is stronger, and no effect on polymer mobility should be visible. Using this approach, good correlations between increased  $W_s$  and an increased glass transition temperature were found [65].

## 2.8 Techniques to investigate nanocomposite systems

As is clear from the previous sections, designing a nanocomposite with desired properties is far from trivial. Nevertheless, the presented theoretical frameworks supply a lot of insight into compatible particle/polymer combinations that allow the creation of a homogeneous nanoparticle distribution, resulting in the formation of an interphase region and ultimately in improved bulk properties. The nanoparticle and polymer surface energy,  $\sigma_{agg}$  and  $E_{agg}$ , and

the thickness of the interphase are key for that, and in this section we discuss different techniques to quantify these parameters.

### **2.8.1 Surface energies**

The surface energy has shown to be a crucial parameter for the quantification of the interfacial compatibility between nanoparticle and polymer matrix. Amongst others, the free energy of immersion (equation (2-1)), the ratio between the work of adhesion of the filler-polymer and the work of adhesion between the filler particles (equation (2-4)), and the work of adhesion (equation (2-14)) were previously mentioned. In these equations, a division of the total surface energy into a dispersive and a polar component (equation (2-2)) is used, which can be quantified with different methods such as direct contact angle measurement, the Wilhelmy method, or inverse gas chromatography. In **Appendix 2-1**, we give an overview of the various values that we found in the consulted references, and that we compiled to give our readers direct access to values that can be used in nanocomposite design. It is clear that the actual values vary greatly, as is the split between polar and dispersive components. Further, the surface energy is temperature dependent [153]; e.g., organoclay had higher surface energies than HDMP and PS at room temperature, but the situation was reversed at processing temperature [154].

#### **2.8.1.1 Direct contact angle measurements**

Contact angle measurement is one of the most common techniques to determine the surface properties of solids. It uses the contact angle between a surface (e.g., a plastic film or a pellet of nanoparticles) and the edge of a liquid droplet, which amongst others gives information about the hydrophobicity and wettability of a certain surface.

For solids, the surface energy can only be derived indirectly, and different methods can be used, for instance Fowkes [155] and Owens-Wendt [89]. We take the Owens-Wendt approach as an example, which considers the surface free energy as the sum of a dispersive and polar component (equation (2-2)). The surface energy and individual components for a material of choice can be calculated using at least two liquids of which these previously mentioned dispersive and polar values are known. The dispersive ( $\gamma_s^d$ ) and polar component ( $\gamma_s^p$ ) of the material of choice can be calculated using:

$$(\gamma_s^d)^{0.5} = \frac{\gamma_i(\cos \theta_i + 1) - \sqrt{(\gamma_i^p / \gamma_j^p)} \gamma_j(\cos \theta_j + 1)}{2(\sqrt{\gamma_i^d} - \sqrt{\gamma_i^p} \left( \frac{\gamma_j^p}{\gamma_j^d} \right))} \quad (2-16)$$

and

$$(\gamma_s^p)^{0.5} = \frac{\gamma_j(\cos \theta_j + 1) - 2\sqrt{\gamma_s^d / \gamma_j^d}}{2\sqrt{\gamma_j^p}} \quad (2-17)$$

where  $\gamma_i$  and  $\gamma_j$  are the total surface energies of liquid  $i$  and  $j$ ,  $\gamma_i^p$  and  $\gamma_j^p$  are the polar component of liquid  $i$  and  $j$ ,  $\gamma_i^d$  and  $\gamma_j^d$  are the dispersive component of liquid  $i$  and  $j$ , and  $\theta_i$  and  $\theta_j$  are the contact angles of liquid  $i$  and  $j$  respectively.

Although the contact angle technique is a relatively straightforward approach, its accuracy relies on many factors including surface rigidity, surface roughness, physical and chemical homogeneity, and surface impurities. The influence of each of these factors is discussed in [156,157].

### 2.8.1.2 Wilhelmy and tilted plate method

Like direct contact angle measurements, also the Wilhelmy method and the tilted plate method use a contact angle to determine the surface free energy. In the case of the Wilhelmy method, particles are fixed at a double-face adhesive plate and immersed and withdrawn from different solutions. The advancing contact angle during immersion of the plate ( $\theta_a$ ), and the receding contact angle ( $\theta_r$ ) during withdrawal are measured (**Figure 2.6A**). In the case of the tilted plate method, the nanoparticles are fixed on a plate on which a sessile droplet is formed. When the plate is tilted, an advancing contact angle is formed at the bottom of the drop, and a receding contact angle is formed at the upper side of the drop (**Figure 2.6B**). Just like the direct contact measurements, the individual components of the total surface energy can be calculated with the Owens-Wendt equation ((2-16) and (2-17)).

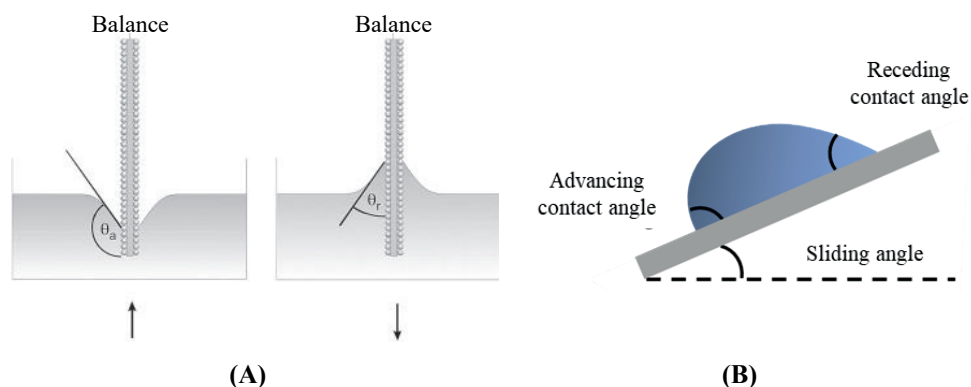


**Figure 2.6:** A schematic illustration of (A) the Wilhelmy technique where a plate is covered by particles. During immersion the advancing contact angle is measured, and during withdrawal the receding contact angle. Retrieved from [63]. (B) The tilting plate technique where a sessile drop is placed on a plate with fixed particles. The drop forms two angles when the plate is tilted, i.e., the advancing contact angle at the lower side of the drop, and the receding contact angle at the upper side of the drop.

### 2.8.1.3 Inverse gas chromatography

Inverse gas chromatography (IGC), has shown to be a valuable tool for the characterization of surface and bulk properties of solid materials including nanoparticles and polymer plastics. One of its most used applications, is for the quantification of the surface free energy [158].

Two methods exist to determine the dispersive and polar component of a sample, i.e., the Dorris-Gray [159] and Schultz method [160]. Here, we only present the Dorris-Gray method because it has been shown to be the more accurate [161]. For information on the Schultz method or IGC in general we refer to the review of Mohammadi-Jam and Waters [158].

Regarding the analysis technique itself, the sample of choice is packed into a column, after which a series of alkanes with known dispersive and polar components are injected. The retention volume  $V_n$  for each of the alkanes is determined, and  $RT \ln(V_n)$  is plotted against the carbon number of the alkanes. This leads to a linear graph, as illustrated in **Figure 2.7** for quarts [158]. The dispersive component of the surface free energy can be determined from the slope of the produced graph.

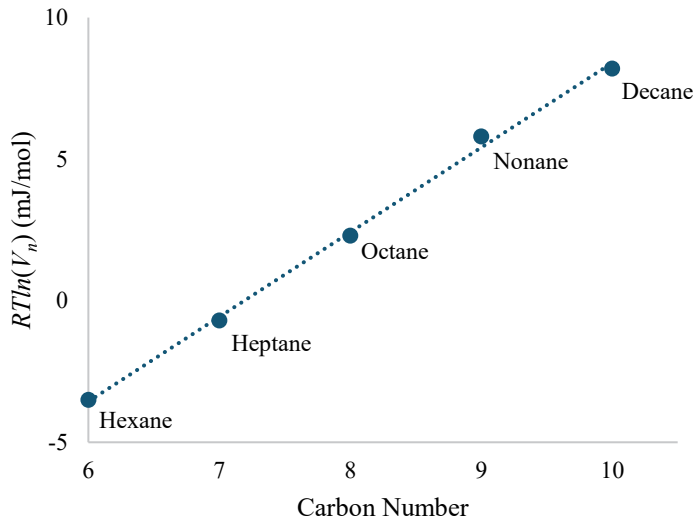


**Figure 2.7:**  $RT\ln(V_n)$  against the carbon number of the alkanes used the Dorris-Gray method; the dispersive free energy is determined from the slope. Modified from [158].

$$\gamma_s^D = \frac{\text{slope}^2}{4N^2(a_{CH_2})^2\gamma_{CH_2}} \quad (2-18)$$

The polar component of the surface free energy can be determined, for example by the polarization method [162]. First, the specific free energy of adsorption of the different probe molecules (i.e.,  $\Delta G^{SP}$ ) is determined from the retention volumes of the polar probe molecules on the sample, from which the molar deformation polarisation  $P_D$  follows:

$$P_D = \frac{M_w (r^2 - 1)}{D (r^2 + 2)} \quad (2-19)$$

where  $M_w$  is the molecular mass of the probe,  $r$  is the refractive index of the probe, and  $D$  is the probe liquid density.

Also, the  $RT\ln(V_n)$  against  $P_D$  plot should produce a linear relationship, where the points of the polar probes are located above the alkane line (**Figure 2.8**). The vertical distance between the alkane line, and the polar probe gives the total free energy of the sample of choice. The polar contribution of the surface free energy can then be calculated using equation (2-2).

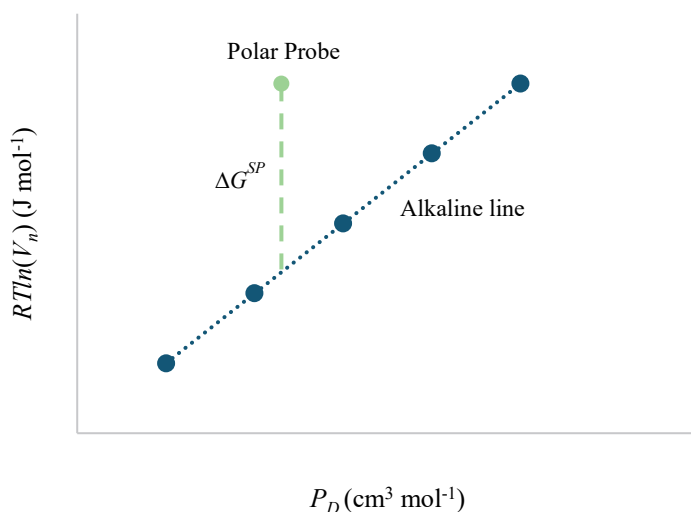


**Figure 2.8:** Schematic representation of  $RT\ln(V_n)$  against the molar deformation polarisation of the probe molecules. The retention volumes of the polar probe molecules are located above the alkane line, from which the total free energy of the compound using the vertical distance between the alkane line and the polar probe. Adjusted from [158].

### 2.8.2 Aggregate strength – Static light scattering

Recently, we have developed a method to quantify the bond energy of nanoparticle aggregates [54]. Dispersions containing aggregates of chitin nanocrystals were subjected to ultrasound treatment, from which the energy input was determined calorimetrically, and static light scattering was used to describe the total scattering behaviour of the particles. When plotted against the applied energy input (**Figure 2.9**), Equation (2-12) was fitted through the static light scattering data points, from which  $E_{agg}$  could be calculated. In principle, every mechanical force can be used as long as the nanoparticle aggregates are broken up, and the applied energy input can be quantified.

### 2.8.3 Region of the interphase – atomic force microscopy

To date, atomic force microscopy (AFM) is the only device which is able to visualize the interphase, and also quantify its local mechanical properties (e.g., Young's moduli). For nanocomposites commonly either the peak force tapping mode (PF-TM) or intermodulation



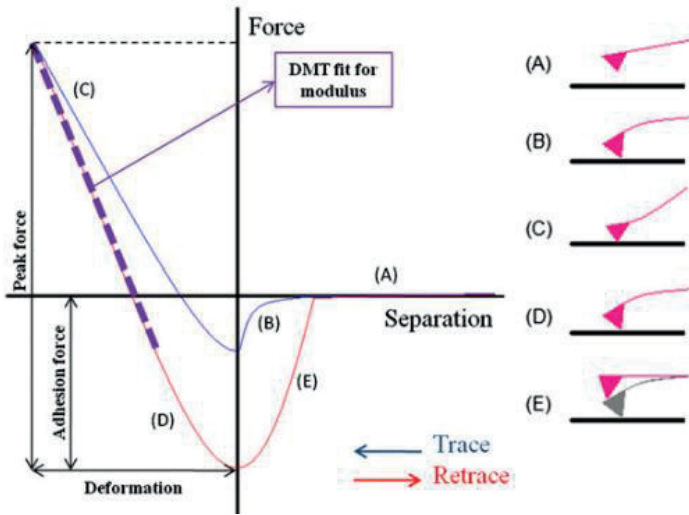


**Figure 2.10:** Schematic representation of the force separation curve obtained in AFM peak force tapping mode. (A) The AFM tip approaches the sample and there is no to little force on the tip. (B) The tip starts to touch the surface as a consequence of attractive tip-surface forces. (C) A maximum deformation because of maximum tip-surface interactions. (D) The tip-surface interactions start to become weaker and the tip comes off the surface. (E) The AFM tip returns to its original position. Retrieved from [118].

properties, the Derjaguin-Muller-Toropov model can be fitted through the initial section of the retrace curve [165]. Although other models exist (e.g., Johnson-Kendall-Roberts model [166]), the Derjaguin-Muller-Toropov model is very suitable for nanocomposites because the deformation of the sample is often lower than the tip radius, and adhesion forces are taken into account (in contrast to the Hertz model):

$$F = \frac{4}{3} E^* \sqrt{Rd^3} + F_a \quad (2-20)$$

where  $F$  is the force on the tip,  $R$  is the tip radius,  $d$  is the deformation,  $F_a$  is the force of adhesion between the tip and the sample, and  $E^*$  is the reduced elastic modulus.

When the Poisson ratio of the sample ( $\nu_s$ ) and the tip ( $\nu_{tip}$ ) are known, the elastic modulus of the sample can be calculated, assuming that the tip has an infinite elastic modulus ( $E_{tip}$ ) [167]:

$$E^* = \left( \frac{1 - \nu_s^2}{E_s} + \frac{1 - \nu_{tip}^2}{E_{tip}} \right)^{-1} \quad (2-21)$$

### 2.8.3.2 Inter modulation AFM (ImAFM)

AFM techniques have been extended using multiple frequencies instead of one to excite the probe, i.e., intermodulation AFM (ImAFM) [168].

During the measurement, the cantilever is excited with two frequencies close to the resonance of the cantilever. At the start of the measurement, there are no tip-sample interactions and a free oscillation spectrum is recorded (**Figure 2.11A** and **C**). When the tip approaches the sample the cantilever is perturbed by a non-linear tip-surface interaction (**Figure 2.11B** and **D**). Consequently, the two frequencies intermodulate (basically they mix), forming a new frequency near the cantilever resonance, i.e., intermodulation products (IMP), which are recorded. These IMPs contain additional information about the tip-surface interactions, which cannot be acquired by peak force AFM; for instance, the viscous behaviour of the material derived from the energy dissipated from the tip-sample [136]. However, the analysis is less straightforward than for other AFM techniques, and more simulation work on the

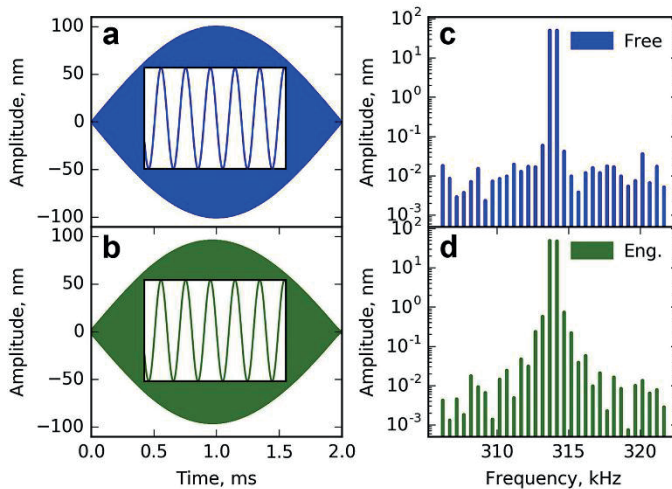


**Figure 2.11:** Schematic overview of free oscillation (upper), engaged oscillation (bottom) recorded in time, (A, B) and frequency domain (C, D). Parts a and b show the amplitude of the individual oscillations. Retrieved from [169].

tip-surface interactions is required to translate these values to, e.g., local Young's moduli [169].

## 2.9 Summary and outlook

Addition of nanoparticles to a polymer matrix holds the promise to obtain advanced products with greatly improved properties. In reality, this goal is not often achieved. We find that the options that are explored do not really follow the theoretical frameworks that are available but are rather trial-and-error in nature. Nanocomposite design would greatly be helped by a description of the theories that are available and how the essential parameters can be measured, and that is what the current review tries to achieve.

We provided thermodynamic and kinetic approaches to improve nanoparticle dispersion. Next to that, we discussed how nanoparticle – polymer interactions on an atomic scale affect the material properties on a nano, micro, and bulk scale. Furthermore, we identified three parameters which are often overlooked when designing nanocomposites, i.e., the polar and dispersive component of the surface energy of the nanoparticle and polymer, the cohesive bond energy of nanoparticle aggregates, and the quantification of the interphase region once added to the matrix. We finished with a section on how to quantify the latter designing parameters.

Considering these fundamental parameters is one step toward a better understanding of why some nanoparticle – polymer combinations are more successful than others. Most theoretical frameworks correctly describe tendencies of certain effects (e.g., nanoparticle aggregation), but better insight into the actual time frames in which these take place is crucial. As pointed out, thermodynamic and kinetic effects dominate at very different time scales, and depending on their relative importance this will lead to very different materials. To be able to differentiate between relative importance, we feel that computer simulations could play a very instrumental role, on the condition that the actual values that are used are established correctly by applying the methods that we presented earlier. Our conclusion would be that there is still a world to gain when practical and simulation tools are used symbiotically, and we believe that this will facilitate the design of the advanced materials our society is in dire need of.

## 2.10 Appendix

*Appendix 2-1: The dispersive, polar, and total surface energy of different nanoparticles in mJ/m.*

Particle	$\gamma^{total}$	$\gamma^D$	$\gamma^P$	Method used
Aerosil 200 [170]	37.3	20.0	17.3	Wilhelmy method
Aerosil R974 [170]	13.1	13.1	0.0	Wilhelmy method
Amino-modified silica [65]	43.6	37.9	5.8	Direct contact angle
CB N121 [170]	28.1	28.1	0.0	Wilhelmy method
CB N234 [170]	30.6	29.5	1.1	Wilhelmy method
CB N339 [170]	27.0	27.0	0.0	Wilhelmy method
CB N990 [170]	27.5	26.8	0.7	Wilhelmy method
Cellulose nanocrystals [70]	71.0	4.3	66.7	Direct contact angle
Cellulose nanocrystals 11% acetylated [70]	63.4	6.1	57.3	Direct contact angle
Cellulose nanocrystals 27% acetylated [70]	53.4	10.0	43.4	Direct contact angle
Cellulose nanocrystals 37% acetylated [70]	47.6	14.2	33.4	Direct contact angle
Cellulose nanocrystals 62% acetylated [70]	42.7	18.8	23.9	Direct contact angle
Cellulose nanocrystals 63% acetylated [70]	42.5	18.6	23.9	Direct contact angle
Chitin nanocrystals [36]	49.7	33.4	16.3	Direct contact angle
Chitin nanocrystals acetylated [36]	28.7	28.0	0.7	Direct contact angle
Chloro-modified silica [65]	36.2	30.5	5.8	Direct contact angle
Coupsil 8113 gran. [170]	36.9	21.1	15.8	Wilhelmy method
Coupsil 8113 pulv. [170]	32.9	22.2	10.8	Wilhelmy method
Montmorillonite [171]	-	216	-	IGC
MWCNT [170]	30.9	30.9	0.0	Wilhelmy method
MWCNT-OH [170]	31.3	31.1	0.0	Wilhelmy method
MWCNT-SH [170]	30.4	30.4	0.0	Wilhelmy method
Nanofil 15 [170]	25.3	24.3	1.0	Wilhelmy method
Nanofil 5 [170]	25.2	22.8	2.4	Wilhelmy method
Nanofil 757 [170]	48.2	17.5	30.6	Wilhelmy method
Octyl-modified silica [65]	31.0	28.0	3.0	Direct contact angle
Organo modified montmorillonite [171]	-	34.0	-	IGC
Silica VN3 gran. [170]	41.3	18.7	22.7	Wilhelmy method
Silica VN3 pulv. [170]	38.3	19.4	18.9	Wilhelmy method



---

# 3

Nanoparticle – polymer interactions  
drive nanoparticle dispersion and thus  
nanocomposite design – a molecular  
dynamics study

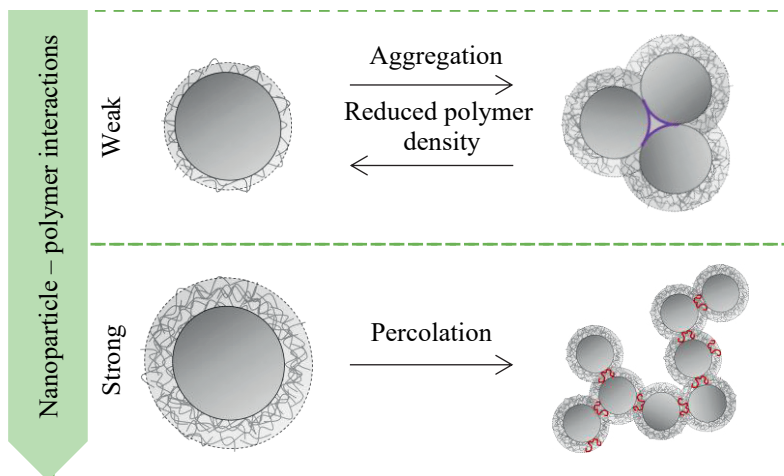
---

### 3.1 Abstract

Nanocomposites have gathered substantial attention as they show amongst others improved mechanical, barrier, and thermal properties compared to the neat polymer. In practice, these enhanced material properties are only observed when the nanoparticles are homogeneously dispersed in the polymer matrix. This is challenging to evaluate since the nature of these systems makes it difficult to observe the overall and local nanocomposite structure.

Within this chapter, we used a coarse-grained model to investigate nanoparticle dispersion inside a highly entangled polymer matrix throughout a wide temperature range. We investigated the effect of nanoparticle – polymer interaction strength and nanoparticle loading, on interphasial architecture and overall nanocomposite structure.

Generally, our results show that nanoparticle – polymer interactions facilitate nanoparticle dispersion. This led to properties that have been related to enhanced material properties such as an increased polymer density at the nanoparticle interface, an increased interphasial layer thickness, the formation of polymer bridges, and a higher glass transition temperature. We interpret this as follows: the local nanocomposite structure is crucial for inducing changes in dynamics, that are transferred to the bulk through the overall nanoparticle dispersion. This clearly points to nanoparticle – polymer interactions being at the core of nanocomposite design.



*Graphical abstract*

## 3.2 Introduction

Both in academia and industry, nanocomposites have gathered great attention due to - amongst others - improved mechanical, barrier, and thermal properties compared to the neat polymer [26,31,33,56,58,172]. As such, nanocomposites are expected to be of added value for a wide variety of applications including the automotive, aviation, and packaging industry.

It is generally accepted that improved material properties are the consequence of nanoparticle – polymer interactions that alter polymer dynamics within the interphasial region (**Chapter 4**). Due to the small size of the nanoparticles, the interphasial region occupies most of the material at low nanoparticle loading if particles are homogeneously distributed. However, nanoparticles have the tendency to aggregate because of strong interparticle interactions and/or a poor compatibility with the polymer matrix. However, investigating nanoparticle aggregation inside materials is far from trivial. Nanocomposite observation commonly relies on methods with a limited depth resolution such as scanning electron microscopy (SEM) (**Chapter 4**, **Chapter 6**, and [49,147,173,174]) or TEM [65,175], which cannot provide information on the architecture of the interphasial layer. In addition, the nature of composites, and composite manufacturing makes it difficult to investigate the effect of specific parameters on the resultant matrix. For instance, altering nanoparticle – polymer interactions is only useful if the interactions can be quantified. As a consequence, in practice, nanocomposite production and design mostly rely on ‘trail-and-error’ approaches. To make a next step toward the rational design of nanocomposites, insights in nanoparticle – polymer interactions in relation to interphasial and overall nanocomposite structure are crucial. Molecular dynamics simulations are ultimately suited to vary environment and (inter)particle properties [176,177], and thus elucidate the local nanocomposite structure including the interphasial region [177].

In the current chapter, we used a coarse grained model to investigate nanoparticle dispersion inside a highly entangled polymer matrix over a wide temperature range. We investigated different nanocomposite structures by simply altering loading and interaction strength with the polymer, and show how the interphasial structure and overall structure are affected. Finally, we discuss how different length scales are interlinked and collectively result in properties that have been related to enhanced material characteristics.

### 3.3 Model and simulation method

We used the bead-spring model of Kremer and Grest [129] to simulate polymer chains consisting of  $N_p = 500$  beads (degree of polymerization) with a diameter of  $1 \sigma^1$  and an entanglement length of  $N_e = 85$  at a monomer density of 0.85 [178,179]. The bonded monomeric units interacted with the finite extensible nonlinear elastic (FENE) potential:

$$U_{FENE} = -0.5 k R_0^2 \ln \left( 1 - \left( \frac{r}{R_0} \right)^2 \right) \quad (3-1)$$

with  $k = 30 \epsilon / \sigma^2$  and  $R_0 = 1.5 \sigma$  to ensure a certain stiffness while still avoiding high frequency modes and chain crossing [75]. Nanoparticles with a diameter of  $10 \sigma$  ( $\sigma_{NP}$ ) were modelled as Lennard Jones spheres. We simulated the nanoparticles with approximately the same mass density as the polymer monomers ( $m_m$ ); as  $m_{NP} = m_m (\sigma_{NP} / \sigma)^3$  the nanoparticles had a higher mass density than the polymers. In contrast to the regular Lennard Jones potential, the expanded Lennard Jones potential ensures the “hardness” of the nanoparticles and is commonly regarded as more accurate when simulating nanoparticle – polymer mixtures [75,180]. For differently sized particles  $i$  and  $j$ , the expanded Lennard Jones potential is defined as:

$$U_{ij}(r) = 4\epsilon \left[ \left( \frac{\sigma_j}{r - \Delta_{ij}} \right)^{12} - \left( \frac{\sigma_j}{r - \Delta_{ij}} \right)^6 \right] \quad (3-2)$$

where  $\Delta_{ij} = (\sigma_i + \sigma_j) / 2 - \sigma_j$  is a quantity that offsets the interaction caused by the excluded volume effects of different interaction sites. To reduce computational expense, the Lennard Jones potential was truncated and shifted:

$$U_{ij,ts}(r) = \begin{cases} U_{ij}(r) = 4\epsilon \left[ \left( \frac{\sigma_j}{r - \Delta_{ij}} \right)^{12} - \left( \frac{\sigma_j}{r - \Delta_{ij}} \right)^6 \right] - U_{ij}(r_c) & \text{for } r - \Delta_{ij} \leq r_c \\ 0 & \text{for } r - \Delta_{ij} > r_c \end{cases} \quad (3-3)$$

---

<sup>1</sup> Throughout the chapter units are provided in their reduced form based on the Lennard-Jones potential.

where  $r_c$  is the potential cut-off distance. The exact values for the Lennard Jones parameters can be found in **Table 3.1**. Different  $\epsilon$  were chosen to investigate the effect of pair interactions on the dispersion state of the nanoparticles in the polymer matrix.

**Table 3.1:** Absolute values used for the extended Lennard Jones potential.  $r_c^*$  is given excluding  $\Delta_{ij}$ .

Interaction	$\Delta_{ij}$	$r_c^*$	$\epsilon$
Monomer – monomer	$\sigma - \sigma$	$2^{1/6}$	1
Monomer – nanoparticle	$(\sigma_N - \sigma)/2$	$2^{7/6}$	0.1, 1, 2, 3
Nanoparticle – nanoparticle	$\sigma_N - \sigma$	$2^{1/6}$	1

Every system consisted of  $N_P = 1000$  polymers with a nanoparticle volume fraction  $\Phi_{NP} = \sigma_{NP}^3 N_{NP} / (\sigma_{NP}^3 N_{NP} + \sigma^3 N)$ , with  $N$  the number of monomers. All simulations were carried out in the software Large-scale Atomic/Molecular Massively parallel Simulator (LAMMPS) [177], and performed in a cubic simulation box with periodic boundary conditions in all directions. The velocity-Verlet algorithm was applied to integrate the equations of motion with a time step  $dt = 0.005 \tau$ . The Nose-Hoover thermostat and barostat were used to control the pressure and temperature [177,181].

The initial configurations were prepared with the software Moltemplate [182]; the polymer chains were present in a fully stretched position and the nanoparticles were placed on lattice points within the box (**Appendix 3-1**). To relax the initial configurations, we first equilibrated this system in an NVE ensemble for  $10^5 dt$  with a limited particle displacement ( $0.01 \sigma/dt$ ) to prevent the generation of huge forces acting on the atoms. The systems were further equilibrated in an NVE ensemble without limit for  $2 \cdot 10^6 dt$ , with an added mixing step in an NPT ensemble at a  $T^* = 4.0$  and  $P^* = 0$  for  $10^6 dt$  (**Appendix 3-2B**). It is good to point out that this mixing step was needed. Without this step, an improper mixture of nanoparticles and polymers was obtained (**Appendix 3-2A and E**); a high temperature was used to allow sufficient and fast mixing by expanding the volume of the system. After, the temperature was decreased to  $T^* = 1$  in  $10^5 dt$  and equilibrated for  $10^6 dt$  (**Appendix 3-2C**). All systems reached equilibrium after  $\sim 5 \cdot 10^4 dt$  where the slope of the total energy ( $U_{total}^*$ ) was  $< 10^{-11}$  and did not fluctuate more than  $\pm 0.002$  ( $\sim 0.01\%$  of the absolute value) over  $10^5 dt$ .

It is well-established that the linear dependency of various material properties – including density – changes at the glass transition temperature ( $T_g^*$ ) [176]. We therefore plotted density ( $\rho^*$ ) as function of  $T^*$  to identify  $T_g^*$ .  $T^*$  and  $\rho^*$  were determined and averaged over  $10^5 dt$  for systems at full equilibrium (**Appendix 3-3**); we found  $T_g^*$  using the least squares method.

The software OVITO was used to visualize the simulation system, generate the radial distribution functions, and perform cluster analysis [183].

### 3.4 Results and discussion

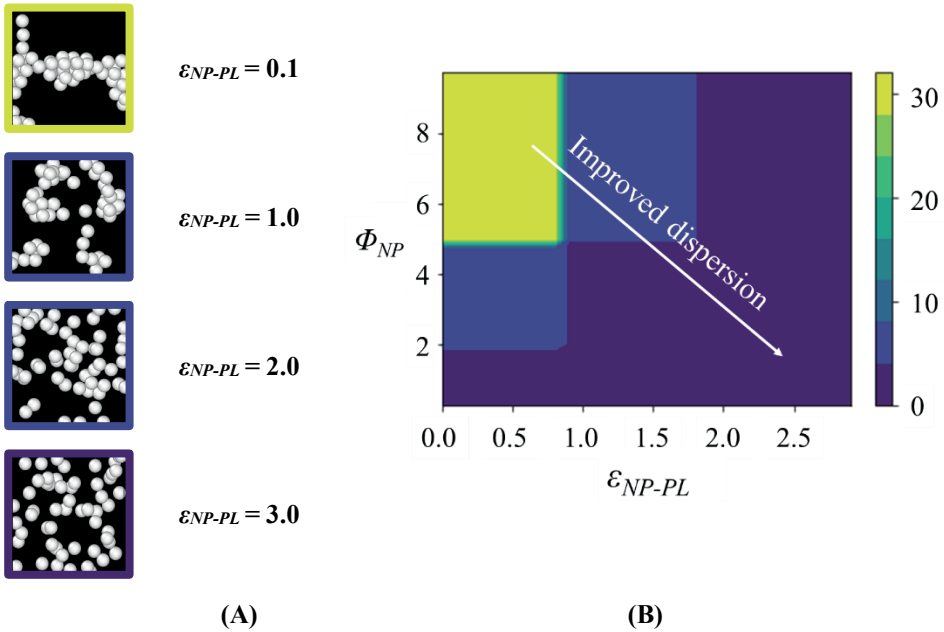
We investigated nanoparticle – polymer interaction strength ( $\epsilon_{NP-PL}$ ) and nanoparticle loading ( $\Phi_N$ ) as function temperature ( $T^*$ ) in relation to interphasial and nanocomposite structure.

#### 3.4.1 Nanoparticle – polymer interactions and nanoparticle dispersion

The overall nanocomposite structure after equilibrium was highly affected by the interaction strength between the nanoparticle and the polymer ( $\epsilon_{NP-PL}$ ) and between nanoparticles ( $\epsilon_{NP-NP} = 2.0$  for all systems) (**Appendix 3-4**). In the dispersibility map we considered nanoparticles to be of the same cluster when the interparticle distance was  $\leq 10.2 \sigma$  (**Figure 3.1**).

Very weak nanoparticle – polymer interactions ( $\epsilon_{NP-PL} = 0.1$ ) resulted in systems with heavily aggregated nanoparticles, eventually leading to completely phase separated systems at high loading. Increasing the interaction strength to  $\epsilon_{NP-PL} = 1.0$  substantially improved dispersion, although aggregation occurred at high nanoparticle loading. When  $\epsilon_{NP-PL} \geq \epsilon_{NP-NP}$  dispersion was favoured and full dispersion was achieved regardless of the loading. In general, the trends observed in our simulations correspond well with experimental data suggesting that the work of adhesion ( $W_a$ ) between the nanoparticle and the polymer needs to be higher than the work of cohesion ( $W_c$ ) between the nanoparticles themselves to facilitate dispersion (**Chapter 2**, **Chapter 4**, and [65,184]). In practical applications, nanoparticle aggregation should be prevented as this creates local weak spots that are detrimental to the material.

Increased mechanical strength and viscoelastic properties have been related to the emergence of a three-dimensional percolation network [31,57,185,186], for which certain nanoparticle loading and dispersion is needed. In general, at 2 – 10 vol % particles, viscoelastic or mechanical properties have been reported to substantially change [31,70,74,175], although

Dispersion at  $\Phi_{NP} = 10\%$ 

**Figure 3.1:** Dispersion states for varying  $\epsilon_{NP-PL}$  (0.1, 1.0, 2.0, or 3.0) and  $\epsilon_{NP-NP} = 2.0$  at  $T^* = 1.0$ . (A) Snapshots at  $\Phi_{NP} = 10\%$ . (B) Cluster size at different  $\Phi_{NP}$  and  $\epsilon_{NP-PL}$ . Nanoparticles at interparticle distance  $\leq 10.2 \sigma$  were considered part of one cluster.

also higher and lower percolation thresholds have been reported. This is expected to be dependent on nanoparticle dispersion that in practice can be affected by changing nanoparticle – polymer interactions by using different nanoparticles [65,66,184], or by surface modification (**Chapter 6**).

It is important to mention that nanoparticle loadings  $> 5$  wt. % are very substantial and aggregation is commonly observed at even higher loadings in experiments, ([39] & **Chapter 4**). The main difference with simulation studies is that empirical nanocomposites are most probably in a meta-stable state. For example, various studies have shown that the final nanocomposite structure is affected by the fabrication method and/or the solvent quality [40,41]. Considering this, it is a pity that most simulation and experimental studies investigating (interphasial) dynamics are limited to well-dispersed systems [34,38].

### 3.4.2 Nanoparticle – polymer interactions and glass transition temperature

An increase in  $T_g^*$  is an indicator of dynamics reduction [187,188], and here we investigated  $T_g^*$  as function of nanoparticle concentration (**Figure 3.2**).

Very poor nanoparticle – polymer interaction ( $\varepsilon_{NP-PL} = 0.1$ ) led to reduced  $T_g^*$  compared to the neat polymer, which was more obvious at higher  $\Phi_{NP}$ . In general, stronger nanoparticle – polymer interactions increased  $T_g^*$ , depending on the overall nanocomposite structure (**Figure 3.2**). For  $\varepsilon_{NP-PL} = 1.0$  and  $\Phi_{NP} \leq 2\%$ ,  $T_g^*$  increased with nanoparticle loading, while at  $\Phi_{NP} \geq 5\%$  when the system started to aggregate (**Figure 3.1**),  $T_g^*$  slightly decreased. Experimentally, similar results were reported by Qiao et al. [189] who qualitatively showed that aggregation leads to smaller changes in  $T_g$ . This is a clear indication that material properties are affected by the overall nanocomposite structure. In contrast, the  $T_g^*$  of compatible systems ( $\varepsilon_{NP-PL} = 2.0$  and  $\varepsilon_{NP-PL} = 3.0$ ) increased upon increasing  $\Phi_N$ , and this increase plateaued at  $\Phi_{NP} \geq 5\%$ . The latter suggests that the percolation threshold of these systems lies around this loading.

Although the nanoparticle's effect on  $T_g^*$  seems low, it is worth mentioning that similar magnitudes were found experimentally; typically  $T_g$  alters with a maximum of

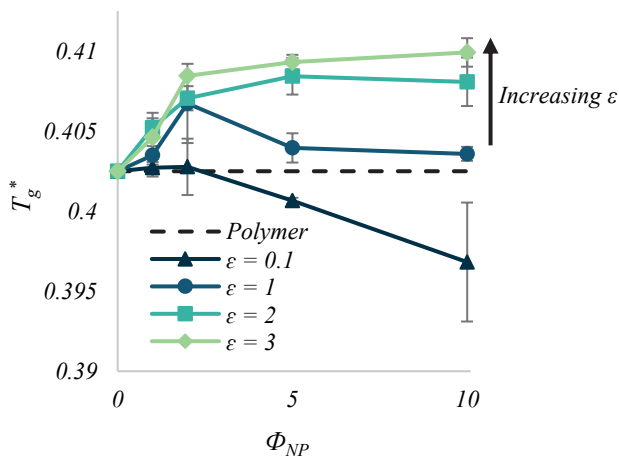


**Figure 3.2:** Glass transition temperature ( $T_g^*$ ) as function of nanoparticle loading ( $\Phi_{NP}$ ) at a constant nanoparticle interaction strength  $\varepsilon_{NP-NP} = 2.0$ . The error bars represent the standard deviation from two independent simulations. The  $T_g^*$  of each system was found by the method of least squares (**Appendix 3-3**).

$\pm 5$  °C [65,128]. Commonly, these effects are explained by local alteration in chain relaxation at the interface of the nanoparticle [56]. In the next section, we explored interphasial architecture further, and discuss how this affects overall material properties.

### 3.4.3 Nanoparticle-polymer interactions and interphasial properties

Recent insights suggest that altered interphasial dynamics are caused by an increased or reduced polymer density at the interphasial region [56,132,190]. For that reason, we determined the local structure by means of the radial distribution function:

$$g_{ij} = - \frac{\langle n_j(r) \rangle_\alpha}{\rho_j V_{shell}(r)} \quad (3-4)$$

where  $\langle n_j(r) \rangle_\alpha$  is the average number of particles  $j$  at distance  $r$  from nanoparticle  $i$ ,  $\rho_j$  the number density of particles  $j$  (either the nanoparticle or monomeric units of the polymer), and  $V_{shell}(r)$  the volume of a shell centred around particle  $i$ . First, we determined the radial distribution function between the nanoparticle and the polymer at  $\Phi_N = 0.5\%$  (**Figure 3.3**); this loading was sufficiently low for nanoparticles to not physically touch even at weak  $\varepsilon_{NP-PL}$ . Please note that the first 5.5  $r/\sigma$  were inaccessible as they correspond to the radius of the nanoparticle ( $\sigma_{NP} = 10$ ) and the monomeric unit of the polymer ( $\sigma_m = 1$ ). When completely mixed,  $g(r)$  should theoretically approach  $\sim 1$ , an increased or reduced  $g(r)$  illustrates higher or lower monomer density near the surface of the nanoparticle, respectively.

The nanoparticle – polymer interaction strength highly impacted monomer density directly at and near the interface of the nanoparticle. For both  $T^* = 0.2$  and 0.6, an interaction strength of  $\varepsilon_{NP-PL} = 0.1$ ,  $g_{NP-PL}$  mostly fluctuated  $\sim 1$ . A higher  $\varepsilon_{NP-PL}$  clearly increased  $g_{NP-PL}$ ; at  $\varepsilon_{NP-PL} = 3.0$  even to 1.7 for  $T^* = 0.2$ . Interestingly, the polymer density increased for  $\varepsilon_{NP-PL} = 1.0$ , meaning that this interaction strength can be considered attractive despite its aggregated nature (**Figure 3.1**). The effect of temperature on  $g_{NP-PL}$  was small, although it is somewhat higher for  $T^* = 0.2$ , most probably due to the reduced volume of the system that essentially pushed nanoparticles together at low temperatures (**Appendix 3-5**).

Furthermore,  $\varepsilon_{NP-PL}$  influenced the range over which the polymers were affected by the nanoparticle. To get an impression of the interphasial layer thickness, we quantified the layer thickness ( $h_i$ ) as the furthest point in  $g(r)$  where  $|g(r) - 1.0| > 0.05$  (**Figure 3.4**), and found

that  $\epsilon_{NP-PL}$  affected the range of influence of the nanoparticle over the polymers. For  $\epsilon_{NP-PL} = 0.1$ , the interphasial thickness was  $\sim 1 \sigma$ , whereas this is  $\sim 4 \sigma$  for higher  $\epsilon_{NP-PL}$ . This dependency of the interphasial thickness on interaction strength is probably an important reason why the percolation threshold in some systems is higher than in others (as discussed in **section 3.4.1**). An increased layer thickness essentially increases the chance for interphasial zones to interact. Stronger nanoparticle – polymer interactions are therein more effective, and do so independently of temperature.

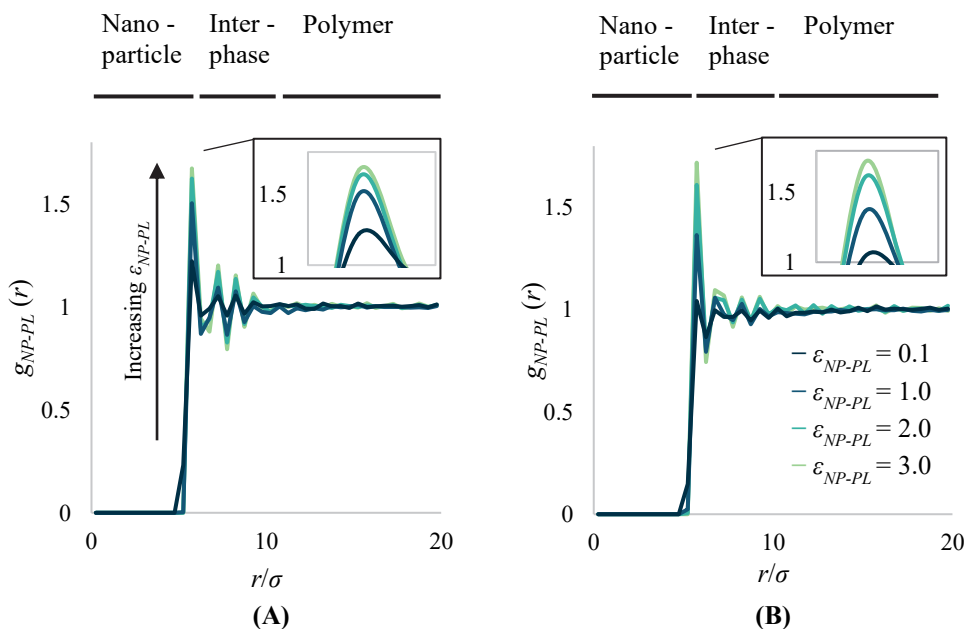


**Figure 3.3:** The radial distribution function between nanoparticle and polymer at a temperature of (A)  $T^* = 0.2$  and (B)  $T^* = 0.6$ ; the nanoparticle – nanoparticle interaction strength ( $\epsilon_{NP-NP} = 2.0$ ) and loading ( $\Phi_N = 0.5\%$ ) were constant, while nanoparticle – polymer interaction strength varied from  $\epsilon_{NP-PL} = 0.1$  to  $3.0$  for non-touching nanoparticles.

Our results are consistent with other simulation studies that show similar trends [129,132]. For attractive nanoparticle – polymer interactions, we found an interphasial layer in the order of  $\sim 4 \sigma$  (**Figure 3.4**), which seems realistic as empirical studies estimate the interphasial layer at  $1.5 - 9 \text{ nm}$  [191–193]. When comparing with Zhang et al [132] who used a similar simulation approach for a single particle, we found a discrepancy in regard to temperature

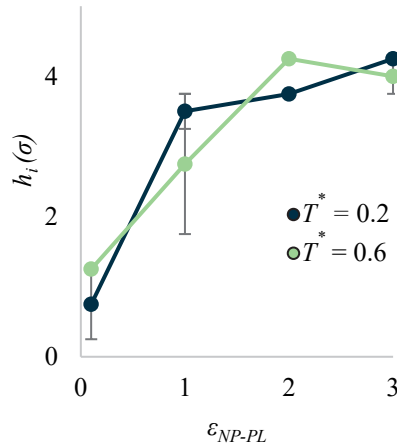


**Figure 3.4:** The thickness of the interphasial region ( $h_i$ ) as function of nanoparticle - polymer interaction strength ( $\epsilon_{NP-PL}$ ) at temperatures  $T^* = 0.2$  and  $0.6$ ; the nanoparticle - nanoparticle interaction strength ( $\epsilon_{NP-NP} = 2.0$ ) and loading ( $\Phi_N = 0.5\%$ ) were constant. The error bars represent the standard deviation between two independent simulations, and fall mostly within the data points.

effects. They observed an increased interphasial layer upon cooling, while we found no effect (**Figure 3.4**).

In brief, our results clearly indicate that attractive nanoparticle – polymer interactions are needed to develop a thick interphasial layer, and a high polymer density at the nanoparticle surface. As such,  $\epsilon_{NP-PL}$  dictates  $T_g^*$  and the extent of its change (**Figure 3.3**).

#### 3.4.4 Nanoparticle dispersion, interphasial structure, material properties

To evaluate how nanocomposite dispersion affects  $T_g^*$  (**Figure 3.1** and **Figure 3.2**), we determined the radial distribution function amongst nanoparticles (**Figure 3.5**) and between the nanoparticle and the polymer (**Figure 3.6**) at a loading of  $\Phi_N = 10\%$ . To be complete,  $g_{NP-PL}$  for  $\Phi_N = 2$  and  $5\%$  are given in **Appendix 3-6** and **Appendix 3-7** respectively.

Systems with  $\epsilon_{NP-PL} = 0.1$  were highly aggregated (**Figure 3.1**), as was clearly visible in the radial distribution function (**Figure 3.5A**). A peak at  $g_{NP-NP} \sim 10 r/\sigma$  appeared corresponding to two nanoparticles directly touching. At  $T^* > T_g^*$  the aggregation peak slightly shifted to

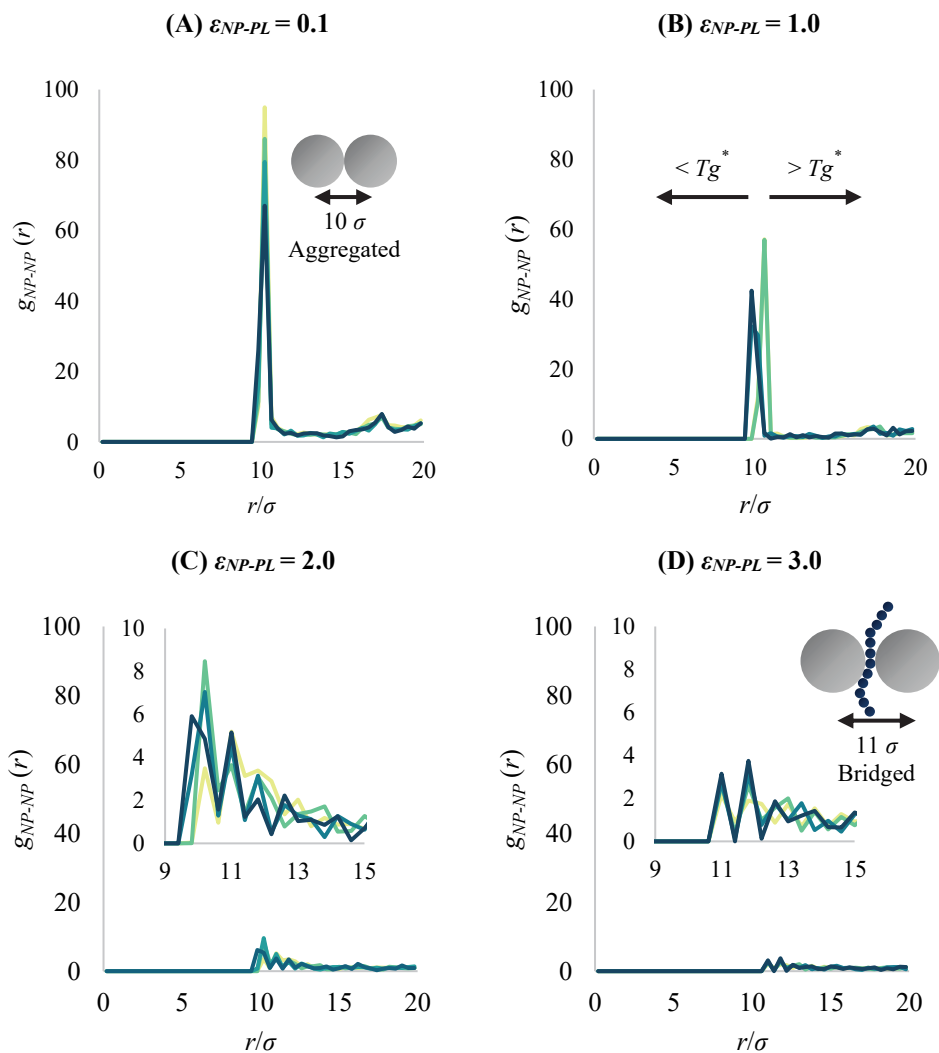


**Figure 3.5:** Radial distribution function of the nanoparticle with respect to the nanoparticle at different temperatures  $\bullet T^* = 0.25$   $\bullet T^* = 0.35$   $\bullet T^* = 0.45$   $\bullet T^* = 0.55$ . The nanoparticle – nanoparticle interaction strength ( $\epsilon_{NP-NP} = 2.0$ ) and loading ( $\Phi_N = 10\%$ ) were constant, while we varied the nanoparticle – polymer interaction strength  $\epsilon_{NP-PL}$  (A) = 0.1 (B) 1.0 (C) 2.0 (D) 3.0.

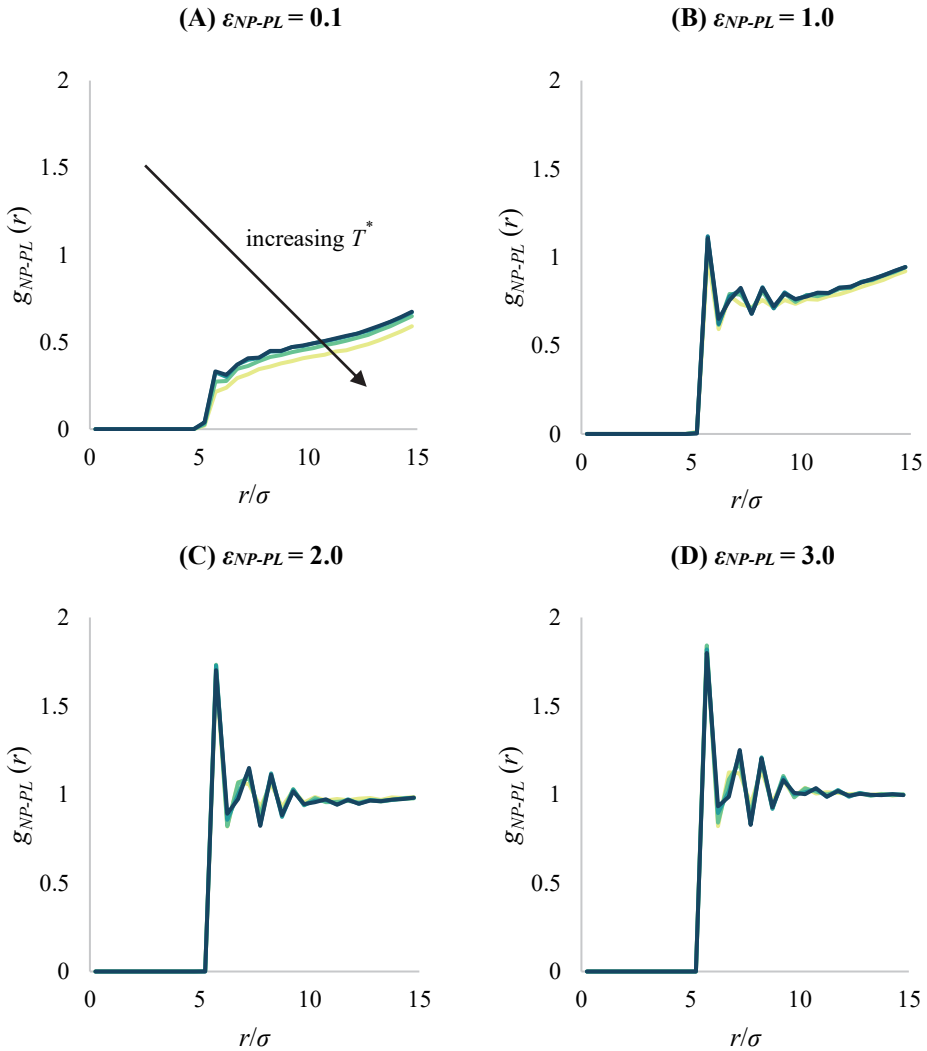


**Figure 3.6:** Radial distribution function of the nanoparticle with respect to the polymer at different temperatures  $\bullet T^* = 0.25$   $\bullet T^* = 0.35$   $\bullet T^* = 0.45$   $\bullet T^* = 0.55$ . The nanoparticle - nanoparticle interaction strength ( $\epsilon_{NP-NP} = 2.0$ ) and loading ( $\Phi_N = 10\%$ ) were constant, while we varied the nanoparticle - polymer interaction strength  $\epsilon_{NP-PL}$  (A) = 0.1 (B) 1.0 (C) 2.0 (D) 3.0.

$g_{NP-NP} \sim 10.1 r/\sigma$ ; most likely the kinetic energy was sufficient for polymer reorientation, thus created some distance between nanoparticles due to repulsive interactions among nanoparticles, and with the polymer (**Appendix 3-8**). The  $g_{NP-PL}$  of these systems was far below 1 (**Figure 3.6A**), meaning that overall polymer density at the interphasial region was low, and this effect increased at higher temperatures (see **Appendix 3-5**; repulsive interaction between nanoparticle – polymer, and amongst nanoparticles led to system expansion). Since melt mixing is often the preferred production method for plastics; our results hint that for weak nanoparticle – polymer interactions, elevated temperatures may be used to facilitate nanoparticle separation.

Stronger nanoparticle – polymer interactions reduced the ‘aggregation’ peak at  $\sim 10 r/\sigma$ , until it completely vanished at an interaction strength of  $\epsilon_{NP-PL} = 3.0$  (**Figure 3.5A, B, C**). Furthermore, we observed additional peaks for well-dispersed systems ( $\epsilon_{NP-PL} \geq 2.0$ ) that are located at  $\sim 11$ ,  $\sim 12$ , and  $\sim 13 r/\sigma$ . These peaks correspond to single, double, or triple monomeric units being sandwiched between two nanoparticles (**Figure 3.5C & D**). This is consistent with Lui et al. who reported a sandwich structure for attractive nanoparticle dispersion [75]. Additionally, the volume of these systems decreased because of the attractive forces between nanoparticles and polymers (**Appendix 3-5**), which led to an increased monomer density at the nanoparticle surface (**Figure 3.6A & B**). This was more pronounced for  $\epsilon_{NP-PL} = 3.0$  than 2.0.

Interestingly, we found that the interphasial structure was highly affected by the polymer - nanoparticle interaction strength. We hypothesize that the multiscale interactions from **Figure 3.7** are key for this. Nanoparticle aggregation taking place at low  $\epsilon_{NP-PL}$  hinders percolation network formation (**Figure 3.5A & B**), and affects the space polymers could occupy in the interphase. This effect increases with cluster size (**Figure 3.1**), and reduces  $T_g^*$ . In contrast, strong  $\epsilon_{NP-PL}$  leads to large interphasial regions (**Figure 3.4**) with higher polymer density (**Figure 3.3**) leading to the emergence of a percolation network connected by polymer bridges (**Figure 3.5**) that increases the glass transition temperature. When considering  $T_g^*$  a measure for dynamics reduction [187,188], it is fair to suggest that these well-dispersed systems reduce material dynamics and thereby enhance mechanical strength.

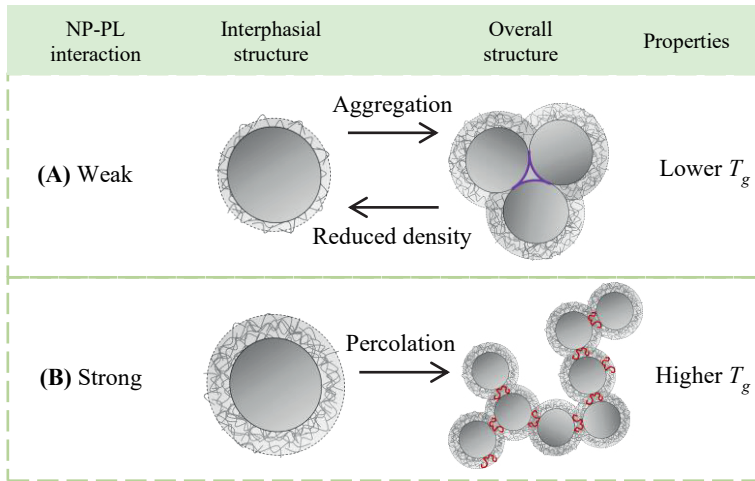


**Figure 3.7:** (A) Weak nanoparticle – polymer interactions result in a small interphasial layer and cause aggregation. The latter prevents interaction with the polymer (indicated in purple), thereby decreasing the polymer density at the surface of the nanoparticle consequently reducing the glass transition temperature. (B) Strong nanoparticle – polymer interactions result in an increased interphasial region, and result in polymer bridges (indicated in red) which can form a percolation network. Consequently, an increased glass transition temperature is observed.

In essence, the local and overall nanocomposite structure are the consequence of enthalpic and entropic contributions which are classically described by Gibb’s free energy ( $\Delta G$ ):

$$\Delta G = H - T\Delta S \quad (3-5)$$

where  $H$  is the enthalpic component and  $\Delta S$  the entropic one. We directly computed  $H^*$  and illustrate the enthalpic contribution normalized against  $H^*$  of the neat polymer (**Figure 3.8**). For nanoparticles with  $\epsilon_{NP-PL} < \epsilon_{NP-NP}$  the enthalpy of the system increased with higher  $\Phi_{NP}$ , while for nanoparticles with  $\epsilon_{NP-PL} \geq \epsilon_{NP-NP}$  the enthalpic component decreased with  $\Phi_{NP}$ . In literature, the overall opinion seems to be that the enthalpic factor is highly influential to induce polymer perturbations [56,190], but in our systems the absolute enthalpic differences between well-dispersed and aggregated ones were very small ( $< 1.0\%$ ). This could be an indication that the entropic component plays a more important role than commonly assumed. Unfortunately, the entropic contribution of the entire system cannot be directly computed via LAMMPS, but this would be highly interesting to do.

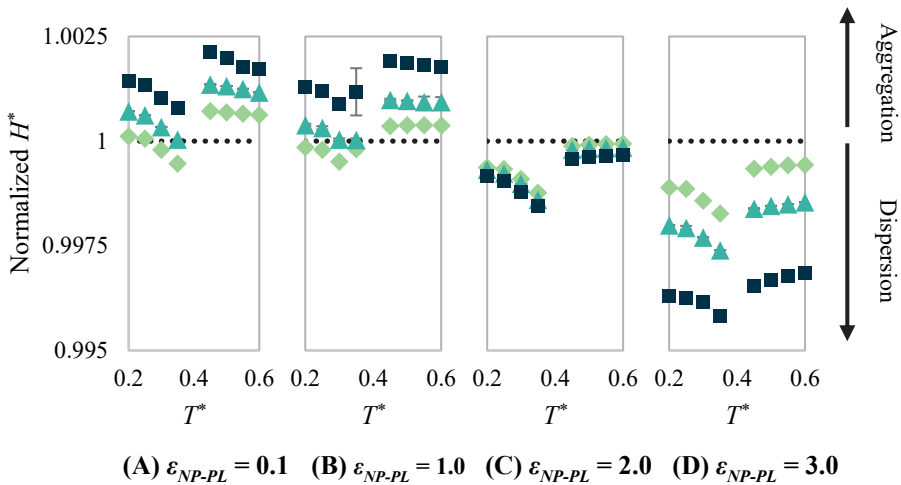


**Figure 3.8:** The enthalpic factor of the nanocomposites (normalized  $H^*$ ) normalized to that of the neat polymer for different nanoparticle loading: ..  $\Phi_{NP} = 0\%$ ,  $\diamond$   $\Phi_{NP} = 2\%$ ,  $\triangle$   $\Phi_{NP} = 5\%$ ,  $\blacksquare$   $\Phi_{NP} = 10\%$  at different temperatures ( $T^*$ ). The interaction strength between the nanoparticle and the polymer ( $\epsilon_{NP-PL}$ ) varied (A-D) and the interaction strength between the nanoparticles was kept constant ( $\epsilon_{NP-NP} = 2.0$ ).

### 3.5 Conclusions

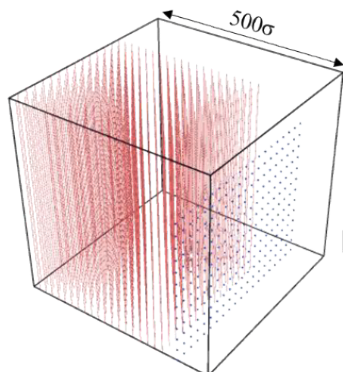
Our results indicate that nanoparticle – polymer interactions greatly affect the interphasial and nanocomposite structure, and collectively contribute to ‘enhanced material properties’.

Nanoparticle – polymer interactions of which the strength exceeded that of the interaction between particles resulted in large interphasial regions of relatively high polymer density. In these systems nanoparticles were connected by a single, double, or triple monomeric polymer unit. This is key for percolation network formation that reduces polymer dynamics, and in turn increased the glass transition temperature. For weak nanoparticle – polymer interactions nanoparticle aggregation greatly reduced the polymer density in the interphasial region, even for attractive nanoparticle – polymer interactions, which inhibited the formation of a percolation network and reduced the glass transition temperature.

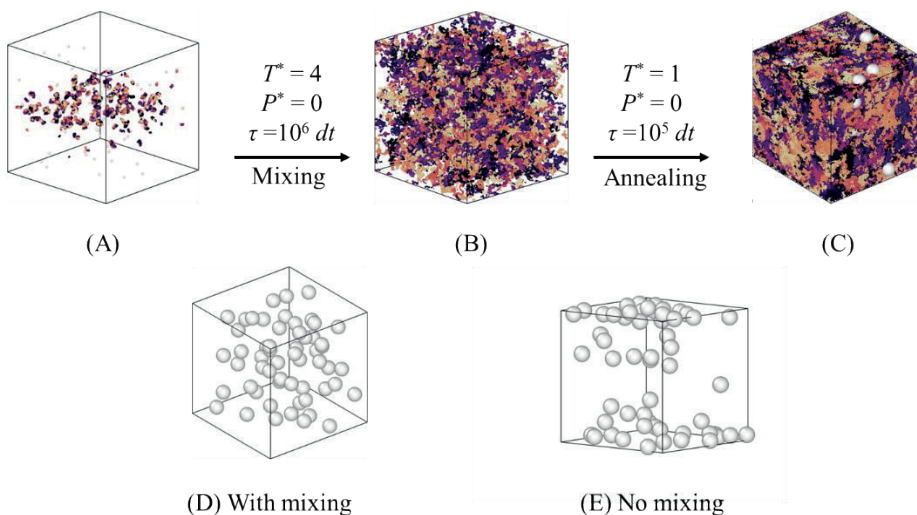
Generally, our results show great similarity with experimental data, which makes us confident that these results provide valuable insights for practice. For nanocomposite design, it is important to match the properties of the nanoparticle to the polymer, which can be done

by simply choosing an appropriate nanoparticle, or when not available, to tune particle properties by surface modification when needed.

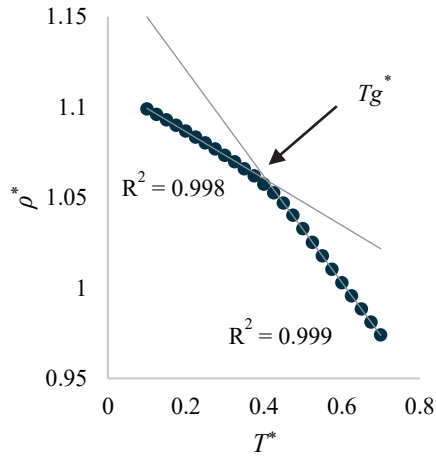
## 3.6 Appendix



**Appendix 3-1:** Starting configuration created with Moltemplate [182] with nanoparticles and polymers equally distributed through the simulation box.

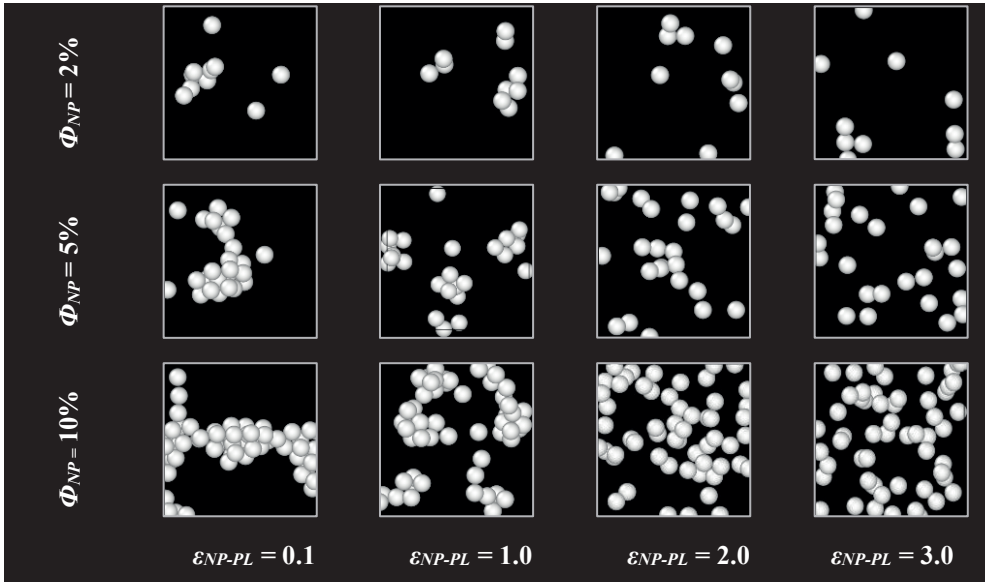


**Appendix 3-2:** Development of simulation procedure: (A) nanocomposite structure after NVE ensemble with nanoparticles mainly located on top and bottom of the simulation system. (B) The included mixing step, and (C) annealing the system for  $10^6 dt$ , resulted in (D) properly mixed systems. (E) If the mixing step was not applied particles remained present at the top and the bottom of the simulation system. Different colours in (A)-(C) are assigned to individual polymers.

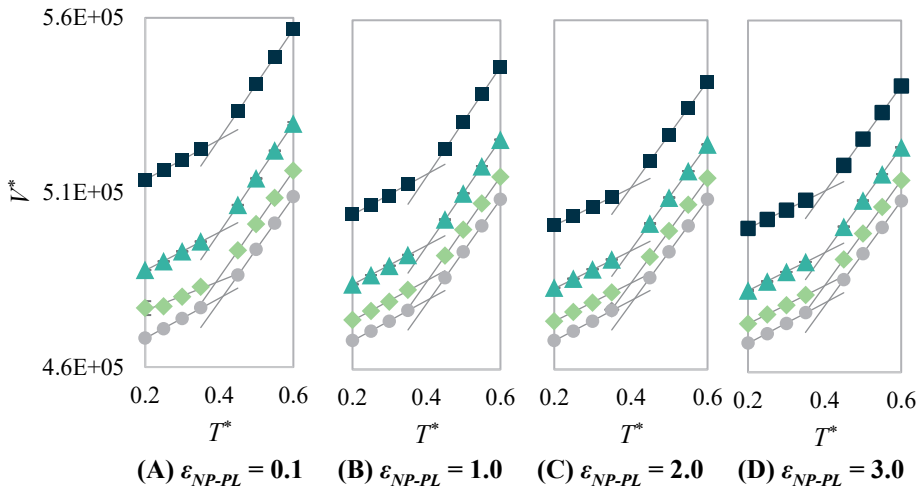


**Appendix 3-3:** By plotting the density of each system ( $\rho^*$ ) as function of temperature ( $T^*$ ) the glass transition temperature ( $T_g^*$ ) was found using the least sum of squares. This is an example for  $\epsilon_{NP-PL} = 2.0$  and  $\Phi_{NP} = 5\%$ .

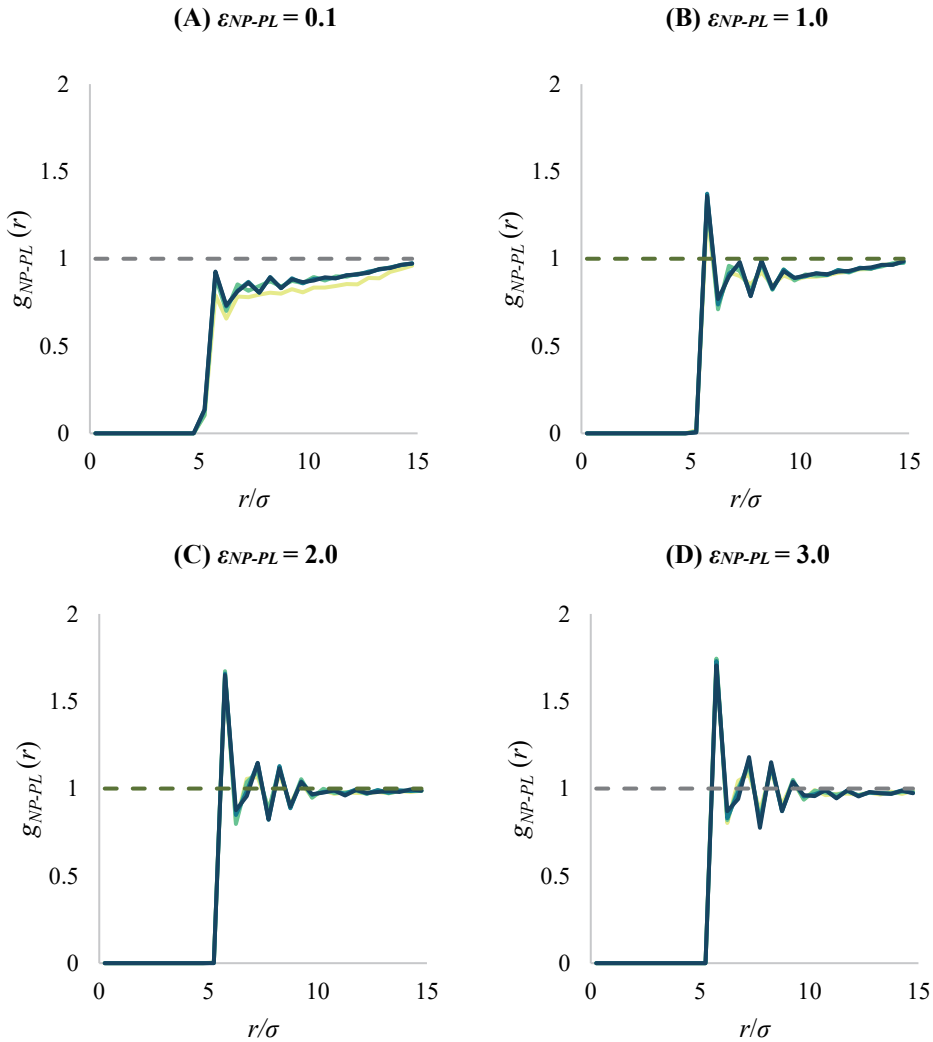
3



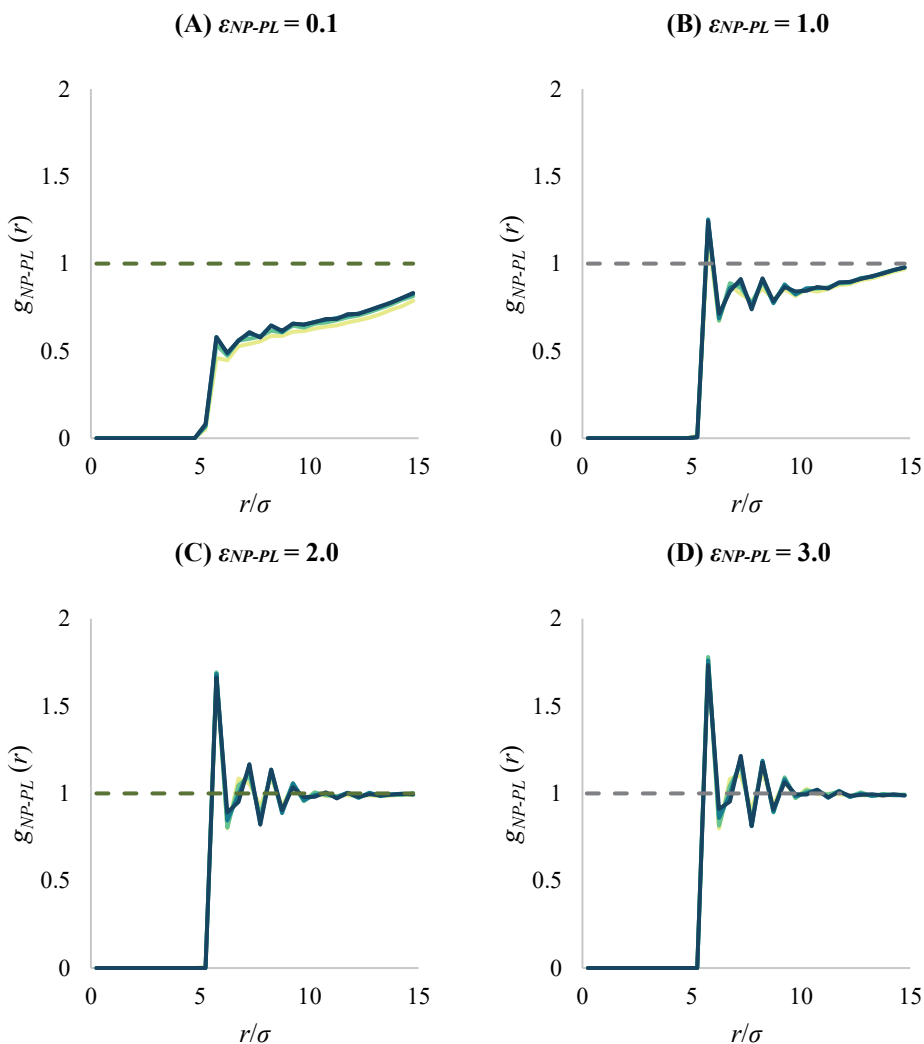
**Appendix 3-4:** Nanoparticles dispersed in the polymer matrix as function of nanoparticle loading ( $\Phi_{NP}$ ) and interaction strength with the polymer ( $\epsilon_{NP-PL}$ ). Interaction strength between nanoparticles ( $\epsilon_{NP-NP} = 2.0$ ) and temperature ( $T^* = 1.0$ ) were kept constant.



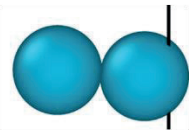
**Appendix 3-5:** The system volume ( $V^*$ ) of the simulation box as function of nanoparticle loading :  $\circ \Phi_{NP} = 0\%$ ,  $\diamond \Phi_{NP} = 2\%$ ,  $\triangle \Phi_{NP} = 5\%$ ,  $\blacksquare \Phi_{NP} = 10\%$  at different temperatures ( $T^*$ ). The interaction strength between the nanoparticle and the polymer ( $\epsilon_{NP-PL}$ ) varied (A-D) and the interaction strength between the nanoparticles was kept constant ( $\epsilon_{NP-NP} = 2.0$ ). Error bars of two independent simulations fall within marker symbols.



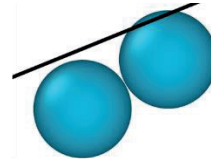
**Appendix 3-6:** Radial distribution function of the nanoparticle with respect to the polymer at different temperatures  $\bullet T^* = 0.25$   $\bullet T^* = 0.35$   $\bullet T^* = 0.45$   $\bullet T^* = 0.55$ . The nanoparticle – nanoparticle interaction strength ( $\epsilon_{NP-NP} = 2.0$ ) and loading ( $\Phi_N = 2\%$ ) were constant, while we varied the nanoparticle – polymer interaction strength  $\epsilon_{NP-PL}$  (A) 0.1 (B) 1.0 (C) 2.0 (D) 3.0. To guide the eye a dotted line is presented at  $g(r) = 1$ .



**Appendix 3-7:** Radial distribution function of the nanoparticle with respect to the polymer at different temperatures  $\bullet T^* = 0.25$   $\bullet T^* = 0.35$   $\bullet T^* = 0.45$   $\bullet T^* = 0.55$ . The nanoparticle – nanoparticle interaction strength ( $\epsilon_{NP-NP} = 2.0$ ) and loading ( $\Phi_N = 5\%$ ) were constant, while we varied the nanoparticle – polymer interaction strength  $\epsilon_{NP-PL}$  (A) = 0.1 (B) 1.0 (C) 2.0 (D) 3.0. To guide the eye a dotted line is presented at  $g(r) = 1$ . To guide the eye a dotted line is presented at  $g(r) = 1$ .



(A)  $T^* < T_g^*$



(B)  $T^* > T_g^*$

**Appendix 3-8:** Below the glass transition temperature (A) aggregated particles were in direct contact with each other. Above the glass transition temperature (B) aggregated particles had a minimum distance due to the repulsive forces among the nanoparticles and the kinetic energy that allowed this separation.



---

# 4

## Particle dispersion drives nano to bulk dynamics required for nanocomposite design

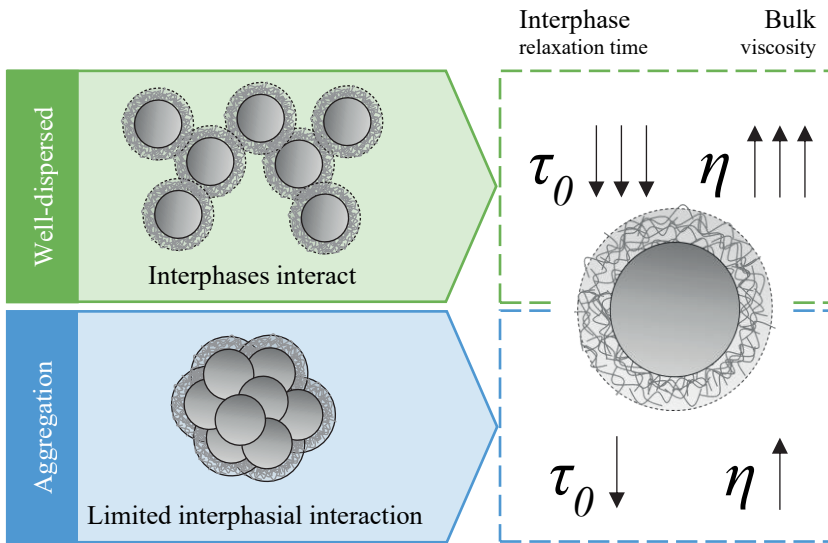
---

*Submitted as “Ivanna Colijn, Erik Postma, Raoul Fix, Hanne van der Kooij, Karin Schroën.  
Particle dispersion governs nano to bulk dynamics for tailored nanocomposite design”*

## 4.1 Abstract

The addition of nanoparticles to bioplastics has shown great potential to expand their practical use, as the resultant bioplastic nanocomposites feature improved thermal, barrier, and/or mechanical properties. It is well-established that these enhancements are the consequence of nanoparticle – polymer interactions that alter polymer dynamics within an interphasial region of a few nanometers. However, the translation of nanoscale phenomena to bulk properties is challenging, as traditional techniques that probe interphasial dynamics are limited to well-dispersed samples, which is usually not the case in practice. Laser speckle imaging (LSI) does enable the measurement of interphasial dynamics inside realistic nanocomposites with great sensitivity. In this chapter, we investigated the effect of nanoparticle surface chemistry on interphasial polymer motion. We bridged nano- and macroscale observations by comparing the LSI-derived relaxation times with rheological quantities.

On a macroscale, nanocomposites with well-dispersed PDMS coated nanoparticles showed the highest melt viscosity compared to nanocomposites containing highly aggregated PVP and PAA coated nanoparticles. On the nanoscale – within the interphasial region – the presence of nanoparticles increased relaxation times by a factor  $10^1 - 10^2$ , eventually reaching ultraslow relaxations in the order of  $\sim 10^3$  s. As such, embedded nanoparticles essentially play the role of physical crosslinks, constraining the motions of polymer chains locally. In nanocomposites with well-dispersed PDMS coated nanoparticles, the relaxation times plateaued at 5 wt. % whereas this was 10 wt. % for nanocomposites containing aggregated nanoparticles with a coating of PAA or PVP. We hypothesize that spatially separated yet mechanically connected interphasial regions can interact with each other, which is facilitated by improved dispersion and nanoparticle loading. In fact, our results highlight that nanoparticle dispersion is the key parameter for mechanical reinforcement as opposed to nanoparticle – polymer interactions that are commonly considered most important.



Graphical abstract

## 4.2 Introduction

Bioplastics tackle environmental issues related to our current linear plastics economy, but their properties do often not meet the requirements for their intended use [13,14]. The addition of nanoparticles has shown great promise to expand the application of bioplastics from niche to mainstream, as the resultant bioplastic nanocomposites often feature enhanced thermal, barrier, and/or mechanical properties [31,194,195].

Plastic products – including nanocomposites – are commonly produced via melt mixing where the viscoelastic behaviour of the melt highly impacts its processability. The addition of nanoparticles greatly increases the viscoelastic properties depending on design parameters such as nanoparticle nature or the molecular weight of the polymer. Although rheological insights are abundantly reported and reviewed [74,196–198], current knowledge is mainly of phenomenological nature rather than providing knowledge on the nano/micro level.

Nevertheless, it is well-established that nanoparticle – polymer interactions alter polymer dynamics within a region of  $\sim 1.5 - 9$  nm from the nanoparticle's surface [191–193]. Due to the small size of the nanoparticles, the interphasial region easily occupies most of the material

already at low nanoparticle loading [184]. At higher nanoparticle loading, interphasial regions potentially overlap resulting in a much higher reinforcement.

Recent studies reveal that the structure and dynamics of the interphasial region are transferred to the bulk [190], yet the governing mechanisms are ill-understood, mainly because the measurement of interphasial dynamics is not so trivial. Polymer melts – and nanocomposites specifically – exhibit a wide range of dynamic processes that are interrelated and take place at different length and time scales [56]. Today’s knowledge is therefore primarily founded on molecular dynamics simulations and advanced experimental techniques such as broad dielectric spectroscopy (BDS), neutron spin echo (NSE), and quasi-elastic neutron scattering (QENS) [56,190]. These techniques commonly rely on well-dispersed systems, as contaminants, aggregates or heterogeneity severely complicate data analysis [199]. This is a major drawback considering that nanoparticles tend to aggregate into microscale entities due to interparticle interactions and/or a poor compatibility with the polymer matrix [65,184]. To truly translate interphasial to bulk scale dynamics, a technique is required which enables the measurement of nanoscale dynamics in the interphasial region of aggregated nanoparticles.

In the current chapter, we show that the relatively unexplored optical method laser speckle imaging (LSI) is well suited for this challenge. LSI allows non-invasive, in situ visualisation of nanometric motions deep inside turbid materials [200–204], which can contain aggregates. It uses a powerful laser beam and camera, combined with quantitative image processing algorithms, that enables the elucidation of nanoscale dynamics of polymers close to the nanoparticle’s (aggregate) surface over a wide spectrum of relaxation times inherent to viscoelastic properties. Using this technique, we unveiled that nanoparticle dispersion is a key parameter affecting both nano and bulk scale dynamics.

## **4.3 Experimental**

### **4.3.1 Materials**

TiO<sub>2</sub> nanoparticles, coated with polyacrylic acid (PAA), polyvinylpyrrolidone (PVP), and polydimethylsiloxane (PDMS), with a diameter of ~ 18 nm were purchased from US Research Nanomaterials Inc (USA). Polylactic acid (PLA) Ingeo D3052 and D4043 were from NatureWorks LLC (USA), and chloroform was from Sigma-Aldrich (Germany).

### 4.3.2 Nanocomposite production

Nanoparticles were suspended in 5 w/v % PLA chloroform solution and stirred overnight. This mixture was sonicated to facilitate nanoparticle dispersion; 50 J per 30 ml sample was applied with an amplitude of 10%, in pulses of 10 s with 5 s rest to prevent excessive heating (Branson Sonifier SFX550, Emerson, the Netherlands). Thereafter, 30 ml was poured into an aluminium tray, and the chloroform was left to evaporate overnight. Drying was continued at 40 °C for 24 h (VD53, Binder, Germany) followed by drying in an air dryer at 80 °C for 9 days (TTM 2/100 ES, Gerco Kunststofftechnik GmbH, Germany). The resulting ~ 0.5 mm thick samples were stored in a vacuum desiccator to prevent moisture uptake.

### 4.3.3 Nanocomposite characterization

#### 4.3.3.1 Scanning electron microscopy

Scanning Electron Microscopy (SEM; FEI Magellan 400, FEI Electron Optics B.V., the Netherlands) was used to observe nanoparticle distribution and morphology in the PLA matrix. To expose the material core, samples were cryo-fractured in liquid nitrogen, mounted onto 90° SEM stubs with the cross-section facing upward, and sputter-coated with ~ 9 nm tungsten (Leica EM SCD500, Leica Microsystems, the Netherlands) to prevent charging. Imaging was done at a working distance of ~ 4 mm, with SE detection at 5 kV and 25 pA, at a magnification of 25000 x.

#### 4.3.3.2 Laser speckle imaging

A similar set-up as described in [205] was used to investigate nanoscale dynamics. Prior to measuring, the sample was kept at 200 °C (MHCS400, Microptik, the Netherlands) for ~ 3 min to ensure complete melting. During the measurement, the sample was cooled with a ramp rate of ~ 0.5 °C/min. Simultaneously, an expanded coherent 532-nm laser beam was shone onto the sample. Within the sample, laser photons undergo multiple scattering events due to the presence of TiO<sub>2</sub> nanoparticles, resulting in different light paths as each photon undergoes statistically independent scattering events. The backscattered light was recorded with a camera (Dalsa Genie M640-1/2, Stemmer Imaging); an area of 200 by 200 pixels, i.e., 0.9 by 0.9 mm, was analyzed with an initial average grey value of 50 – 55 (every pixel has a grey value between 0 – 255). A linear polarizer was placed perpendicular to the polarization of the incident laser beam in order to filter specular and low-order scattering paths. The

resulting snapshots are easily recognized by their typical random pattern of black and white spots, called ‘speckles’. These snapshots were analyzed with Matlab to extract the characteristic relaxation time  $\tau_0$ ; for which a similar fitting procedure as described in [205] was used. In short, differences in speckle intensity/contrast were quantified by means of the intensity autocorrelation function:

$$g_2(\tau, t) = \frac{\langle [I(t) \cdot I(\tau + t)] \rangle}{\langle I(t) \rangle \langle I(\tau + t) \rangle} \quad (4-1)$$

where we averaged over speckles in space; the denominator derives the standard deviation and the numerator normalizes the intensity fluctuations ( $I$ ) within a certain timeframe ( $\tau$ ). We quantified nanoscale dynamics by the characteristic relaxation time ( $\tau_0$ ) that we derived by fitting the  $g_2(\tau)$  correlation curves over time with a generalized exponential decay:

$$\sqrt{g_2(\tau, t) - 1} = \sqrt{\beta_{fit}(t)} \cdot \exp \left[ -\gamma \left( \frac{\tau}{\tau_0(t)} \right)^\alpha \right] + P \quad (4-2)$$

where  $\beta_{fit}$  represents the actual decay of the correlation function  $g_2$  (equation (4-1)),  $P$  represents a small plateau value as  $g_2$  does not equal zero at high  $\tau$  values,  $\alpha$  represents the slope of the decorrelation, and  $\tau_0$  the typical relaxation time of the sample. To remove outliers, the fitted  $\tau_0$  values were subjected to the Thompson test with an alpha of 0.01 in blocks of 50 measurements [206].

#### 4.3.3.3 Rheology – complex viscosity

Rheometer MCR501 (Anton Paar, Australia) was used to measure the zero shear complex viscosity from 180 – 140 °C. The sample was placed within a plate-plate configuration consisting of a 25 mm plate (PP25-SN52020, Anton Paar, Australia), with a gap size of 0.7 mm at 180 °C, and stabilized for 3 min prior to the measurement. Thereafter, an oscillatory measurement was performed with a strain amplitude of 2.0% and a frequency 0.1 s<sup>-1</sup>; this was sufficiently low to measure zero shear viscosity, while preventing polymer degradation over the total measurement time.

## 4.4 Results

We used a multiscale approach to investigate the reinforcement effect of nanoparticles in polylactic acid matrixes with a degree of polymerization of  $\sim 300$  (PLA300), and  $\sim 500$  (PLA500) (**Appendix 4-1**). We altered nanoparticle – polymer interactions by using TiO<sub>2</sub> nanoparticles with a coating of either PAA (NP<sub>PAA</sub>), PVP (NP<sub>PVP</sub>) or PDMS (NP<sub>PDMS</sub>).

### 4.4.1 Interaction forces nanoparticles – polymers

To quantitatively describe nanoparticle – polymer and nanoparticle – nanoparticle interaction forces, we calculated the work of adhesion ( $W_a$ ), the work of cohesion ( $W_c$ ), and their related dispersibility factor ( $W_a/W_c$ ) (**Table 4.1**) based on surface energy values reported in literature; in **Appendix 4-2** we provide more details.

Theoretical frameworks suggest that nanoparticle dispersion is favoured when  $W_a/W_c > 1$ , whereas nanoparticle aggregation is favoured when  $W_a/W_c < 1$  [65,184]. Based on this distinction, we anticipated NP<sub>PDMS</sub> to be readily dispersible in the PLA matrix, in contrast to NP<sub>PVP</sub> and NP<sub>PAA</sub> which feature a  $W_a/W_c < 1$ . The work of adhesion generally indicates the interaction strength between two components, from which we expect that the interaction with the PLA matrix is strongest for NP<sub>PAA</sub>, followed by NP<sub>PVP</sub>, and finally NP<sub>PDMS</sub>.

**Table 4.1:** Calculated work of adhesion ( $W_a$ ), work of cohesion ( $W_c$ ), and dispersibility factor ( $W_a/W_c$ ) based on surface energy values reported in literature (**Appendix 4-2**).

NP <sub>coating</sub>	$W_a$ (mJ/m <sup>2</sup> )	$W_c$ (mJ/m <sup>2</sup> )	$W_a/W_c$ (-)	reference
PDMS	54.3	39.6	1.37	[207]
PVP	87.4	92.1	0.95	[208]
PAA	91.6	118.2	0.78	[209]

### 4.4.2 Nano-/microscale nanoparticle dispersion

We used scanning electron micrographs to obtain an impression of the dispersion state of the nanoparticles embedded in the polymer matrix (**Figure 4.1**). Irrespective of their loading, NP<sub>PAA</sub> and NP<sub>PVP</sub> heavily aggregated within the PLA matrix, with typical aggregate sizes varying between 100 – 2000 nm that contain air-filled gaps. These are generally considered

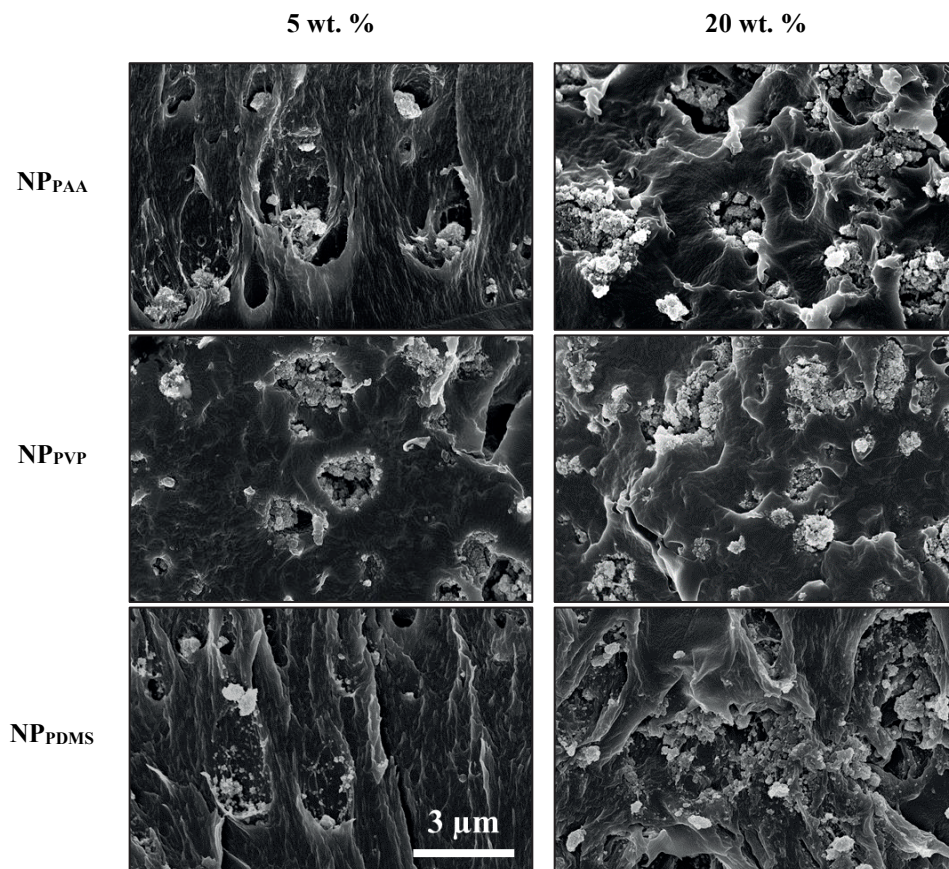


**Figure 4.1:** Nanoparticles with different coatings dispersed in PLA500 at loadings of 5 and 20 wt. %. The scale bar accounts for all images.

indications of poor compatibility between the nanoparticles and polymer. NP<sub>PDMS</sub> dispersed substantially better compared to NP<sub>PAA</sub> and NP<sub>PVP</sub>. Average aggregate sizes were in the order of  $\sim 100$  nm and  $\sim 500$  nm for a loading of 5 and 20 wt. % respectively. At 5 wt. % loading, we observed many individual nanoparticles together with small aggregates (5-10 particles).

#### 4.4.3 Macroscale dynamics – Viscoelastic properties of nanocomposites

To investigate material dynamics at the bulk scale, we measured the complex viscosity (**Figure 4.2**). Generally, the presence of nanoparticles substantially increased the complex viscosity compared to their neat counterparts, but the extent to which this occurred greatly depended on the molecular weight of the polymer, the surface chemistry, and loading of the

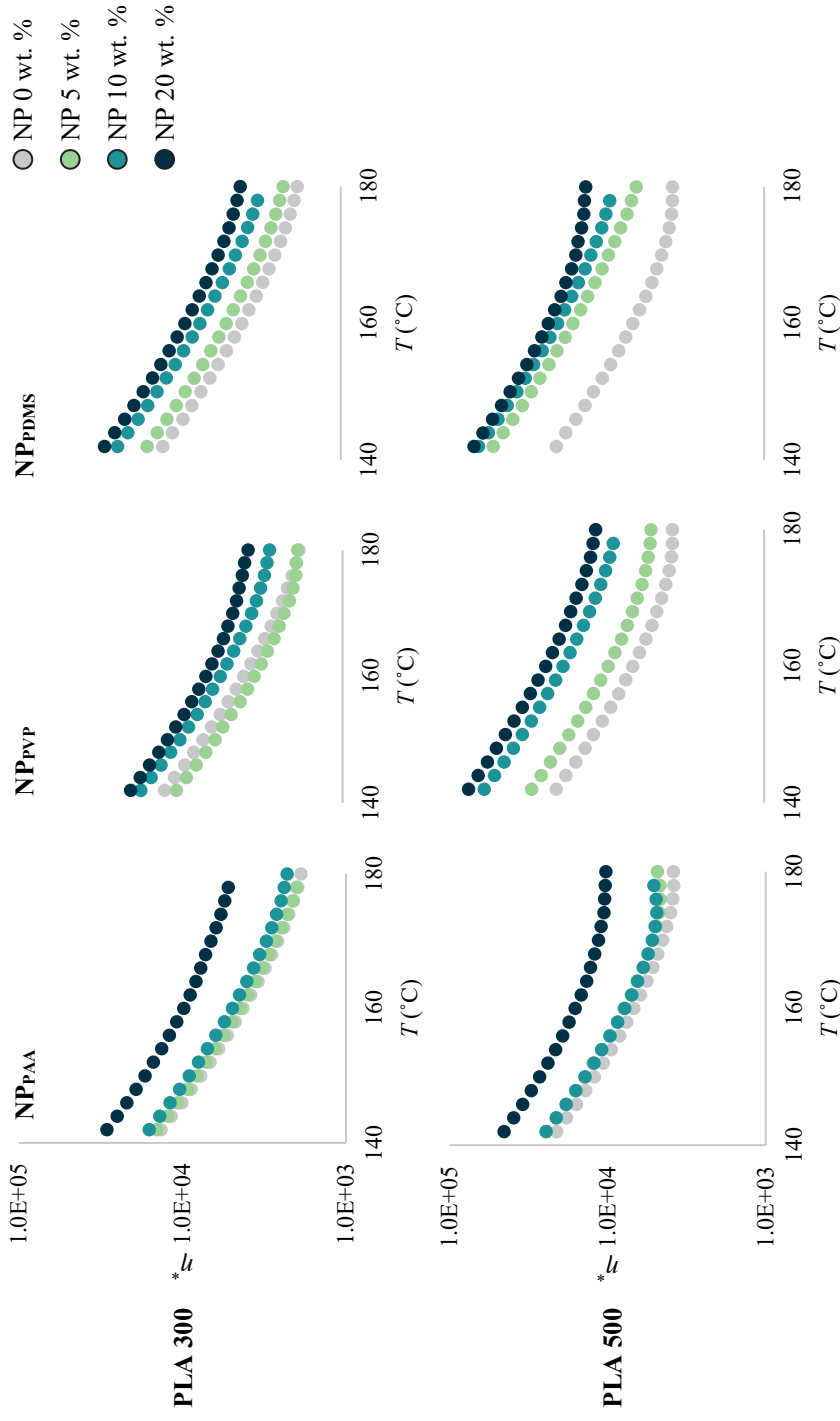


**Figure 4.2:** Complex viscosity ( $\eta^*$ ) of nanocomposites measured with macroscale oscillatory rheometry at different temperatures ( $T$ ).

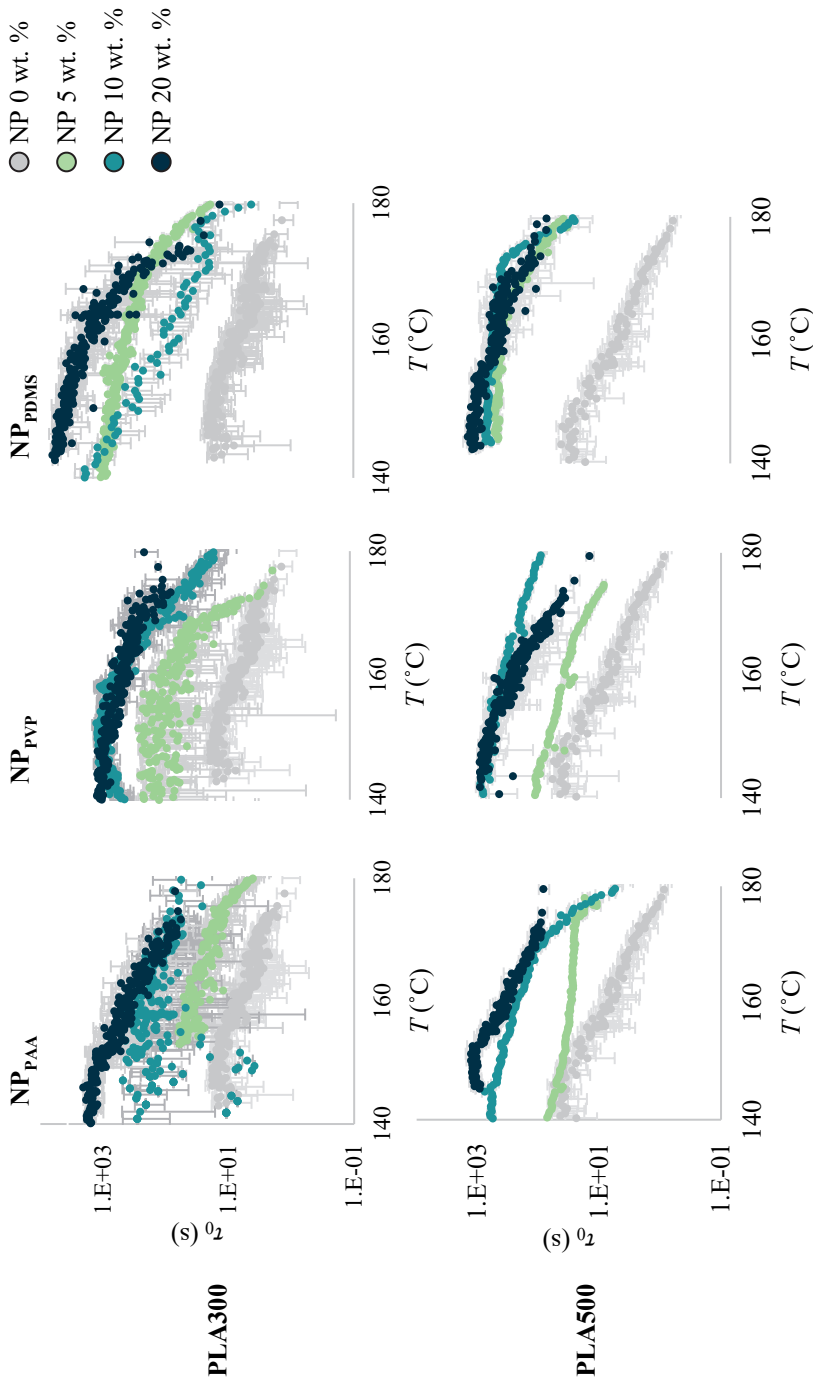


**Figure 4.3:** Nanoscopic relaxation times ( $\tau_0$ ) of nanocomposites during a cooling ramp ( $T$ ) measured by laser speckle imaging.

nanoparticles. Specifically, the complex viscosities of nanocomposites made from PLA500 were a factor  $\sim 2$  higher than those containing PLA300. In both matrixes, the reinforcing effect was more prominent for NP<sub>PDMS</sub> than for NP<sub>PVP</sub> and NP<sub>PAA</sub>. To illustrate, the complex viscosity at 180 °C was  $\sim 6.5$  kPa·s for 5 wt. % NP<sub>PDMS</sub> in PLA500 compared to  $\sim 4.8$  kPa·s for 5 wt. % NP<sub>PAA</sub>. For NP<sub>PDMS</sub> and NP<sub>PVP</sub>, an increasing nanoparticle loading manifested itself in a monotonically increasing complex viscosity. In the case of NP<sub>PAA</sub>, a nanoparticle loading of 20 wt. % was needed to substantially increase the complex viscosity.

#### 4.4.4 Nanoscale dynamics measured with LSI

To bridge the gap between the nano/microstructure and macro rheology, we used LSI, which offers highly resolved insights into the nano dynamics of the nanocomposites; **Figure 4.3** presents the relaxation times ( $\tau_0$ ).

PLA300 and PLA500 featured  $\tau_0$  values in the order of  $10^0 - 10^1$  s above the melting temperature ( $T_m$  of pristine PLA is  $\sim 150$  °C), and  $10^1 - 10^2$  s below the melting temperature. The presence of nanoparticles drastically increased these time scales to  $10^2 - 10^4$  s. The extent of this increase depended strongly on the nanoparticle coating and loading. At 150 °C, a nanoparticle loading of 5 wt. % raised the  $\tau_0$  of PLA to  $\sim 40$  s,  $\sim 65$  s, and  $\sim 700$  s for NP<sub>PAA</sub>, NP<sub>PVP</sub>, and NP<sub>PDMS</sub>, respectively. For NP<sub>PDMS</sub> nanocomposites a saturation effect was reached at 5 wt. %, after which a further increase in nanoparticle loading did not increase  $\tau_0$  much further. For NP<sub>PAA</sub> and NP<sub>PVP</sub>, saturation was achieved at 10 wt. %.

### 4.5 Discussion

Nanoparticle dispersion is key for nanocomposite reinforcement with effects ranging from the nano- to bulk scale (**Figure 4.2** & **Figure 4.3**). NP<sub>PDMS</sub> showed by far the best dispersion (**Figure 4.1**), and resulted in a higher complex viscosity than NP<sub>PVP</sub> and NP<sub>PAA</sub> (**Figure 4.2**). Generally, higher nanoparticle loadings increased the complex viscosity, and this effect was more pronounced for PLA500 compared to PLA300. These findings align with the abundant literature data that report an increased melt viscosity upon improved nanoparticle dispersion, nanoparticle loading, and increased chain length [196,197].

Traditionally, the nanoparticle's reinforcing effect is explained by the emergence of percolation regions where nanoparticles are (in)directly linked together, to ultimately form a

micro/macro network [196]. Recent studies suggest that the structure and dynamics of the interphasial layer are crucial determinants for the bulk mechanical and viscoelastic properties [56,190,210]. How these phenomena act across different length scales, relate, and interact is not really known, and we were curious to find out.

The interphasial region was investigated by LSI (**Figure 4.3**). Technically, LSI provides access to the relaxation times ( $\tau_0$ ) of scattering particles. Due to the highly entangled nature of PLA, (aggregated) nanoparticles were trapped within the effective cages imposed by the matrix, consequently mirroring the dynamics of the polymers surrounding them. The independence of  $\tau_0$  on aggregate size confirms the latter (**Figure 4.1 & Figure 4.3**). Thanks to the excellent sensitivity inherent to multiple light scattering, these times reflect local displacements of only 1 – 10 nm, being similar to the interphasial region that is estimated at 1.5 – 9 nm [191–193]. Generally, nanocomposites featured substantially longer  $\tau_0$  compared to their neat counterparts, even at temperatures far beyond the glass transition temperature (**Figure 4.3**). The addition of 5 wt. % NP<sub>PVP</sub> and NP<sub>PAA</sub> increased  $\tau_0$  by a factor 10, while a factor 100 was found for NP<sub>PDMS</sub>. The relaxation times increased even further at a nanoparticle loading of 20 wt. %, reaching an order of  $10^3$  s (**section 4.4.4**).

Our LSI results suggest that nanoparticles cause local constraints, thereby effectively playing the role of physical crosslinking points within the material. Data about interphasial dynamics is limited, due to the experimental challenges encountered when endeavouring to probe interphasial dynamics. Interestingly, albeit of a different dynamic nature and system, the authors of [193] also mentioned that segmental dynamics of P2VP located far from the silica nanoparticle interface exhibited relaxation times  $\sim 100$  times longer than the bulk [193].

We observed no clear dependence of interphasial dynamics (i.e.,  $\tau_0$ ) on  $M_w$ . In literature, the effect of  $M_w$  on the interphasial thickness is still up for debate; some studies suggest that the thickness of the interphasial region scales with the polymer's  $R_g$ , whereas others dispute this due to an entropic penalty [56,211,212]. Our results for limited variation in molecular weight do not suggest that  $M_w$  plays a crucial role in the dynamics experienced in the interphasial region (**Figure 4.3**), which makes this different from the bulk behaviour (**Figure 4.2**).

Noteworthy is the independence of nano- and bulk scale dynamics on the enthalpic component (**Table 4.1**). Aggregated nanocomposites, i.e., NP<sub>PAA</sub> ( $W_a = 91.6$  mJ/m<sup>2</sup>) and

NP<sub>PVP</sub> ( $W_a = 87.4 \text{ mJ/m}^2$ ) featured shorter  $\tau_0$  and lower  $\eta^*$  compared to their well-dispersed NP<sub>PDMS</sub> nanocomposite counterpart ( $W_a = 54.3 \text{ mJ/m}^2$ ). Additionally, the relaxation time of aggregated nanocomposites was saturated at 10 wt. % loading (**Figure 4.2**), whereas the complex viscosity increased upon loading **Figure 4.3**. This is remarkable, at 5 wt. % PLA500-NP<sub>PVP</sub> and PLA500-NP<sub>PAA5%</sub> contained locations low in nanoparticles due to their heavily aggregated state (**Figure 4.1**). The complex viscosity of NP<sub>PDMS</sub> nanocomposites in which particles were well dispersed, increased with nanoparticle loading, but this was not reflected by in  $\tau_0$  values. In fact, a loading of 5 wt. % seemed to saturate the interphasial layer completely, showing relaxation times in the order of  $\sim 10^3 \text{ s}$ . This suggests that different phenomena may occur in the interphasial region; we hypothesize that the individual interphasial layers of NP<sub>PDMS</sub> can affect each other, facilitated by their favourable dispersion state (**Figure 4.1**). Zhang et al. [138] found that overlapping interphases can increase stiffness by 5%; compared to the substantial increase in  $\tau_0$  observed in our study, these effects were rather small. In the case of entangled polymers, Cui et al. [210] showed that adsorbed polymers can reduce the mobility of polymers that are not in direct contact with the nanoparticle's surface. Our results highlight that nanoparticle dispersion is the key parameter affecting dynamics at nano- and bulk scale, instead of nanoparticle – polymer interactions that are commonly considered paramount for reinforcement.

Optimal nanoparticle dispersion can be achieved by effectively matching the nanoparticle's surface chemistry with that of the polymer (**Table 4.1**) [184]. Interestingly, based on our calculations (**Table 4.1**), the work of adhesion between polylactic acid and PDMS was not particularly high, and our calculations therefore suggest that the favourable dispersibility was mainly due to the low interparticle forces between the particles themselves. Contrarily, NP<sub>PVP</sub> and especially NP<sub>PAA</sub> had a higher  $W_c$ , giving rise to a  $W_a/W_c < 1$  and these samples heavily aggregated within PLA500.

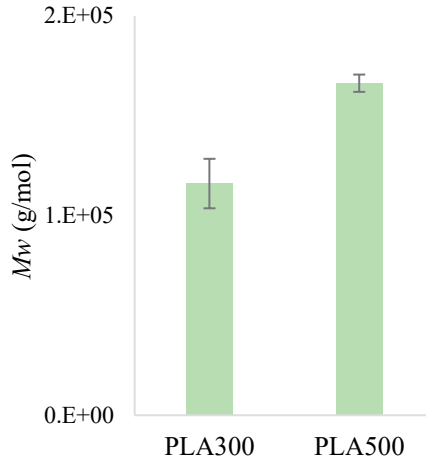
Finally, it is noteworthy to point out that nanoparticle loadings  $> 5 \text{ wt. \%}$  are very substantial, resulting in considerable effects in terms of material properties. Simultaneously, nanoparticle aggregation is – especially at high loadings – inevitable in practice. This renders virtually all traditional nano-analysis methods unsuitable, and illustrates the urgency of a technique such as LSI that allows the measurement of nanoscale dynamics inside nanocomposite systems

as LSI that allows the measurement of nanoscale dynamics inside nanocomposite systems that are not perfectly dispersed.

## 4.6 Conclusion

Nanoparticle dispersion is a factor determining both nano- and bulk scale dynamics in polymer nanocomposites. On a macro scale, nanoparticles coated with PDMS ( $NP_{PDMS}$ ) showed by far the best dispersion in a PLA matrix compared to PAA ( $NP_{PAA}$ ) and PVP ( $NP_{PVP}$ ) coated nanoparticles, consequently resulting in the highest melt complex viscosity. On the nanoscale, interphasial relaxation times were  $\sim 10^2 - 10^3$  longer than that of the neat PLA matrix, illustrating that nanoparticles essentially play the role of long-lived physical crosslinks. The relaxation times of well-dispersed  $NP_{PDMS}$  nanocomposites plateaued at 5 wt. % whereas this was 10 wt. % for aggregated  $NP_{PAA}$  and  $NP_{PVP}$  nanocomposites. We hypothesize that individual interphasial regions can affect each other, which is facilitated by improved dispersion and higher nanoparticle loading. In fact, our results offer thought-provoking indications that dispersion is more important than nanoparticle – polymer interactions, whereas the latter is commonly considered the most important.

## 4.7 Appendix



**Appendix 4-1:** Weight-averaged molecular weight of PLA with a degree of polymerization of  $\sim 300$  (PLA300) or  $\sim 500$  (PLA500) as determined by gel permeation chromatography.

**Appendix 4-2:** Calculation of work of adhesion, work of cohesion, dispersibility factor, and work of spreading.

The  $W_a$  (J/m<sup>2</sup>) was calculated as follows:

$$W_a = 2(\sqrt{\gamma_P^d \gamma_{NP}^d} + \sqrt{\gamma_P^p \gamma_{NP}^p}) \quad (4-3)$$

where  $\gamma_P^d$  and  $\gamma_{NP}^d$  are the dispersive components of the nanoparticle and the polymer's surface energy, respectively, and  $\gamma_P^p$  and  $\gamma_{NP}^p$  the polar components. The work of cohesion ( $W_c$ ) was calculated as follows:

$$W_c = 2 \gamma_{NP} \quad (4-4)$$

As several studies suggest that the balance between the two, i.e.,  $W_a/W_c$  can be used to predict the tendency of nanoparticle dispersion in a certain matrix [65,184], we also provide this in **Table 4.1**.  $W_a/W_c > 1$  suggests favourable dispersion, and  $W_a/W_c < 1$  unfavourable nanoparticle dispersion in a certain matrix.



**P**art II  
Biobased systems



---

# 5

## Quantification of energy input required for chitin nanocrystal aggregate size reduction through ultrasound

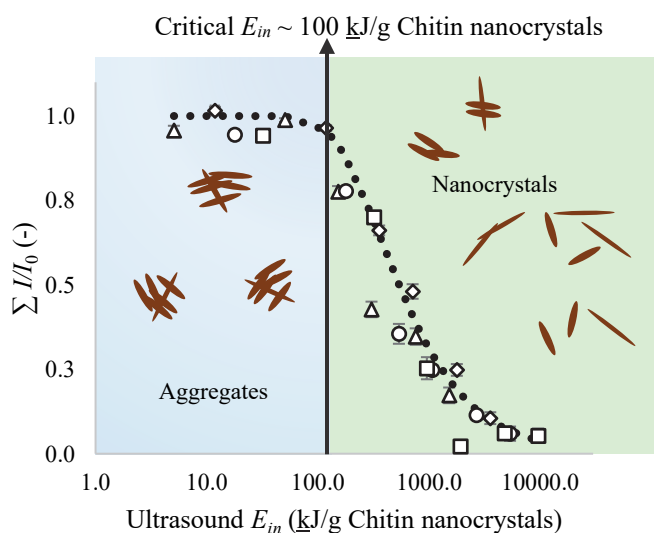
---

*Published as “Ivanna Colijn, Remco Fokkink and Karin Schroën. 2021. Quantification of Energy Input Required for Chitin Nanocrystal Aggregate Size Reduction through Ultrasound. Scientific Reports 11 (1): 1–9.”*

## 5.1 Abstract

Nanoparticles have been claimed to contribute efficiently to, e.g., the mechanical strength of composite materials when present as individual particles. However, these particles tend to aggregate. In this chapter, we prepare nanocrystals from chitin, a product with high potential added value for application in biobased materials, and investigate the effect of ultrasound on de-aggregation.

Chitin nanocrystals with a length  $\sim 200$  nm and a diameter  $\sim 15$  nm, were obtained via acid hydrolysis of crude chitin powder. Freeze drying resulted in severe aggregation and after redispersion sizes up to  $\sim 200$   $\mu\text{m}$  were found. Ultrasound treatment was applied and break-up behaviour was investigated using static light scattering, dynamic light scattering, and laser diffraction. Our results suggest that the cumulative energy input was the dominant factor for chitin nanocrystal aggregate break-up. When a critical energy barrier of  $\sim 100$   $\text{kJ/g}$  chitin nanocrystals was exceeded, the chitin nanocrystal aggregates broke down to the nanometer range. The break-up was mostly a result of fragmentation: the aggregation energy of chitin nanocrystal aggregates was quantified to be  $\sim 370$   $\text{kJ/g}$  chitin nanocrystals and we hypothesize that mainly van der Waals interactions and hydrogen bonds are responsible for aggregation.



Graphical abstract

## 5.2 Introduction

The versatile physical and chemical properties of nanoparticles give them outstanding properties for different applications [213], including enhanced catalysis [214], or drug release compared to their more macroscopic counterparts [215]. Also when embedded within a material, nanoparticles can alter the material's properties such as the mechanical strength or give it antioxidant activity if the nanoparticles possess that property. A great example are carbon nanotubes for the production of flexible electronic devices or the use of biobased polysaccharide nanocrystals which improve mechanical and barrier properties of polymeric materials [53,216,217]. These options to introduce unique properties make nanoparticles increasingly important as building blocks for different applications, e.g., in the material, medical, and electronic science fields and industry.

Nanoparticles can be produced from various natural sources. Chitin, the second most abundant polysaccharide next to cellulose, is getting more and more attention [51–53]. It is present in the cell walls of fungi, in insects, and in marine sponges [218], but mainly in the exoskeletons of arthropods such as shrimps. The latter sources are currently considered waste materials produced by the fishery industry, but they could become the source for a high added-value product, because chitin can easily be extracted. Chitin is a polysaccharide composed of N-acetyl-2-amido-2-deoxy-D-glucoside units linked by  $\beta(1\rightarrow4)$  bonds. The use of chitin can be expanded if the powder is hydrolysed into smaller chitin nanocrystals that have an increased exposed surface area in either solution or within a bulk material.

Chitin based nanofillers in particular possess special properties including a high aspect ratio, low density, and it was even reported that they retain their antioxidant and antimicrobial activity in polymeric matrixes [36,53,217,219–221]. In addition, their hydroxyl and amine groups allow surface modification, which can be used to tune nanoparticle properties practically at will, which is an important lead for further functionalisation. From this it is clear that chitin nanocrystals are versatile building blocks; in the current study, we especially consider them as bio fillers in polymeric matrixes for the medical and food packaging industry.

For the envisioned application it is important to prevent degradation and reduce transportation costs, which can be achieved by drying. However, drying nanoparticles often

leads to the formation of strong agglomerates because of its high surface area [85,222–226], and in the case of chitin nanocrystals due to the formation of strong hydrogen bonds [52]. Consequently, it remains difficult to redisperse the chitin nanocrystal aggregates in polymer melts, or aqueous solutions depending on the application [51,55,227–229]. A common approach to facilitate nanoparticle dispersion is the use of surfactants and compatibilizers [222,224,225,230–232]. Alternatively, nanoparticles can be re-dispersed by the use of mechanical force, e.g., ultrasound or extrusion. In contrast to extrusion, ultrasound has been shown to effectively lead to a stable aqueous dispersion of nanoparticles [53]. Interestingly, this difference in dispersibility with treatment method has been observed for multiple nanoparticles such as cellulose nanocrystals [87,233], or carbon nanotubes [234,235].

Theoretically, aggregate break-up occurs once the applied forces exceed the cohesive forces keeping the nanoparticles together. Aggregate break-up can occur in two ways, i.e., fragmentation or erosion. Erosion is characterized by the removal of single or small parts from the parent aggregate, whereas fragmentation is characterized by the break-up into pieces of similar sizes. Also the time scales of the two break-up mechanisms are different as erosion occurs over much longer time scales compared to fragmentation [236]. To the best of our knowledge, the aggregation energy of chitin nanocrystal aggregates and their break-up behaviour are unknown, yet for the preparation of biobased material reinforced with chitin nanocrystals these are essential design parameters.

The current study aims to quantify the aggregate energy of chitin nanocrystals and investigate its break-up behaviour in terms of fragmentation and erosion. This will be investigated on a small scale by dispersing freeze dried chitin nanocrystal powder in Milli-Q water, and measuring particle size after ultrasound treatment by static light scattering, laser diffraction, and dynamic light scattering. We find a distinct transition in particle size as function of applied energy input. The data is compared to literature of polymer systems with chitin nanocrystals, and linked energy input in production systems.

## 5.3 Materials and Methods

### 5.3.1 Materials

Shrimp chitin powder with > 98% purity and a high molecular weight was purchased from Glentham Life Sciences (UK). For dilutions, only ultra-pure water was used (Milli-Q) (Millipore MilliQ system, Q-POD with Millipak Express 40 0.22  $\mu\text{m}$  filter, Merck Millipore, USA).

### 5.3.2 Sample preparation

Chitin nanocrystals were prepared via a slightly adjusted protocol of Broers et al. [237]. In short, chitin nanocrystals were prepared via acid hydrolysis of crude chitin powder in 3 M hydrochloric acid (HCl) at 85 °C for 90 minutes; 1 gram of chitin powder per 15 ml HCl was added. The mixture was cooled on ice to stop the reaction, after which it was centrifuged at 2000 g for 5 minutes (Sorvall LYNX 4000 superspeed centrifuge, Thermo Scientific™ 46910, MA, USA) to remove the HCl. The supernatant was discarded and an equal amount of Milli-Q water was added to redisperse the pellet. The latter step was repeated three times. Two final centrifugation steps were performed at 1000 g for 5 minutes, after which the supernatant containing chitin nanocrystals was collected. After production, the 2.85 wt. % chitin nanocrystal solution (pH ~ 2.0) was freeze dried at -20 °C for at least 48 hours (Christ Epsilon 2-6D Freeze Dryer, Martin Christ Gefriertrocknungsanlagen GmbH, Germany).

Dispersions of 0.01 wt. % chitin nanocrystals in Milli-Q water (pH ~ 4.5) were prepared for static light scattering and dynamic light scattering experiments. Dispersions of 0.1 wt. % chitin nanocrystals in Milli-Q water were prepared for laser diffraction and observations with fluorescent microscopy.

### 5.3.3 Aggregate break-up by sonication

A Branson sonifier 250 connected to a 1/4' microtip (Branson Ultrasonics, USA) was used to sonify 10 ml sample at power 3, 5, 7, and 10 at a constant amplitude of 40%. This device had a horn frequency of 19.8 – 20.0 MHz. Samples were continuously cooled on ice to prevent excessive heating. The energy input ( $E_{in}$ ) was determined calorimetrically [238–240] (Appendix 5-1) :

$$E_{in} = C_{p,water} m_{water} \frac{\Delta T}{\Delta t} \quad (5.1)$$

where  $C_p$  is the thermal capacity of water (4.18 J/K),  $m$  is the mass of water (0.2 kg) and  $\Delta T/\Delta t$  is the rise in temperature per time. Different power settings were used to differ the instantaneous power supplied; the measured instantaneous  $E_{ins}$  were 5, 12, 18, and 32 Js<sup>-1</sup> for the power settings 3, 5, 7, 10 respectively (**Appendix 5-1**). We enabled an  $E_{in}$  between 0 - 9.6 MJ/g chitin nanocrystals. The heat loss to the environment was neglected because of the small volumes used.

### 5.3.4 Characterization

#### 5.3.4.1 Morphology

After acid hydrolysis, JOEL-JEM1400Plus – 120 kV (spot size 1) was used to observe the chitin nanocrystals, which were negatively stained in 2% uranylactate solution.

After ultrasound treatment, chitin nanocrystal dispersions were labelled with 0.01 wt. % fluorescein isothiocyanate (FITC) for 24 hours. The samples were centrifuged at 20.000 g, after which the supernatant was discarded and an equal amount of Milli-Q water was added. The latter step was repeated 5 times. FITC grafting was confirmed with Fourier Transform Infrared (Bruker, Alpha II, Germany); FTIR spectra were taken in absorbance mode over a wavenumber range of 400 – 4000 cm<sup>-1</sup> with a resolution of 4 cm<sup>-1</sup> and after 60 scan accumulations. The absence of FITC's isothiocyanate characteristic peak (N=C=S stretching) at 2000 cm<sup>-1</sup> [241,242] suggested that this group was involved in the reaction with the chitin nanocrystals (**Appendix 5-2**). Afterwards, the samples were observed with Axioscope in fluorescent mode (Zeiss, Germany).

#### 5.3.4.2 Degree of acetylation

<sup>13</sup>C cross-polarization magnetic angle spinning (CP-MAS) NMR spectroscopy (Bruker Avance III HD spectrometer 700 MHz, Bruker, USA) was used to determine the degree of acetylation of the crude chitin powder and the produced chitin nanocrystals. Samples were packed into 4 mm zirconia rotors. The rotors were spun at MAS frequency of 11 kHz at 25 °C. the <sup>13</sup>C CP MAS spectra were recorded with a recycle delay of 5 s, and a contact time of 3 ms. The <sup>13</sup>C NMR spectra were referenced with respect to adamantane

( $^{13}\text{C}$ , 29.456 ppm). The degree of acetylation (DA%) was determined with the following equation [243]:

$$DA\% = \frac{I_{CH_3}}{\frac{1}{6} I_{C1-C6}} \quad (5.2)$$

where  $I_{CH_3}$  and  $I_{C1-C6}$  correspond to the peak integrals associated with the  $\text{CH}_3$  and carbon backbone respectively. MestRenova software was used to determine the peak integrals. As determined from the  $^{13}\text{C}$  NMR spectra (**Appendix 5-3**), chitin nanoparticle production resulted in a slight decrease in degree of acetylation; a DA of 99% and 94% were found for crude chitin powder and the produced chitin nanocrystals respectively.

#### 5.3.4.3 Thermal stability

The thermal stability of chitin powder and the produced chitin nanocrystals were determined with thermogravimetric analysis (TGA) (PerkinElmer TGA 4000, Waltham, USA). The samples were heated from 30 °C to 450 °C, at a heating rate of 10 °C/min under a constant nitrogen flow of 20 mL/min. Pyris software was used to examine the data (Pyris, 11.1.1.0492). For chitin powder an initial degradation temperature and maximum temperature of 216 °C and 334 °C were found respectively. For chitin nanocrystals an initial degradation and maximum degradation temperature of 148 °C and 260 °C respectively.

#### 5.3.4.4 Particle size distribution

The particle size distributions of the chitin nanocrystal dispersions were measured with laser diffraction (Mastersizer 3000, Malvern Instruments Ltd., UK) and dynamic light scattering (Zetasizer Ultra, Malvern Instruments Ltd, UK). The absorption index was set to 0.01, and a refractive index of 1.560 and 1.330 was used for chitin nanocrystals and Milli-Q water, respectively. All samples were measured in triplicate.

Please note that the measurement angle used for laser diffraction (0.015° - 144°) and dynamic light scattering (173°) was different. Consequently, as mainly forward scattering was used for laser diffraction, it was more sensitive toward particles with a size above the wavelength of the device laser (i.e.,  $\lambda_{device} = 632.8$  nm for the red source and  $\lambda_{device} = 470$  nm for the blue source). As backscattering was used during dynamic light scattering measurements, also

particles with a size below  $\lambda_{device}$  could be observed (i.e.,  $\lambda_{device} = 632.7$  nm). Because of the very polydisperse nature of our chitin nanocrystal aggregate sample, we find a combination of these techniques crucial to obtain a good overall impression of the size distribution (**Figure 5.1**).

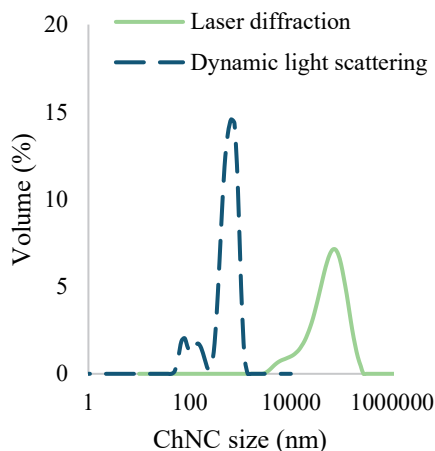


**Figure 5.1:** Volume % as function of chitin nanocrystal (ChNC) size at an  $E_{in}$  of 0  $\underline{\text{kJ/g}}$  chitin nanocrystals measured with laser diffraction and dynamic light scattering. The average of three measurements is given.

#### 5.3.4.5 Static light scattering

A HeNe 2 mW 633 nm polarized laser (product 19064, LASOS, USA) was shone through 8 ml 0.01 wt. % chitin nanocrystal dispersion which was added to the small angle light scattering cell (Anton Paar, Austria). The incoming beam was blocked by an in-house made beam stop, that was placed on a ground glass diffuser (gritt 600, Edmund Optics, USA). The distance between the SALS cell and the ground glass diffuser was 31 cm. A charged coupled device camera (CCD Thorland 125 IM SERIES, Edmund Optics, USA) with a lens of 16 mm/F1.4 59879 (Edmund Optics, USA) was used to capture 50 images per sample. The scattering patterns were further analyzed with Fiji [244] (**Appendix 5-4**). The Radial Profile Extended plugin developed by Baggethun [245] was used to derive the scattering intensity as function of scattering path (**Appendix 5-5**). The total scattering intensity is defined as the integral of the scattering intensity as function of the scattering path, which was corrected for

the background intensity (**Appendix 5-5**). The first 120 pixels of the path lengths were not considered as this corresponded to the position of the beam stop.

## 5.4 Results

The application of ultrasound has shown to be an effective way to break down nanoparticle aggregates [53,87,234], and was for that reason used to quantify the aggregation energy ( $E_{agg}$ ) within chitin nanocrystal aggregates. The energy input ( $E_{in}$ ) produced by ultrasound was determined calorimetrically for different sonication power settings, enabling an  $E_{in}$  up to 9.7 MJ/g chitin nanocrystals (**Appendix 5-1**).

### 5.4.1 Morphology of chitin nanocrystals and their aggregates after ultrasound

The morphology and size of the individual chitin nanocrystals and their aggregates were observed with transmission electron microscopy and fluorescence microscopy, respectively. **Figure 5.2** shows the morphology of individual chitin nanocrystals that have a clear needle like morphology. The chitin nanocrystals had a length between 50 – 400 nm and a diameter between 10 – 20 nm. The geometry of the nanocrystals corresponded well with sizes found in literature [51,53,217,237]; chitin nanocrystals commonly show a crystallinity index of 85 - 90% [53,229,246,247].

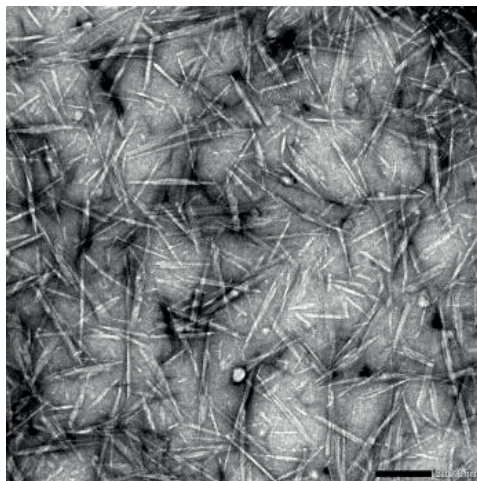


**Figure 5.2:** Needle shaped chitin nanocrystals derived after acid hydrolysis observed with transmission electron microscopy. The scale bar has a size of 200 nm.

After ultrasound treatment, the chitin nanocrystal aggregates were labelled with FITC to enable observation with fluorescent microscopy (**Figure 5.3**). After freeze drying, aggregates with sizes up to 200  $\mu\text{m}$  were observed in the chitin nanocrystal dispersion that was very polydisperse. Ultrasound clearly decreased the chitin nanocrystal aggregates; at an  $E_{in} \sim 1.9 \text{ MJ/g}$  chitin nanocrystal hardly any aggregates were visible, and if visible they had a size  $< 40 \mu\text{m}$ . As the resolution of the microscopy is  $\sim 2 \mu\text{m}$ , this probably suggests that most chitin nanocrystal particles were smaller than that, assuming no reduced signal intensity as function of size.

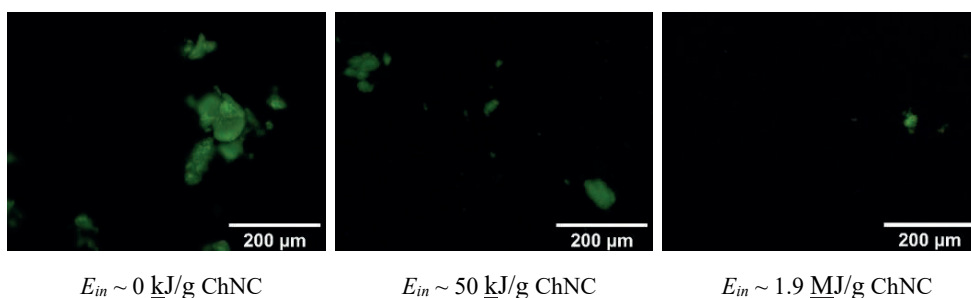


**Figure 5.3:** Microscopic pictures of FITC labelled chitin nanocrystals (ChNC) after sonication treatments at different  $E_{in}$ .

### 5.4.2 Aggregate strength

Static light scattering was used to capture the overall aggregate break-up behaviour. According to the classical Raleigh scattering theory a  $I \sim r^6$  relationship exists, meaning that the total scattering intensity decreases when an aggregate breaks up into two smaller particles of the same total volume. The scattering intensity clearly decreased as a consequence of ultrasound treatment (**Appendix 5-4 & Appendix 5-5**) and this is summarized in **Figure 5.4**, showing the normalized total scattering intensity as function of  $E_{in}$  produced by ultrasound.

The effect of ultrasound on scattering intensity could be divided into three regimes. In the first regime  $< 100 \text{ kJ/g}$  chitin nanocrystal, no effect of  $E_{in}$  on scattering intensity was observed. In the second regime,  $100 \text{ kJ/g}$  chitin nanocrystal  $< E_{in} < 5.0 \text{ MJ/g}$  chitin nanocrystal, the total intensity decreased as a consequence of either a decreased particle size, or decreased number of aggregates, but most likely a combination of both. At  $E_{in} > 5.0 \text{ MJ/g}$

chitin nanocrystal, the scattering intensity was very close to the background intensity and did not decrease any further.

The dimensionless number *Prob* has been suggested to determine the break-up probability of an aggregate at a certain shear rate [97,98,248]:

$$Prob = e^{-\sigma/\tau} \quad (5.3)$$

where  $\sigma$  is the mechanical bonding strength of an aggregate in  $\text{N}\cdot\text{m}^{-2}$  and  $\tau$  represents the shear stress in  $\text{N}\cdot\text{m}^{-2}$ . A slightly modified version was used in the current study. To describe the break-up probability of an aggregate at a certain  $E_{in}$ ,  $\sigma$ , and  $\tau$  were replaced with  $E_{agg}$  and  $E_{in}$  respectively. In addition, the mirrored value was taken to fit the equation to the static light scattering data points:

$$Prob = 1 - e^{-\left(\frac{E_{agg}}{E_{in}}\right)} \quad (5.4)$$

From the fit of equation (5.4) to the static light scattering data points, an  $E_{bond}$  of 373  $\text{kJ/g}$  chitin nanocrystal was derived, that is put into a wider perspective in the discussion section.

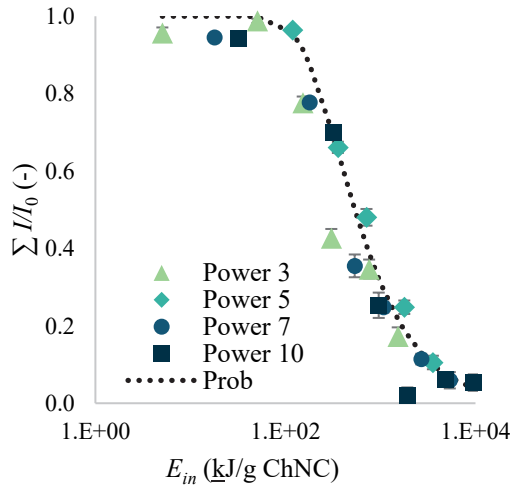


**Figure 5.4:** Normalized total intensity as function of ultrasound energy ( $E_{in}$ ) in  $\text{kJ/g}$  chitin nanocrystals (ChNC) determined via static light scattering.

### 5.4.3 Particle size distribution

To distinguish between aggregate break-up occurring in particles of different sizes, size distributions after ultrasound treatment were measured using different techniques. **Figure 5.5** shows size distributions obtained with laser diffraction and dynamic light scattering. The size averages are given as  $D_{[4,3]}$  for laser diffraction and  $D_{[6,5]}$  for dynamic light scattering as function of  $E_{in}$ , and are not the same (**Figure 5.6**).

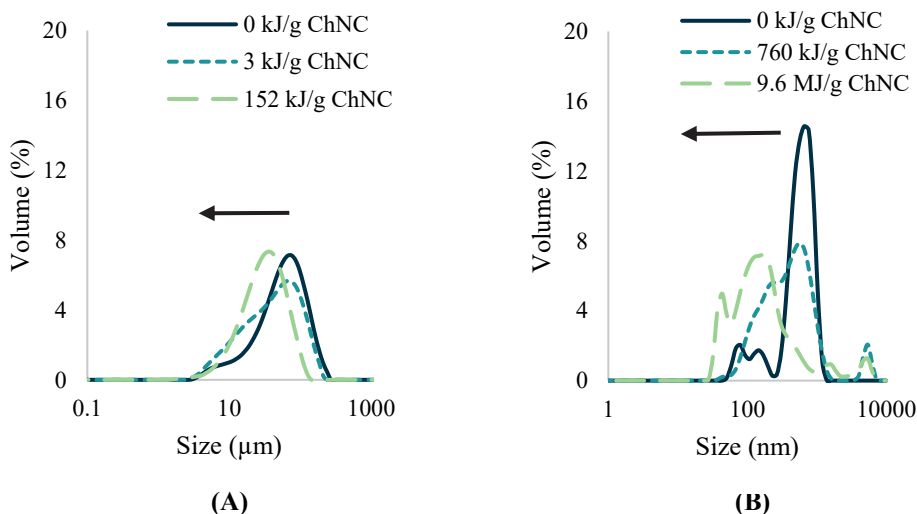


**Figure 5.5:** The volume % as function of chitin nanocrystal (ChNC) size at different  $E_{in}$  measured with (A) laser diffraction and (B) dynamic light scattering.

Chitin particle sizes between 5 - 500  $\mu\text{m}$  and 50 - 100 nm were observed with laser diffraction and dynamic light scattering, respectively. We interpret this as follows: only a very small number of large particles ( $> 5 \mu\text{m}$ ) was present, and these particles scatter mostly in the forward direction and are dominant at low angles. At a larger detection angle as used for dynamic light scattering, their contribution is negligible and does not contribute to the overall signal. If there would have been many large particles, they would have given a signal during this measurement, and that is not the case, not even at 10-fold higher concentration. Thus, the overall behaviour is dominated by break-up events happening in small(er) chitin aggregates, and this was well captured by static light scattering (**Figure 5.4**).

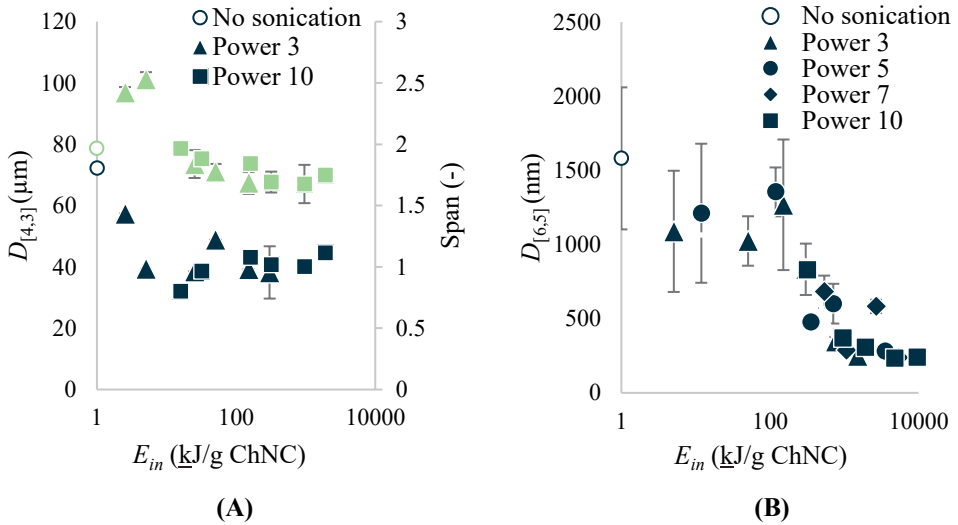


**Figure 5.6:** The chitin nanocrystal (ChNC) size (in blue) and span (in green) as function of ultrasound  $E_{in}$  at different power settings measured with (A) laser diffraction and (B) dynamic light scattering. The error bars represent the standard deviation within three different measurements, some of them being within the data marks.

On a more general level, at an  $E_{in} < 16 \text{ kJ/g}$  the chitin nanocrystal size was reduced from  $72 \mu\text{m}$  to approximately  $40 \mu\text{m}$  (Figure 5.6), leading to higher polydispersity. This effect was supported by results obtained by dynamic light scattering; the chitin nanocrystal size shifted to lower values and broader distributions ( $E_{in} \sim 3 \text{ kJ/g}$  chitin nanocrystals) (Figure 5.5). At  $16 < E_{in} < 100 \text{ kJ/g}$  chitin nanocrystals, no further decrease in chitin nanocrystal size was observed, and the span remained equal, which corresponds well with the static light scattering results (Figure 5.4). At higher  $E_{in}$  values, most of the chitin nanocrystal aggregates broke up to a size of  $\sim 240 \text{ nm}$  which is similar to the length of the original chitin nanocrystals before freeze drying (Figure 5.2). Although ultrasound treatment clearly shifted the chitin nanocrystal size to lower values, also when no ultrasound treatment was applied, chitin nanocrystal particles in the nano range were found, and at the highest  $E_{in}$ , the chitin nanocrystal particles showed a considerable size distribution (Figure 5.5).

## 5.5 Discussion

Ultrasound treatment clearly reduced the chitin nanocrystal aggregate size (Figure 5.3 & Figure 5.6), as was found for different nanoparticles including carbon nanotubes [234] and

cellulose nanocrystals [87]. Our results suggest that weakly bound micro meter agglomerates can be broken down at low  $E_{in} < 16 \text{ kJ/g}$  chitin nanocrystals (**Figure 5.6**), which corresponds to the general observation that break-up occurs at the weakest spot inside the aggregate. However, a much higher critical  $E_{in}$  of  $\sim 100 \text{ kJ/g}$  chitin nanocrystals was required to decrease the aggregates to the size range of the original chitin nanocrystals (**Figure 5.4 & Figure 5.6**). This is common for particles, and far from trivial for nanoparticles because the  $E_{in}$  required increases as the particle diameter decreases [249,250].

An aggregation energy ( $E_{agg}$ ) of  $\sim 370 \text{ kJ/g}$  chitin nanocrystals was found (**Figure 5.4**). We would like to emphasize that this number corresponds to the break-up of interparticle interactions within an aggregate, rather than the interactions within a nanocrystal (**Figure 5.4, Figure 5.5, and Figure 5.6**). It is good to point out that extreme sonication conditions, e.g., 300 W for 30 minutes, are capable of separating chitin nanofibrils from the chitin matrix but are not able to break the nanofibrils themselves [251–253]. It is expected that mainly van der Waals interactions and hydrogen bonds formed after drying are responsible for the high aggregation strength [251,254]. Interestingly, these latter interactions are also believed to be responsible for keeping individual chitin polymers within a chitin nanocrystal together [255], although the actual strength can be different. Within a nanocrystal, chitin polymers have an extremely evolved hierarchical structure [255], which results in a strong material built by relatively weak interactions, i.e., van der Waals interactions ( $\sim 1 k_bT$ ) and hydrogen bonds ( $\sim 10 k_bT$ ) [110]. In a freeze dried sample irregular aggregates are present (**Figure 5.3**), that likely do not have as many interactions as the chitin nanocrystals would have, which explains the differences between both materials.

We expect these high  $E_{in}$  values needed to break up aggregates to be one of the reasons why it remains difficult to achieve homogeneous chitin nanocrystal distributions in polymeric matrixes without any surface modification or the use of a compatibilizer. Extrusion is often used to process thermoplastic polymers, where typical specific mechanical energy inputs lay in the range of 0.17 – 0.27 kWh/kg. Considering a maximum residence time of 10 minutes and a chitin nanocrystal content of 5 wt. %, an  $E_{in}$  of around  $\sim 1 \text{ kJ/g}$  material would be achieved. Assuming  $E_{in}$  is equally distributed through the whole material,  $\sim 50 \text{ mJ/g}$  chitin nanocrystals is available for aggregate breakdown, being lower than the critical energy

barrier of  $\sim 100$  kJ/g chitin nanocrystals that we identified before. Thus, in this example the  $E_{in}$  provided by extrusion should be increased by at least a factor 2000. Even if we consider that not all acoustical energy is transferred into cavitation breaking energy ( $\sim 35\%$  [240]), a serious increase in  $E_{in}$  is required for break up to occur. This difference becomes more pronounced using the argument of maximum local shear stress that can be achieved. Huang & Terentjev [234] calculated a local shear stress of 20 kPa for mechanical shear mixing in high viscosity polymer melts, whereas 100 MPa could be achieved for ultrasound treatment in low viscosity solvents; this is a factor 5000 different [234]. Please note that in the latter study it was assumed that all stress from an imploding bubble contributed to the localized shear stress.

The dominant break-up mechanism is expected to be fragmentation as deduced from the various size distributions (**Figure 5.5 & Figure 5.6**), which also corresponds well with observations of others [87,256,257]. Like Graves et al. [257] we find that the  $E_{in}$  was the dominant factor for nanoparticle aggregate break-up. However, the reported dependency on  $E_{in}$  is not always observed [87]. This may be related to the calculation of the energy input through the implosion of a bubble in the case of Beuguel et al. [87] and determined calorimetrically by Graves et al. [257] and the current study. The reasons for this strong dependency on  $E_{in}$  are not yet elucidated.

As the next step toward application in, e.g., polymer melts other factors like interfacial compatibility should be considered as well. When relatively hydrophilic chitin nanocrystals are added to hydrophobic matrixes, there will be a continuous competition between the hydrodynamic forces breaking the chitin nanocrystal particles up and the cohesive forces bringing the chitin nanocrystal particles together. This is commonly observed for nanoparticles in polymer and aqueous systems [82,87,107,108]. So ways to reduce  $E_{agg}$ , away from the use of compatibilizers, are relevant. Interestingly,  $E_{agg}$  does not solely depend on the interaction forces, for example, Khoshkava & Kamal [85] found that cellulose nanocrystal aggregates with a more porous structure require less energy to break up. Van der Waals interactions act over a longer range (0.32 nm) compared to hydrogen bonds (up to 100 nm), thereby explaining why less  $E_{in}$  is needed to break down larger nanoparticles compared to smaller ones. Higher porosity can be achieved using other drying methods such as spray

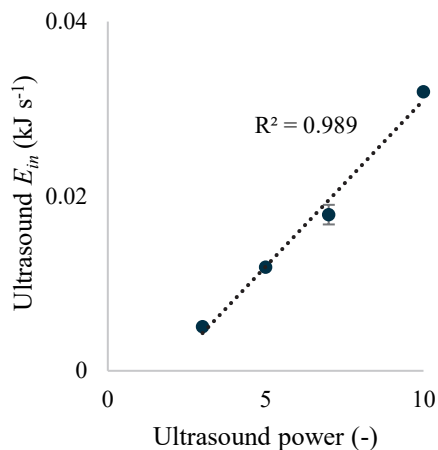
drying or by using lower chitin nanocrystal concentrations during freeze drying [85,86]. Another way to decrease the  $E_{in}$  required for chitin nanocrystal break-up would be to increase the interfacial compatibility with the solvent or polymer melt. This can be achieved amongst others by surface modification which is part of our follow-up research.

## 5.6 Conclusion

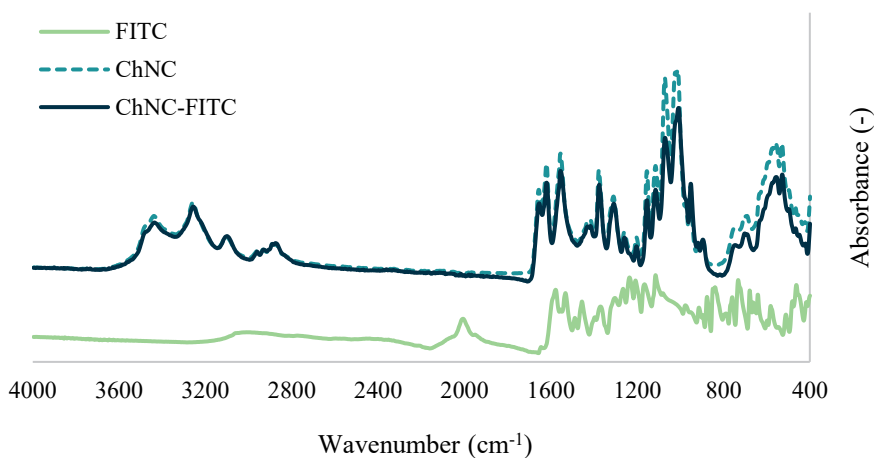
We have demonstrated that the critical energy barrier for aggregate break-up as well as aggregation energies can be quantified with a combination of ultrasound and static light scattering. Ultrasound treatment was shown to effectively decrease the size of chitin nanocrystal aggregates that were held together by van der Waals interactions and hydrogen bonds ( $\sim 370$  kJ/g chitin nanocrystals) formed during freeze drying. The reason for the strong relationship between the cumulative applied energy input and the break-up behaviour of the chitin nanocrystals is not yet elucidated.

Although ultrasound can easily overcome the critical energy input needed to break up chitin nanocrystal aggregates, the energy input achieved during extrusion of polymer melts is expected to be too low to achieve this, which is in line with the common observation that nanoparticles do not disperse well in polymer melts. Still, the current study very clearly sheds light on the importance of energy input as a design parameter for nanocomposite preparation, and also directs toward which strategies should be applied to achieve nanoparticle dispersion (e.g., surface modification).

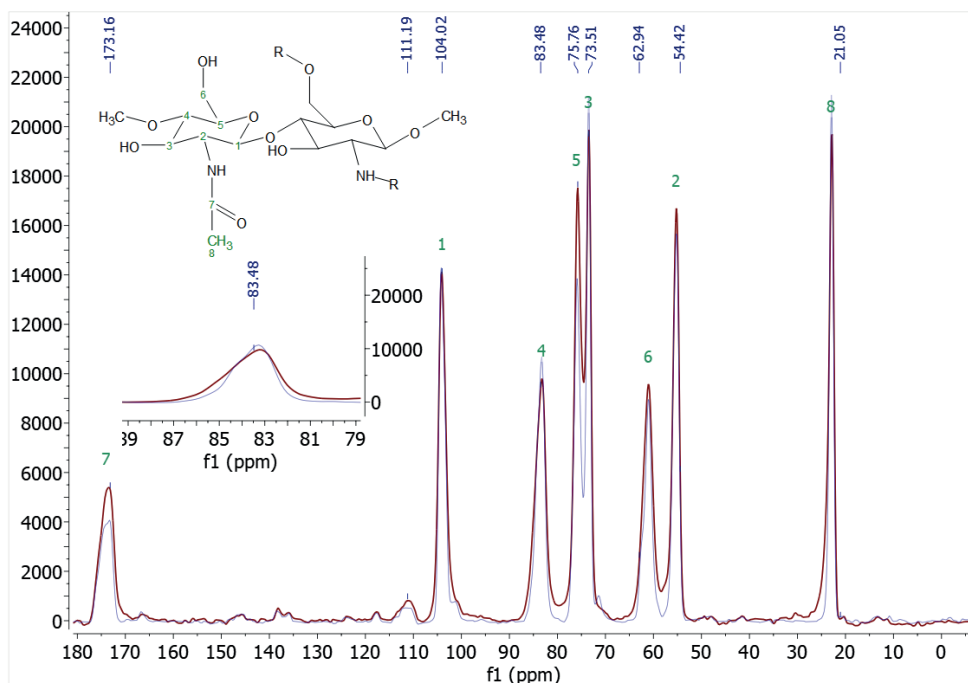
## 5.7 Appendix



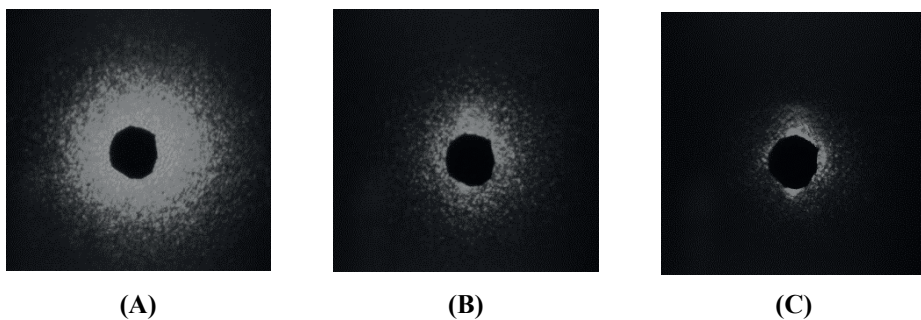
**Appendix 5-1:** The sonication energy in  $\text{kJ s}^{-1}$  for different ultrasound power settings determined calorimetrically.



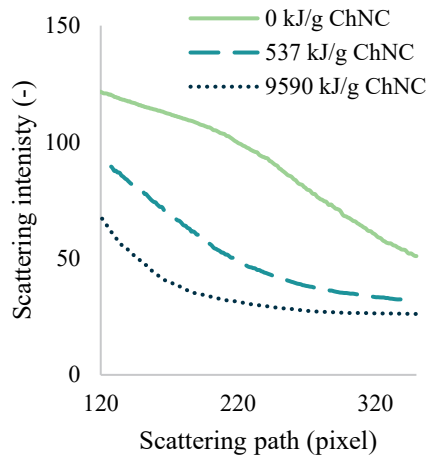
**Appendix 5-2:** FTIR spectra of FITC, chitin nanocrystals (ChNC), and FITC labelled chitin nanocrystals (ChNC-FITC). The absence of the characteristic peak of FITC's isocyanate group at  $2000 \text{ cm}^{-1}$  confirms the conjugation of FITC with the amine groups of the chitin nanocrystals.



**Appendix 5-3:**  $^{13}\text{C}$  NMR spectra of crude chitin powder (red) and produced chitin nanocrystals (blue). The green numbers indicate the peaks that were assigned to their corresponding carbon atoms as represented in the chemical drawing.



**Appendix 5-4:** Scattering patterns derived with static light scattering (A) at an  $E_{in} \sim 0 \text{ MJ/g ChNC}$ , (B)  $E_{in} \sim 0.5 \text{ MJ/g ChNC}$ , and (C)  $E_{in}$  of  $\sim 9.6 \text{ MJ/g ChNC}$ .



**Appendix 5-5:** Scattering intensity as function of scattering path at different  $E_{in}$  before background correction and normalization.



---

# 6

## Chitin nanocrystal hydrophobicity adjustment by fatty acid esterification for improved polylactic acid nanocomposites

---

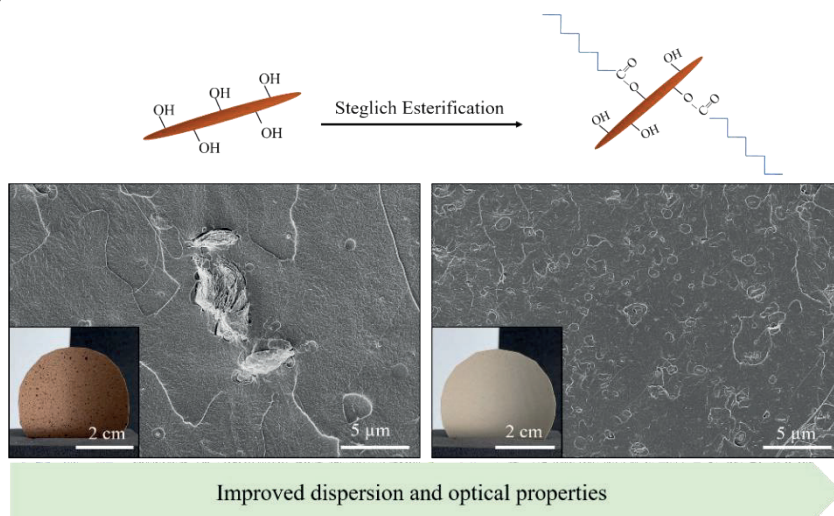
*Published as “Ivanna Colijn, Murat Yanat, Geertje Terhaerd, Karin Molenveld, Carmen G Boeriu, and Karin Schroën. 2022. Chitin Nanocrystal Hydrophobicity Adjustment by Fatty Acid Esterification for Improved Polylactic Acid Nanocomposites, Polymers 14 (13):2619.”*

## 6.1 Abstract

Bioplastics may solve environmental issues related to the current linear plastic economy, but they need improvement to be viable alternatives. To achieve this, we targeted to add chitin nanocrystals (ChNC) to polylactic acid (PLA), which is known to alter material properties while maintaining a fully biobased character. However, ChNC are not that compatible with PLA, and surface modification with fatty acids was used to improve this. We used fatty acids that are different in carbon chain length (C4 – C18), and degree of saturation (C18:2).

We successfully used Steglich esterification and confirmed covalent attachment of fatty acids to the ChNC with FTIR and solid-state  $^{13}\text{C}$  NMR. The morphology of the ChNC remained intact after surface modification, as observed by TEM. ChNC modified with C4 and C8 showed higher degrees of substitution compared to fatty acids with a longer aliphatic tail; while particles modified with the longest fatty acid showed the highest hydrophobicity.

The addition of ChNC to the PLA matrix resulted in brown colour formation that was reduced when using modified particles, leading to higher transparency, most probably as a result of better dispersibility of modified ChNC, as observed by SEM. In general, addition of ChNC provided high UV-protection and improved barrier protection; this is an additional feature that can be created through addition of ChNC, which was not at the expense of the mechanical strength.



*Graphical abstract*

## 6.2 Introduction

To tackle environmental issues related to the use and production of fossil-based plastics, biobased and biodegradable plastics have been proposed as alternatives. Amongst them, polylactic acid (PLA) is often considered the most promising material because of its availability, low environmental footprint, low costs, good optical properties, and high tensile modulus [14]. However, its current application is limited because its properties are not as good as their fossil-based counterparts, such as polyethylene terephthalate [26,258].

Nanoparticle – polymer interactions are known to alter material properties including mechanical and barrier functions [31–33,58,59]. To retain a plastic's biobased character, the particles also need to comply with this requirement, and different polysaccharide nanoparticles have been considered for this purpose such as starch or cellulose nanoparticles, that are abundant in nature, and have low toxicity [51]. Another promising nanoparticle source is chitin, which is a polysaccharide composed of N-acetyl-2-amido-2-deoxy-D-glucoside units linked by  $\beta$  (1  $\rightarrow$  4) bonds. After cellulose, it is the second most abundant polysaccharide and mainly present in exoskeletons of arthropods, such as shrimps and crabs.

Currently, these exoskeletons are considered waste, which is a missed opportunity as chitin can be easily extracted and made into a high-added-value product. Chitin nanocrystals (ChNC) can be produced by acid hydrolysis of chitin powder. Like the chitin powder, the degree of acetylation (presence of amino groups) at the nanocrystal surface is thought to relate to antifungal and antibacterial activity, even when ChNC are present in polymer films [39,259,260], which is of special interest for medical devices or food packages [261,262]. ChNC clearly have high potential as building blocks in nanocomposites, albeit are rather unexplored.

For a functional biopolymer, homogeneous distribution of ChNC throughout the PLA film is crucial [184]. When starting from ChNC, the relatively hydrophobic PLA drives the ChNC to agglomerate. During particle preparation, interparticle hydrogen bonds lead to strong ChNC agglomerates upon drying [54], which are difficult to break up under conditions commonly used during extrusion processes. In order to mitigate this, ChNC can be modified which is possible through their hydroxyl and amino groups [53,263].

Surface acetylation with fatty acids has been shown to effectively increase the hydrophobicity of starch crystals [264] and chitin nanocrystals [263]. Commonly this is done by converting the fatty acids into their noxious chloride forms, which is less desirable from a human health and environmental point of view. Alternatively, direct esterification (Steglich esterification) that circumvents the formation of toxic components and is efficient under mild conditions can be used, but to the best of our knowledge, this has not been demonstrated for chitin nanocrystals.

Here we used, fatty acids of different carbon chain length (C4 - C18) and saturation (C18:0 and C18:2), and characterized the modified particles by FTIR and solid-state NMR. We expect the polarity to depend on the length of the carbon tail, and this was investigated using two-phase-liquid-systems of various  $\log P$ . Next, (modified) ChNC were added to a polymer matrix, and dispersibility was investigated through SEM. Furthermore, the characteristics of the obtained nanocomposites were evaluated (e.g., UV-protection, color, mechanical strength, barrier function). This modification is expected to open up possibilities to successfully use chitin nanocrystals as fillers for bio-nanocomposites.

## 6.3 Materials and Methods

### 6.3.1 Materials

Shrimp chitin powder ( $\geq 98\%$  purity) was purchased from Glentham Life Sciences (UK). Butyric acid ( $\geq 99.5\%$ ) was from Thermo Fisher Scientific (USA). The following chemicals were bought from Sigma Aldrich: octanoic acid ( $\geq 99\%$  purity), lauric acid ( $\geq 98\%$  purity), stearic acid ( $\geq 99\%$  purity) linoleic acid ( $\geq 99\%$  purity), N-(3-dimethyl aminopropyl)-N'-ethyl carbodiimide hydrochloride (EDC), hexane tert-butyl acetate ( $\geq 99\%$  purity), and 4-dimethyl aminopyridine (DMAP). Palmitic acid ( $\geq 99\%$  purity) and dry tetrahydrofuran (THF) ( $\geq 99\%$  purity) were purchased from Merck (Germany). Polylactic acid Ingeo 4043D was from NatureWorks LLC (USA). All other chemicals and solvents were analytical grade and used as received. For dilutions, only ultrapure water was used (Millipore MilliQ system, Q-POD with Millipak Express 40 0.22  $\mu\text{m}$  filter, Merck Millipore, USA).

## 6.3.2 Sample preparation

### 6.3.2.1 Chitin nanocrystal preparation

A general acid hydrolysis procedure was used to prepare chitin nanocrystals, as described in [237,265]; the effects of production conditions on nanocrystal properties are extensively reviewed in [53]. Crude chitin powder was hydrolyzed in 3 M HCl for 90 minutes at 90 °C after which the reaction was stopped by cooling the mixture on ice. To remove the HCl, the mixture was centrifuged at 4000 g for 5 minutes, after which the supernatant was discarded, and the pellet redispersed in water. The latter steps were repeated three times. This suspension was sonicated with the Branson Sonifier SFX550 (Emerson, the Netherlands) equipped with a sonication tip 1/8' tapered microtip (Branson, Emerson, the Netherlands), in pulses of 100 J at an amplitude of 40% with 10 seconds rest and a total sonication energy of ~ 150 J/ml while cooled on ice. To collect the chitin nanocrystals (ChNC), two centrifugation steps were applied (1000 g, 15 minutes), after which the pellet was discarded.

### 6.3.2.2 Surface acetylation

Before modification, the ChNC and the chemicals were dried in a desiccator with silica for 5 days. The ChNC had a water activity ( $a_w$ ) ~ 0.25. A dispersion of 5.0 w/v % freeze dried ChNC was made in THF and stirred for > 24 h at room temperature. This suspension was sonicated in pulses of 100 J at an amplitude of 40% with 10 seconds of rest and total sonication energy of ~ 150 J/ml while cooled on ice. After sonication, the sample was kept on ice and the fatty acids (1 fatty acid : 5 chitin monomers) and DMAP (3 DMAP : 1 fatty acid) were added. EDC was slowly added, and the mixture was stirred for 5 more minutes after addition. The reaction was started by increasing the temperature to 45 °C. The mixture was kept at this temperature for 45 minutes, and the reaction was stopped by centrifugation at 4700 rpm. The pellet was rinsed one more time with THF, followed by two rinsing steps with methanol and acetone. The pellet was dried in a vacuum oven (VD53, Binder, Germany) under constant nitrogen flow at 40 °C for > 24 h. The supernatants containing the unbound fatty acids, EDC, and DMAP were pooled and saved for further analysis with GC-FID. All modifications were performed in independent duplicates. Washed ChNC refers to ChNC that were subjected to the same washing steps as the modified ChNC, whereas unwashed ChNC refer to ChNC that were used directly after production.

### 6.3.3 Nanocomposite production

Prior to production, PLA 4043 was dried in an air dryer (TTM 2/100 ES, Gerco Kunststofftechnik GmbH, Germany) at 80 °C for > 48 h. The (modified) ChNC were dried at 50 °C in a vacuum oven; this was done under continuous nitrogen flow for > 48 h while allowing minimal vapour to escape the oven. Thereafter, a micro compounder (MC 15 HT, Xplore, the Netherlands) was used to produce nanocomposites consisting of 95 wt. % PLA and 5 wt. % (modified) chitin nanocrystals at 180 °C. During sample addition, a maximum torque of 40 Nm and screw speed of 40 rpm/s<sup>2</sup> was used. During compounding, the screw speed was increased to 100 rpm/s<sup>2</sup>, and mixing was continued for approximately 2 minutes. After extrusion, samples were pressed into sheets using a hot press (LabEcon 600, Fontijne Presses, the Netherlands) at 190 °C; a pressure of 10 kN was applied for the first three minutes followed by a pressure of 50 kN for two minutes. An in-house made mould from aluminium was used to control the sample thickness at ~ 400 µm. The pressed samples were cooled for 2 minutes in an in-house made cooling unit consisting of two plates that were continuously cooled by rinsing tap water.

### 6.3.4 Nanoparticle characterization

#### 6.3.4.1 TEM

Transmission electron microscopy (TEM) images were taken using JO-EL-JEM1400Plus – 120 kV (spot size 1). Before observation, the ChNC were negatively stained with a 2% uranyl acetate solution. Three images per sample were further analysed with Fiji [244]. To determine particle diameter, length, and aspect ratio, 52 ChNC were analysed per image.

#### 6.3.4.2 FTIR

FTIR spectra of (un)modified ChNC were obtained using a Bruker Equinox 55 (Germany) in attenuated reflectance mode (400 – 4000 cm<sup>-1</sup>), with a resolution of 4 cm<sup>-1</sup> and after 64 accumulations. Calibration and baseline placement of [266] was applied to determine the degree of acetylation; using the ratio between amide II (1560 cm<sup>-1</sup>) and glycosidic bond (1030 cm<sup>-1</sup>) for quantification.

#### 6.3.4.3 *Solid-state $^{13}\text{C}$ NMR*

The  $^{13}\text{C}$  cross-polarization magic angle spinning CP-MAS NMR spectrum was obtained on a Bruker Avance III HD spectrometer operating at 700.13 MHz (16.4 T). All particles were packed into 4 mm zirconia rotors that were spun at MAS frequency of 11 kHz at 298 K. The  $^{13}\text{C}$  CP MAS spectra were recorded with a recycle delay of 5 s, and a contact time of 3 ms. The  $^{13}\text{C}$  NMR spectra were referenced with respect to adamantane ( $^{13}\text{C}$ , 29.456 ppm). The spectra were analyzed using MestRenova software.

#### 6.3.4.4 *GC-FID*

The supernatant containing unbound fatty acid (with the exception of butyric acid), and the remaining EDC and DMAP was evaporated under constant nitrogen flow (Reacti-Therm III, Thermo Fisher Scientific, US). Prior to analysis, fatty acid methyl esters (FAMES) were derived following a similar protocol as described in [267]. In short, the remaining components were redispersed in methanol (0.3 ml/mg fatty acid added for modification) and stirred overnight. Next, the samples were sonicated at an amplitude of 40% with a total energy input of 100 J/ml (SFX150, Branson Ultrasonics, US). As reference, a known amount of pentanoic acid (C15:0) was added to each sample. An amount of 200  $\mu\text{l}$  HCl in methanol (8 : 92 v/v %) was added per ml sample. FAMES were derived by heating this mixture at 90 °C for 1 hour. The samples were cooled to room temperature, subsequently 1 ml hexane and 1 ml Milli-Q were added and vortexed. This was left to sit for 10 minutes, after which the hexane layer was taken and diluted 10 times prior to GC-FID analysis. For the quantification of unreacted butyric acid, a calibration curve of butyric acid in a mixture of acetone : tetrahydrofuran : methanol (1 : 1 : 1) was made. A known and equal amount of acetic acid was added as internal standard; this was added to the supernatant containing unreacted butyric acid and to each calibration curve point.

The unbound butyric acid and FAMES were quantified by gas chromatography (Focus GC, Thermo Scientific, USA) in combination with a flame ionization detector (Interscience, the Netherlands); the CP-FAAPCB column (Agilent, USA) and rxi-5 ms capillary column (Restek Corp, USA) were used for butyric acid, and the FAMES, respectively. During butyric acid analysis, the oven was held at a temperature of 100 °C for 30 seconds, after which the temperature was increased to 180 °C with a ramp of 8 °C per minute. The temperature was

kept at 180 °C for 1 minute, after which it was increased to 200 °C with a ramp of 20 °C per minute. The sample was injected into the column (CP-FAAPCB, Agilent, USA) with a split flow of 40 ml per minute, while the oven was kept at 200 °C for 5 minutes. Nitrogen was used as carrier gas and applied at a constant pressure of 20 kPa. The detector was kept at a temperature of 240 °C. During FAMES quantification, the oven was held at a temperature of 40 °C for 2 minutes, after which the temperature was increased to 250 °C with a ramp of 10 °C per minute and held at this temperature for 5 minutes. The temperature of the injector and detector was 240 °C and 250 °C respectively.

The degree of substitution, DS, was calculated as follows:

$$DS = \frac{F_{added} - F_{unbound}}{4 ChNC} \cdot 100 \quad (6-1)$$

where  $ChNC$ ,  $F_{added}$ ,  $F_{unbound}$  represent the amount of chitin added in moles, the amount of moles fatty acid added, and the unbound fraction in moles, respectively. To calculate the total of available target groups,  $ChNC$  is multiplied by 4 to compensate for the hydroxyl groups of chitin.

#### 6.3.4.5 $\zeta$ -potential

The  $\zeta$ -potential of (un)modified  $ChNC$  in Milli-Q water was measured using Zetasizer Ultra (Malvern Instruments Ltd., U.K.). Prior to analysis, the pH of these dispersions was adjusted to 5.0, and thereafter these were loaded into capillary cells (DTS1080, Malvern Instruments Ltd., U.K.). All samples were measured in triplicate, where an absorption index was set to 0.01, and a refractive index of 1.56 and 1.33 was used for chitin nanocrystals and Milli-Q water respectively.

### 6.3.5 Nanocomposite characterization

#### 6.3.5.1 SEM

Neat PLA and nanocomposite films were cryo-fractured, glued on an aluminium sample holder with conductive carbon tape (Leit-C, Neubauer Chemikalien, Germany) and sputter-coated with ~ 10 nm Tungsten (Leica EM SCD500, Leica Microsystems, the Netherlands). The surfaces were observed with FESEM (FEI Magellan 400, FEI Electron

Optics B.V., the Netherlands) at room temperature at a working distance of 4 mm, with SE detection at 2 kV and 13 pA.

#### 6.3.5.2 *Colour analysis*

The colour values ( $L^*$ ,  $a^*$ ,  $b^*$ ) of nanocomposite films were measured using a Minolta CR-400 colorimeter (Minolta Camera Co., Osaka, Japan). The colorimeter was calibrated with a standard white plate (D65,  $Y = 94.4$ ,  $x = 0.3158$ ,  $y = 0.3334$ ) before use.  $L^*$ ,  $a^*$ , and  $b^*$  values were measured under D65 illumination. The measurement was performed in triplicate for all samples.

#### 6.3.5.3 *Spectroscopy*

The light transmittance of nanocomposite films was measured with a UV–VIS spectrophotometer (DU720, Beckman Coulter, USA) in the range of 200 – 700 nm at room temperature. Instead of a cuvette the pressed film was placed inside the sample holder of the UV-VIS, and air was used as background. Values were corrected based on film thickness.

#### 6.3.5.4 *Barrier Properties*

The water vapour transmission rate (WVTR) of PLA and nanocomposite films were determined according to ASTM E96. Samples were cut into circular films with a diameter of 3.8 cm, and fixed between an aluminium cup containing dry silica beads. During the measurement, the cups were placed in a conditioning chamber (PR-4J, Espec, Japan) at 23 °C and 85% RH; the samples were approximately daily weighted with a four-digit analytical balance (ME204E, Mettler Toledo, USA) for a period of 14 days. The WVTR was calculated as follows:

$$WVTR = \frac{m}{tA} \quad (6-2)$$

where  $m$  is the water uptake by the silica beads (g),  $t$  is the testing time (days), and  $A$  is the surface area ( $m^2$ ) of the sample of choice.

#### 6.3.5.5 *Mechanical properties*

Prior to analysis, a mould (DIEFAC stansvormen, the Netherlands) was used to produce tensile test samples from the pressed sheets. After that, the samples were conditioned at a

relative humidity of 50%, at 20 °C for 1 week. Tensile strength measurements were performed according to ISO 527-2 using a Zwick Z010 (Zwick Roell, the Netherlands); a clamp distance of 80 mm, an extensometer distance of 30 mm, an *E*-modulus speed of 1 mm/min, and a testing speed of 10 mm/min were used. The dimensions of the tensile strength measurement samples can be found in **Appendix 6-1**.

## **6.4 Results and discussion**

All tested fatty acids: butyric acid (C4:0), octanoic acid (C8:0), lauric acid (C12:0), stearic acid (C18:0), and linoleic acid (C18:2) were successfully coupled to chitin nanocrystals (ChNC) using Steglich esterification in the presence of *N*-ethyl-*N*'-carbodiimide (EDC) and 4-dimethylaminopyrine (DMAP). We first characterized the modified chitin nanocrystals, and thereafter the properties of PLA containing 5 wt. % (modified) chitin nanocrystals.

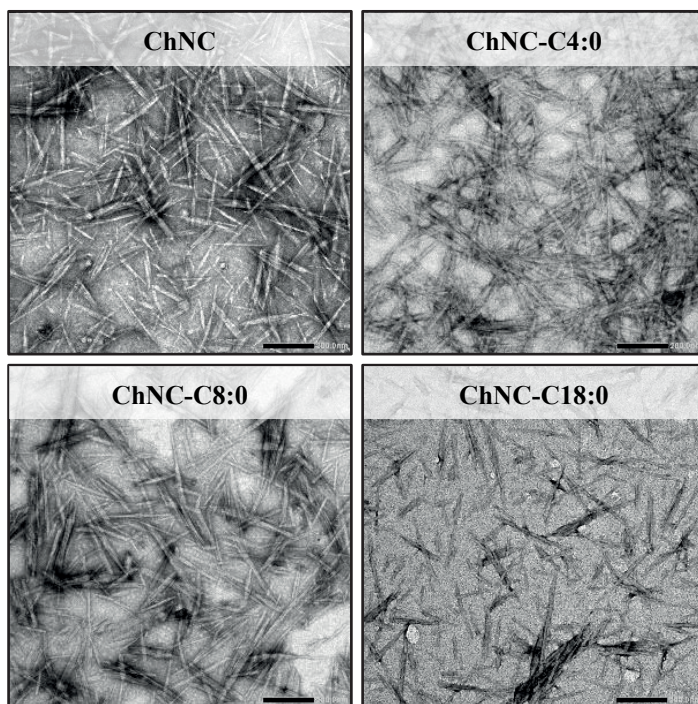
### **6.4.1 Nanoparticle characterization**

#### **6.4.1.1 Morphology and size of (modified) ChNC**

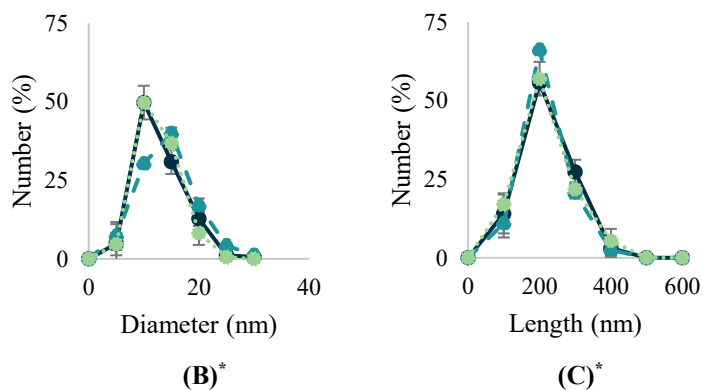
Transmission electron microscopy was used to image all ChNC (**Figure 6.1A**). The length and diameter distribution as determined from three different regions in the sample are given in **Figure 6.1B** and **C**. Irrespective of the modification method used, ChNC particles were rod like with an average length of ~ 200 nm and diameter of ~ 10 nm, and thus have an aspect ratio of ~ 20. These dimensions are well within the ranges commonly found in literature, confirming successful chitin nanocrystal production [51,53,237]. In contrast to other esterification reactions where chloride intermediates were used [36,264], Steglich esterification did not affect the morphology nor the size of the ChNC, thus confirming Steglich esterification is rather mild.

#### **6.4.1.2 Degree of substitution, degree of acetylation, and $\zeta$ -potential**

The FTIR spectra of (un)modified chitin nanocrystals can be found in **Figure 6.2**; the full spectra of all samples can be found in **Appendix 6-2**. The stretching behaviour of unmodified ChNC corresponds well with values reported in literature [268]. The first broad peaks at 3430 cm<sup>-1</sup> and 3258 cm<sup>-1</sup> were assigned to the -OH and -NH stretch vibrations respectively. The peaks at 1658 cm<sup>-1</sup>, 1628 cm<sup>-1</sup>, and 1563 cm<sup>-1</sup> correspond to amide I, amide II, and amide III bands, which is typical stretching behaviour of  $\alpha$ -chitin [268]. The absorption bands



(A)



(B)\*

(C)\*

**Figure 6.1:** (A) Transmission electron microscopy images of ● ChNC as such and ChNC modified with ● C4:0, ● C8:0, and ● C18:0. (B) The particle diameter and (C) particle length distribution determined from TEM images. The error bars represent the standard deviation of three different regions; 50 particles were measured per region. \*It was not possible to determine the particle diameter and length of ChNC-C18:0 due to lower resolution of the pictures of this sample. By eye, this sample looked similar to the other three.

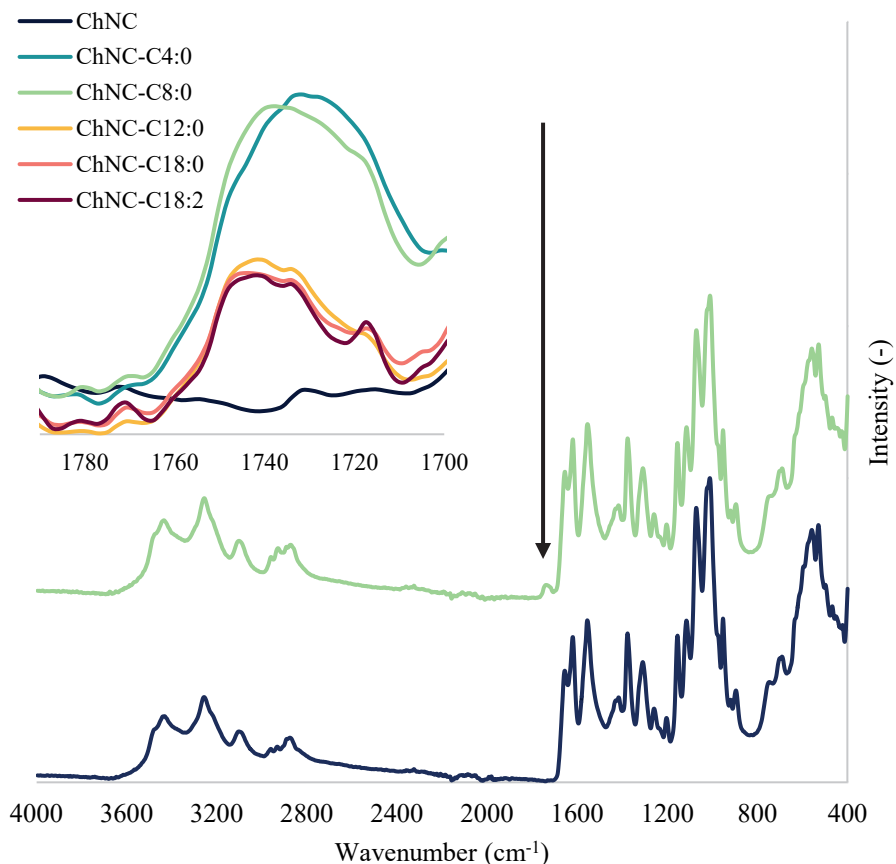


**Figure 6.2:** FTIR spectra of unmodified chitin nanocrystals and nanocrystals modified with fatty acids. The presence of the ester group at 1735 - 1750  $\text{cm}^{-1}$  is highlighted in the inset; its intensity is dependent on the fatty acid of choice.

between 1000 – 1200  $\text{cm}^{-1}$  correspond to -C-O-stretching present in the polysaccharide backbone. An increased intensity was found upon modification in the region 2860 – 2900  $\text{cm}^{-1}$  corresponding to the aliphatic chains of the fatty acids ( $\text{CH}_2$ ). In the region 1735 – 1750  $\text{cm}^{-1}$ , the formed ester linkages (C=O) appeared, with lower peak intensity for carbon chain lengths > 12.

**Figure 6.3** shows the  $^{13}\text{C}$  NMR spectra of (un)modified ChNC; the full spectra of all samples can be found in **Appendix 6-3**. The spectra for unmodified ChNC show peaks corresponding to carbons  $\text{C}^1 - \text{C}^6$  (104.1 ppm, 55.3 ppm, 73.5 ppm, 83.5 ppm, 75.9 ppm, 61.1 ppm), the  $\text{CH}_3$  ( $\text{C}^8$ , 22.9 ppm), and the acetyl group carbon ( $\text{C}^7=\text{O}$ , 174.9 ppm). Modifications

introduced new peaks in the region of 13.4 – 38.0 ppm; these could be assigned to the CH<sub>3</sub> (25.3 ppm) and CH<sub>2</sub> groups of the aliphatic tail of the fatty acids. Modification shifted the peak at 174.9 ppm to ~ 173 ppm, indicative of an ester link between the fatty acid and the ChNC (**Table 6.1**). Furthermore, the amide group present in the unmodified ChNC typically show a chemical shift at ~ 175 ppm, but the consistent chemical shift of 1.7 ppm at this wavelength indicates successful esterification.

**Table 6.2** presents the degree of substitution determined with GC-FID, the degree of acetylation, and the  $\zeta$ -potential of the (un)modified ChNC. Generally, the degree of substitution was ~ 2 – 4% upon modification, which did not affect the  $\zeta$ -potential and had a minor effect on the degree of acetylation. In line with FTIR (**Figure 6.2**), GC-FID showed that the degree of substitution was higher for aliphatic tail lengths shorter than 12 carbons. This all indicates that the hydroxyl groups are modified and not the amine groups.

**Table 6.1:** The <sup>13</sup>C NMR chemical shift of C<sup>7</sup> for unmodified ChNC and C<sup>1</sup>' for modified ChNC, including the peak area compared to C<sup>1</sup>.

Particle	Chemical shift C <sup>7*</sup> or C <sup>1</sup> '	Area compared to C <sup>1</sup>
ChNC*	174.9	0.35
ChNC – C4:0	173.0	0.65
ChNC – C8:0	172.9	0.65
ChNC – C12:0	173.1	0.62
ChNC – C18:0	172.9	0.65
ChNC – C18:2	173.0	0.63

**Table 6.2:** The degree of substitution (DS%), degree of acetylation (DA%), and  $\zeta$ -potential at pH = 5.0 of (modified) chitin nanocrystals.

Sample	DS%	DA%	$\zeta$ -potential (mV)
ChNC	(-)	74.5	35.3 ± 0.5
ChNC – C4:0	2.6 ± 0.2	78.4	33.9 ± 0.6
ChNC – C8:0	3.9 ± 0.0	78.5	34.7 ± 0.3
ChNC – C12:0	2.2 ± 0.1	71.3	35.0 ± 1.0
ChNC – C18:0	1.7 ± 0.0	60.7	35.7 ± 0.5
ChNC – C18:2	2.0 ± 0.5	62.9	34.3 ± 0.2

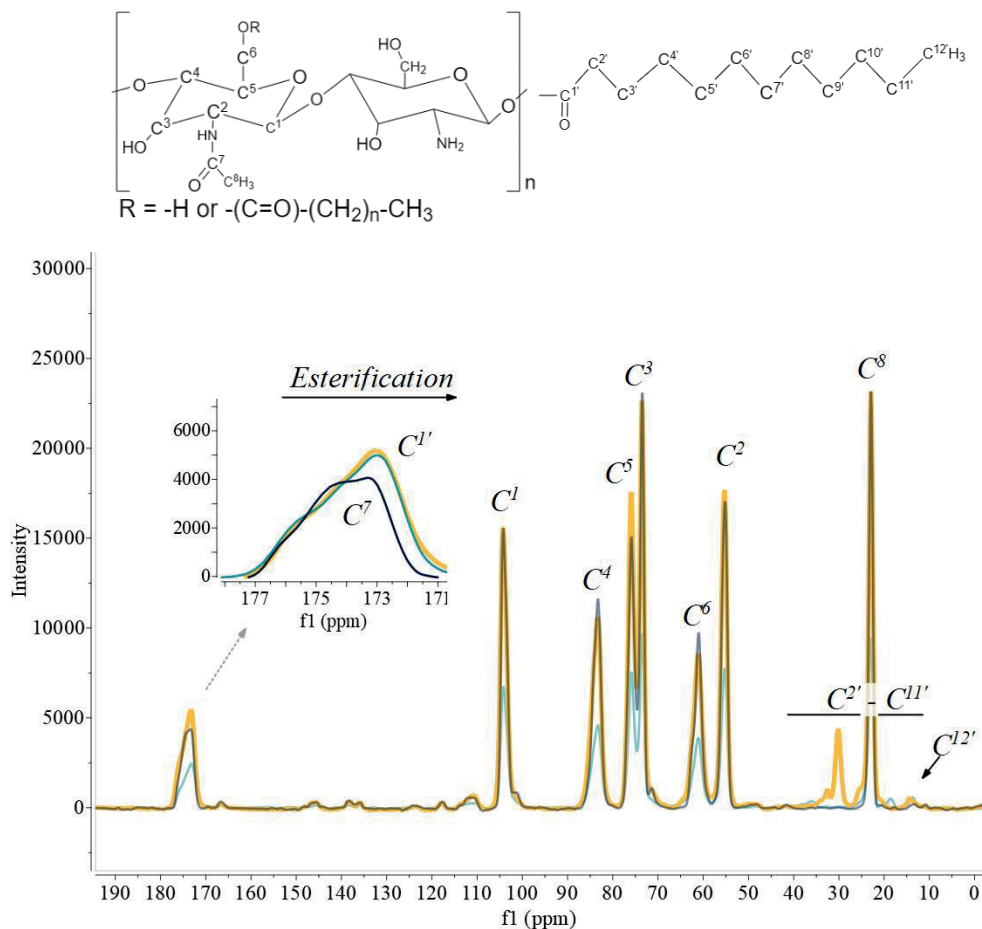


**Figure 6.3:**  $^{13}\text{C}$  NMR spectra of ChNC (blue), ChNC-C4:0 (yellow), and ChNC-C12:0 (turquoise). The chemical structure of chitin and the fatty esters is provided, where  $n$  can be 2, 6, 10, or 16 depending on the fatty ester considered.

#### 6.4.1.3 Wettability test

ChNC particles were added to two-phase systems consisting of Milli-Q water and either butanol ( $\log P$  0.88), tertbutyl acetate ( $\log P$  1.76), or toluene ( $\log P$  2.73) (**Figure 6.4**). Modification clearly changed the phase behaviour of particles; the unmodified ChCN always migrated to the Milli-Q phase irrespective of the organic solvent used suggesting a rather polar character. The modified particles partitioned increasingly toward the organic phase as the length of the fatty acid increases, and ultimately rather fully accumulated in the solvent with the highest  $\log P$ . We expected all modified particles to have increased hydrophobicity

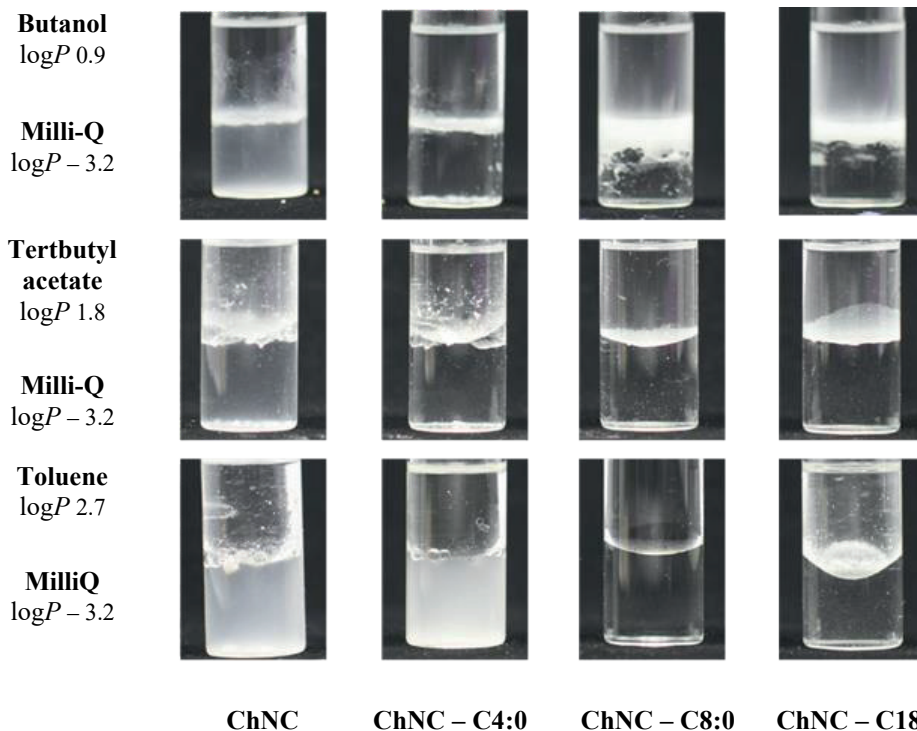


**Figure 6.4:** Phase behaviour of (un)modified ChNC in two-phase systems, indicative of their hydrophobicity.

compared to the starting material, which was also found. The fact that the degree of modification was lower for the longer chain fatty acids, was apparently compensated for by the longer fatty acids attached that thus overall lead to higher hydrophobicity. We did not find any difference between saturated (C18:0) and unsaturated fatty acids (C18:2). For that reason, we now only report for C18:0 modification. We expect that the current modification makes the particles suitable for application in polylactic acid that is hydrophobic, as tested in the next section. If successful, this most probably implies that modified ChNC are also suitable for application in other hydrophobic plastics such as polypropylene (PP), or polyethylene terephthalate (PET).

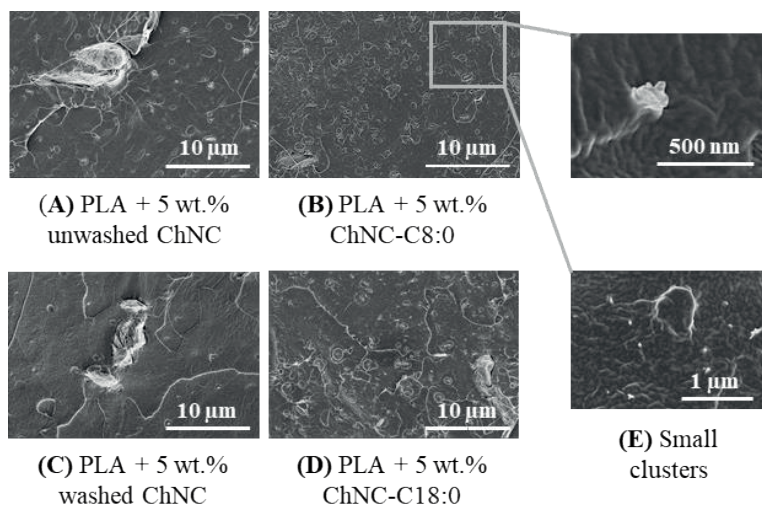
#### 6.4.2 Nanocomposite characterization

As a next step, nanocomposites were made, characterized and compared to neat polylactic acid.

#### 6.4.2.1 Nanocrystal dispersion in the PLA matrix

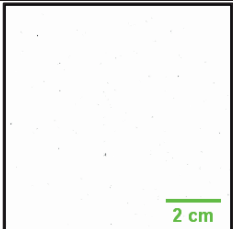
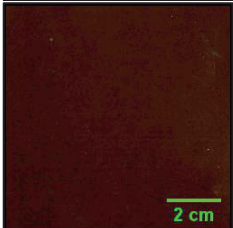
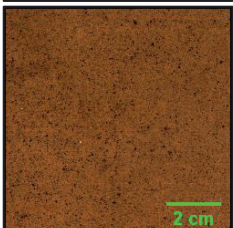
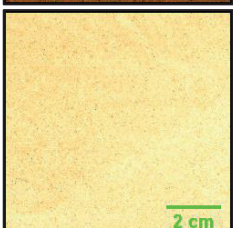
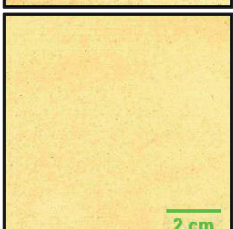
We used scanning electron microscopy (SEM) to observe the dispersibility of ChNC in PLA (**Figure 6.5**). To be complete, PLA without ChNC is shown in **Appendix 6-4**. Nanocomposites with unmodified ChNC contained highly aggregated nanocrystals even  $> 50 \mu\text{m}$  (**Figure 6.5A** and **C**). When the nanoparticles were washed before application, the number of small aggregates seemed less (**Figure 6.5C**). PLA samples containing modified ChNC mainly showed aggregates with a size around  $\sim 200 \text{ nm}$  (**Figure 6.5B, D**, and **E**). This indicates that surface modification facilitates ChNC dispersion. Bigger aggregates with a size  $> 20 \mu\text{m}$  were also observed, although they were much less abundant.

**Table 6.3** shows pictures of PLA containing 5 wt. % (modified) ChNC; *Lab*<sup>\*</sup> colour scores are provided to quantify colour differences. **Figure 6.6** shows film transmittance in the UV- and visible light range. As expected, PLA had a high transparency of 83.7% at wavelength 500 nm. The addition of 5 wt. % (modified) ChNC introduced a yellow to deep brown colour depending on the treatment used. This is in line with other studies that observed colour formation upon extrusion [237]. Glucosamine-derived products, such as chitin, are known to undergo Maillard reactions at elevated temperatures, giving rise to a brownish colour [269].



**Figure 6.5:** Scanning electron microscopy pictures of PLA containing (A) 5 wt. % unwashed ChNC, (B) 5 wt. % ChNC-C8:0, (C) 5 wt. % washed ChNC, and (D) 5 wt. % ChNC-C18:0. (E) Samples containing ChNC-C8:0 and ChNC-C18:0 had many small aggregates with a size of  $\sim 500 \text{ nm}$ .

**Table 6.3:** Pictures of nanocomposites containing 5 wt. % (modified) chitin nanocrystals and their corresponding  $L^*$ ,  $a^*$ ,  $b^*$  scores.

Sample	$L^*$	$a^*$	$b^*$	Picture
100% PLA	$88.8 \pm 0.0$	$2.1 \pm 0.0$	$-0.4 \pm 0.0$	
PLA + 5 wt. % unwashed ChNC	$27.4 \pm 0.1$	$15.4 \pm 0.3$	$24.9 \pm 0.2$	
PLA + 5 wt. % washed ChNC	$43.0 \pm 0.2$	$16.2 \pm 0.1$	$24.9 \pm 0.2$	
PLA + 5 wt. % ChNC-C8:0	$77.4 \pm 0.1$	$4.8 \pm 0.1$	$20.0 \pm 0.1$	
PLA + 5 wt. % ChNC-C18:0	$75.2 \pm 0.2$	$5.9 \pm 0.1$	$23.5 \pm 0.3$	

Interestingly, the presence of unmodified ChNC resulted in darker films compared to their modified counterparts (**Table 6.3**). One possible explanation is the better dispersibility of modified ChNC in PLA (**Figure 6.5**), which resulted in a higher overall transparency. Alternatively, the introduction of fatty acids to the ChNC's surface may inhibit Maillard reactions.

Regardless of its treatment, the addition of ChNC reduced transmittance throughout the whole wavelength range measured (**Figure 6.6**), i.e.,  $\lambda = 250 - 650$  nm. For instance, at a wavelength of  $\lambda = 500$  nm, the transmittance was 1.9% for PLA with unmodified unwashed ChNC (dark film) and 16.1% in the presence of ChNC-C8:0 (light film). This is an important clue for the development of food packaging materials that are less UV transparent making food products thus less prone to oxidation reactions, and other reactions that are light-induced.

#### 6.4.2.2 Barrier properties

**Table 6.4** presents the water vapour transmission rate (WVTR) of neat PLA and nanocomposites containing 5 wt. % ChNC. Generally, the WVTR of the nanocomposites was  $\sim 7\%$  lower than neat PLA, with the exception of nanocomposites containing washed ChNC

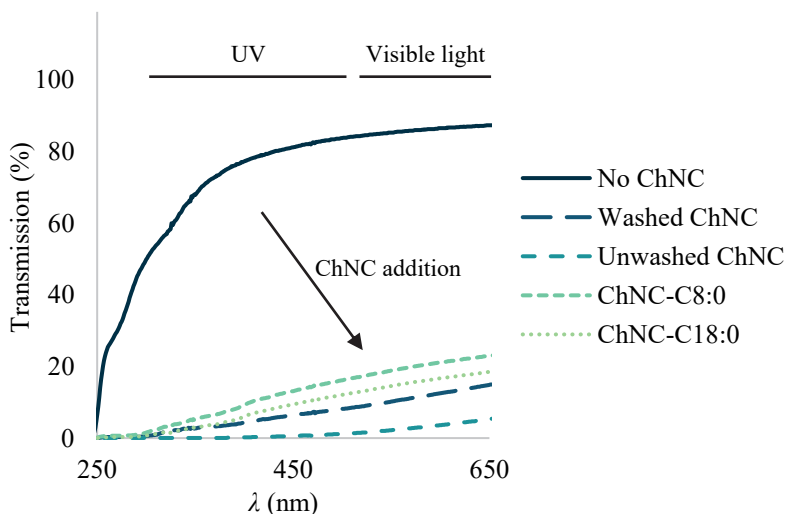


**Figure 6.6:** Transmittance of PLA films containing 5 wt. % (modified) ChNC. Wavelengths in UV- and visible ranges are highlighted.

**Table 6.4:** Water vapour transmission rate (WVTR) of PLA nanocomposites containing 5 wt. % (modified) ChNC.

Sample	WVTR (g/m <sup>2</sup> ·day)*	WVTR compared to PLA
PLA	38.2 ± 2.2	-
PLA + 5 wt. % washed ChNC	99.7 ± 73.3	+ 261.4%
PLA + 5 wt. % unwashed ChNC	35.6 ± 0.9	- 6.7%
PLA + 5 wt. % ChNC-C8:0	35.6 ± 0.5	- 6.3%
PLA + 5 wt. % ChNC-C18:0	34.6 ± 2.3	- 9.4%

\*100  $\mu$ m thickness, 23 °C, 85% gradient RH

that showed a high WVTR of  $\sim$  260% compared to PLA. In the latter nanocomposites, substantial aggregation took place, most probably leading to ‘weak spots’ in the material, which was mitigated in the other nanocomposites. Improved barrier properties are commonly reported for nanocomposites [194,270,271], and many authors explain this by an increased tortuous diffusion path caused by nanoparticle addition. This may also be the reason for the improved performance of our other nanocomposites in which the particles are much better dispersed.

#### 6.4.2.3 Mechanical properties

**Figure 6.7** shows the Young’s modulus (A), maximum stress (B), and elongation at break (C) of neat PLA and the nanocomposites. The addition of ChNC particles resulted in a slightly higher Young’s modulus and slightly lower elongation at break. For instance, a Young’s modulus of  $3030 \pm 70$  and  $3154 \pm 438$  MPa was found for neat PLA and upon addition of 5 wt. % unwashed ChNC, respectively. It is good to point out that these differences are very small, and most probably insignificant. Others have reported increased maximum stress and Young’s modulus upon polysaccharide nanocrystal addition to PLA [237,271]. This is commonly explained by the formation of a percolation network of polysaccharide nanocrystals that gives rise to increased mechanical properties. The difference with our work is that commonly substantial amounts of plasticizers are used to facilitate ChNC dispersion, or PLA and ChNC are mixed with other plastics such as PBAT; this may not only facilitate

nanoparticle dispersion but also influence the mechanical film properties beyond what is possible within our experimental conditions.

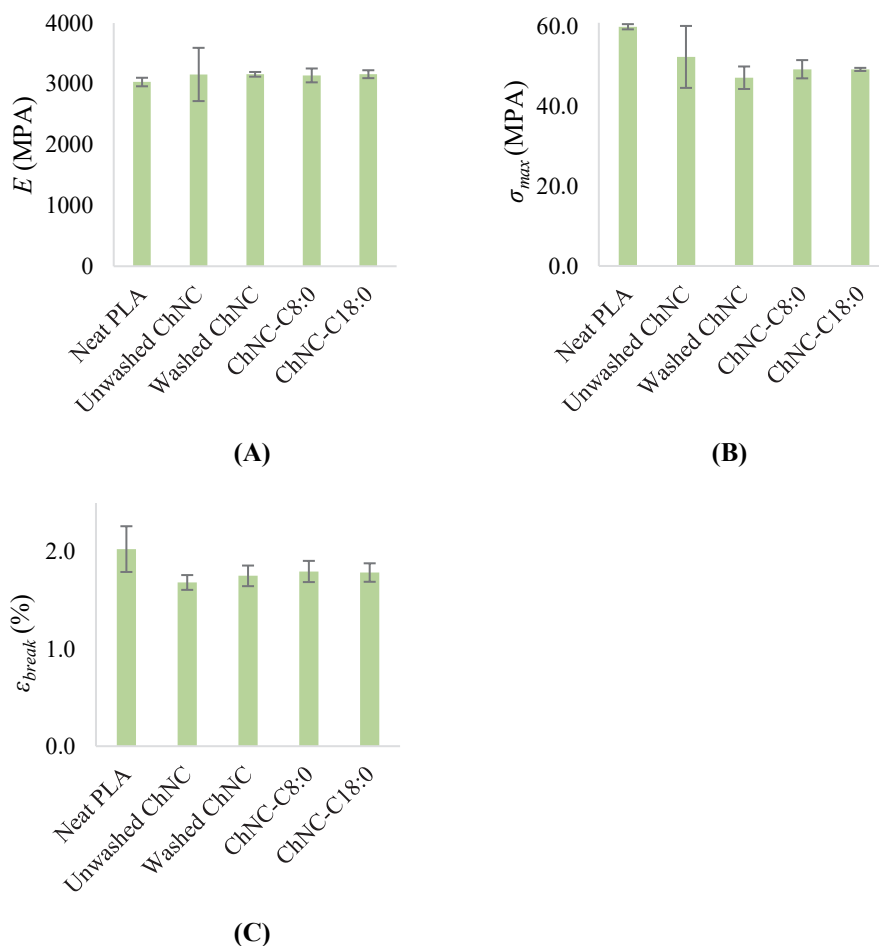


**Figure 6.7:** Young's modulus (A), maximum stress (B), and elongation at break (C) of neat PLA and nanocomposites containing unmodified (unwashed and washed), and modified chitin nanocrystals (ChNC-C8:0 and ChNC-C18:0).

## 6.5 Conclusions

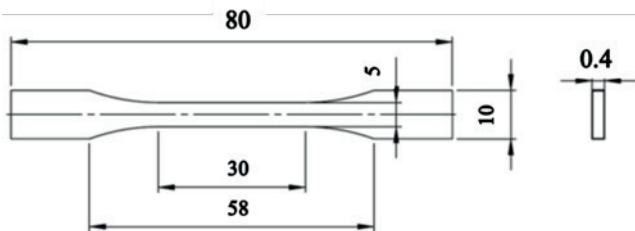
Steglich esterification was successfully used to modify chitin nanocrystals with fatty acids differing in carbon chain length and degree of saturation; covalent attachment was confirmed with FTIR and  $^{13}\text{C}$  NMR. We demonstrated that substitution of 2 – 4% influenced phase

behaviour greatly, with ChNC modification with the longest fatty acid leading to the highest hydrophobicity.

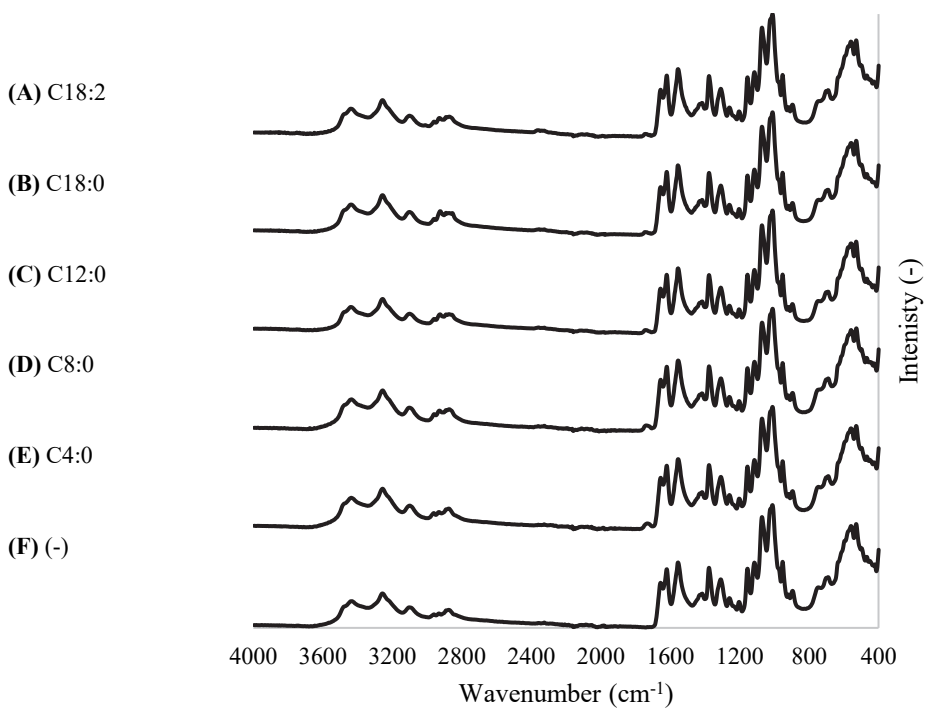
SEM observations suggested that modified ChNC dispersed better in the PLA matrix compared to their unmodified counterparts. This reduced brown colour formation and improved transparency. Generally, the addition of ChNC provided high UV-protection and improved barrier protection, which was without being at the expense of mechanical strength.

The prepared nanocomposites are relevant for application in, e.g., food for which it can be expected that light-induced reactions will be slowed down considerably. The modified particles as such are also expected to be compatible with other hydrophobic polymers, and may contribute to the development of other advanced packaging materials.

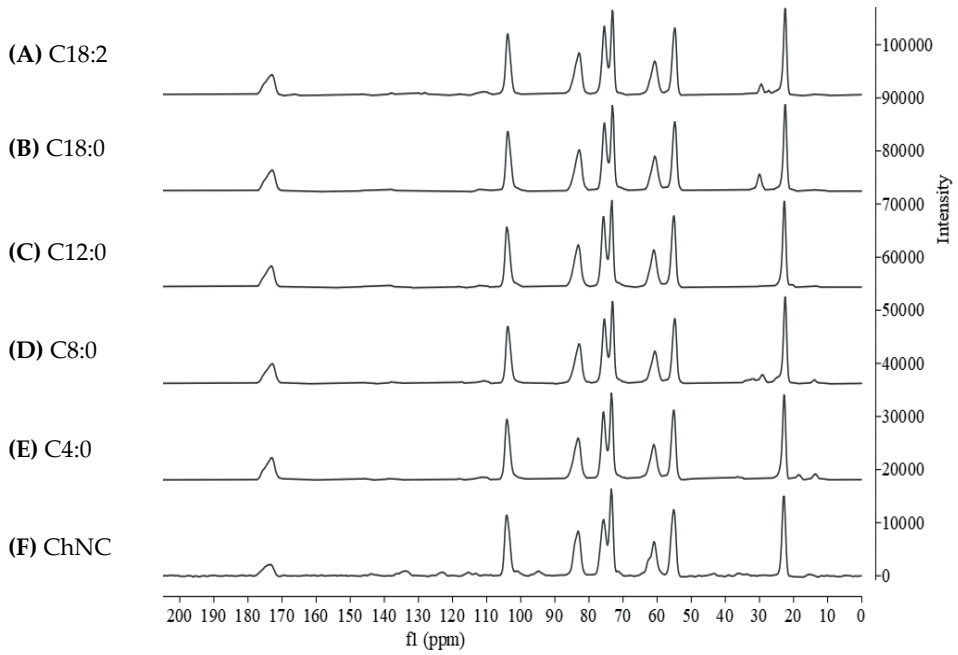
## 6.6 Appendix



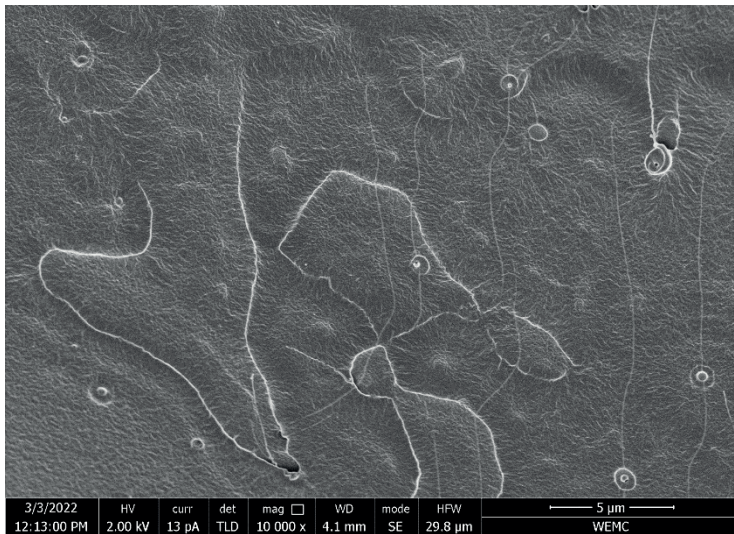
*Appendix 6-1: Geometry and dimensions of the samples used for the tensile test strength measurements.*



*Appendix 6-2: FTIR spectra of ChNC modified with (A) C18:2, (B) C18:0, (C) C12:0, (D) C8:0, (E) C4:0, (F) unmodified.*



**Appendix 6-3:**  $^{13}\text{C}$  NMR spectra of (A) ChNC-C18:2, (B) ChNC-C18:0, (C) ChNC-C12:0, (D) ChNC-C8:0, (E) ChNC-C4:0, and (F) ChNC.



**Appendix 6-4:** Scanning electron microscopy picture of neat PLA.



**P**art III  
Plastics and society



---

# 7

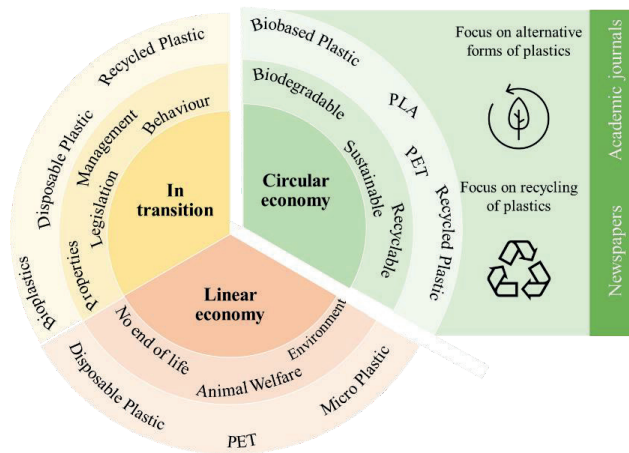
## Science and media framing of the future of plastics in relation to transitioning to a circular economy

---

*Published as “Ivanna Colijn, Fabrice Fraiture, Efrat Gommeh, Karin Schroën and Tamara Metze. 2022. Science and Media Framing of the Future of Plastics in Relation to Transition to a Circular Economy. Journal of Cleaner Production 370:133472.”*

### 7.1 Abstract

Plastics play an important role in the transition from the current linear economy to a more circular one, but ideas differ about this role. These ideas were studied in this article as a form of futurity framing. These framings may hinder or contribute to a transition toward a circular bio-economy by opening up or closing down alternative paradigms for thinking about plastics in the future. Based on a media analysis of four Dutch national newspapers and international academic papers, three futurity frames were found regarding the role of different types of plastics in a linear economy, a circular economy, or an economy in transition. (1) In newspapers and academic sources, traditional plastics were considered part of a linear economy. (2) In both sources, all sorts of actors saw a future for plastics with improved material properties in a transition toward a circular economy, but in combination with a change in consumer behaviour and waste management systems. (3) In both academic journals and newspapers, a role for plastics was envisioned in a future circular economy. However, in academic journals, the discussions focused mainly on the improvement of alternative forms of plastics such as biobased and/or biodegradable, whereas, in newspapers, recycling traditional plastics was emphasized. These findings indicate that a transition to a more circular economy may accelerate if both the closing-the-loop argument and the argument for technological innovations for biobased and biodegradable products receive equal attention in newspapers and academic journals, and are taken more into account in a societal future vision for the circular economy.



Graphical abstract

## 7.2 Introduction

As today's linear economy is increasingly contributing to sustainability issues [272,273], it is important to work toward a circular economy, where the resource-manufacture-use-waste loop is closed [274]. The European Union identified five priorities, one of which is plastics. The main application of plastics is packaging (40% of its total use [275]), and packaging is also the main waste stream (60% of post-consumer waste [275]). Currently, 32% leaks out of the collection system, meaning that it is either not collected or collected but then illegally dumped or mismanaged [12]. In short, plastic packaging creates an environmental problem.

In 2018, the European Commission published *A European Strategy for Plastics in a Circular Economy*, presenting key commitments for action at the European level [276]. The Netherlands has deployed numerous plastics strategies [277,278] and was therefore chosen as a focus of this study. In 2019, the Plastics Pact was signed in the Netherlands by 75 companies that were using or producing plastics and by the Dutch Ministry of Infrastructure and Water Management [10]. Involved parties acknowledge that, to accelerate the transition to a closed plastics loop, innovative collaborations between industry, governments, and societal actors are needed [279].

These various groups of actors that need to collaborate envision new roles for (new sorts of) plastics in the circular economy. They have contrasting or similar ideas about what a circular economy implies, and about whether and how plastic packages will be used. Consequently, they *frame* plastics, meaning that they select information and highlight certain aspects of it based on “*a perspective from which a situation can be made sense of and acted on*” ([280] page 146). These aspects of plastics include, for example, the environmental impact, benefits, technical characteristics, or the development of alternatives (like bioplastic) depending on actors' idea about what a future may entail. In other words, all actors frame plastics coming from a broader idea, for example a future that they desire, detest, or think might be feasible. Current research illustrates the need to study these framings in a circular economy, as they can open up or close down opportunities for futurity framings [281]. Yet, futurity framing is hardly ever connected to the role of specific materials in it.

Therefore, in this chapter, these ideas were studied as a form of *futurity framing* [282] that may open up alternative paradigms for thinking about – in this case – plastics in a circular

economy and that can hinder or contribute to a transition toward this. In the literature on emerging technologies, this is also known as *narratives of futurity* [283]. In futurity frames, actors envision future societies (a broader perspective), and, as part of those often-implicit visions, give meaning to aspects of a reality. Futurity framing is influential and guides policy decisions, business models, and societal responses to new technologies and to sustainability transitions [284,285]. Envisioning futures may create room for technological, behavioural, market, and governance innovations [282,284,286]. The importance of conflicting or congruent framings, or understandings of the circular economy, is pointed out in studies that describe the contested nature of a circular economy [273,287]. Conflicting conceptualizations and framings of the circular economy influence not only research programs and their empirical focus, but also how the general public perceives and supports this transition, and may hinder the much-needed innovative collaborations between directly involved actors, such as governments, industry, and citizens.

To contribute to innovative collaborations and to acceptable forms of transition toward a circular economy, better insights are required in terms of differences and similarities in the futurity framing of plastics in a circular economy. There is particular interest in how traditional media and academic sources envision the role of different types of plastics and in whether there are differences and similarities in these visions. This may be very influential for the development and production of particular (biodegradable, biobased) plastic packaging; the public responses to, and acceptance of, those plastic packages; and their governance.

The research question guiding this chapter is: What futures are envisioned for plastics by all sorts of actors in traditional media sources and in academic sources? This question was answered by a frame analysis of 133 international academic journal publications and 207 newspapers articles published between 2010 and 2019 in the Netherlands. First, the conceptual framework of futurity framing is developed, followed by a description of the methods. Then the results are presented and discussed.

### 7.3 Conceptual framework: futurity framing of plastics in a circular economy

Many scholars agree that the transition to an inclusive circular economy requires drastic changes to current systems [273,288]. However, the ideas and definitions of what a circular economy entails vary among scholars and also among societal actors, including the general public. It is an essentially contested concept and is defined in many different ways [287,289]. Studies on media framing of the circular economy point out the importance of framing in public responses to this transition and argue that, for example, media coverage should widen in scope to reflect the multisectoral nature of the circular economy ([290], page 16). Framing by media sources plays an important role in engaging society in the (circular) bio-economy. Through valid and informative media reporting, the general public may change their opinion [290,291]. Hence, framing can be defined as a communicative activity in which actors highlight certain aspects of an issue [292,293]. The way in which academics define the circular economy may also influence public opinion and at least give focus to their objects of study. In addition, depending on how actors handle different framings of an issue, collaboration may or may not be successful [294]. This may influence the much-needed innovative collaborations for a plastics transition. Hence, insights into the contested nature of the circular economy concept – and in this case the role of plastics in it – need to be complemented by insights from studies into framings by societal actors. A particular type of framing – futurity framing – is the special focus of this research.

Transitions always entail forward-looking narratives. Policy visions, business strategies, designs, scenarios, and ideological paradigms are all subjective, forward-looking depictions of something that has not yet been realized [283]. Different societal actors envision new roles for (innovative) technologies and materials in a particular future. These visions are influential and – as paradigms – guide policy decisions, business models, and societal responses to new technologies and sustainability transitions [284,285]. Through narratives of the future, new possibilities open up, thereby creating room for technological, behavioural, market, and governance innovations [282,284,286]. However, these imaginaries can also hinder these transitions [286]. In this chapter, broader visions of society were studied as a form of futurity

framing<sup>2</sup>; the idea of narratives of the future were combined [283] with framing as defined by van Hulst and Yanow in [293]. Futurity framing is defined as the study of interpretive schema in talk and text that comprise the following interrelated elements:

(1) *A forward-looking frame*, which is a broader collectively imagined form of social life and social order, such as a degrowth ideal or other (political) visions.

Forward-looking framing enables people to make sense of a current situation and they “*can start to imagine what could or should happen next in light of prior notions concerning the ways certain problems can and should be handled*” ([295] cited in [293]).

(2) *The label actors use for – in this case – a material, product, or technology*. How people refer to plastics makes a difference: as a general category, or biodegradables, or PET, as part of a particular future (see also page 8 in [293]) on naming, categorizing, and selecting as framing devices).

(3) *Arguments* given for the role of plastics in those social futures. This is the storytelling part of framing: elements are woven together in a plot (page 10 in [293]).

In this case, futurity frames are the broader collectively imagined futures of a circular economy, a linear economy, or an economy in transition and, within that, the narratives by groups of actors regarding the (non)use and development of particular sorts of plastic. The circular economy is one of those framings, and it is a hopeful one, as it depicts an escape from an economy in which Earth is depleted. A linear economy and a transition to a circular economy are two other broader collectively imagined forms of social life.

## 7.4 Methods

### 7.4.1 Data gathering

Futurity framing was analyzed in four Dutch newspapers (De Telegraaf, Volkskrant, NRC Handelsblad, and Trouw) because the Netherlands can be considered a frontrunner in the plastics strategy [278]. As the academic world is international, international academic papers

---

<sup>2</sup> The word *futurity* was used rather than futures, as it conveys the infinite range of possibilities better than furthers (see also [283]).

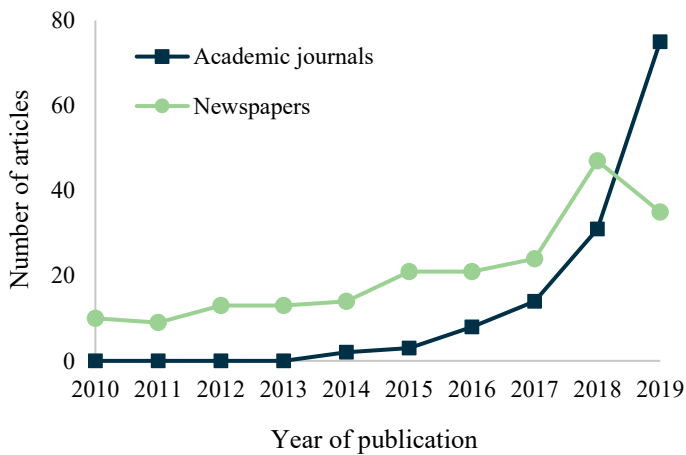


**Figure 7.1:** Total number of articles about plastic food packaging in academic journals and newspapers.

were collected. The timeframe for the search was 2010 – 2019, as awareness of the need for a plastics transition clearly increased over the last decade, as was visible in both academic journals and newspapers (**Figure 7.1**)

To construct a dataset, articles from the four Dutch newspapers were retrieved from the database Nexis Uni, and academic papers were collected from the scientific database Scopus. A Boolean search was conducted for each database. The following search string was used in Nexis Uni (in Dutch) ‘plastic’ or ‘polymer’ or ‘kunststof’ and ‘verpak’ or ‘voedselverpak’ or ‘levensmiddelverpak’ and ‘voedsel’ or ‘levensmiddel’ or ‘eetwaar’ or ‘eetwa’ or ‘voeding’<sup>3</sup>. Different keywords were used for academic papers to prevent the collection of papers containing information about plastics without making a statement about its transition toward a circular economy. The following search string was used in Scopus: TITLE-ABS-KEY (plastic or polymer) AND TITLE-ABS-KEY (circular AND economy).

All articles were manually checked for relevance after collection. Newspaper articles were considered relevant when they discussed plastic, plastic food packaging, and its global

<sup>3</sup> The Dutch words translate as: synthetic material (*kunststof*), package (*verpak*), food package (*voedselverpak*, *levensmiddelverpak*), nutrition or food (*voedsel*, *levensmiddel*, *eetwaar*, *eetwa*, *voeding*).

impacts. Academic papers were considered relevant when plastics were discussed in general, or when plastic food packaging was mentioned. The final dataset consisted of 133 academic articles and 207 newspaper articles.

### 7.4.2 Data analysis

An interpretative analysis was performed in the software ATLAS.ti. **Figure 7.2** gives a schematic overview of the coding procedure performed on newspapers and academic articles.

Actors were coded as a representation of a stakeholder group involved in the plastics chain (code 1). Labels were the names that actors used for a material such as ‘polymer’, but also specific types of plastics such as ‘PET’ (code 2). The frame coding consisted of two parts: one to identify the type of future, i.e., linear, transition, circular, the second to identify arguments that give meaning to the use of plastics in that type of future (code 3). These were inductively developed by manual coding of a sample of newspapers and academic sources; a grouping of codes in conversations between the researchers (**Figure 7.2**) represents the final code book for the frames. Five arguments were observed that were not considered to be supportive of a specific frame (indicated in grey **Figure 7.2** code 3).

Second, the strength of the relation between two codes was explored, e.g., the relation between the actor ‘policymakers’ and the label ‘PET’. Atlas-ti’s co-occurrence calculation function was used [296]. Co-occurrence is expressed as a co-occurrence coefficient value, which describes how frequently two codes are assigned to the same text excerpt. The resulting co-occurrence coefficient fluctuates between zero and one; the higher the co-occurrence, the stronger the relationship.

From the 207 newspaper articles, a total of 934 excerpts were coded, and, from the 133 academic papers, a total of 1002 excerpts were coded. These provided sufficient codes to calculate the co-occurrence. In the results, Atlas.ti indicated when there was possible distortion by a too low co-occurrence. Please note that the data are qualitative and therefore the c-coefficient is different from, for instance, a Pearson correlation coefficient and consequently no p-values are provided.

Code 1	
<u>Actor</u> : Citizens, Consumers, Industry, Journalists, NGOs, Policymakers, Scientists	
Code 2	
<u>Label</u> : e.g., Plastic, Polymer, Microplastic, PET, PLA	
Code 3	
<u>Frame + Argument</u> :	
Linear	Animal welfare – Plastics: plastic waste in the environment causes harm to animals End-of-life – Plastics: the end-of-life treatment does not contribute to a circular economy Environmental – Plastics: plastics harm nature by its production or as waste in the environment
Transition	Language – Alternatives: terms used for different plastics are complex/confusing, affecting the transition toward a circular economy Technical – Alternatives: alternative plastics need improvement, e.g., technical characteristics, production, scale, or efficiency to be successfully used in a circular economy Change management – Plastics: transitioning to alternatives requires people to develop a new mindset Consumer behaviour – Plastics: transitioning towards a new plastics economy requires a change in consumer behaviour and awareness End-of-life – Plastics: end-of-life of alternative plastics need improvement to become suitable to use in a circular economy End-of-life – Alternatives: alternative plastics have a low(er) environmental impact than traditional plastics Legal – Plastics: legislation still needs to be optimized to stimulate the transition towards a new plastic economy
Circular	Environmental – Alternatives: alternative plastics have a low(er) environmental impact than traditional plastics Resources – Alternatives: renewable resources are available for the production of alternative plastics, and this is better than using fossil resources Technical – Alternatives: alternative plastics can equal the technical characteristics of traditional plastics or perform even better, while contributing to a circular economy. End-of-life – Traditional: if recycled, the end-of-life treatment of traditional plastics contributes to the aim of a circular economy
None	Necessity – No: plastics can be removed because they serve no purpose Necessity – Yes: plastics are needed, e.g., for protection or during transport Necessity – Yes but less: plastics are needed but should be reduced Others over plastics: other materials are preferred over plastics Plastics over others: plastics are preferred over other materials

**Figure 7.2:** Schematic overview of the interpretative analysis performed in academic journals and newspapers; each excerpt consisted of 1) an actor, 2) a label, and 3) a frame connected to an argument. Note: This is a schematic representation of the method applied and not a representation of a futurity frame. The arguments presented are those collected in newspapers and academic journals.

## 7.5 Results

It was aimed to answer the question: what futures are envisioned for plastics by all sorts of actors in traditional media sources and in academic sources?

### 7.5.1 Futurity framing in academic journals and traditional media

This study identified three futurity frames: 1) plastics are part of a linear economy, 2) plastics are in transition toward a circular economy, and 3) plastics are part of a circular economy. All futurity frames were relatively equally present in academic journals and newspapers (**Table 7.1**), although differences were observed among actors represented by the co-occurrence coefficients in academic journals and newspapers (**Table 7.2**). In this section, these differences are elaborated on, whereas in the next section the different arguments actors used to frame plastics are elaborated on.

#### 7.5.1.1 Academic journals

In academic journals, actors generally used the frames ‘plastics are in transition’ and ‘plastics are part of a circular economy’ in similar frequency as ‘plastics are part of a linear economy’ frame (**Table 7.2**). NGOs ( $C = 0.23$ ) and policymakers ( $C = 0.33$ ) mainly framed plastics as in transition, whereas journalists ( $C = 0.31$ ), scientists ( $C = 0.26$ ), and consumers ( $C = 0.35$ ) mostly framed plastics as part of a circular economy. The actor industry equally co-occurred in the linear economy frame and the in transition economy frame ( $C = 0.22$ ) (**Table 7.2**).

#### 7.5.1.2 Newspapers

In newspapers, the actors citizens ( $C = 0.32$ ) and consumers (**Table 7.2**;  $C = 0.09$ ) showed the highest co-occurrence with the linear economy frame. The actors NGOs ( $C = 0.26$ ) and policymakers ( $C = 0.29$ ) mostly framed plastics as in transition, whereas the actors industry

*Table 7.1: Relative frequency of occurrence of broad futurity frames in the two types of sources.*

Futurity frame	Academic journals	Newspapers
Linear economy	33%	38%
In transition	31%	31%
Circular economy	36%	31%

( $C = 0.37$ ) and journalists ( $C = 0.43$ ) showed the highest co-occurrence with the circular economy frame. An equal co-occurrence was found between scientists and the frames ‘plastics are in transition’ and ‘plastics are part of a circular economy’ ( $C = 0.25$ ).

**Table 7.2:** Co-occurrence coefficients of actor and broad futurity frames in newspapers (NP) and academic journals (AJ).

Actor	Linear economy		In transition		Circular economy	
	AJ	NP	AJ	NP	AJ	NP
Citizen $n_{AJ} = 1^a$ ; $n_{NP} = 66$	(-) <sup>a</sup>	0.32	(-) <sup>a</sup>	0.11	(-) <sup>a</sup>	0.04
Consumer $n_{AJ} = 15$ ; $n_{NP} = 16$	0.08	0.09	0.14	0.03	0.35	0.00
Industry $n_{AJ} = 78$ ; $n_{NP} = 181$	0.06	0.08	0.22	0.16	0.22	0.37
Journalist $n_{AJ} = 19$ ; $n_{NP} = 462$	0.11	0.19	0.17	0.11	0.31	0.43
NGO $n_{AJ} = 43$ ; $n_{NP} = 89$	0.12	0.17	0.23	0.26	0.08	0.10
Policymaker $n_{AJ} = 27$ ; $n_{NP} = 39$	0.17	0.20	0.33	0.29	0.04	0.10
Scientist $n_{AJ} = 819$ ; $n_{NP} = 81$	0.14	0.16	0.14	0.25	0.26	0.25

<sup>a</sup> Presence in the dataset was too limited to accurately calculate co-occurrence.

### 7.5.2 Futurity framing of plastics

Within each broad frame, different labels for plastic and different arguments were used. Observations indicated that actors in scientific journals and newspapers used different labels to identify plastics, and different arguments as to why particular plastics are needed. **Figure 7.3** presents an overview of the futurity frames, the role of plastics in them, and the labels mentioned. The co-occurrence values between the actors and their arguments are presented in **Table 7.3**.

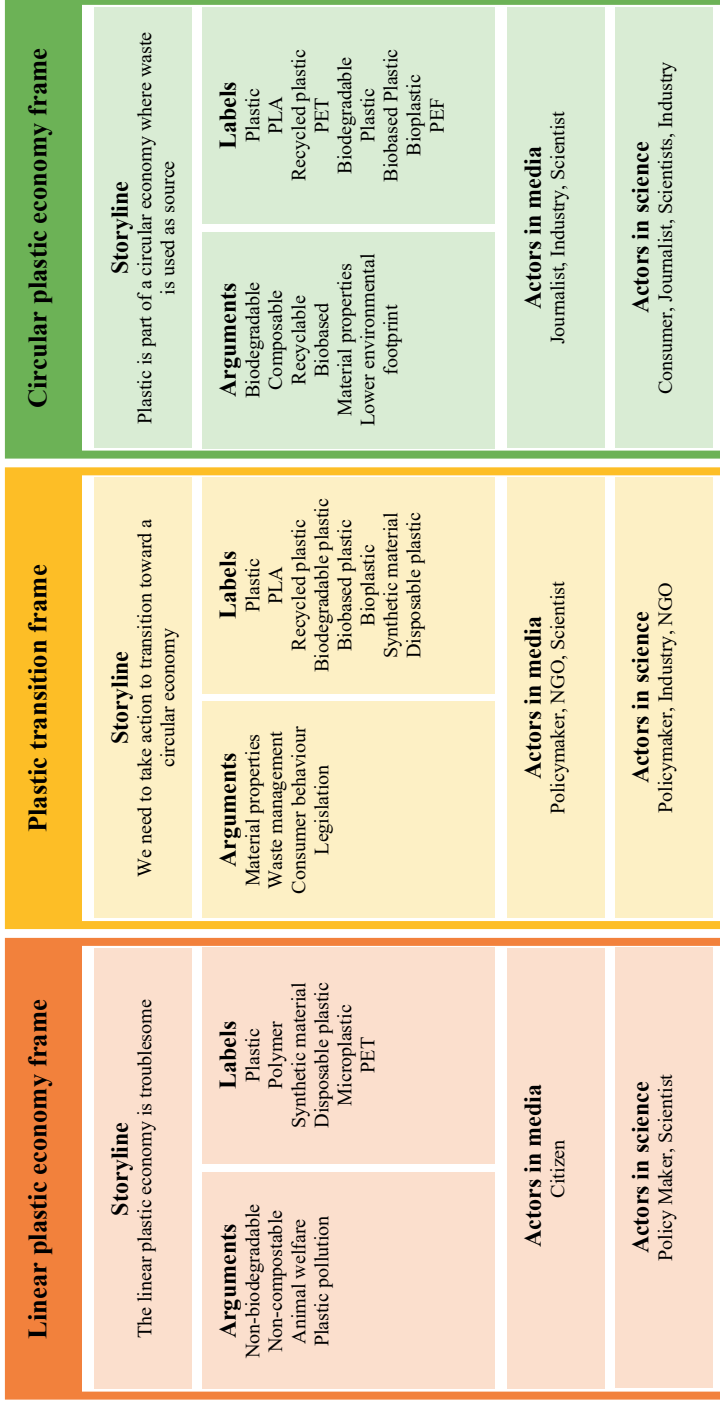


**Figure 7.3:** Overview of the three futurity frames (linear, in transition, circular economy) in terms of a circular biobased economy; most occurring labels, actors, and arguments in each futurity frame are presented.

**Table 7.3:** Co-occurrence coefficients for arguments and actors in academic journals (AJ) and newspapers (NP). Empty cells refer to a co-occurrence of  $C = 0$ , bold numbers correspond to co-occurrences of  $C \geq 0.06^a$ . This result should not be overinterpreted, as this actor's frequency was very low.

	Citizen		Consumer		Industry/ Business		Journalist		NGO		Policymaker		Scientists	
	AJ	NP	AJ	NP	AJ	NP	AJ	NP	AJ	NP	AJ	NP	AJ	NP
Linear	Animal welfare – Plastics	<b>0.13</b>						0.02	0.04					0.01
	End-of-life – Plastics	<b>0.11</b>			0.03	0.03	<b>0.08</b>	0.05	<b>0.07</b>	<b>0.07</b>	<b>0.06</b>	0.04	<b>0.07</b>	<b>0.06</b>
	Environmental – Plastics	0.01 <sup>a</sup>	<b>0.09</b>	<b>0.08</b>	<b>0.11</b>	0.02	0.02	0.05	0.04	0.04	<b>0.06</b>	<b>0.16</b>	0.03	0.03
Transition	Language – Alternatives		<b>0.06</b>		0.01									
	Technical – Alternatives		<b>0.25</b>		0.02	0.02	<b>0.26</b>	0.02					0.03	0.02
	Change management – Plastics	0.01			0.05	0.01			<b>0.12</b>	0.04	<b>0.06</b>		0.02	<b>0.09</b>
	Consumer behaviour – Plastics	<b>0.06</b>			0.03	0.05	0.02	0.02	0.02	<b>0.08</b>	<b>0.07</b>	0.02	0.02	0.02
	End-of-life – Plastics	0.02			<b>0.06</b>	<b>0.07</b>	0.01	0.01	0.05	0.01	<b>0.25</b>	<b>0.22</b>	0.02	0.02
	End-of-life – Alternatives				0.02	0.02	0.02		0.03	0.03			0.02	0.03
Circular	Legal – Plastics	<b>0.06</b>			0.01	0.01		0.01	0.04	<b>0.11</b>	<b>0.07</b>	<b>0.12</b>	0.03	0.03
	Environmental – Alternatives			<b>0.17</b>		0.02	<b>0.08</b>						0.04	
	Resources – Alternatives			<b>0.07</b>									0.02	
	Technical – Alternatives			<b>0.10</b>		0.05		<b>0.12</b>	0.02				0.05	
	End-of-life – Traditional					0.05				0.01				0.03
	Economic – Alternatives					0.04	0.01		0.02	0.02			0.02	0.05
	Necessity no	<b>0.12</b>		<b>0.33</b>	0.01	0.03		0.01	<b>0.07</b>	0.04				
	Necessity yes	0.01		<b>0.05</b>		<b>0.08</b>	0.03	0.03	0.03			0.02	0.02	0.02
	Necessity yes but less			<b>0.16</b>		0.02	0.02	0.02				<b>0.06</b>		0.03
	Others over plastic	0.01		<b>0.07</b>	<b>0.06</b>	0.01	0.01	0.01	0.02	0.02			0.01	0.01
	Plastics over others					0.01	0.01	0.01	0.04					0.01

### 7.5.2.1 *Futurity framing of plastics in a linear economy: a plastic monster*

The linear economy frame was identified by issues related to how plastics are nowadays used, produced, and treated. Remarkably, the tone of voice seemed quite pessimistic, as nicely demonstrated by the following quote “*The current plastic system – a crisis called ‘plastic monster’ – needs to be fundamentally changed*” [297]. Generally, actors used similar arguments in both academic journals and newspapers to frame plastics as part of a linear economy (**Table 7.3**).

#### *Academic journals*

The frame ‘plastics are part of a linear economy’ was used with a similar frequency as the two other frames (**Table 7.2**). When using the linear economy frame, the actors focused mostly on the material’s non-biodegradability, non-compostability, or non-recyclability, which do not contribute to the aim of a circular economy (**Table 7.3**). There was a high co-occurrence of this argument with the actors journalists ( $C = 0.08$ ), NGOs ( $C = 0.07$ ), policymakers ( $C = 0.06$ ), and scientists ( $C = 0.07$ ) (**Table 7.3**). In fact, scientists often presented this argument as their biggest motivation to conduct certain research.

#### *Newspapers*

The lack of end-of-life treatment was also the most dominant argument in newspapers, where high co-occurrence coefficients were found for the actors citizens ( $C = 0.11$ ), NGOs ( $C = 0.07$ ), and scientists ( $C = 0.06$ ) (**Table 7.3**). However, in newspapers, the linear economy frame was applied with a broader set of arguments compared to academic journals. Actors in newspapers argued that accumulating plastics in the environment is harmful and has deleterious consequences for animal welfare. The effects of plastic production on the environment were also mentioned. Citizens ( $C = 0.09$ ), consumers ( $C = 0.11$ ), and policymakers ( $C = 0.16$ ) in particular co-occurred highly with the argument of polluting the environment, and citizens co-occurred highly with animal welfare ( $C = 0.13$ ): “*Here it serves as food for birds, fish, and marine mammals*” [298] (**Table 7.3**).

Interestingly, the actors citizens ( $C = 0.12$ ) and consumers ( $C = 0.33$ ) mostly mentioned that the use of plastics is now common but not needed for many applications, and this was often expressed in a negative or sarcastic tone: “*What is the use of putting a plastic suit on every*

*eggplant, since when do cucumbers become unwell if they are not tightly wrapped in a plastic film?”* [299] (**Table 7.3**). Additionally, the actor consumers argued that other materials should be used instead of plastics (**Table 7.3**;  $C = 0.06$ ). Citizens and consumers were the only actors using the frame ‘plastics are part of a linear economy’ more often than the other two frames (**Table 7.2**).

Industrial actors, on the other hand, were most often quoted when they expressed the necessity of plastics ( $C = 0.08$ ) and argued why plastics are better in comparison to other materials (**Table 7.3**). This may be a response to consumers and citizens who often questioned the necessity of plastics. Industrial actors argued, for example: *“It must not be forgotten that plastics have unequalled qualities for the time being; they keep food fresh, they are safe to use, and protect food, hence they prevent food waste”* [300].

Academics quoted in newspapers were talking mostly about the issues of today’s linear economy (**Table 7.3**;  $C = 0.06$ ); they argued that the linearity creates an economic loss, that repurposing the material is inefficient, or that degradation takes forever.

### **7.5.2.2 Futurity frame plastics in a transition: we can do it!**

Whereas the linear economy frame was used to highlight today’s problems with plastics, the transition frame was used to highlight various pathways toward a circular economy. The tone of voice appeared much more positive. The actors commonly discussed the issue as if the transition to a circular economy is guaranteed, and a rather high ‘we can do it’ spirit could be noticed: *“Currently, one of the biggest barriers to the adaptation of bioplastics is the versatility of biodegradable polymer materials...”*, and *“... We’ll see scientists work to overcome the issues in 2019 and beyond”* [301].

#### **Academic journals**

There were clear differences in arguments used among the actors (**Table 7.3**). Remarkably, policymakers and NGOs used similar arguments to frame plastics as in transition. It is good to point out that the European Commission was the most observed policy actor in academic journals. The following two quotes clearly show their narrative: *“According to the European Commission, the potential for recycling plastic waste in the European Union remains unfulfilled...”* [302] and *“... the EU has pointed out that designing appropriate measures for*

*recycling plastic materials may contribute to improve competitiveness and create economic activities and, consequently, new jobs*” [303]. Thus, whereas policymakers argued that the end-of-life treatments of plastics are still complex ( $C = 0.06$ ), they still considered that it is promising and holds potential ( $C = 0.25$ ) (**Table 7.3**). Interestingly, policymakers acknowledged their own responsibility where they reasoned that legislation to change the current use of plastics needs to be optimized to enable or stimulate the transition toward a new plastic economy (**Table 7.3**;  $C = 0.07$ ).

Generally, the actors NGOs and policymakers were very united in the argument that change is needed to make the plastic transition happen; it requires a new mindset for people to adapt to something new (policymakers  $C = 0.06$ ; NGO  $C = 0.12$ ) (**Table 7.3**). As Linder [304] stated: *“it is a start of a journey focusing on system-wide solutions, which hopefully leads to intensified effort with a revised perspective, both in academia and business”*. However, the actor NGOs seemed to adopt a more critical tone of voice, with arguments less focused on changing consumer behaviour compared to policymakers (policymakers  $C = 0.07$ ; NGO  $C = 0.02$ ) (**Table 7.3**). The feeling of responsibility was not unique to policymakers and NGOs; industry also mentioned the need to change the way of managing plastics for food packaging used for their products or produced by them. Like the actors NGOs and policymakers, industry acknowledged the complexity of the end-of-life treatments of plastics (**Table 7.3**;  $C = 0.05$ ). They mentioned that transitioning toward a circular economy is difficult and not yet possible for all materials, but they stressed the possibilities and the will to transition toward a circular economy (**Table 7.3**;  $C = 0.06$ ). Although the actor industry did discuss the economic feasibility of alternative plastics, its co-occurrence was not extremely high (**Table 7.3**;  $C = 0.04$ ). Lastly, the actor journalists focused mainly on labels used for alternative forms of plastics, which they consider to be complex and confusing (**Table 7.3**;  $C = 0.25$ ): *“... the idea that bioplastics were synonymous with biodegradable plastics became fixed in the minds of the public and the industry alike, a misconception the bioplastics industry is wrestling with to this day”* [305].

#### ***Newspapers: legal incentives and consumer behaviour***

In newspapers, a similar set of arguments about the role of plastics in a transition were used as in academic journals. The actors NGOs and policymakers used the ‘plastics are in

transition' frame more than the other two frames (**Table 7.2**). From a technical point of view, consumers discussed the biodegradability or compostability of alternatives, which needs development ( $C = 0.06$ ), whereas industry ( $C = 0.07$ ) and policymakers ( $C = 0.22$ ) focused mainly on the development required in recyclability (**Table 7.3**). Moreover, much more emphasis was put on the legal aspects of currently used plastics (citizen  $C = 0.06$ ; NGO  $C = 0.11$ ; policymaker  $C = 0.12$ ), and this should stimulate the transition toward a circular economy, as well as the required change in consumer behaviour (citizen  $C = 0.06$ ; NGO  $C = 0.08$ ) (**Table 7.3**). It is noteworthy that there was not a high co-occurrence of scientists and the argument 'management should change' ( $C = 0.09$ ) in academic journals (**Table 7.3**;  $C = 0.02$ ).

### 7.5.2.3 *Futurity framing of plastics in a circular economy: plastics have a place*

An optimistic tone of voice was observed when actors were envisioning plastics as part of a future circular economy. The role ascribed to plastics in the future was remarkable; all actors agreed that plastics are important and will be part of a future circular economy: "*The question, therefore, is not whether plastics have a place in a circular future, but what that place may be, both for conventional plastics and bioplastics*" [306].

#### *Academic journals: innovating plastic forms*

In academic journals, mostly consumers, journalists, and scientists framed plastics as part of a circular economy (**Table 7.2**). They framed plastics as materials with better technical properties (consumer  $C = 0.10$ ; journalist  $C = 0.12$ ; scientists  $C = 0.05$ ) simultaneously being biobased (consumer  $C = 0.07$ ) and having a low environmental footprint (consumer  $C = 0.17$ ; journalist  $C = 0.08$ ) (**Table 7.3**). "*PBS is a biodegradable aliphatic polyester with properties that are comparable to polypropylene*" [306].

#### *Newspapers: closing the loop*

In newspapers, the actors industry, journalists, and scientists mostly framed plastics as part of a circular plastic economy (**Table 7.2**). Whereas academic journals highlighted mostly the alternative forms of plastics, newspapers focused mostly on closing the loop for traditional plastics in a circular economy; the material was not considered as end-of-life waste but rather as a resource. This is an interesting note, as these are visuals of a future that has yet to be

realized. As Speksnijder states: “*When you consider how much we still depend on fossil resources, we still have a long way to go before we have fully replaced them with sustainable alternatives*” [307].

### 7.5.3 The role of different plastics in a circular economy

This section presents a more detailed analysis of how plastics were labelled within different futurity frames (**Figure 7.4**).

Remarkably, many labels that were often framed as part of a linear economy were also frequently framed as materials that are in transition or even part of a circular economy. These labels included ‘plastics’, ‘synthetic material’, and ‘polymer’. Interestingly, these are all terms to describe the material in general, although there are small nuances. The label ‘polymer’, for instance, often refers to the molecular structure, the name ‘synthetic material’ refers to a material that can be produced by mankind, and the term ‘plastic’ is a more general term to describe the material itself. When framed as part of a linear economy, the issues related to the linearity of plastics were mostly emphasized, accompanied by a seemingly negative tone of voice. When these labels were used in the transition or circular economy frame, the tone of voice appeared optimistic and the actors framed plastics in a new light. The label ‘microplastic’, often referring to plastic materials with a size 1–1000  $\mu\text{m}$  and not to a specific plastic type, was the only label that co-occurred highly only with the linear economy frame (academic journals and newspapers  $C = 0.07$ ) where actors highlighted the consequences of microplastics for the environment and animal welfare.

The role of different plastics reflected mostly the envisioned circular economy presented in the two sources. For instance, in newspapers, PET – a synthetic polymer produced from fossil resources and non-biodegradable – was strongly associated with the circular economy frame ( $C = 0.12$ ), because of its good recyclability. In academic journals, a much lower co-occurrence was found ( $C = 0.06$ ), because the term ‘recycled plastics’ was often expressed as a material that was not there yet ( $C = 0.09$ ) rather than a material corresponding to a circular economy ( $C = 0.05$ ) (**Figure 7.4**): “... *is the loss of strength in the material as a result of the recycling process, [...], inherently weakening the final product. This means that typically, recycled PET cannot be used on its own to produce new bottles or packaging*

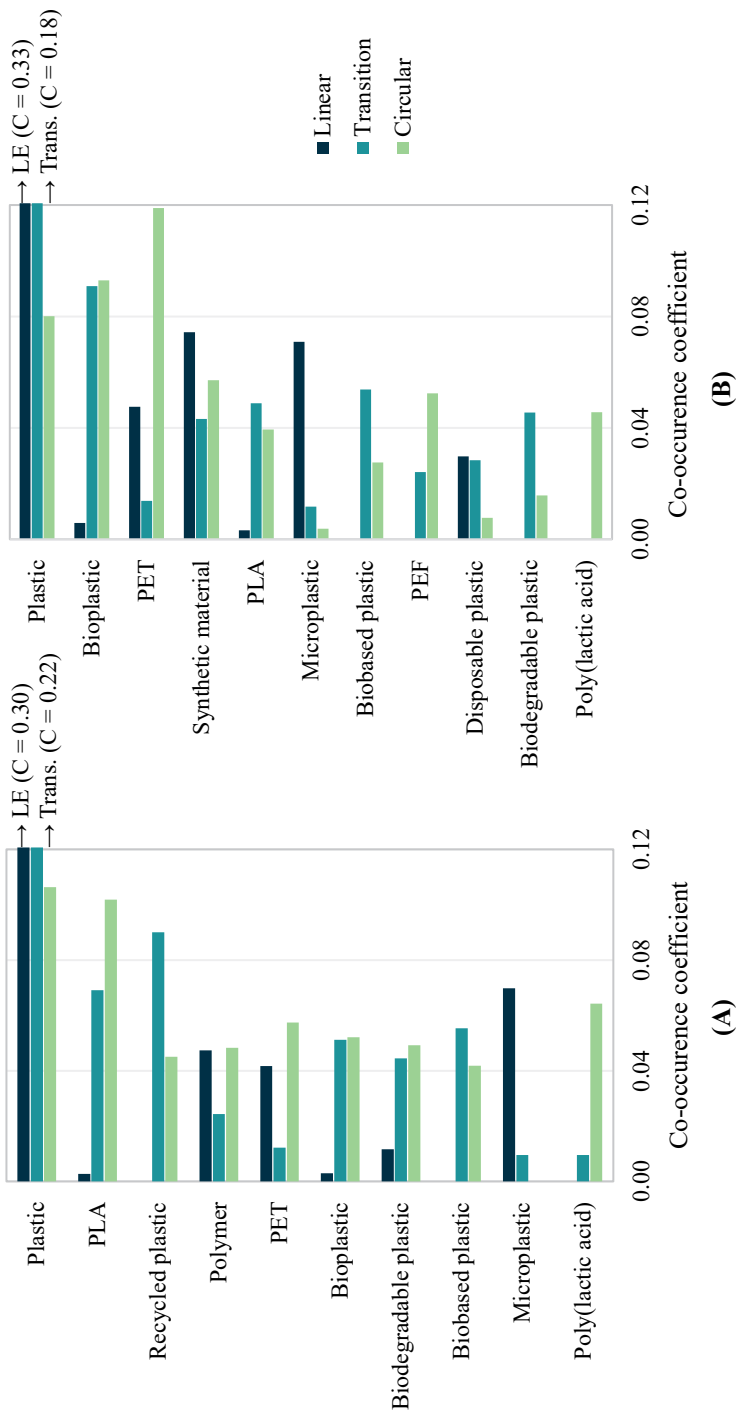


**Figure 7.4:** Co-occurrence coefficient of most used names and frames in (A) academic journals and (B) newspapers. When no bar is visible, the label does not co-occur with a frame. Note: The label 'plastic' continues beyond the boundary of the figure, a maximum value for frame 'linear economy' is  $C = 0.30$  for journals and  $C = 0.33$  for newspapers and, for the frame 'transition from circular to linear economy', the value is  $C = 0.22$  in academic journals and  $C = 0.18$  in newspapers.

*but requires blending with virgin material to achieve the same performance” [308].*

Mostly alternative forms of plastics were framed as part of a circular economy in academic journals. This is nicely demonstrated by the label ‘polylactic acid’ (PLA), which is a biobased polymer that can be composted under industrial composting conditions. In academic journals, this plastic was strongly associated with a circular economy (**Figure 7.4**;  $C = 0.11$ ) because of the combination of its biobased and compostable nature as well as its good technical properties. As stated: *“Among biopolymers, polylactic acid (PLA) is one of the most used compostable, biobased polymeric matrixes, since it exhibits processability and mechanical properties comparable with a wide range of applications” [309].* A much lower co-occurrence was found in newspapers (**Figure 7.4**;  $C = 0.04$ ), where more emphasis was put on the recycling of plastics. This is less evident for the label ‘bioplastics’. Observations indicated that academic actors used PLA in their research as an example of bioplastics, and the fact that PLA is commonly considered the most promising bioplastic [299] could be an easy explanation for the high co-occurrence found for the label ‘PLA’ but not necessarily for the label ‘bioplastics’.

Thus, the expected role of a circular plastic does not depend solely on its properties but rather on actors’ vision in regard to the economy. In fact, a specific type of plastic was often framed in multiple ways. For instance PET, which was framed as part of a linear economy: *“causes relatively high environmental impacts at primary production” [310]*, but also as part of a circular economy: *“Using renewable feedstock to produce PET will reduce dependence on petro-based resources, reduce carbon emission, and contribute to a circular economy” [311].*

## **7.6 Discussion**

This chapter elaborated on the role of the futurity framing of plastics in a transition to a circular economy. The framing of plastics in three different future visions was explored: a linear economy, a circular economy, and a transitions vision. This section presents a discussion on how the results contribute to the governance of, and the public debate about, transitions; plastic packaging for food purposes plays an important role in this transition and we therefore also elaborate on that.

First, the results indicate that all sorts of actors, as quoted in traditional media and academic sources, envision a role for plastics in a circular economy, but they also emphasize that the current linear use of plastics is troublesome and that a transition is needed. Second and remarkably, the current research clearly identified two competing roles for plastics in a circular economy. In academic sources, there was a focus on alternative forms of plastic for a circular and biobased economy. In newspapers, the reporting related mainly to closing the loop for traditional plastics<sup>4</sup>. There seemed to be two different ‘worlds of meaning’: one in which developing biobased and biodegradable forms of plastic is most important to reach circularity; and one in which closing the loop for fossil-based plastics is the main strategy. One option seems relatively invisible in both sources: a combination in which biobased resources are used for bioplastic production and bioplastics are recycled after usage. Practically, this means that the opportunities seen in academic journals to develop alternative forms of plastics in a circular economy could be reported on in newspapers in order to reach a larger public, and vice versa: academics need to be aware that the recycling of traditional plastics is paramount for governmental, industry, and other societal actors. Additionally, in pursuing possibilities to recycle biodegradable plastics, academics, governmental actors, and others need to collaborate to make recycling policies, behaviour, and techniques compatible with alternative forms of plastics.

Third, the results indicate that within the transition futurity frame, both in academic and in newspaper sources, the necessary processes and steps to achieve a circular economy are central. In this futurity frame, industry, academics, policymakers, and NGOs envisioned specific tasks for their sectors to contribute to a more circular economy, and they all have expectations about citizens and consumers changing their behaviour. The collection, separation, and recycling of waste by consumers are considered crucial for achieving circularity. However, in the traditional media reporting and academic studies analyzed, the voice of citizens and consumers was underrepresented. Other studies have shown that consumers are generally aware of the environmental issues that plastic waste and production are causing [312]. They even agree that behavioural solutions are required [312,313].

---

<sup>4</sup> The different roles ascribed to plastics labels co-occurred with the type of future vision for the plastic economy rather than with the properties of that specific plastic itself.

Interestingly, a study among German consumers showed that consumers seem to be more attracted to bioplastics, which are compostable, rather than to recyclable fossil-based plastics. However, this was not translated into proper disposal behaviour to make full use of the environmental benefits of either compostable or recyclable packages [314]. Potentially, this can be explained by the complexity of the various compostable bioplastics labels, which can be misleading or confusing. Although these studies provide insight into consumers' attitudes and behaviour with respect to plastics, more in-depth knowledge about how citizens and consumers envision the role of plastics in the future would be a welcome input for the development of a more realistic and practical redesign of circular plastic food packaging, reuse, collecting, separating, and recycling systems. Such studies may also make visible alternative imaginaries [286], for instance, the existing package-free supermarkets where consumers reuse their own packaging [315] or edible food packages where the package is considered as food [316].

Lastly, the current study was rather exploratory in nature, but it took a first step in the direction of understanding futurity framing and the roles of materials in it. In contrast to other studies, this study enabled a reflection on the futurity framings of materials – in our case plastics – in two different type of sources, opening up the possibility to explore new strategies for governmental actors, industry, academics, and other societal actors [317,318]. This is important, because our study has indicated that current research focuses mainly on alternative forms of plastics and that recycling systems are mainly geared toward recycling traditional plastics [319]. This exclusivity may eventually limit the possibilities and benefits gained by recycling traditional plastics. Additional research could lead to possible solutions and different interpretations for our future biobased and circular plastic economy. Although clear differences were found in the futurity framing used by the identified actors, other factors such as background, education, or norms and values might be more important. More detailed analysis of co-occurrences of arguments, storylines, and labels could identify this.

Furthermore, it is worth pointing out that whether actors frame consciously or unconsciously cannot be concluded from our study. Interviews could reveal how and why different actors communicate about plastics in a certain way, thereby providing more insights into how these materials are framed. Additionally, although our research nicely demonstrates differences

between plastic framing in scientific journals and newspapers, it must be kept in mind that both sources are written for different audiences and purposes. Moreover, outcomes could potentially be different if newspaper articles from countries other than the Netherlands are included.

## **7.7 Conclusions**

This research distinguished three futurity frames: plastics are part of a linear economy, plastics are in transition toward a circular economy, and plastics are part of a circular economy. The linear economy futurity frame focuses on today's issues with plastic, emphasizing its non-biodegradability, non-compostability, or non-recyclability. The vision for a transition toward a circular economy framed plastic as requiring improved material properties – such as improved recyclability and compostability – and emphasized the processes and steps needed for change: a change in consumer behaviour, social structures, and waste management systems. In the envisioning of a circular economy, academic papers focused mainly on alternative forms of plastic, and in newspapers the reporting related mainly to closing the loop for traditional forms of plastic. In both sources, the quoted actors framed plastics as important and as part of a future circular economy. Interestingly, the role of plastics in this future circular economy was framed positively. This is a good sign, as positive images of the future trigger action, which is urgently needed. In light of that, an opportunity is seen to combine the framing of a need to develop alternative biobased and biodegradable forms of plastics with recycling. The further development of this future vision of recyclable bioplastics and biodegradable plastics by industry, academics, governments, and NGOs, including citizens, may contribute to a more fully biobased plastic and circular economy.



---

# 8

## General Discussion

---

# Introduction

Today, we are running a race against the clock that humanity cannot afford to lose. Various industries – including the plastics industry – need urgent transition toward circularity. Within this thesis, we discussed the possibility of thermoplastic (bio)nanocomposites as advanced materials that fit within this concept. We aimed to investigate and characterize the multiscale physical and chemical properties of nanoparticles and nanoparticle – reinforced plastics that are needed to transition toward a (more) circular economy.

It is well-established that the structure and dynamics of the interphasial region are crucial for nanocomposite characteristics. However, the translation from fundamental insights at the molecular scale, to their consequences on macro- and bulk scale is difficult to capture; a multidisciplinary approach is required to connect these insights and get the whole picture. Unfortunately, nanocomposite understanding and design are often seen as individual fields, whereas these should be – in our humble opinion – considered as an interwoven effort to improve materials far beyond what is currently possible.

Within this general discussion, we provide a route from fundamental insights to the rational design of nanocomposite systems (**Figure 8.1**). We start with a summary of events occurring at the molecular scale (**section 8.1.1**), where our results highlight that nanoparticle dispersion is crucial at nanoscale and beyond (**section 8.1.2**). The section thereafter is dedicated to particle interactions that are relevant to prevent aggregation from equilibrium and kinetic points of view (**section 8.2**). We take learnings from the previous two sections and give guidelines for bio-nanocomposite design, which includes additional functionality that can be created (**section 8.3**). We finish with an outlook on if, and how, bio-nanocomposites are expected to find a place in a circular economy (**section 8.4**).

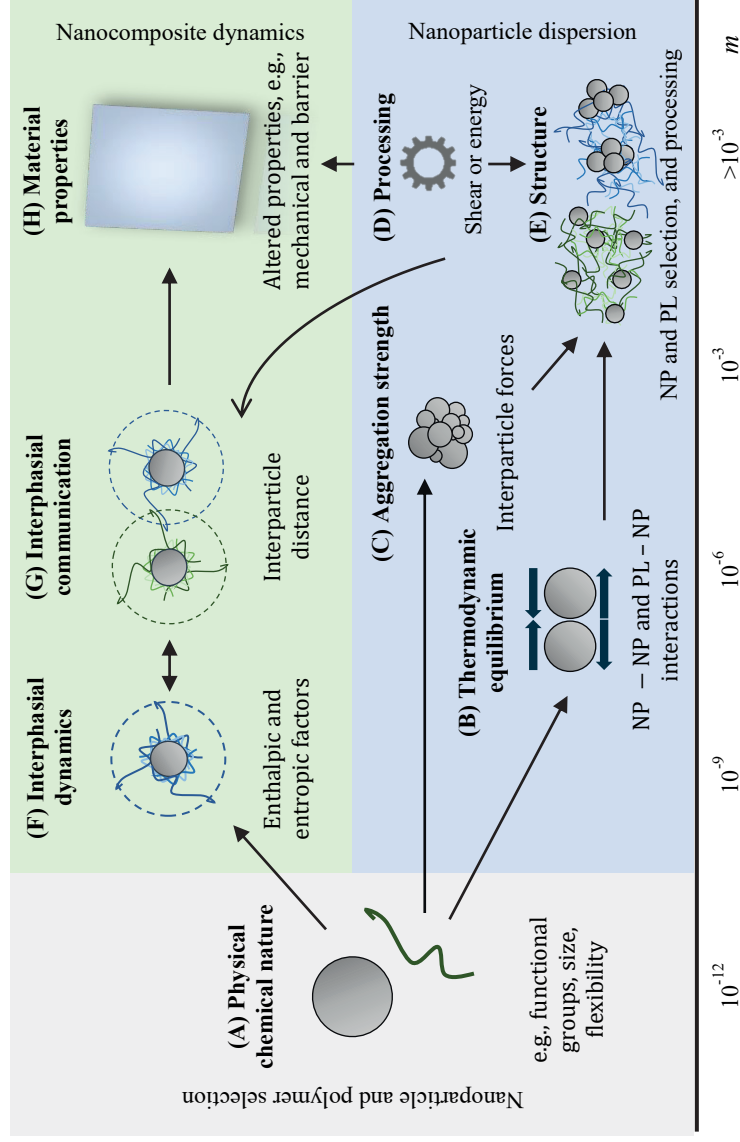


**Figure 8.1:** (A) The physical chemical nature of the nanoparticle and polymer determine (B) the thermodynamic equilibrium of the system, (C) and interparticle forces determine the aggregate strength. (D) Applied shear forces bring the system in a new equilibrium, (E) resulting in the final nanocomposite structure. In addition, the physical chemical nature of the polymer and the nanoparticle affect (F) interphal dynamics and depending on the interparticle distance (G) different interphal layers can communicate (H) resulting in materials with altered properties compared to the neat polymer.

## 8.1 Nanoparticle–polymer interactions: structure and dynamics

### 8.1.1 Interphasial region – enthalpic and entropic effects

It is widely accepted that the enhanced material properties of nanocomposites are the consequence of altered polymer dynamics near the interface of the particle [56,191,192]. The interphasial region is generally estimated to extend 1.5 – 9.0 nm from the particle surface [118,191–193], which seems in line with our modelling results from **Chapter 3**. In **Chapter 4** we showed that interphasial relaxation in the interphasial region can be up to  $10^3$  seconds, which was  $\sim 100$  times longer than that of the neat polymer. This implies that nanoparticles constrain local dynamics, and effectively play the role of long-lived physical crosslinks. Although the relevance of the interphasial region is acknowledged, its architecture and dynamics are still poorly understood.

A continuous interplay between enthalpic and entropic contributions determines if and how polymer segments adsorb at the nanoparticle surface (**Figure 8.2**). In essence, the enthalpic factor describes the nanoparticle - polymer affinity [56,190]. Attractive nanoparticle – polymer interactions increase the polymer density at the nanoparticle interface (**Chapter 3**), and consequently reduce the polymer’s segmental dynamics, while weakly attractive or repulsive nanoparticle – polymer interactions decrease polymer density and increase segmental dynamics. The enthalpic factor is rather well understood, and quantified by the interaction strength ( $\epsilon$ ) in the Lennard Jones potential used in molecular dynamics simulations [75,320] (**Chapter 3**), the work of adhesion ( $W_a$ ) between the nanoparticle and polymer measured in practice (**Chapter 2 & Chapter 3**) [65,184,321], or by calculating, e.g., the number of hydrogen or covalent bonds [210].

In our simulations we did not find a great difference in the enthalpy between systems (**Chapter 3**), and entropic contributions are possibly more important as generally assumed. The entropic component dictates the conformation of free chains near the nanoparticle surface; for instance, the polymers experience an entropic penalty when the interparticle distance is small [212]. Metaphorically speaking, it simply gets ‘too crowded’. As a consequence, the polymer density at the interface decreases, and the reduction in dynamics is less than may be expected. The entropic factor is rather difficult to quantify, and its effect on interphasial structure and dynamics thus difficult to predict.

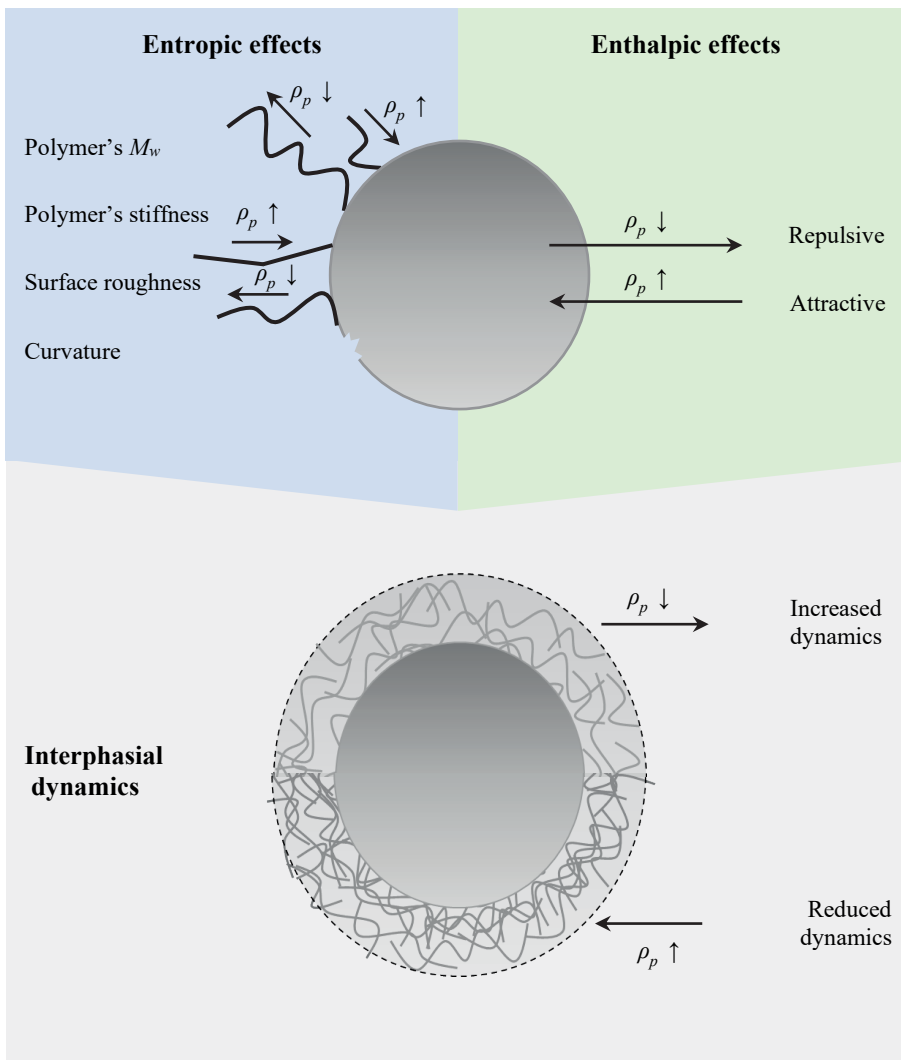


**Figure 8.2:** Entropic and enthalpic factors that reduce or increase the polymer density at the nanoparticle surface ( $\rho_p$ ) which has been related to interphasial dynamics.

The overall conclusion is that the polymer density at the nanoparticle's interface needs to be maximized in order to minimize segmental relaxations in the interphasial region. Potential routes to do so are surface modification (altering the enthalpic factor) or polymer grafting (entropic factor) (**Chapter 6** & [190]), which we further discuss in **section 8.3.4** and directly relate to material properties.

For the development of biobased systems, it is important to keep in mind that nanoparticles may have widely differing shapes and sizes including the chitin nanocrystals used in this thesis (**Chapter 5 & Chapter 6**). To which extent polymers experience chain frustration has been related to nanoparticle surface chemistry, curvature (related to size and geometry), and roughness, although their actual effect is rather unknown [56]. Additionally, the presence of abundant hydroxyl groups in, e.g., chitin [51] complicates the matter further; adsorption of polymer segments is highly dependent on the activation energy of the hydrogen bonds ( $k_b T$ ), and the polymer's attempt frequency related to the relaxation time of the polymer. Both factors are temperature dependent and thus affected by production conditions. Although, the interdependency of these factors still needs to be unravelled [56].

### 8.1.2 Nanoparticle dispersion as key parameter for nanocomposite design

Interphasial dynamics are commonly explained by events occurring at the interface of the nanoparticle (**section 8.1**). Remarkably, our results from **Chapter 3** and **Chapter 4** highlight that the overall dispersion state of the nanocomposite can greatly impact interphasial architecture (**Chapter 3**) and as such its relaxation time (**Chapter 4**); we visualize this in **Figure 8.3**.

On one hand, nanoparticle aggregation negatively impacts the build-up of the interphasial layer. In **Chapter 3** we used molecular dynamics simulations to investigate how nanoparticle – polymer interactions affect the overall and interphasial nanocomposite structure. At very low nanoparticle loadings where the nanoparticles did not physically touch (**Chapter 3**; **Figure 3.3**), the polymer density at the nanoparticle surface clearly increased upon increasing nanoparticle – polymer interactions. At higher loadings, an overall reduction in polymer density was observed in systems that started to aggregate, even for attractive nanoparticle - polymer interaction. This can be explained by part of the nanoparticle surface area becoming inaccessible for the polymer (**Figure 8.3**).

As reported in **Chapter 4**, PDMS coated nanoparticles showed substantially better dispersion states compared to PVP and PAA coated nanoparticles. At a nanoparticle loading of 5 wt. %, aggregated systems (PAA and PVP coating) increased  $\tau_0$  by a factor 10 whereas a factor 100 was found for well-dispersed systems (PDMS coating). Noteworthy was the independence of the relaxation time on the enthalpic component of the interaction; the work of adhesion

with PLA is 91.6, 87.4, and 54.3 mJ/m<sup>2</sup> for PAA, PVP, and PDMS, respectively. We speculated that individual interphasial layers can affect each other which is facilitated by favourable dispersion states. Reduced dynamics directly translated to a higher complex viscosity which is a thought-provoking indication that dispersion is more important than maximizing the interaction force between the nanoparticle and polymer.

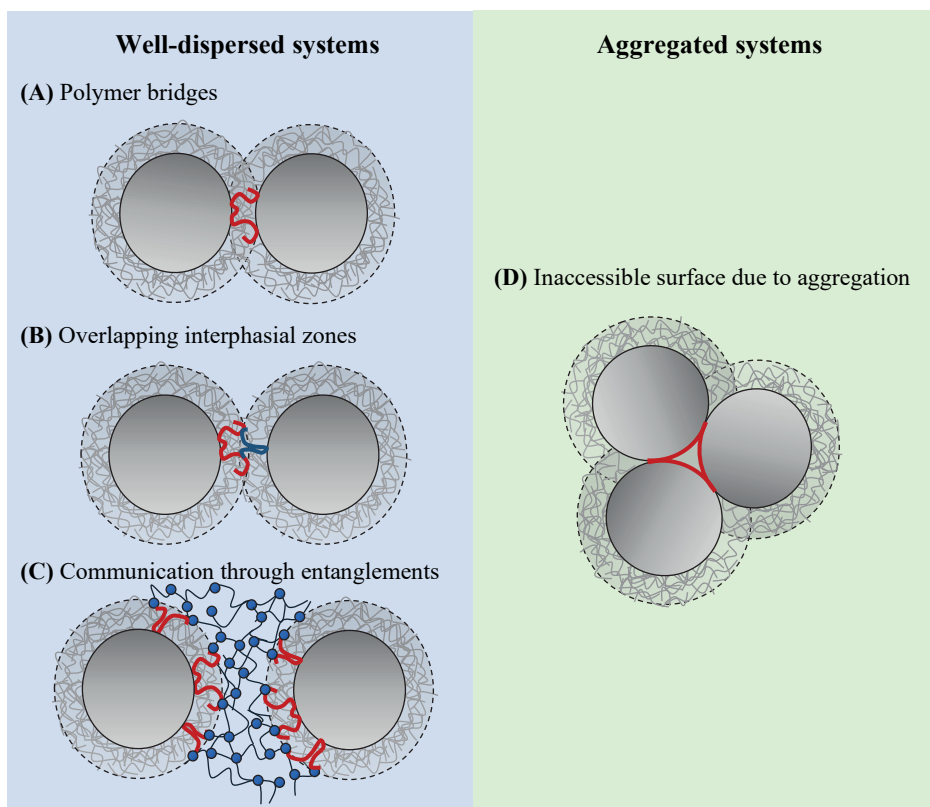


**Figure 8.3:** In well-dispersed systems, individual interphasial regions can affect each other, this potentially happens via (A) polymer bridges where a single polymer string (indicated in red) is attached to multiple nanoparticles (B) overlapping interphasial zones, where adsorbed polymers of different nanoparticles (indicated in blue and red) can interact (C) through entangled polymers, nanoparticles can possibly interact with polymers (indicated in black) beyond the adsorbed layer (indicated in red) via entanglement points (indicated as blue dots). In aggregated systems (D) part of the interphase becomes inaccessible automatically reducing the overall polymer density, and hindering interphasial communication.

How individual interphasial layers interact is not really known, although several hypotheses exist which we illustrate in **Figure 8.3**:

- The formation of polymer bridges between nanoparticles (**Chapter 3** & [57,185,322]), which can eventually form a strong nanoparticle network.
- Overlapping interphasial layers [184].
- In case applicable, polymer entanglement allows interactions with polymers beyond the directly adsorbed layer [210].

To be complete, the effect of nanoparticle dispersion on interphasial dynamics has long been a blind spot, and through the work in this thesis we have shed some light on this. Current knowledge of the interphase is mostly based on molecular dynamics simulations (**Chapter 3** and [56,191]), and advanced techniques such as neutron spin echo spectroscopy (NSE) or quasi-elastic neutron scattering (QENS) [56,323,324]. The latter require well-dispersed systems because heterogeneity largely complicates data analysis [199]. Ironically, in most systems, some degree of nanoparticle aggregation seems unpreventable when using conventional methods such as melt mixing (**Chapter 6**) or solvent casting (**Chapter 4**); this inevitably has a negative effect on data gathered, and obscures their interpretation. Techniques such as laser speckle imaging (LSI) [200–204] allow distinguishing these effects, and bring phenomena such as multiscale interaction and the importance of nanoparticle dispersion to light (**Chapter 4**).

Yet, the translation from interphasial properties to bulk characteristics is extremely challenging, especially as the empirical observation of the interphasial structure is virtually inaccessible. To unravel such events, molecular dynamics simulations can be used to systematically vary and understand the effect of parameters (**Chapter 3**). The choice of a simulation method, e.g., quantum, molecular dynamics, mesoscopic, or finite element, largely depends on the time scales of the phenomena of interest [176]. It is expected that the interphasial region largely affects bulk scale properties, and ideally simulation techniques should also cover larger time scales. Unfortunately, today, the computation expense to do so is still rather high. Alternatively, multiscale simulations could be interesting to answer how interphasial events are translated to the bulk.

In brief, we conclude that the overall nanoparticle dispersion state determines if and how interphasial layers interact and influence interphasial dynamics. It is a key parameter for nanocomposite design, and therefore we focus on the design of homogenous nanocomposites in the next section.

## 8.2 Thermodynamic and kinetic routes for nanoparticle dispersion

### 8.2.1 Nanoparticle dispersion and aggregation

Nanocomposite design often follows a rather trial-and-error approach, despite the various theoretical frameworks available to prevent nanoparticle aggregation. In **Chapter 2** we discussed these frameworks, which show that nanoparticle aggregation is mostly governed by two factors:

- The work of adhesion between the nanoparticle and the polymer:  $W_a$  (a.k.a.  $W_{PF}$ ).
- The work of cohesion between the nanoparticles themselves:  $W_c$  (a.k.a.  $W_{FF}$ ).

When  $W_a/W_c > 1$ , nanoparticle dispersion is favoured whereas at  $W_a/W_c < 1$  aggregation is favoured. This clearly goes beyond the ‘like-dissolves-like’ approach that is commonly used in engineering fields. In fact, according to the dispersibility factor, the interparticle forces ( $W_c$ ) are equally important as the interaction forces between the nanoparticle and the polymer ( $W_a$ ), but unfortunately often not considered in practice.

To be complete,  $W_a$  and  $W_c$  can be calculated using surface energies derived from contact angle measurements. As the contact angle is sensitive to many effects including surface roughness and heterogeneity [325,326], some experts in the field question whether experimental values should be used as a basis to calculate surface energies [325]. Currently, methods are being developed to measure the most-stable-contact-angle, which is the angle believed to be closest to thermodynamic equilibrium [325,326]; complementary tools have been used, e.g., reviewed by Kung et al. [327]. Despite the uncertainty in  $W_a/W_c$ , this factor could describe the dispersibility of TiO<sub>2</sub> nanoparticles with different coatings in PLA (**Chapter 4**). Likewise, in **Chapter 6**, chitin nanocrystals modified with octanoic acid ( $W_a/W_c \sim 0.80$ ; **Appendix 8-1**) dispersed better in PLA compared to unmodified chitin nanocrystals ( $W_a/W_c \sim 0.64$ ; **Appendix 8-1**). From this we conclude that, in practice, frameworks that use  $W_a/W_c$  are the best tools currently available for nanocomposite design

[65,102,170,184]. From a scientific point of view techniques to quantify interaction strengths or simply hydrophobicity/hydrophilicity of different materials would be needed to make a next step. For nanocomposites specifically, ideally, these techniques allow the evaluation of heterogeneous samples over a wide temperature range as is relevant in practice during production and storage.

### 8.2.2 Aggregate strength

In **Chapter 6** we used Steglich esterification with fatty acids to increase the hydrophobicity of chitin nanocrystals. Despite that surface modification improved the dispersibility of chitin nanocrystals in PLA [172], it cannot be ignored that aggregates of a substantial size (up to  $\sim 50 \mu\text{m}$ ) were present (**Figure 6.5; Chapter 6**). This is a common observation, especially when nanoparticles are dried to, e.g., reduce transport costs. Depending on interactions between nanoparticles these aggregates can be very strong. Polysaccharide nanocrystals (such as cellulose or chitin) possess abundant hydroxyl groups that form strong hydrogen bonds. In **Chapter 5** we have shown that a sonication energy input  $> 100 \text{ kJ/g}$  ChNC was required to break up freeze dried chitin nanocrystal aggregates when redispersed in Milli-Q water [54]. This exceeds the energy input generated by common extrusion processes and hampers the application of dried particles. Surface modification on the other hand seems an effective method to reduce aggregate strength by affecting  $W_c/W_a$  (**Chapter 6**).

Predicting the aggregation tendency of nanoparticles is not trivial as many phenomena may occur that either favour or oppose aggregation [328]. For instance, nanoparticle aggregation can be promoted through nanoparticle surface charge reduction upon drying, while nanoparticle aggregates may be partly broken up by the mechanical stress induced by crystal formation during freeze drying [328,329].

In principle, the DLVO theory [330,331] can be a basis to understand nanoparticle aggregation under various conditions including drying [332,333]. For practical systems, it is advisable to include surface heterogeneity, hydration forces, hydrophobic interactions, steric, and Helfrich repulsion [328,332], which is far from simple. Extended DLVO models have been suggested, although it can be very difficult to quantify parameters, due to small size, variable geometry, roughness, and possibly grafted molecules [332]. Considerable efforts are currently made to cover conditions relevant to the pharma, paint, and food industries.

### 8.2.3 The role of processing on nanoparticle dispersion

In industry, melt mixing is by far the most commonly used technique for plastic processing, meaning that the applied shear forces can potentially facilitate nanoparticle dispersion. It allows dispersion of nanoparticles in a rather cheap and easy way based on kinetics (processing). Theoretically, two energy barriers need to be overcome:

- The thermodynamic equilibrium related to  $W_a/W_c$ .
- A certain aggregate strength (when nanoparticles are not individually added).

In **Chapter 2** we discussed processing to facilitate nanoparticle dispersion. Shear forces can decrease the nanoparticle aggregate size [84,108]. Some studies suggest that  $W_a/W_c$  determines which break-up mechanism occurs in addition to the thermodynamic equilibrium [102,321]. In **Figure 8.4** we illustrate that for favourable nanoparticle – polymer interactions rupture dominates, which is facilitated by polymer infiltration in the aggregate pores, thus reducing cohesion strength [321] (**Chapter 2; equation (2-8)**). The pore sizes play an important role in this, which may - to some extent - be tailored by using different drying techniques. For instance, spray dried cellulose nanocrystals required less energy to break up compared to freeze dried nanoparticles due to a difference in porosity [51,87,334]. However, for unfavourable nanoparticle – polymer interactions, erosion dominates or may not even be possible without compromising the polymer.

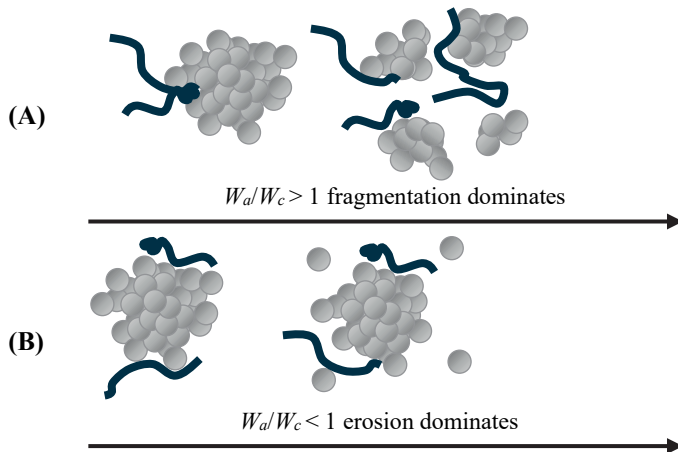


**Figure 8.4:** Depending on the magnitude of interaction forces between the nanoparticle and polymer ( $W_{PF}$ ) and interaction forces between nanoparticles ( $W_{FF}$ ) (A) fragmentation or (B) erosion dominates.

This emphasizes the importance of matching the nanoparticle's surface chemistry to that of the polymer. With regard to chitin nanocrystals, its interaction forces are likely so high that disaggregation is not possible without compromising the polymer, i.e., degradation (**Chapter 5**). Surface modification such as performed in **Chapter 6** or discussed elsewhere [53,254,335,336] can be used to improve compatibility.

In the last decade, quite some advances have been made in understanding the effect of parameters – such as  $W_{FP}/W_{FF}$  and aggregation strength – on the final dispersion state of nanocomposites also under non-equilibrium conditions. However, models that accurately describe these effects are largely missing, or need additional fitting parameters. To illustrate this, Hassinger et al., [102] used data mining techniques to derive a mathematical expression that describes the final dispersion state of nanocomposites under non-equilibrium conditions:

$$\bar{I}_{filler} = f(matrix) \sinh^2 \left( \frac{2W_{PF}}{W_{FF}} - 1 \right) \log(E_y + 1) + C_0 \quad (8-1)$$

To reach a satisfactory description, an additional parameter  $f(matrix)$  needed to be introduced. Whereas the authors hypothesized that  $f(matrix)$  describes the mobility and crystallinity of the polymer matrix, alternative explanations are possible. Most theoretical frameworks correctly describe tendencies such as nanoparticle aggregation, but they do not provide information on the time scales at which these processes take place. This is quite crucial, as thermodynamic and kinetic effects dominate at different time scales and result in different materials.

### 8.3 Toward rational design of practical bio-nanocomposites

To make an impact beyond the scientific community, it is relevant to ask how nanocomposite architecture and dynamics affect material properties. In this section, we aim to translate fundamental insights – mostly investigated at the nano/microscale – to practical applications. We pay special attention to polysaccharide nanocrystals derived from cellulose, starch, and chitin, because these are abundantly present in nature, and ideal candidates for the production of bio-nanocomposites that fit a circular plastics economy (**Chapter 1; section 1.3**).

### 8.3.1 Mechanical properties

Improved mechanical and viscoelastic properties of nanocomposites compared to the base polymer are probably the most reported effects, although it is rather unknown how this can be the result of interphasial properties that translate into bulk behaviour. In the most general form, it is often argued that – due to the small size of the nanoparticles – the total interphasial region is already large at low nanoparticle loading [56,184]. **Figure 8.5** shows the critical loading required (in volume %) to create a material fully consisting of nanoparticles and their corresponding interphasial layers. Yet, for the interphasial layer to correspond to the whole material, a substantial amount of nanoparticles would be needed and it is questionable whether this is the case for the nanocomposites made in this thesis (e.g., **Chapter 4** & **Chapter 6**).

An alternative explanation for improved material properties is the formation of a percolation network, i.e., a three-dimensional network in which nanoparticles are connected [175]. It has been suggested that strong polysaccharide nanocrystals (cellulose nanocrystals  $\sim 7.5$  GPa [337]) result in a network connected through hydrogen bonds [338], leading to a stronger material. However, this hypothesis has been contested [339]. For regular dimensions of polysaccharide nanocrystals (diameter 5 – 20 nm, and length 100 – 400 nm), a concentration

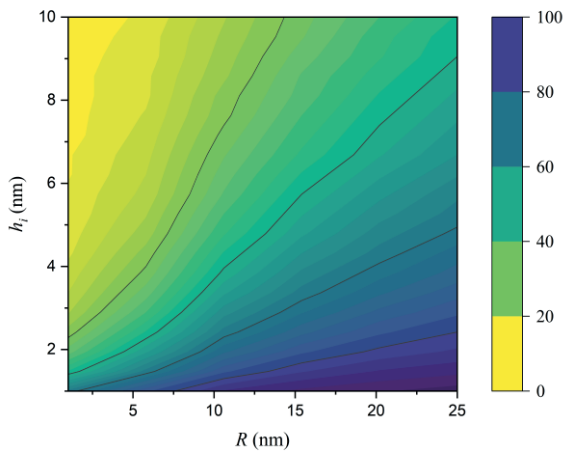


**Figure 8.5:** Critical nanoparticle loading (vol %) required to create a material fully consisting of nanoparticles and its corresponding interphasial layer. This is determined for various nanoparticle radii ( $R$ ) and interphasial thicknesses ( $h_i$ ).

of  $\sim 5$  vol. % would be required for network formation [340]. Higher values have been reported for spherical nanoparticles (theoretical percolation threshold  $\sim 16$  vol % [341]).

Although both the interphasial volume as such and the occurrence of a percolation network carry interesting elements, we feel that it is not for nothing these theories fail to accurately describe experimental data [339]. Others have suggested that the interphasial layer should be taken into account in the percolation theory, i.e., nanoparticles are connected through their interphasial layers [342,343]. As discussed in **section 8.1.2** this can potentially happen via overlapping interphasial zones, polymer bridges [344], or via entanglements (**Figure 8.3**). These pseudo-percolation networks have a lower percolation threshold than the ‘original’ ones depending on the interphasial thickness and nanoparticle size considered. For instance, Chen et al. [57] used a percolation model where nanoparticles were linked by polymer bridges, and the surrounding polymer was affected by hydrodynamic interactions. In that way, they were able to fairly well predict the linear viscoelastic response of the polymer nanocomposites consisting of silica particles in P2VP. Through the work in **Chapter 4**, the link to interphasial relaxation times has become within reach.

To be complete, other phenomena may occur at substantially higher nanoparticle loadings. For instance, for entangled polymers, molecular dynamics simulations have suggested that the addition of nanoparticles decreases the tube diameter through geometric constraints.

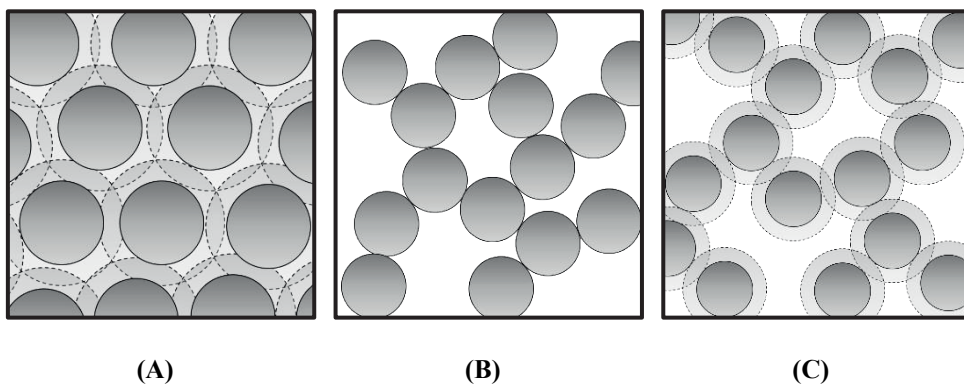


**Figure 8.6:** Several hypotheses exist to explain enhanced mechanical properties including (A) a composite where most of the material exists of the interphasial region (B) the formation of a percolation network where nanoparticles are in direct contact (C) the formation of a pseudo-percolation network in which interphasial zones affect each other.

Thereby they effectively increase the entanglement density, giving rise to a reinforcing effect that increases with specific surface area [345]; rather high nanoparticle loadings ( $> 30\%$ ) are required, which is quite far beyond the amounts used in our study, and used in practice (commonly  $\leq 5$  wt. %).

Although the exact mechanism behind the reinforcing effect of nanoparticle addition remains unclear, the altered bulk properties directly affect material processability. At temperatures exceeding the glass transition temperature, generally, attractive nanoparticle – polymer interactions result in a substantial increase in viscosity (**Chapter 4**), which is also reported for polysaccharide-filled polymers [55,334,346]. An altered melt flow viscosity can improve or worsen the processability of a material and directly influence the choice of processing method, e.g., extrusion or injection moulding. In general, at temperatures below  $T_g$ , nanoparticles improve mechanical strength compared to the base polymer as extensively reviewed [51,347].

### 8.3.2 Thermal properties

Nanoparticle addition alters segmental dynamics and thereby directly the material's thermal profile. Our results from **Chapter 3** illustrate that  $T_g$  increases in the case of attractive nanoparticle – polymer interactions and decreases when the nanoparticle – polymer interaction is very poor (**Chapter 3; Figure 3.2**). Experimentally, similar effects have been observed for various nanoparticles such as  $\text{TiO}_2$ ,  $\text{SiO}_2$ , or chitin nanocrystals [65,192,229,348,349], although generally the effect is rather small, i.e., max.  $\pm 5$  °C [65].

To be complete,  $T_g$  is defined as the temperature where relaxation times become infinitely slow [187,188], and is therefore not only an indication of altered material properties, but can also be used as a relatively easy tool to understand material dynamics at the Ångström scale [350]. However, the difference in  $T_g$  is commonly small and difficult to measure as it is within the error range of a DSC. For instance, our results in **Chapter 4** clearly show increased relaxation times upon nanoparticle addition, but no increase in  $T_g$ .

### 8.3.3 Barrier properties

Various studies – including **Chapter 6** – have shown improved barrier function (e.g., water vapour or oxygen) upon nanoparticle addition [194,351,352]. This reduction can easily be

50 – 70% depending on nanocomposite design and processing methods [194,351,352]. Classically, this is explained by an increased tortuous path, thus limiting diffusion (**Figure 8.7**). It is often suggested that nanocrystals or nano clays could be of interest as their geometry allows an even longer tortuous path (**Figure 8.7**), although it is good to keep in mind that in a 3D-network the actual pathlength may be rather shorter as presented in **Figure 8.7**, due to the smallest dimension of the particles. Several models exist that predict permeability of nanocomposites as reviewed by, e.g., [351,353].

The increase in a tortuous path often fails to describe the data [352]; for well-dispersed systems, a large part of the material consists of the interphasial region or is affected by the interphasial region provided that the nanoparticles are sufficiently present (**Chapter 4**). As this region possesses different properties as the base polymer it may explain differences in permeability. Furthermore, several nanoparticles including chitin and cellulose nanocrystals have shown nucleation effects in the polymers they were dispersed in [349,354–356], meaning that the overall crystallinity increases upon nanoparticle addition. These explanations are – in our humble opinion – quite valid but seem largely overlooked.

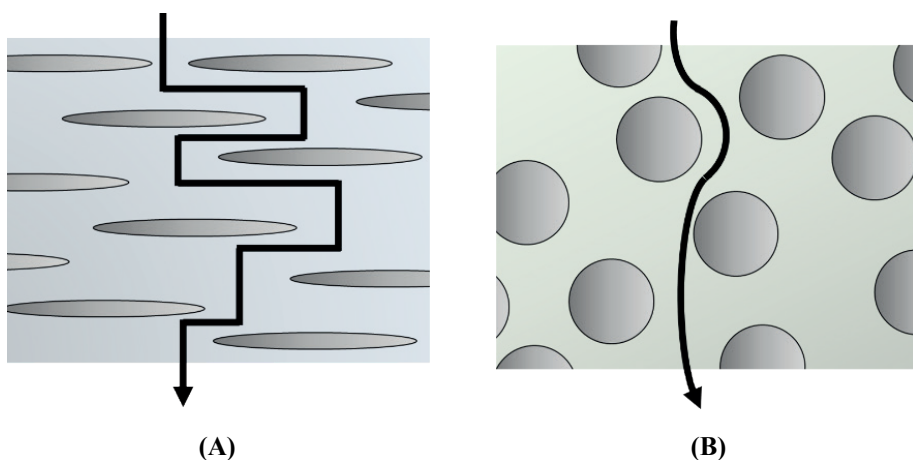


**Figure 8.7:** Needle shaped particles (A) are expected to provide superior barrier properties compared to sphere shaped particles (B) due to an increased tortuous diffusion path.

### 8.3.4 Directly linking nanocomposite dynamics to material properties

One obvious question remains unanswered: how can one finetune nanocomposites in such a way that desired material properties are created? Today, clear design models are missing, and as pointed out before, interphasial and overall nanocomposite architecture are interlinked and play a pivotal role in the final material properties:

- Nanoparticle – polymer interactions determine interphasial layer thickness and polymer density (**Chapter 3**).
- Nanoparticle dispersion determines if and how interphasial properties are translated to the bulk (**Chapter 2 & Chapter 4**).

Various routes can be considered which we schematically present in **Figure 8.8**. The following options generally reduce the polymer density in the interphasial layer, resulting in unaltered or even increased dynamics, which may decrease the mechanical strength, glass transition temperature, and increase permeability:

- Repulsive nanoparticle – polymer interactions (**Chapter 3**).
- Plasticizers are commonly added to facilitate nanoparticle dispersion [55,237]; which also tends to increase the overall dynamics.

The following routes generally increase the polymer density in the interphasial layer, resulting in reduced dynamics, which may increase mechanical strength and the glass transition temperature, and reduce permeability:

- Attractive nanoparticle – polymer interactions lead to increased polymer density at the interphase, as well as homogeneous nanoparticle dispersion in the polymer matrix (**Chapter 3**). This is commonly regarded as the ‘enthalpic route’ (**section 8.1.1 & 8.2**).
- Grafting with a low molecular weight molecule may improve nanoparticle dispersion. It is good to point out that it can also result in a localized plasticizing effect [346], thereby reducing the melt viscosity and/or mechanical properties.
- Grafting with a high molecular weight molecule may improve nanoparticle dispersion (**Chapter 6**), potentially through interaction with the surrounding polymer. This is commonly regarded as the ‘entropic route’ (**sections 8.1.1 & 8.2**).

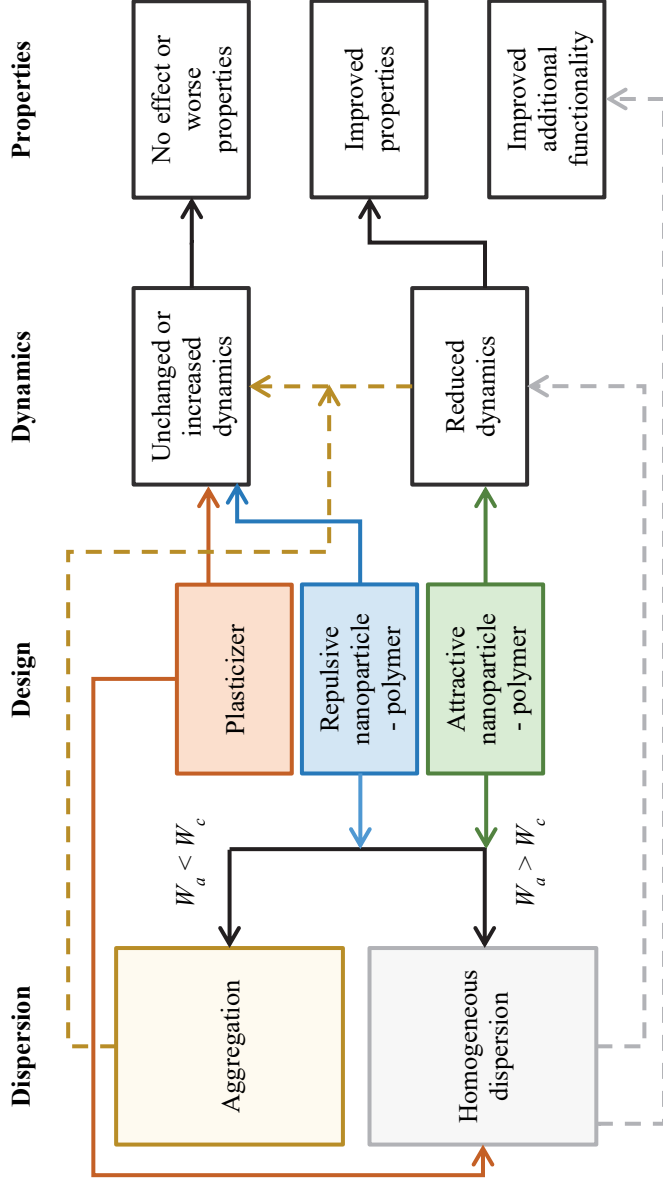


**Figure 8.8:** Design chart illustrating how design parameters are expected to affect material properties. Dispersion strategies include (A) compatibilizers (B) source selection and (C) surface modification. Homogeneous dispersion is expected when a plasticizer is used and  $W_a > W_c$ , whereas aggregation is expected when  $W_a < W_c$ . The dotted lines present the effect of the overall nanocomposite structure, on interphasial dynamics. Generally reduced dynamics are expected for surface modification and attractive nanoparticle – polymer interactions. Repulsive nanoparticle – polymer interactions and plasticizers increase interphasial dynamics.

The above expectations are based on information available in various fields. In reality, more factors determine the success or failure of materials. To illustrate, very fast crystallization is required for injection blowing of PET bottles, a factor that we have not covered here. To truly link interphasial dynamics to material properties, techniques are required that measure nanoscale dynamics during use and production.

In **Chapter 4**, we have shown the potential of laser speckle imaging (LSI), to investigate material dynamics in situ during solidification. The beauty of this technique is that it can be used during for instance a tensile test, or measurement of barrier properties (cup-test). In that way, nanoscale dynamics can be directly related to macro-/bulk dynamics, which accelerates the rational design of these materials. It is good to point out that tremendous amounts of data are produced during LSI measurements. Provided that the sample is homogeneous, this opens possibilities to use LSI in combination with artificial intelligence. The large data sets generated by LSI may in that way lead to reliable models and algorithms that predict large-scale properties that are currently either lacking or simply not considered good enough [186,357].

### **8.3.5 Additional features of nanocomposites**

Besides altering physical properties of polymers, the addition of nanoparticles also opens up the possibility to introduce additional features to existing polymers such as optical, antioxidant, or antimicrobial properties.

#### **8.3.5.1 Optical properties**

As a rule of thumb, the size of a particle needs to be smaller than the wavelength of visible light ( $\lambda = 300 - 500$  nm) to obtain transparent films, and for this dispersion of particles is of great relevance. It is even more challenging to obtain transparent films when polysaccharide nanocrystals are used, because these nanocrystals commonly undergo browning when heated.

In **Chapter 6** we have shown that surface modification is a viable way to decrease browning and improve nanocrystal dispersion in the PLA matrix, and as such resulted in nanocomposites with increased transparency (**Chapter 6; Figure 6.6**). This highly affected the appeal of the resultant nanocomposite (**Figure 8.9**), which is of great importance for consumer acceptance.

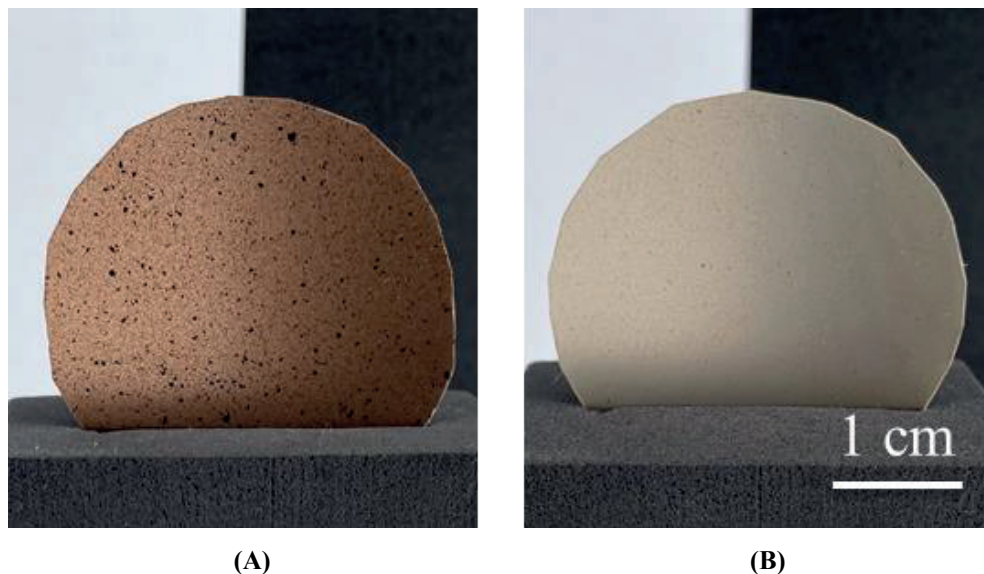


**Figure 8.9:** (A) Large chitin nanocrystal aggregates visible at 5 wt. %; fatty acid surface modification (C18:0) improves dispersibility and film transparency (B) (**Chapter 6**).

#### 8.3.5.2 Antioxidant and antimicrobial activity

Addition of nanoparticles may lead to additional functionality of packaging material, that can be instrumental in ‘active packaging concepts’ (**Figure 8.10**). Chitin based products (including chitosan) have antifungal and antioxidant properties [36,358–362], and there are indications that these properties remain when used in combination with polymers. This is an important lead for the food industry that aims toward more natural ways to protect its products. Within a sister project, DPPH radical scavenging activity (antioxidant) was found when particles were included in a polylactic acid packaging concept. When particles are at the surface their activity was 5 times higher than when used as integral part of the film (**Figure 8.10**).

Antioxidant functionality can be boosted by surface modification, and a potential route to do so is the Steglich esterification that we used in **Chapter 6**. The selection of a fatty acid with a phenolic moiety may even create a double effect, i.e., increased dispersibility in the polymer matrix and antioxidant activity, which is a concept that needs to be further tested.

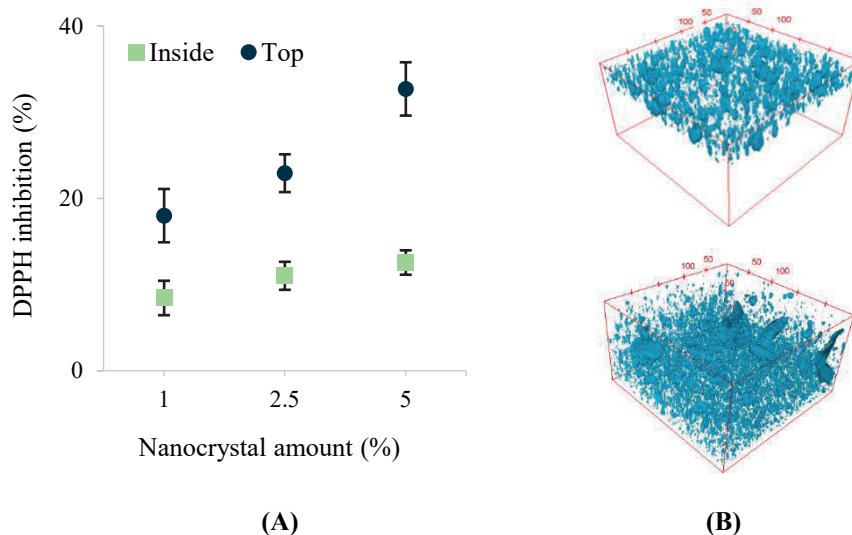


**Figure 8.10:** (A) DPPH inhibition as function of nanocrystal addition (B) where PLA nanocomposites show higher activity when chitin nanocrystals were placed on top of the plastic film instead of inside [358].

## 8.4 Outlook – How to arrive at a circular biobased plastics economy?

### 8.4.1 The missing vision of a circular economy

Direct action is urgently needed to limit climate change, but this is challenging as the transition towards a circular plastics economy goes beyond technical challenges; hurdles that are societal, political, legislative, infrastructural, or economical in nature need to be overcome as well [363]. In other words, a holistic approach is required to transform our current linear economy into a more circular one.

Our results from **Chapter 7** indicate that the vision of a future circular economy is far from united; actors (e.g., policymakers, scientists, and industry) have different ideas about what this circular plastics economy implies, and what the role of different plastics in this economy is. Because of this, it is questionable whether certain research findings are in line with what is desired or looked for in society. For example, bioplastics positively contribute to sustainability, but they do not solve the huge amounts of plastic litter in the environment. To mitigate the litter problem, behavioural changes are needed. To address this, collaborations between natural and social science are of essence [364]. It is therefore crucial to look beyond

the material dynamics and consider the social dynamics as well, although this is not straightforward due to different terminology and views on methodology.

Today, collaboration largely depends on individuals initiatives, whereas some frameworks exist that facilitate this. For instance, the RRI framework – Responsible Research and Innovation – is developed by the European Union to form a shared understanding of the roles and responsibilities of stakeholders, and create public trust toward advanced technologies including novel materials [365]. From a business and government perspective, the Ellen Mac Arthur Foundation aims to actively unite various organizations through, e.g., ‘Global Commitment’ [366] and ‘Plastics Pact Network’ [367]. These are ways to change the individual random man walks into a united march towards a circular economy that is required to meet climate’s deadline.

#### **8.4.2 The route toward a circular economy**

In **Chapter 7** we observed that societal actors prioritize traditional plastic’s recyclability, whereas academic actors focus on alternative forms of plastics in a circular economy. Today, bioplastics have a disputative reputation. On one hand, bioplastics have an excellent CO<sub>2</sub> footprint compared to petroleum-based plastics [368]. On the other hand, they interfere with current recycling processes. In a polluted world where fossil-based sources are scarce and prices fluctuate, it is inevitable to focus on biobased resources in the long run. Having said that, it is good to consider that one vision does not necessarily exclude the other, but may simply take place at different time frames, which we illustrate in **Figure 8.11**.

On the short term, much can be gained by the first 8 steps of the 9R-framework, including recycling, reusing [369], or reducing traditional fossil-based plastics (**Table 8.1**). The current footprint of food production must not be underestimated [370]; plastic packages effectively increase the food’s shelf life and reduce food waste, thus contributing to lowering the footprint. In conjunction, the potential of alternative forms of plastics should be investigated and developed; for example, the (bio)nanocomposites of this thesis (**Chapter 6**).

Inevitably, there will be a transition phase, during which traditional and alternative forms of plastics co-exist. In this stage, we have to adjust alternative plastics so they can be traditionally processed, and/or adjust our processes to make them suitable for alternative

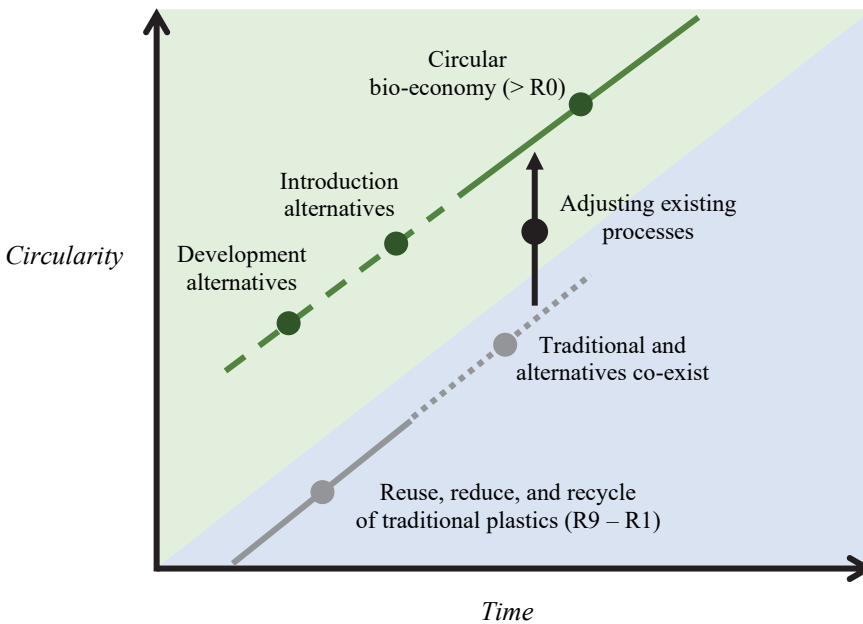


**Figure 8.11:** The transition towards a fully biobased circular plastics economy where traditional plastics are eventually replaced by alternative forms of plastics.

forms of plastics. Eventually, we arrive at a completely biobased circular plastics economy where plastics are made from biobased resources that can be recycled after use. To be complete, the last step within the 9R-framework – R0: Refuse – can be applied in the broadest sense, e.g., bioplastics, (bio)nanocomposites, edible plastics, or materials we simply do not yet know, are examples that fall within this category (Chapter 7).

### 8.4.3 Future materials – do (bio)nanocomposites have a place in society?

Looking at, e.g., the automotive or aviation industry, there is a role for nanocomposites in society, but whether these kinds of materials will also find their way within the packaging industry still needs to be seen. The astonishing material properties of (bio)nanocomposites may potentially expand plastic properties as we currently know them, and make them even more effective at, e.g., reducing food waste. For fossil-based plastics, these improvements may allow a reduction of resource usage which directly leads to an environmentally and financially favourable picture (R2: reduce; Table 8.1). Fully biobased nanocomposites can be regarded as completely novel materials (R0: Refuse; Table 8.1), and therefore may

**Table 8.1:** 9R-framework: steps that can be taken to arrive at a circular economy.

Circular economy	Smarter product use and manufacture	<ul style="list-style-type: none"> <li>• <b>R0 Refuse:</b> make a product redudant by abandoning its function or by offering the same function with another product.</li> <li>• <b>R1 Rethink:</b> prolong product use (e.g., sharing the product).</li> <li>• <b>R2 Reduce:</b> increase material productivity in product manufacturing.</li> </ul>
	Extend the lifespan of the product and its parts	<ul style="list-style-type: none"> <li>• <b>R3 Reuse:</b> Reuse by another consumer of discarded product which is still in good condition and fulfils its original function.</li> <li>• <b>R4 Repair:</b> repair and maintenance of defective product so it can be used with its original function.</li> <li>• <b>R5 Refurbish:</b> restore an old product and bring it up to date.</li> <li>• <b>R6 Remanufacture:</b> use parts of the discarded product in a new product with the same function.</li> <li>• <b>R7 Repurpose:</b> use the discarded product or its parts in a new product with a different function.</li> </ul>
Linear economy	Useful application of materials	<ul style="list-style-type: none"> <li>• <b>R8 Recycle:</b> process materials to obtain the same or lower quality</li> <li>• <b>R9 Recover:</b> incineration of material with energy recover</li> </ul>

contribute to the ultimate goal of a circular biobased plastics economy provided that they are recycled.

Potential ‘deal-breakers’ should be investigated before these novel concepts can become successful in society. These include:

- Scalability; can we produce these materials at large scale? Will the heterogeneous nature of, e.g., polysaccharide nanocrystals allow large-scale processing?
- Accessibility; are the envisioned nanoparticles/crystals and polymers sufficiently available?

- End-of-life possibilities; are these materials fully compostable and/or recyclable? What is the effect of nanoparticles on these processes?
- Sustainability; what is the environmental footprint of production? And that of end-of-life processes? Are these advanced processes more sustainable than current ones?
- Toxicology; do nanoparticles/crystals migrate out of the package? If so, what is its physiological effect on humans and the environment?
- Consumer acceptance and handling; do consumers know how to separate nanocomposites from other materials? What happens if they do not separate these materials accordingly?

It is clear that the rational design of nanocomposites from just a technical point of view is challenging, but when including societal aspects, the picture becomes even more multifaceted. In particular, if one wishes to create a fully biobased nanocomposite that not only fits within circular economy concepts, but that also leads to consumer acceptance in the widest sense.

In the introduction of this thesis, we asked ourselves the following question (**Chapter 1; section 1.1; page. 11**):

*“There is a clear need for new materials with comparable properties to plastics [...] We therefore need to question ourselves what these novel materials should look like, and what their role is within a future circular economy.”*

It may be obvious that there is no simple answer to this question, and it is important to consider that the use of bioplastics – and bio-nanocomposites specifically – is one possible solution to the linearity of the current plastics economy. If we put this in a broader context and look back at materials we used and preferred in the past (**Chapter 1; section 1.1**), one task seems clear: we ‘simply’ need to make materials that are better than the plastics we currently know.

## 8.5 Appendix

*Appendix 8-1: Dispersive and polar surface energy of unmodified chitin nanocrystals (ChNC), chitin nanocrystals modified with octanoic acid (ChNC-C8:0) produced in Chapter 6.*

Sample	$\gamma^d$	$\gamma^p$	$\gamma^{total}$
ChNC	86.7	12.9	99.6
ChNC-C8:0	52.6	11.0	63.8

---

# References

- [1] Rasmussen SC. From Parkesine to Celluloid: The Birth of Organic Plastics. *Angew Chemie* 2021;133:8090–4. <https://doi.org/10.1002/ange.202015095>.
- [2] Philippe Chalmin. The history of plastics: from the Capitol to the Tarpeian Rock. *F Actions Sci Reports* 2019;19:6–11.
- [3] Mulder KF. Sustainable Consumption and Production of Plastics? *Technol Forecast Soc Change* 1998;58:105–24. [https://doi.org/10.1016/s0040-1625\(97\)00129-7](https://doi.org/10.1016/s0040-1625(97)00129-7).
- [4] Barthes R. *Plastic*. New York: Hill and Wang; 1972.
- [5] Europe P. *Plastics – the facts 2020*. PlasticEurope. 2020; 1: 1-64
- [6] Shen M, Zhang Y, Zhu Y, Song B, Zeng G, Hu D, et al. Recent advances in toxicological research of nanoplastics in the environment: A review. *Environ Pollut* 2019;252:511–21. <https://doi.org/10.1016/j.envpol.2019.05.102>.
- [7] Plastics, a growing environmental and climate concern: how can Europe revert that trend? 28th January 2021. <https://www.eea.europa.eu/highlights/plastics-environmental-concern> (accessed February 18, 2022).
- [8] Agency EE. Greenhouse Gas Inventory. May 31 2021. <https://doi.org/https://www.eea.europa.eu/data-and-maps/data/national-emissions-reported-to-the-unfccc-and-to-the-eu-greenhouse-gas-monitoring-mechanism-17>.
- [9] Agreement P. Paris agreement. Rep. Conf. parties to united nations Framew. Conv. Clim. Chang., Paris: 2015. <https://doi.org/10.4324/9789276082569-2>.
- [10] Ministry of Infrastructure and Water Management, Plastics-using companies, Plastics-producing companies. *Plastics Pact NL 2019-2025*. 2019.
- [11] Crippa M, De Wilde B, Koopmans R, Leyssens J, Muncke J, Ritschkoff A-C, et al. A circular economy for plastics – Insights from research and innovation to inform policy and funding decisions. Brussels: European Commission; 2019. <https://doi.org/https://doi.org/10.2777/269031>.
- [12] World Economic Forum, Ellen MacArthur Foundation, McKinsey & Company. *The New Plastics Economy — Rethinking the future of plastics*. 2016.
- [13] Molenveld K, Bos H, van der Spa M. *Biobased Plastics 2020*. 2020. Wageningen Food & Biobased Research.
- [14] van den Oever M, Molenveld K, van der Zee M, Bos H. Bio-based and biodegradable plastics : facts and figures : focus on food packaging in the Netherlands. 2017. <https://doi.org/10.18174/408350>.
- [15] Bioplastics Europe. *Relevant standards and labels for bio-based and biodegradable plastics 2016*.
- [16] Iles A, Martin AN. Expanding bioplastics production: Sustainable business innovation in the chemical industry. *J Clean Prod* 2013;45:38–49. <https://doi.org/10.1016/j.jclepro.2012.05.008>.
- [17] Jamshidian M, Tehrani EA, Imran M, Jacquot M, Desobry S. Poly-Lactic Acid: Production, applications, nanocomposites, and release studies. *Compr Rev Food Sci Food Saf* 2010;9:552–71. <https://doi.org/10.1111/j.1541-4337.2010.00126.x>.
- [18] Auras RA, Harte B, Selke S, Hernandez R. Mechanical, physical, and barrier properties of poly(lactide) films. *J Plast Film Sheeting* 2003;19:123–35. <https://doi.org/10.1177/8756087903039702>.
- [19] Plichta A, Lisowska P, Kundys A, Zychewicz A, Dębowski M, Florjańczyk Z. Chemical recycling of poly(lactic acid) via controlled degradation with protic (macro)molecules. *Polym Degrad Stab* 2014;108:288–96. <https://doi.org/10.1016/j.polymdegradstab.2014.03.006>.
- [20] Gupta AP, Kumar V. New emerging trends in synthetic biodegradable polymers - Polylactide: A critique. *Eur Polym J* 2007;43:4053–74. <https://doi.org/10.1016/j.eurpolymj.2007.06.045>.
- [21] European Bioplastics. *Bioplastics market data 2022*. <https://www.european-bioplastics.org/market/>.

- (Accessed on Februari 18, 2022)
- [22] Peelman N. Characterization of barrier properties and temperature resistance of biobased plastics for food packaging. Doctoral dissertation, Ghent Univeristy, 2015.
- [23] Peelman N, Ragaert P, De Meulenaer B, Adons D, Peeters R, Cardon L, et al. Application of bioplastics for food packaging. *Trends Food Sci Technol* 2013;32:128–41. <https://doi.org/10.1016/j.tifs.2013.06.003>.
- [24] Petersen K, Væggesø Nielsen P, Bertelsen G, Lawther M, Olsen MB, Nilsson NH, et al. Potential of biobased materials for food packaging. *Trends Food Sci Technol* 1999;10:52–68. [https://doi.org/10.1016/S0924-2244\(99\)00019-9](https://doi.org/10.1016/S0924-2244(99)00019-9).
- [25] Schmid M, Dallmann K, Bugnicourt E, Cordoni D, Wild F, Lazzeri A, et al. Properties of whey-protein-coated films and laminates as novel recyclable food packaging materials with excellent barrier properties. *Int J Polym Sci* 2012;2012:5–7. <https://doi.org/10.1155/2012/562381>.
- [26] Yanat M, Schroën K. Preparation methods and applications of chitosan nanoparticles; with an outlook toward reinforcement of biodegradable packaging. *React Funct Polym* 2021;161. <https://doi.org/10.1016/j.reactfunctpolym.2021.104849>.
- [27] Hassouna F, Raquez JM, Addiego F, Toniazzo V, Dubois P, Ruch D. New development on plasticized poly(lactide): Chemical grafting of citrate on PLA by reactive extrusion. *Eur Polym J* 2012;48:404–15. <https://doi.org/10.1016/j.eurpolymj.2011.12.001>.
- [28] Mekonnen T, Mussone P, Khalil H, Bressler D. Progress in bio-based plastics and plasticizing modifications. *J Mater Chem A* 2013;1:13379–98. <https://doi.org/10.1039/c3ta12555f>.
- [29] Usuki A, Mizutani T, Fukushima Y, Fujimoto M, Fukumori K, Kojima Y, et al. Composite Material containing a Layered Silicate. US4739007A, 1989.
- [30] Novais RM, Covas JA, Paiva MC. The effect of flow type and chemical functionalization on the dispersion of carbon nanofiber agglomerates in polypropylene. *Compos Part A Appl Sci Manuf* 2012;43:833–41. <https://doi.org/10.1016/j.compositesa.2012.01.017>.
- [31] Li B, Zhong WH. Review on polymer/graphite nanoplatelet nanocomposites. *J Mater Sci* 2011;46:5595–614. <https://doi.org/10.1007/s10853-011-5572-y>.
- [32] Müller K, Bugnicourt E, Latorre M, Jorda M, Echegoyen Sanz Y, Lagaron J, et al. Review on the Processing and Properties of Polymer Nanocomposites and Nanocoatings and Their Applications in the Packaging, Automotive and Solar Energy Fields. *Nanomaterials* 2017;7:74. <https://doi.org/10.3390/nano7040074>.
- [33] Vasile C. Polymeric nanocomposites and nanocoatings for food packaging: A review. *Materials* 2018;11. <https://doi.org/10.3390/ma11101834>.
- [34] Attaran SA, Hassan A, Wahit MU. Materials for food packaging applications based on bio-based polymer nanocomposites : A review 2017. <https://doi.org/10.1177/0892705715588801>.
- [35] Youssef AM. Polymer Nanocomposites as a New Trend for Packaging Applications. *Polym - Plast Technol Eng* 2013;52:635–60. <https://doi.org/10.1080/03602559.2012.762673>.
- [36] Salaberria AM, Diaz RH, Andrés MA, Fernandes SCM, Labidi J. The antifungal activity of functionalized chitin nanocrystals in poly (Lactid Acid) films. *Materials* 2017;10:1–16. <https://doi.org/10.3390/ma10050546>.
- [37] Han Y, Lee S, Ho K, Park I. Journal of Physics and Chemistry of Solids Preparation and characterization of chitosan – clay nanocomposites with antimicrobial activity. *J Phys Chem Solids* 2010;71:464–7. <https://doi.org/10.1016/j.jpcs.2009.12.012>.
- [38] Răpă M, Miteluț AC, Tănase EE, Grosu E, Popescu P, Popa ME, et al. Influence of chitosan on mechanical, thermal, barrier and antimicrobial properties of PLA-biocomposites for food packaging. *Compos Part B Eng* 2016;102:112–21. <https://doi.org/10.1016/j.compositesb.2016.07.016>.
- [39] Salaberria AM, Diaz RH, Labidi J, Fernandes SCM. Role of chitin nanocrystals and nanofibers on physical, mechanical and functional properties in thermoplastic starch films. *Food Hydrocoll* 2015. <https://doi.org/10.1016/j.foodhyd.2014.12.016>.
- [40] Naser AZ, Deiab I, Defersha F, Yang S. Expanding poly(Lactic acid) (pla) and polyhydroxyalkanoates

- (phas) applications: A review on modifications and effects. *Polymers* 2021;13. <https://doi.org/10.3390/polym13234271>.
- [41] Qadeer A, Kirsten KL, Ajmal Z, Jiang X, Zhao X. Alternative Plasticizers As Emerging Global Environmental and Health Threat: Another Regrettable Substitution? *Environ Sci Technol* 2022;56:1482–8. <https://doi.org/10.1021/acs.est.1c08365>.
- [42] Liu H, Zhang J. Research progress in toughening modification of poly(lactic acid). *J Polym Sci Part B Polym Phys* 2011;49:1051–83. <https://doi.org/10.1002/polb.22283>.
- [43] Murariu M, Da Silva Ferreira A, Duquesne E, Bonnaud L, Dubois P. Poly lactide (PLA) and highly filled PLA - calcium sulfate composites with improved impact properties. *Macromol Symp* 2008;272:1–12. <https://doi.org/10.1002/masy.200851201>.
- [44] Notta-cuvier D, Odent J, Delille R, Murariu M, Lauro F, Raquez JM. Tailoring poly lactide ( PLA ) properties for automotive applications : Effect of addition of designed additives on main mechanical properties. *Polym Test* 2014;36:1–9. <https://doi.org/10.1016/j.polymertesting.2014.03.007>.
- [45] Choochottiros C, Chin I. Potential transparent PLA impact modifiers based on PMMA copolymers. *Eur Polym J* 2013;49:957–66. <https://doi.org/10.1016/j.eurpolymj.2012.12.008>.
- [46] Kamal MR, Carreau PJ, Sacligil D, Heuzey M-C, Nofar M. Poly (lactic acid) blends: Processing, properties and applications. *Int J Biol Macromol* 2018;125:307–60. <https://doi.org/10.1016/j.ijbiomac.2018.12.002>.
- [47] Imre B, Renner K, Pukánszky B. Interactions, structure and properties in poly(lactic acid)/thermoplastic polymer blends. *Express Polym Lett* 2014;8:2–14. <https://doi.org/10.3144/expresspolymlett.2014.2>.
- [48] Lee JH, Park TG, Park HS, Lee DS, Lee YK, Yoon SC, et al. Thermal and mechanical characteristics of poly(L-lactic acid) nanocomposite scaffold. *Biomaterials* 2003;24:2773–8. [https://doi.org/10.1016/S0142-9612\(03\)00080-2](https://doi.org/10.1016/S0142-9612(03)00080-2).
- [49] Balakrishnan H, Hassan A, Wahit MU, Yussuf AA, Razak SBA. Novel toughened polylactic acid nanocomposite: Mechanical, thermal and morphological properties. *Mater Des* 2010;31:3289–98. <https://doi.org/10.1016/j.matdes.2010.02.008>.
- [50] Ates B, Koytepe S, Ulu A, Gurses C, Thakur VK. Chemistry, structures, and advanced applications of nanocomposites from biorenewable resources. *Chem Rev* 2020;120:9304–62. <https://doi.org/10.1021/acs.chemrev.9b00553>.
- [51] Scaffaro R, Botta L, Lopresti F, Maio A, Sutura F. Polysaccharide nanocrystals as fillers for PLA based nanocomposites. *Cellulose* 2017;24:447–78. <https://doi.org/10.1007/s10570-016-1143-3>.
- [52] Zeng JB, He YS, Li SL, Wang YZ. Chitin whiskers: An overview. *Biomacromolecules* 2012;13:1–11. <https://doi.org/10.1021/bm201564a>.
- [53] Salaberria AM, Labidi J, Fernandes SCM. Different routes to turn chitin into stunning nano-objects. *Eur Polym J* 2015;68:503–15. <https://doi.org/10.1016/j.eurpolymj.2015.03.005>.
- [54] Colijn I, Fokkink R, Schroën K. Quantification of energy input required for chitin nanocrystal aggregate size reduction through ultrasound. *Sci Rep* 2021;11:1–9. <https://doi.org/10.1038/s41598-021-96657-1>.
- [55] Herrera N, Singh AA, Salaberria AM, Labidi J, Mathew AP, Oksman K. Triethyl citrate (TEC) as a dispersing aid in polylactic acid/chitin nanocomposites prepared via liquid-assisted extrusion. *Polymers* 2017;9. <https://doi.org/10.3390/polym9090406>.
- [56] Bailey EJ, Winey KI. Dynamics of polymer segments, polymer chains, and nanoparticles in polymer nanocomposite melts: A review. *Prog Polym Sci* 2020;105:101242. <https://doi.org/10.1016/j.progpolymsci.2020.101242>.
- [57] Chen Q, Gong S, Moll J, Zhao D, Kumar SK, Colby RH. Mechanical reinforcement of polymer nanocomposites from percolation of a nanoparticle network. *ACS Macro Lett* 2015;4:398–402. <https://doi.org/10.1021/acsmacrolett.5b00002>.
- [58] Ma P, Siddiqui NA, Marom G, Kim J. Composites : Part A Dispersion and functionalization of carbon nanotubes for polymer-based nanocomposites : A review. *Compos Part A* 2010;41:1345–67. <https://doi.org/10.1016/j.compositesa.2010.07.003>.

- [59] Oksman K, Aitomäki Y, Mathew AP, Siqueira G, Zhou Q, Butylina S, et al. Review of the recent developments in cellulose nanocomposite processing. *Compos Part A Appl Sci Manuf* 2016;83:2–18. <https://doi.org/10.1016/j.compositesa.2015.10.041>.
- [60] Sahraee S, Milani JM, Ghanbarzadeh B, Hamishehkar H. Physicochemical and antifungal properties of bio-nanocomposite film based on gelatin-chitin nanoparticles. *Int J Biol Macromol* 2017;97:373–81. <https://doi.org/10.1016/j.ijbiomac.2016.12.066>.
- [61] Salaberria AM, Diaz RH, Andrés MA, Fernandes SCM, Labidi J. The antifungal activity of functionalized chitin nanocrystals in poly (Lactid Acid) films. *Materials* 2017;10:1–16. <https://doi.org/10.3390/ma10050546>.
- [62] Ngo DH, Kim SK. Antioxidant effects of chitin, chitosan, and their derivatives. vol. 73. 1st ed. Elsevier Inc.; 2014. <https://doi.org/10.1016/B978-0-12-800268-1.00002-0>.
- [63] Stöckelhuber KW, Das A, Jurk R, Heinrich G. Contribution of physico-chemical properties of interfaces on dispersibility, adhesion and flocculation of filler particles in rubber. *Polymer* 2010;51:1954–63. <https://doi.org/10.1016/j.polymer.2010.03.013>.
- [64] Tang Q, Wang F, Guo H, Yang Y, Du Y, Liang J, et al. Effect of coupling agent on surface free energy of organic modified attapulgite (OAT) powders and tensile strength of OAT/ethylene-propylene-diene monomer rubber nanocomposites. *Powder Technol* 2015;270:92–7. <https://doi.org/10.1016/j.powtec.2014.09.005>.
- [65] Natarajan B, Li Y, Deng H, Brinson LC, Schadler LS. Effect of interfacial energetics on dispersion and glass transition temperature in polymer nanocomposites. *Macromolecules* 2013;46:2833–41. <https://doi.org/10.1021/ma302281b>.
- [66] Khoshkava V, Kamal MR. Effect of surface energy on dispersion and mechanical properties of polymer/nanocrystalline cellulose nanocomposites. *Biomacromolecules* 2013;14:3155–63. <https://doi.org/10.1021/bm400784j>.
- [67] Starr FW, Douglas JF, Glotzer SC. Origin of particle clustering in a simulated polymer nanocomposite and its impact on rheology. *J Chem Phys* 2003;119:1777–88. <https://doi.org/10.1063/1.1580099>.
- [68] Zhang L, Dong H, Li M, Wang L, Liu Y, Wang L, et al. Fabrication of Poly(lactic Acid)-Modified Carbon Black Composites into Improvement of Levelness and Mechanical Properties of Spun-Dyeing Poly(lactic Acid) Composites Membrane. *ACS Sustain Chem Eng* 2019;7:688–96. <https://doi.org/10.1021/acsschemeng.8b04264>.
- [69] Castellano M, Conzatti L, Turturro A, Costa G, Busca G. Influence of the silane modifiers on the surface thermodynamic characteristics and dispersion of the silica into elastomer compounds. *J Phys Chem B* 2007;111:4495–502. <https://doi.org/10.1021/jp0702144>.
- [70] Gan L, Liao J, Lin N, Hu C, Wang H, Huang J. Focus on Gradientwise Control of the Surface Acetylation of Cellulose Nanocrystals to Optimize Mechanical Reinforcement for Hydrophobic Polyester-Based Nanocomposites. *ACS Omega* 2017;2:4725–36. <https://doi.org/10.1021/acsomega.7b00532>.
- [71] Bee SL, Abdullah MAA, Bee ST, Sin LT, Rahmat AR. Polymer nanocomposites based on silylated-montmorillonite: A review. *Prog Polym Sci* 2018;85:57–82. <https://doi.org/10.1016/j.progpolymsci.2018.07.003>.
- [72] Karnati SR, Agbo P, Zhang L. Applications of silica nanoparticles in glass/carbon fiber-reinforced epoxy nanocomposite. *Compos Commun* 2020;17:32–41. <https://doi.org/10.1016/j.coco.2019.11.003>.
- [73] Xu GR, Wang JN, Li CJ. Strategies for improving the performance of the polyamide thin film composite (PA-TFC) reverse osmosis (RO) membranes: Surface modifications and nanoparticles incorporations. *Desalination* 2013;328:83–100. <https://doi.org/10.1016/j.desal.2013.08.022>.
- [74] Saravanan N, Rajasekar R, Mahalakshmi S, Sathishkumar TP, Sasikumar K, Sahoo S. Graphene and modified graphene-based polymer nanocomposites - A review. *J Reinf Plast Compos* 2014;33:1158–70. <https://doi.org/10.1177/0731684414524847>.
- [75] Liu J, Gao Y, Cao D, Zhang L, Guo Z. Nanoparticle dispersion and aggregation in polymer nanocomposites: Insights from molecular dynamics simulation. *Langmuir* 2011;27:7926–33. <https://doi.org/10.1021/la201073m>.

- [76] Ray SS, Okamoto M. Polymer / layered silicate nanocomposites : a review from preparation to processing 2003;28:1539–641. <https://doi.org/10.1016/j.progpolymsci.2003.08.002>.
- [77] Ray SS. Processing of polymer-based nanocomposites: processing-structure-property-performance relationships. Cham: Springer; 2018. <https://doi.org/10.1007/978-3-319-97792-8>.
- [78] Koval AA, Shevchenko VG, Shchegolikhin AN, Nedorezova PM, Klyamkina AN, Aladyshev AM. Effect of Carbon Nanotube Functionalization on the Structural and Mechanical Properties of Polypropylene / MWCNT Composites 2008;7536–42. <https://doi.org/10.1021/ma801599q>.
- [79] Velasco-Santos C, Martínez-Hernández AL, Fisher FT, Ruoff R, Castaño VM. Improvement of Thermal and Mechanical Properties of Carbon Nanotube Composites through Chemical Functionalization. *Chem Mater* 2003;15:4470–5. <https://doi.org/10.1021/cm034243c>.
- [80] Buffa F, Abraham GA, Grady BP, Resasco D. Effect of Nanotube Functionalization on the Properties of Single-Walled Carbon Nanotube / Polyurethane Composites 2007;490–501. <https://doi.org/10.1002/polb>.
- [81] Cantor KM, Watts P. *Plastics Processing*. Elsevier; 2011. <https://doi.org/10.1016/B978-1-4377-3514-7.10012-1>.
- [82] Rishi K, Narayanan V, Beaucage G, McGlasson A, Kuppa V, Ilavsky J, et al. A thermal model to describe kinetic dispersion in rubber nanocomposites: The effect of mixing time on dispersion. *Polymer* 2019;175:272–82. <https://doi.org/10.1016/j.polymer.2019.03.044>.
- [83] Móczó J, Pukánszky B. Polymer micro and nanocomposites: Structure, interactions, properties. *J Ind Eng Chem* 2008;14:535–63. <https://doi.org/10.1016/j.jiec.2008.06.011>.
- [84] Gaspar H, Teixeira P, Santos R, Fernandes L, Hilliou L, Weir MP, et al. A Journey along the Extruder with Polystyrene:C60Nanocomposites: Convergence of Feeding Formulations into a Similar Nanomorphology. *Macromolecules* 2017;50:3301–12. <https://doi.org/10.1021/acs.macromol.6b02283>.
- [85] Khoshkava V, Kamal MR. Effect of drying conditions on cellulose nanocrystal (CNC) agglomerate porosity and dispersibility in polymer nanocomposites. *Powder Technol* 2014;261:288–98. <https://doi.org/10.1016/j.powtec.2014.04.016>.
- [86] Abdallah W, Kamal MR. Influence of process variables on physical characteristics of spray freeze dried cellulose nanocrystals. *Cellulose* 2018;25:5711–30. <https://doi.org/10.1007/s10570-018-1975-0>.
- [87] Beuguel Q, Tavares JR, Carreau PJ, Heuzey MC. Ultrasonication of spray- and freeze-dried cellulose nanocrystals in water. *J Colloid Interface Sci* 2018;516:23–33. <https://doi.org/10.1016/j.jcis.2018.01.035>.
- [88] Abdallah W, Tan V, Kamal MR. The Effect of Spray-Freeze Drying of Montmorillonite on the Morphology, Dispersion, and Crystallization in Polypropylene Nanocomposites. *Polym Eng Sci* 2020;60:168–79. <https://doi.org/10.1002/pen.25270>.
- [89] Owens D. Estimation of the surface free energy of polymers. *J Appl Polym Sci* 1969;13:1741–7.
- [90] Good RJ, Girifalco LA. A theory for estimation of surface and interfacial energies. III. Estimation of surface energies of solids from contact angle data. *J Phys Chem* 1960;64:561–5. <https://doi.org/10.1021/j100834a012>.
- [91] Cheung O, Zhang P, Frykstrand S, Zheng H, Yang T, Sommariva M, et al. Nanostructure and pore size control of template-free synthesised mesoporous magnesium carbonate. *RSC Adv* 2016;6:74241–9. <https://doi.org/10.1039/c6ra14171d>.
- [92] Shavit A, Riggelman RA. The dynamics of unentangled polymers during capillary rise infiltration into a nanoparticle packing. *Soft Matter* 2015;11:8285–95. <https://doi.org/10.1039/c5sm01866h>.
- [93] Supple S, Quirke N. Rapid Imbibition of Fluids in Carbon Nanotubes. *Phys Rev Lett* 2003;90:1–4. <https://doi.org/10.1103/PhysRevLett.90.214501>.
- [94] Yao Y, Butt HJ, Floudas G, Zhou J, Doi M. Theory on Capillary Filling of Polymer Melts in Nanopores. *Macromol Rapid Commun* 2018;39:1–5. <https://doi.org/10.1002/marc.201800087>.
- [95] Dimitrov DI, Milchev A, Binder K. Capillary Rise in Nanopores: Molecular Dynamics Evidence for the Lucas-Washburn Equation. *phys Rev Lett*. 2007; 1:17–20.
- [96] Hu G, Cao B. Flows of polymer melts through nanopores: Experiments and modelling. *J Therm Sci*

- Technol 2013;8:363–9. <https://doi.org/10.1299/jtst.8.363>.
- [97] Xiao F, Xu H, Li XY, Wang D. Modeling particle-size distribution dynamics in a shear-induced breakage process with an improved breakage kernel: Importance of the internal bonds. *Colloids Surfaces A Physicochem Eng Asp* 2015;468:87–94. <https://doi.org/10.1016/j.colsurfa.2014.11.060>.
- [98] Odriozola G, Schmitt A, Moncho-Jordá A, Callejas-Fernández J, Martínez-García R, Leone R, et al. Constant bond breakup probability model for reversible aggregation processes. *Phys Rev E - Stat Physics, Plasmas, Fluids, Relat Interdiscip Top* 2002;65:1–8. <https://doi.org/10.1103/PhysRevE.65.031405>.
- [99] Duan B, Chang C, Ding B, Cai J, Xu M, Feng S, et al. High strength films with gas-barrier fabricated from chitin solution dissolved at low temperature. *J Mater Chem A* 2013;1:1867–74. <https://doi.org/10.1039/c2ta00068g>.
- [100] Calderón BA, McCaughey MS, Thompson CW, Barinelli VL, Sobkowicz MJ. Evaluating the Influence of Specific Mechanical Energy on Biopolymer Blends Prepared via High-Speed Reactive Extrusion. *ACS Appl Polym Mater* 2019;1:1410–9. <https://doi.org/10.1021/acscpm.9b00177>.
- [101] Domenech T, Peuvrel-Disdier E, Vergnes B. The importance of specific mechanical energy during twin screw extrusion of organoclay based polypropylene nanocomposites. *Compos Sci Technol* 2013;75:7–14. <https://doi.org/10.1016/j.compscitech.2012.11.016>.
- [102] Hassinger I, Li X, Zhao H, Xu H, Huang Y, Prasad A, et al. Toward the development of a quantitative tool for predicting dispersion of nanocomposites under non-equilibrium processing conditions. *J Mater Sci* 2016;51:4238–49. <https://doi.org/10.1007/s10853-015-9698-1>.
- [103] Mack C, Sathyanarayana S, Weiss P, Mikonsaari I, Hübner C, Henning F, et al. Twin-screw extrusion of multi walled carbon nanotubes reinforced polycarbonate composites: Investigation of electrical and mechanical properties. *IOP Conf Ser Mater Sci Eng* 2012;40. <https://doi.org/10.1088/1757-899X/40/1/012020>.
- [104] Villmow T, Kretschmar B, Pötschke P. Influence of screw configuration, residence time, and specific mechanical energy in twin-screw extrusion of polycaprolactone/multi-walled carbon nanotube composites. *Compos Sci Technol* 2010;70:2045–55. <https://doi.org/10.1016/j.compscitech.2010.07.021>.
- [105] Diemer J, Chilles C, Colbert J, Miri T, Ingram A, David P, et al. Flow visualisation in co-rotating twin screw extruders: Positron emission particle tracking and numerical particle trajectories. *Int Polym Process* 2011;26:540–50. <https://doi.org/10.3139/217.2475>.
- [106] Wagner JR, Mount EM, Giles HF. Plastic Behavior in the Extruder. *Extrusion* 2014:47–70. <https://doi.org/10.1016/b978-1-4377-3481-2.00004-1>.
- [107] Xu HN, Tang YY, Ouyang XK. Shear-Induced Breakup of Cellulose Nanocrystal Aggregates. *Langmuir* 2017;33:235–42. <https://doi.org/10.1021/acs.langmuir.6b03807>.
- [108] Vilaverde C, Santos RM, Paiva MC, Covas JA. Dispersion and re-agglomeration of graphite nanoplates in polypropylene melts under controlled flow conditions. *Compos Part A Appl Sci Manuf* 2015;78:143–51. <https://doi.org/10.1016/j.compositesa.2015.08.010>.
- [109] Wang T, Keddie JL. Design and fabrication of colloidal polymer nanocomposites. *Adv Colloid Interface Sci* 2009;147–148:319–32. <https://doi.org/10.1016/j.cis.2008.06.002>.
- [110] Lee G. *Physical Chemistry of Foods*. vol. 57. New York: Marcel Dekker inc.; 2004. <https://doi.org/10.1016/j.ejpb.2003.10.013>.
- [111] Shen XJ, Yang S, Shen JX, Ma JL, Wu YQ, Zeng XL, et al. Improved mechanical and antibacterial properties of silver-graphene oxide hybrid/poly(lactid acid) composites by in-situ polymerization. *Ind Crops Prod* 2019;130:571–9. <https://doi.org/10.1016/j.indcrop.2019.01.018>.
- [112] Luong ND, Hippel U, Korhonen JT, Soininen AJ, Ruokolainen J, Johansson LS, et al. Enhanced mechanical and electrical properties of polyimide film by graphene sheets via in situ polymerization. *Polymer* 2011;52:5237–42. <https://doi.org/10.1016/j.polymer.2011.09.033>.
- [113] Chi-Yan Li S, Sun YC, Guan Q, Naguib H. Effects of chitin nanowhiskers on the thermal, barrier, mechanical, and rheological properties of polypropylene nanocomposites. *RSC Adv* 2016;6:72086–95. <https://doi.org/10.1039/c6ra11623j>.

- [114] Nunes RCR, Fonseca JLC, Pereira MR. Polymer-filler interactions and mechanical properties of a polyurethane elastomer. *Polym Test* 2000;19:93–103. [https://doi.org/10.1016/S0142-9418\(98\)00075-0](https://doi.org/10.1016/S0142-9418(98)00075-0).
- [115] Nunes RCR, Pereira RA, Fonseca JLC, Pereira MR. X-ray studies on compositions of polyurethane and silica. *Polym Test* 2001;20:707–12. [https://doi.org/10.1016/S0142-9418\(01\)00007-1](https://doi.org/10.1016/S0142-9418(01)00007-1).
- [116] Singh RP, Aggarwal P. Effect of nanosilica on the properties of cement mortar. *Cem Int* 2015;13:65–70.
- [117] Bistričić L, Baranović G, Leskovac M, Bajsić EG. Hydrogen bonding and mechanical properties of thin films of polyether-based polyurethane-silica nanocomposites. *Eur Polym J* 2010;46:1975–87. <https://doi.org/10.1016/j.eurpolymj.2010.08.001>.
- [118] Pakzad A, Simonsen J, Yassar RS. Gradient of nanomechanical properties in the interphase of cellulose nanocrystal composites. *Compos Sci Technol* 2012;72:314–9. <https://doi.org/10.1016/j.compscitech.2011.11.020>.
- [119] Wong M, Paramsothy M, Xu XJ, Ren Y, Li S, Liao K. Physical interactions at carbon nanotube-polymer interface. *Polymer* 2003;44:7757–64. <https://doi.org/10.1016/j.polymer.2003.10.011>.
- [120] Tan H, Jiang LY, Huang Y, Liu B, Hwang KC. The effect of van der Waals-based interface cohesive law on carbon nanotube-reinforced composite materials. *Compos Sci Technol* 2007;67:2941–6. <https://doi.org/10.1016/j.compscitech.2007.05.016>.
- [121] Li C, Chou T. Multiscale modeling of compressive behavior of carbon nanotube / polymer composites. *Compos Sci Technol* 2006;66:2409–14. <https://doi.org/10.1016/j.compscitech.2006.01.013>.
- [122] Panhuis M, Maiti A, Dalton AB, Van Den Noort A, Coleman JN, McCarthy B, et al. Selective interaction in a polymer-single-wall carbon nanotube composite. *J Phys Chem B* 2003;107:478–82. <https://doi.org/10.1021/jp026470s>.
- [123] Rahmat M. Carbon Nanotube – Polymer Interaction in nanocomposites. Doctoral dissertation, McGill University, 2011.
- [124] Gou J, Liang Z, Zhang C, Wang B. Computational analysis of effect of single-walled carbon nanotube rope on molecular interaction and load transfer of nanocomposites. *Compos Part B Eng* 2005;36:524–33. <https://doi.org/10.1016/j.compositesb.2005.02.004>.
- [125] Odent J, Raquez JM, Dubois P, Giannelis EP. Ultra-stretchable ionic nanocomposites: From dynamic bonding to multi-responsive behavior. *J Mater Chem A* 2017;5:13357–63. <https://doi.org/10.1039/c7ta04101b>.
- [126] Karatrantos A, Koutsawa Y, Dubois P, Clarke N, Kröger M. Miscibility and Nanoparticle Diffusion in Ionic Nanocomposites. *Polymers* 2018;10:1–16. <https://doi.org/10.3390/polym10091010>.
- [127] van Zanten JH, Wallace WE, Wu W. Effect of strongly favorable substrate interactions on the thermal properties of ultrathin polymer films. *Phys Rev E* 1996;53:2053–6.
- [128] Fryer DS, Peters RD, Kim EJ, Tomaszewski JE, De Pablo JJ, Nealey PF, et al. Dependence of the glass transition temperature of polymer films on interfacial energy and thickness. *Macromolecules* 2001;34:5627–34. <https://doi.org/10.1021/ma001932q>.
- [129] Desai T, Koblinski P, Kumar SK. Molecular dynamics simulations of polymer transport in nanocomposites. *J Chem Phys* 2005;122. <https://doi.org/10.1063/1.1874852>.
- [130] Long D, Lequeux F. Heterogeneous dynamics at the glass transition in van der Waals liquids, in the bulk and in thin films. *Eur Phys J E* 2001;4:371–87. <https://doi.org/10.1007/s101890170120>.
- [131] Liu H, Brinson LC. Reinforcing efficiency of nanoparticles: A simple comparison for polymer nanocomposites. *Compos Sci Technol* 2008;68:1502–12. <https://doi.org/10.1016/j.compscitech.2007.10.033>.
- [132] Zhang W, Emany H, Pazmiño Betancourt BA, Vargas-Lara F, Starr FW, Douglas JF. The interfacial zone in thin polymer films and around nanoparticles in polymer nanocomposites. *J Chem Phys* 2019;151. <https://doi.org/10.1063/1.5119269>.
- [133] Houssat M, Lahoud Dignat N, Cambronne JP, Diahm S. AFM Measurements of Polyimide/Silicon Nitride Nanocomposite Interphase. *IEEE Trans Nanotechnol* 2018;17:1146–50. <https://doi.org/10.1109/TNANO.2018.2867159>.

- [134] Huang H. Electrochemical Application and AFM Characterization of Nanocomposites: Focus on Interphase Properties. Doctoral dissertation, KTH Royal Institute of Technology, 2017.
- [135] Voyiatzis E, Rahimi M, Müller-Plathe F, Böhm MC. How thick is the polymer interphase in nanocomposites? Probing it by local stress anisotropy and gas solubility. *Macromolecules* 2014;47:7878–89. <https://doi.org/10.1021/ma500556q>.
- [136] Khorasani MGZ, Silbernagl D, Platz D, Sturm H. Insights into nano-scale physical and mechanical properties of epoxy/boehmite nanocomposite using different AFM modes. *Polymers* 2019;11. <https://doi.org/10.3390/polym11020235>.
- [137] McArthur SL. Thin films of Vanadium Oxide Grown on Vanadium metal. *Surf Interface Anal* 2006;38:1380–5. <https://doi.org/10.1002/sia>.
- [138] Zhang M, Askar S, Torkelson JM, Brinson LC. Stiffness Gradients in Glassy Polymer Model Nanocomposites: Comparisons of Quantitative Characterization by Fluorescence Spectroscopy and Atomic Force Microscopy. *Macromolecules* 2017;50:5447–58. <https://doi.org/10.1021/acs.macromol.7b00917>.
- [139] John Lewis T. Nano-composite dielectrics: The dielectric nature of the nano-particle environment. *IEEJ Trans Fundam Mater* 2006;126:1020–30. <https://doi.org/10.1541/ieejfms.126.1020>.
- [140] Tanaka T. Interpretation of several key phenomena peculiar to nano dielectrics in terms of a multi-core model. *Annu. Rep. - Conf. Electr. Insul. Dielectr. Phenomena, CEIDP*, 2006. <https://doi.org/10.1109/CEIDP.2006.311928>.
- [141] Amraei J, Jam JE, Arab B, Firouz-Abadi RD. Modeling the interphase region in carbon nanotube-reinforced polymer nanocomposites. *Polym Compos* 2019;40:E1219–34. <https://doi.org/10.1002/pc.24950>.
- [142] Maghsoudlou MA, Barbaz Isfahani R, Saber-Samandari S, Sadighi M. Effect of interphase, curvature and agglomeration of SWCNTs on mechanical properties of polymer-based nanocomposites: Experimental and numerical investigations. *Compos Part B Eng* 2019;175:107119. <https://doi.org/10.1016/j.compositesb.2019.107119>.
- [143] Hu H, Onyebueke L, Abatan A. Characterizing and Modeling Mechanical Properties of Nanocomposites- Review and Evaluation. *J Miner Mater Charact Eng* 2010;09:275–319. <https://doi.org/10.4236/jmmce.2010.94022>.
- [144] Zare Y. Development of Halpin-Tsai model for polymer nanocomposites assuming interphase properties and nanofiller size. *Polym Test* 2016;51:69–73. <https://doi.org/10.1016/j.polymertesting.2016.02.010>.
- [145] Wang Y, Zhang Y, Zhao H, Li X, Huang Y, Schadler LS, et al. Identifying interphase properties in polymer nanocomposites using adaptive optimization. *Compos Sci Technol* 2018;162:146–55. <https://doi.org/10.1016/j.compscitech.2018.04.017>.
- [146] Boutaleb S, Zaïri F, Mesbah A, Naït-abdelaziz M, Gloaguen JM, Boukharouba T, et al. International Journal of Solids and Structures Micromechanics-based modelling of stiffness and yield stress for silica / polymer nanocomposites. *Int J Solids Struct* 2009;46:1716–26. <https://doi.org/10.1016/j.ijsolstr.2008.12.011>.
- [147] Li X, Zhang M, Wang Y, Prasad A, Chen W, Schadler L, et al. Rethinking interphase representations for modeling viscoelastic properties for polymer nanocomposites. *Materialia* 2019;6:100277. <https://doi.org/10.1016/j.mtla.2019.100277>.
- [148] Khoshkava V, Ghasemi H, Kamal MR. *Thermochimica Acta* Effect of cellulose nanocrystals ( CNC ) on isothermal crystallization kinetics of polypropylene. *Thermochim Acta* 2015;608:30–9. <https://doi.org/10.1016/j.tca.2015.04.007>.
- [149] Kim SH, Ahn SH, Hirai T. Crystallization kinetics and nucleation activity of silica nanoparticle-filled poly(ethylene 2,6-naphthalate). *Polymer* 2003;44:5625–34. [https://doi.org/10.1016/S0032-3861\(03\)00623-2](https://doi.org/10.1016/S0032-3861(03)00623-2).
- [150] Yuan Q, Awate S, Misra RDK. Nonisothermal crystallization behavior of polypropylene-clay nanocomposites. *Eur Polym J* 2006;42:1994–2003. <https://doi.org/10.1016/j.eurpolymj.2006.03.012>.
- [151] Bhattacharyya AR, Sreekumar T V., Liu T, Kumar S, Ericson LM, Hauge RH, et al. Crystallization and

- orientation studies in polypropylene/single wall carbon nanotube composite. *Polymer* 2003;44:2373–7. [https://doi.org/10.1016/S0032-3861\(03\)00073-9](https://doi.org/10.1016/S0032-3861(03)00073-9).
- [152] Pangelinan AB, McCullough RL, Kelley MJ. Fiber-Matrix Interactions in Thermoplastic Composites. *J Thermoplast Compos Mater* 1994;7:192–207. <https://doi.org/10.1177/089270579400700302>.
- [153] Zitzenbacher G, Dirnberger H, Längauer M, Holzer C. Calculation of the contact angle of polymer melts on tool surfaces from viscosity parameters. *Polymers* 2017;10. <https://doi.org/10.3390/polym10010038>.
- [154] Kamal MR, Calderon JU, Lennox BR. Surface energy of modified nanoclays and its effect on polymer/clay nanocomposites. *J Adhes Sci Technol* 2009;23:663–88. <https://doi.org/10.1163/156856108X379164>.
- [155] Fowkes FM. Donor-acceptor interactions at interfaces. *J Adhes* 1972;4:155–9. <https://doi.org/10.1080/00218467208072219>.
- [156] Æ AR. International Journal of Adhesion & Adhesives Analysis for determining surface free energy uncertainty by the Owen – Wendt method 2009;29:451–7. <https://doi.org/10.1016/j.ijadhadh.2008.09.008>.
- [157] Chau TT, Bruckard WJ, Koh PTL, Nguyen A V. A review of factors that affect contact angle and implications for flotation practice. *Adv Colloid Interface Sci* 2009;150:106–15. <https://doi.org/10.1016/j.cis.2009.07.003>.
- [158] Mohammadi-Jam S, Waters KE. Inverse gas chromatography applications: A review. *Adv Colloid Interface Sci* 2014;212:21–44. <https://doi.org/10.1016/j.cis.2014.07.002>.
- [159] Dorris GM, Gray DG. Adsorption of n-alkanes at zero surface coverage on cellulose paper and wood fibers. *J Colloid Interface Sci* 1980;77:353–62. [https://doi.org/10.1016/0021-9797\(80\)90304-5](https://doi.org/10.1016/0021-9797(80)90304-5).
- [160] Schultz J, Lavielle L, Martin C. Interfacial properties of carbon fibers - epoxy matrix composites. vol. 58. American Chemical Society; 1988.
- [161] Shi B, Wang Y, Jia L. Comparison of Dorris-Gray and Schultz methods for the calculation of surface dispersive free energy by inverse gas chromatography. *J Chromatogr A* 2011;1218:860–2. <https://doi.org/10.1016/j.chroma.2010.12.050>.
- [162] Dong S, Brendle M, Donnet. Study of solid surface polarity by inverse gas chromatography at infinite dilution. *Chromatographia* 1989;28:469–72.
- [163] Xu K, Sun W, Shao Y, Wei F, Zhang X, Wang W, et al. Recent development of PeakForce Tapping mode atomic force microscopy and its applications on nanoscience. *Nanotechnol Rev* 2018;7:605–21. <https://doi.org/10.1515/ntrev-2018-0086>.
- [164] Pittenger B, Erina N CS. Bruker application note 128: Quantitative mechanical mapping at nanosclae with peak force QNM. 2009.
- [165] Derjaguin B V., Muller VM, Toporov YP. Effect of contact deformations on the adhesion of particles. *J Colloid Interface Sci* 1975;53:314–26. [https://doi.org/10.1016/0021-9797\(75\)90018-1](https://doi.org/10.1016/0021-9797(75)90018-1).
- [166] Johnson KL, Kendall K, Roberts AD. Surface energy and the contact of elastic solids. *Proc R Soc London A Math Phys Sci* 1971;324:301–13. <https://doi.org/10.1098/rspa.1971.0141>.
- [167] Smolyakov G, Pruvost S, Cardoso L, Alonso B, Belamie E, Duchet-Rumeau J. AFM PeakForce QNM mode: Evidencing nanometre-scale mechanical properties of chitin-silica hybrid nanocomposites. *Carbohydr Polym* 2016;151:373–80. <https://doi.org/10.1016/j.carbpol.2016.05.042>.
- [168] Platz D, Thoñ EA, Pesen D, Haviland DB. Intermodulation atomic force microscopy. *Appl Phys Lett* 2008;92. <https://doi.org/10.1063/1.2909569>.
- [169] Huang H, Dobryden I, Thorén PA, Ejenstam L, Pan J, Fielden ML, et al. Local surface mechanical properties of PDMS-silica nanocomposite probed with Intermodulation AFM. *Compos Sci Technol* 2017;150:111–9. <https://doi.org/10.1016/j.compscitech.2017.07.013>.
- [170] Stöckelhuber KW, Svistkov AS, Pelevin AG, Heinrich G. Impact of filler surface modification on large scale mechanics of styrene butadiene/silica rubber composites. *Macromolecules* 2011;44:4366–81. <https://doi.org/10.1021/ma1026077>.
- [171] Mravčáková M, Boukerma K, Omastová M, Chehimi MM. Montmorillonite/polypyrrole nanocomposites.

- the effect of organic modification of clay on the chemical and electrical properties. *Mater Sci Eng C* 2006;26:306–13. <https://doi.org/10.1016/j.msec.2005.10.044>.
- [172] Colijn I, Yanat M, Terhaerd G, Molenveld K, Boeriu CG, Schroën K. Chitin Nanocrystal Hydrophobicity Adjustment by Fatty Acid Esterification for Improved Poly(lactic Acid) Nanocomposites. *Polymers* 2022;14:1–15. <https://doi.org/10.3390/polym14132619>.
- [173] Kvien I, Tanem BS, Oksman K. Characterization of cellulose whiskers and their nanocomposites by atomic force and electron microscopy. *Biomacromolecules* 2005;6:3160–5. <https://doi.org/10.1021/bm050479t>.
- [174] Iqbal MZ. Structure-property relationships in graphene / polymer nanocomposites. Colorado School of Mines, 2016.
- [175] Dorigato A, Dzenis Y, Pegoretti A. Filler aggregation as a reinforcement mechanism in polymer nanocomposites. *Mech Mater* 2013;61:79–90. <https://doi.org/10.1016/j.mechmat.2013.02.004>.
- [176] Zhao J, Wu L, Zhan C, Shao Q, Guo Z, Zhang L. Overview of polymer nanocomposites: Computer simulation understanding of physical properties. *Polymer* 2017;133:272–87. <https://doi.org/10.1016/j.polymer.2017.10.035>.
- [177] Plimpton S. Fast parallel algorithms for short-range molecular dynamics. *J Comput Phys* 1995;117:1–19. <https://doi.org/10.1006/jcph.1995.1039>.
- [178] Kalathi JT, Yamamoto U, Schweizer KS, Grest GS, Kumar SK. Nanoparticle diffusion in polymer nanocomposites. *Phys Rev Lett* 2014;112:1–5. <https://doi.org/10.1103/PhysRevLett.112.108301>.
- [179] Hoy RS, Foteinopoulou K, Kröger M. Topological analysis of polymeric melts: Chain-length effects and fast-converging estimators for entanglement length. *Phys Rev E - Stat Nonlinear, Soft Matter Phys* 2009;80:14–6. <https://doi.org/10.1103/PhysRevE.80.031803>.
- [180] Shen J, Lin X, Liu J, Li X. Revisiting stress-strain behavior and mechanical reinforcement of polymer nanocomposites from molecular dynamics simulations. *Phys Chem Chem Phys* 2020;22:16760–71. <https://doi.org/10.1039/d0cp02225j>.
- [181] Hünenberger PH. Thermostat algorithms for molecular dynamics simulations. vol. 173. Berlin: Springer; 2005. <https://doi.org/10.1007/b99427>.
- [182] Jewett AI, Stelter D, Lambert J, Saladi SM, Roscioni OM, Ricci M, et al. Moltemplate: A Tool for Coarse-Grained Modeling of Complex Biological Matter and Soft Condensed Matter Physics. *J Mol Biol* 2021;433:166841. <https://doi.org/10.1016/j.jmb.2021.166841>.
- [183] Stukowski A. Visualization and analysis of atomistic simulation data with OVITO—the Open Visualization Tool. *Model Simul Mater Sci Eng* 2010;18. <https://doi.org/10.1088/0965-0393/18/1/015012>.
- [184] Colijn I, Schroën K. Thermoplastic bio-nanocomposites: From measurement of fundamental properties to practical application. *Adv Colloid Interface Sci* 2021;292:102419. <https://doi.org/10.1016/j.cis.2021.102419>.
- [185] Baeza GP, Dessi C, Costanzo S, Zhao D, Gong S, Alegria A, et al. Network dynamics in nanofilled polymers. *Nat Commun* 2016;7:1–6. <https://doi.org/10.1038/ncomms11368>.
- [186] Jancar J, Douglas JF, Starr FW, Kumar SK, Cassagnau P, Lesser AJ, et al. Current issues in research on structure-property relationships in polymer nanocomposites. *Polymer* 2010;51:3321–43. <https://doi.org/10.1016/j.polymer.2010.04.074>.
- [187] Vogel H. The law of the relation between the viscosity of liquids and the temperature. *Phys Z* 1921;22:645–6.
- [188] Shangguan Y, Chen F, Jia E, Lin Y, Hu J, Zheng Q. New insight into Time-Temperature correlation for polymer relaxations ranging from secondary relaxation to terminal flow: Application of a Universal and developed WLF equation. *Polymers* 2017;9. <https://doi.org/10.3390/polym9110567>.
- [189] Qiao R, Deng H, Putz KW, Brinson LC. Effect of particle agglomeration and interphase on the glass transition temperature of polymer nanocomposites. *J Polym Sci Part B Polym Phys* 2011;49:740–8. <https://doi.org/10.1002/polb.22236>.
- [190] Sattar MA. Interface Structure and Dynamics in Polymer-Nanoparticle Hybrids: A Review on Molecular

- Mechanisms Underlying the Improved Interfaces. *ChemistrySelect* 2021;6:5068–96. <https://doi.org/10.1002/slct.202100831>.
- [191] Schönhalts A, Szymoniak P. *Dynamics of Composite Materials*. Springer; 2022.
- [192] Fragiadakis D, Pissis P, Bokobza L. Modified chain dynamics in poly(dimethylsiloxane)/silica nanocomposites. *J Non Cryst Solids* 2006;352:4969–72. <https://doi.org/10.1016/j.jnoncrysol.2006.02.159>.
- [193] Holt AP, Griffin PJ, Bocharova V, Agapov AL, Imel AE, Dadmun MD, et al. Dynamics at the polymer/nanoparticle interface in poly(2-vinylpyridine)/ silica nanocomposites. *Macromolecules* 2014;47:1837–43. <https://doi.org/10.1021/ma5000317>.
- [194] Tan B, Thomas NL. A review of the water barrier properties of polymer/clay and polymer/graphene nanocomposites. *J Memb Sci* 2016;514:595–612. <https://doi.org/10.1016/j.memsci.2016.05.026>.
- [195] A. Esfandiari; Hossein Nazokdast; Abo- saeed rashidi and M.E. Yazdandshenas. Review of Polymer-organoclay nanocomposites. *J Appl Sci* 2008;8:545–61.
- [196] Cassagnau P. Melt rheology of organoclay and fumed silica nanocomposites. *Polymer* 2008;49:2183–96. <https://doi.org/10.1016/j.polymer.2007.12.035>.
- [197] Jordan J, Jacob KI, Tannenbaum R, Sharaf MA, Jasiuk I. Experimental trends in polymer nanocomposites - A review. *Mater Sci Eng A* 2005;393:1–11. <https://doi.org/10.1016/j.msea.2004.09.044>.
- [198] Wang L, Gardner DJ, Wang J, Yang Y, Tekinalp HL, Li K, et al. Towards industrial-scale production of cellulose nanocomposites using melt processing: A critical review on structure-processing-property relationships. *Compos Part B Eng* 2020;201:108297. <https://doi.org/10.1016/j.compositesb.2020.108297>.
- [199] Jeffries CM, Graewert MA, Blanchet CE, Langley DB, Whitten AE, Svergun DI. Preparing monodisperse macromolecular samples for successful biological small-angle X-ray and neutron-scattering experiments. *Nat Protoc* 2016;11:2122–53. <https://doi.org/10.1038/nprot.2016.113>.
- [200] Van Der Kooij HM, Dussi S, Van De Kerkhof GT, Frijns RAM, Van Der Gucht J, Sprakel J. Laser Speckle Strain Imaging reveals the origin of delayed fracture in a soft solid. *Sci Adv* 2018;4. <https://doi.org/10.1126/sciadv.aar1926>.
- [201] van der Kooij HM, Susa A, García SJ, van der Zwaag S, Sprakel J. Imaging the Molecular Motions of Autonomous Repair in a Self-Healing Polymer. *Adv Mater* 2017;29:1–6. <https://doi.org/10.1002/adma.201701017>.
- [202] Van Der Kooij HM, Broer DJ, Liu D, Sprakel J. Electroplasticization of Liquid Crystal Polymer Networks. *ACS Appl Mater Interfaces* 2020;12:19927–37. <https://doi.org/10.1021/acsami.0c01748>.
- [203] Bajj L, Buijs J, Hermans JJ, Raven L, Iedema PD, Keune K, et al. Quantifying solvent action in oil paint using portable laser speckle imaging. *Sci Rep* 2020;10:1–12. <https://doi.org/10.1038/s41598-020-67115-1>.
- [204] Nagazi MY, Dieudonné-George P, Brambilla G, Meunier G, Cipelletti L. Phase transitions in polymorphic materials probed using space-resolved diffusing wave spectroscopy. *Soft Matter* 2018;14:6439–48. <https://doi.org/10.1039/c8sm00911b>.
- [205] Van Der Kooij HM, Fokkink R, Van Der Gucht J, Sprakel J. Quantitative imaging of heterogeneous dynamics in drying and aging paints. *Sci Rep* 2016;6:1–10. <https://doi.org/10.1038/srep34383>.
- [206] Thompson R. A Note on Restricted Maximum Likelihood Estimation with an Alternative Outlier Model. *J R Stat Soc Ser B* 1985;47:53–5. <https://doi.org/10.1111/j.2517-6161.1985.tb01329.x>.
- [207] Solid surface energy data (SFE) for common polymers. <http://www.surface-tension.de/solid-surface-energy.htm> (accessed June 16, 2022).
- [208] Wang X, Yuan M, Qin M. *Surface Energy-Modulated Inkjet Printing of Semiconductors*. Croatia: IntechOpen; 2016. <https://doi.org/10.5772/63425>.
- [209] Kim S, Moses KJ, Sharma S, Bilal M, Cohen Y. Surface characterization data for tethered polyacrylic acid layers synthesized on polysulfone surfaces. *Data Br* 2019;23:103747. <https://doi.org/10.1016/j.dib.2019.103747>.

- [210] Cui W, You W, Yu W. Mechanism of Mechanical Reinforcement for Weakly Attractive Nanocomposites in Glassy and Rubbery States. *Macromolecules* 2021;54:824–34. <https://doi.org/10.1021/acs.macromol.0c02156>.
- [211] Klonos P, Kulyk K, Borysenko M V., Gun'ko VM, Kyritsis A, Pissis P. Effects of Molecular Weight below the Entanglement Threshold on Interfacial Nanoparticles/Polymer Dynamics. *Macromolecules* 2016;49:9457–73. <https://doi.org/10.1021/acs.macromol.6b01931>.
- [212] Cheng S, Holt AP, Wang H, Fan F, Bocharova V, Martin H, et al. Unexpected Molecular Weight Effect in Polymer Nanocomposites. *Phys Rev Lett* 2016;116:1–5. <https://doi.org/10.1103/PhysRevLett.116.038302>.
- [213] Feynman R. There's plenty of room at the bottom. *Feynman Comput.*, 2018, p. 63–76. <https://doi.org/10.1201/9780429500459>.
- [214] Astruc D. Introduction: Nanoparticles in Catalysis. *Chem Rev* 2020;120:461–3. <https://doi.org/10.1021/acs.chemrev.8b00696>.
- [215] Gelperina S, Kisich K, Iseman MD, Heifets L. The potential advantages of nanoparticle drug delivery systems in chemotherapy of tuberculosis. *Am J Respir Crit Care Med* 2005;172:1487–90. <https://doi.org/10.1164/rccm.200504-613PP>.
- [216] Jayakumar R, Menon D, Manzoor K, Nair S V., Tamura H. Biomedical applications of chitin and chitosan based nanomaterials - A short review. *Carbohydr Polym* 2010;82:227–32. <https://doi.org/10.1016/j.carbpol.2010.04.074>.
- [217] Zeng JB, He YS, Li SL, Wang YZ. Chitin whiskers: An overview. *Biomacromolecules* 2012;13:1–11. <https://doi.org/10.1021/bm201564a>.
- [218] Binnewerg B, Schubert M, Voronkina A, Muzychka L, Wysokowski M, Petrenko I, et al. Marine biomaterials: Biomimetic and pharmacological potential of cultivated *Aplysina aerophoba* marine demosponge. *Mater Sci Eng C* 2020;109:110566. <https://doi.org/10.1016/j.msec.2019.110566>.
- [219] Herrera N, Salaberria AM, Mathew AP, Oksman K. Plasticized polylactic acid nanocomposite films with cellulose and chitin nanocrystals prepared using extrusion and compression molding with two cooling rates: Effects on mechanical, thermal and optical properties. *Compos Part A Appl Sci Manuf* 2016;83:89–97. <https://doi.org/10.1016/j.compositesa.2015.05.024>.
- [220] Lopez O, Garcia MA, Villar MA, Gentili A, Rodriguez MS, Albertengo L. Thermo-compression of biodegradable thermoplastic corn starch films containing chitin and chitosan. *LWT - Food Sci Technol* 2014;57:106–15. <https://doi.org/10.1016/j.lwt.2014.01.024>.
- [221] Shankar S, Reddy JP, Rhim JW, Kim HY. Preparation, characterization, and antimicrobial activity of chitin nanofibrils reinforced carrageenan nanocomposite films. *Carbohydr Polym* 2015;117:468–75. <https://doi.org/10.1016/j.carbpol.2014.10.010>.
- [222] Chung NO, Lee MK, Lee J. Mechanism of freeze-drying drug nanosuspensions. *Int J Pharm* 2012;437:42–50. <https://doi.org/10.1016/j.ijpharm.2012.07.068>.
- [223] Esparza Y, Ngo TD, Fraschini C, Boluk Y. Aggregate Morphology and Aqueous Dispersibility of Spray-Dried Powders of Cellulose Nanocrystals. *Ind Eng Chem Res* 2019;58:19926–36. <https://doi.org/10.1021/acs.iecr.9b03951>.
- [224] Beck S, Bouchard J, Berry R. Dispersibility in water of dried nanocrystalline cellulose. *Biomacromolecules* 2012;13:1486–94. <https://doi.org/10.1021/bm300191k>.
- [225] Abdelwahed W, Degobert G, Stainmesse S, Fessi H. Freeze-drying of nanoparticles: Formulation, process and storage considerations. *Adv Drug Deliv Rev* 2006;58:1688–713. <https://doi.org/10.1016/j.addr.2006.09.017>.
- [226] Choi MJ, Briançon S, Andrieu J, Min SG, Fessi H. Effect of freeze-drying process conditions on the stability of nanoparticles. *Dry Technol* 2004;22:335–46. <https://doi.org/10.1081/DRT-120028238>.
- [227] Paillet M, Dufresne A. Chitin whisker reinforced thermoplastic nanocomposites. *Macromolecules* 2001;34:6527–30. <https://doi.org/10.1021/ma002049v>.
- [228] Li C, Liu H, Luo B, Wen W, He L, Liu M, et al. Nanocomposites of poly(l-lactide) and surface-modified

- chitin whiskers with improved mechanical properties and cytocompatibility. *Eur Polym J* 2016;81:266–83. <https://doi.org/10.1016/j.eurpolymj.2016.06.015>.
- [229] Salaberria AM, Labidi J, Fernandes SCM. Chitin nanocrystals and nanofibers as nano-sized fillers into thermoplastic starch-based biocomposites processed by melt-mixing. *Chem Eng J* 2014;256:356–64. <https://doi.org/10.1016/j.cej.2014.07.009>.
- [230] Yokota H, Kadowaki M, Matsuura T, Imanaka H, Ishida N, Imamura K. The Use of a Combination of a Sugar and Surfactant to Stabilize Au Nanoparticle Dispersion against Aggregation during Freeze-Drying. *Langmuir* 2020;36:6698–705. <https://doi.org/10.1021/acs.langmuir.0c00695>.
- [231] Michen B, Geers C, Vanhecke D, Endes C, Rothen-Rutishauser B, Balog S, et al. Avoiding drying-artifacts in transmission electron microscopy: Characterizing the size and colloidal state of nanoparticles. *Sci Rep* 2015;5. <https://doi.org/10.1038/srep09793>.
- [232] Park HM, Misra M, Drzal LT, Mohanty AK. “Green” nanocomposites from cellulose acetate bioplastic and clay: Effect of eco-friendly triethyl citrate plasticizer. *Biomacromolecules* 2004;5:2281–8. <https://doi.org/10.1021/bm049690f>.
- [233] Arias A, Heuzey M-C, Huneault MA, Ausias G, Bendahou A. Enhanced dispersion of cellulose nanocrystals in melt-processed polylactide-based nanocomposites. *Cellulose* 2015;22:483–98. <https://doi.org/10.1007/s10570-014-0476-z>.
- [234] Huang YY, Terentjev EM. Dispersion of carbon nanotubes: Mixing, sonication, stabilization, and composite properties. *Polymers* 2012;4:275–95. <https://doi.org/10.3390/polym4010275>.
- [235] So HH, Cho JW, Sahoo NG. Effect of carbon nanotubes on mechanical and electrical properties of polyimide/carbon nanotubes nanocomposites. *Eur Polym J* 2007;43:3750–6. <https://doi.org/10.1016/j.eurpolymj.2007.06.025>.
- [236] Harshe YM, Lattuada M, Soos M. Experimental and modeling study of breakage and restructuring of open and dense colloidal aggregates. *Langmuir* 2011;27:5739–52. <https://doi.org/10.1021/la1046589>.
- [237] Broers L, Dongen S van, Goederen V de, Ton M, Spaen J, Boeriu C, et al. Addition of Chitin Nanoparticles improves Poly(lactic Acid) Film Properties. *Nanotechnol Adv Mater Sci* 2018;1:1–8.
- [238] Mentler A, Schomakers J, Kloss S, Zechmeister-Boltenstern S, Schuller R, Mayer H. Calibration of ultrasonic power output in water, ethanol and sodium polytungstate. *Int Agrophysics* 2017;31:583–8. <https://doi.org/10.1515/intag-2016-0083>.
- [239] Booth A, Alstrup Jensen K. SOP for probe sonicator calibration of delivered acoustic power and deagglomeration efficiency for ecotoxicological testing. 2015.
- [240] Mamvura TA, Iyuke SE, Paterson AE. Energy changes during use of high-power ultrasound on food grade surfaces. *South African J Chem Eng* 2018;25:62–73. <https://doi.org/10.1016/j.sajce.2017.12.001>.
- [241] Jiang L, Li X, Liu L, Zhang Q. Cellular uptake mechanism and intracellular fate of hydrophobically modified pullulan nanoparticles. *Int J Nanomedicine* 2013;8:1825–34. <https://doi.org/10.2147/IJN.S44342>.
- [242] Basumallick S, Gabriela Nogueira Campos M, Richardson D, Gesquiere A, Santra S. Hydrothermally treated chitosan spontaneously forms water-soluble spherical particles stable at a wide pH range. *Int J Polym Mater Polym Biomater* 2016;65:751–8. <https://doi.org/10.1080/00914037.2016.1163568>.
- [243] Heux L, Brugnerotto J, Desbrières J, Versali MF, Rinaudo M. Solid state NMR for determination of degree of acetylation of chitin and chitosan. *Biomacromolecules* 2000;1:746–51. <https://doi.org/10.1021/bm000070y>.
- [244] Schindelin J, Arganda-Carreras I, Frise E, Kaynig V, Longair M, Pietzsch T, et al. Fiji: An open-source platform for biological-image analysis. *Nat Methods* 2012;9:676–82. <https://doi.org/10.1038/nmeth.2019>.
- [245] Carl P. Radial Profile Extended 2006. <http://questpharma.u-strasbg.fr/html/radial-profile-ext.html>.
- [246] Goodrich JD, Winter WT. Alpha-Chitin nanocrystals prepared from shrimp shells and their specific surface area measurement. *Biomacromolecules* 2007;8:252–7. <https://doi.org/10.1021/bm0603589>.
- [247] Pereira AGB, Muniz EC, Hsieh Y Lo. Chitosan-sheath and chitin-core nanowhiskers. *Carbohydr Polym* 2014;107:158–66. <https://doi.org/10.1016/j.carbpol.2014.02.046>.

- [248] Xiao F, Li XY. Modelling the kinetics of aggregate breakage using improved breakage kernel. *Water Sci Technol* 2008;57:151–7. <https://doi.org/10.2166/wst.2008.789>.
- [249] Vassileva ND, Van Den Ende D, Mugele F, Mellema J. Fragmentation and erosion of two-dimensional aggregates in shear flow. *Langmuir* 2007;23:2352–61. <https://doi.org/10.1021/la0625087>.
- [250] Rumpf H, Knepper W. The strength of granules and agglomerates. *Int. Symp. Agglom.*, 1962, p. 379–418.
- [251] Lu Y, Sun Q, She X, Xia Y, Liu Y, Li J, et al. Fabrication and characterisation of  $\alpha$ -chitin nanofibers and highly transparent chitin films by pulsed ultrasonication. *Carbohydr Polym* 2013;98:1497–504. <https://doi.org/10.1016/j.carbpol.2013.07.038>.
- [252] Wang Q, Yan X, Chang Y, Ren L, Zhou J. Fabrication and characterization of chitin nanofibers through esterification and ultrasound treatment. *Carbohydr Polym* 2018;180:81–7. <https://doi.org/10.1016/j.carbpol.2017.09.010>.
- [253] Zhao HP, Feng XQ, Gao H. Ultrasonic technique for extracting nanofibers from nature materials. *Appl Phys Lett* 2007;90:65–6. <https://doi.org/10.1063/1.2450666>.
- [254] Ifuku S, Saimoto H. Chitin nanofibers: Preparations, modifications, and applications. *Nanoscale* 2012;4:3308–18. <https://doi.org/10.1039/c2nr30383c>.
- [255] Pillai CKS, Paul W, Sharma CP. Chitin and chitosan polymers: Chemistry, solubility and fiber formation. *Prog Polym Sci* 2009;34:641–78. <https://doi.org/10.1016/j.progpolymsci.2009.04.001>.
- [256] Tajik B, Abbassi A, Saffar-Avval M, Najafabadi MA. Ultrasonic properties of suspensions of TiO<sub>2</sub> and Al<sub>2</sub>O<sub>3</sub> nanoparticles in water. *Powder Technol* 2012;217:171–6. <https://doi.org/10.1016/j.powtec.2011.10.024>.
- [257] Graves JE, Sugden M, Litchfield RE, Hutt DA, Mason TJ, Cobley AJ. Ultrasound assisted dispersal of a copper nanopowder for electroless copper activation. *Ultrason Sonochem* 2016;29:428–38. <https://doi.org/10.1016/j.ulsonch.2015.10.016>.
- [258] Madhavan Nampoothiri K, Nair NR, John RP. An overview of the recent developments in polylactide (PLA) research. *Bioresour Technol* 2010;101:8493–501. <https://doi.org/10.1016/j.biortech.2010.05.092>.
- [259] Armentano I, Bitinis N, Fortunati E, Mattioli S, Rescignano N, Verdejo R, et al. Multifunctional nanostructured PLA materials for packaging and tissue engineering. *Prog Polym Sci* 2013;38:1720–47. <https://doi.org/10.1016/j.progpolymsci.2013.05.010>.
- [260] Ifuku S, Ikuta A, Egusa M, Kaminaka H, Izawa H, Morimoto M, et al. Preparation of high-strength transparent chitosan film reinforced with surface-deacetylated chitin nanofibers. *Carbohydr Polym* 2013;98:1198–202. <https://doi.org/10.1016/j.carbpol.2013.07.033>.
- [261] Pan C, Qian J, Fan J, Guo H, Gou L, Yang H, et al. Preparation nanoparticle by ionic cross-linked emulsified chitosan and its antibacterial activity. *Colloids Surfaces A Physicochem Eng Asp* 2019;568:362–70. <https://doi.org/10.1016/j.colsurfa.2019.02.039>.
- [262] Rozman NAS, Yenn TW, Ring LC, Nee TW, Hasanolbasori MA, Abdullah SZ. Potential antimicrobial applications of chitosan nanoparticles (ChNP). *J Microbiol Biotechnol* 2019;29:1009–13. <https://doi.org/10.4014/jmb.1904.04065>.
- [263] Zhang Q, Wei S, Huang J, Feng J, Chang PR. Effect of surface acetylated-chitin nanocrystals on structure and mechanical properties of poly(lactic acid). *J Appl Polym Sci* 2014;131:2–9. <https://doi.org/10.1002/app.39809>.
- [264] Namazi H, Dadkhah A. Convenient method for preparation of hydrophobically modified starch nanocrystals with using fatty acids. *Carbohydr Polym* 2010;79:731–7. <https://doi.org/10.1016/j.carbpol.2009.09.033>.
- [265] Colijn I, Fokkink R, Schroën K. Quantification of energy input required for chitin nanocrystal aggregate size reduction through ultrasound. *Sci Rep* 2021;11. <https://doi.org/10.1038/s41598-021-96657-1>.
- [266] Shigemasa Y, Matsuura H, Sashiwa H, Saimoto H. Evaluation of different absorbance ratios from infrared spectroscopy for analyzing the degree of deacetylation in chitin. *Int J Biol Macromol* 1996;18:237–42. [https://doi.org/10.1016/0141-8130\(95\)01079-3](https://doi.org/10.1016/0141-8130(95)01079-3).
- [267] Hoppenreijns LJG, Berton-Carabin CC, Dubbelboer A, Hennebelle M. Evaluation of oxygen partial

- pressure, temperature and stripping of antioxidants for accelerated shelf-life testing of oil blends using <sup>1</sup>H NMR. *Food Res Int* 2021;147:110555. <https://doi.org/10.1016/j.foodres.2021.110555>.
- [268] Chang PR, Jian R, Yu J, Ma X. Starch-based composites reinforced with novel chitin nanoparticles. *Carbohydr Polym* 2010;80:420–5. <https://doi.org/10.1016/j.carbpol.2009.11.041>.
- [269] Xavier M. Standardization of Optimum Conditions for the Production of Glucosamine Hydrochloride from Chitin. Doctoral dissertation, Cochin University of Science and Technology, 2006.
- [270] Arora A, Padua GW. Review: Nanocomposites in food packaging. *J Food Sci* 2010;75:43–9. <https://doi.org/10.1111/j.1750-3841.2009.01456.x>.
- [271] Herrera N, Roch H, Salaberria AM, Pino-Orellana MA, Labidi J, Fernandes SCM, et al. Functionalized blown films of plasticized polylactic acid/chitin nanocomposite: Preparation and characterization. *Mater Des* 2016;92:846–52. <https://doi.org/10.1016/j.matdes.2015.12.083>.
- [272] Geueke B, Groh K, Muncke J. Food packaging in the circular economy: Overview of chemical safety aspects for commonly used materials. *J Clean Prod* 2018;193:491–505. <https://doi.org/https://doi.org/10.1016/j.jclepro.2018.05.005>.
- [273] Kirchherr J, Reike D, Hekkert M. Conceptualizing the circular economy: An analysis of 114 definitions. *Resour Conserv Recycl* 2017;127:221–32. <https://doi.org/10.1016/j.resconrec.2017.09.005>.
- [274] Kershaw PJ. Biodegradable plastics and marine litter: misconceptions, concerns and impacts on marine environments. Nairobi: United Nations Environment Programme (UNEP); 2016.
- [275] PlasticsEurope. *Plastics - The facts 2018: An analysis of European plastics production, demand and waste data*. PlasticsEurope; 2018.
- [276] European Commission. *A European Strategy for Plastics in a Circular Economy*. 2018.
- [277] Calisto Friant M, Lakerveld D, Vermeulen WJV, Salomone R. Transition to a sustainable circular plastics economy in the netherlands: Discourse and policy analysis. *Sustain* 2022;14:1–32. <https://doi.org/10.3390/su14010190>.
- [278] Termeer CJAM, Metzke TAP. More than peanuts: Transformation towards a circular economy through a small-wins governance framework. *J Clean Prod* 2019;240. <https://doi.org/https://doi.org/10.1016/j.jclepro.2019.118272>.
- [279] Brown P, Von Daniels C, Bocken NMP, Balkenende AR. A process model for collaboration in circular oriented innovation. *J Clean Prod* 2021;286:125499. <https://doi.org/10.1016/j.jclepro.2020.125499>.
- [280] Rein M, Schön D. *Reframing Policy Discourse. Argumentative Turn Policy Anal. Plan.*, Durham: Duke University Press; 1993, p. 145–66. <https://doi.org/https://doi.org/10.1215/9780822381815>.
- [281] Starke JR, Metzke TAP, Candel JLL, Termeer CJAM. Conceptualizing controversies in the EU circular bioeconomy transition. *Ambio* 2022. <https://doi.org/10.1007/s13280-022-01730-2>.
- [282] Metzke T. Framing the future of fracking: Discursive lock-in or energy degrowth in the Netherlands? *J Clean Prod* 2018;197:1737–45. <https://doi.org/10.1016/j.jclepro.2017.04.158>.
- [283] Raven PG, Elahi S. The New Narrative: Applying narratology to the shaping of futures outputs. *Futures* 2015;74:49–61. <https://doi.org/10.1016/j.futures.2015.09.003>.
- [284] Jasanoff S, Kim S-H, Kennedy JF. Sociotechnical Imaginaries and National Energy Policies. *Sci Cult* 2013;22:189–96. <https://doi.org/10.1080/09505431.2013.786990>.
- [285] Kerschner C, Wächter P, Nierling L, Ehlers MH. Degrowth and Technology: Towards feasible, viable, appropriate and convivial imaginaries. *J Clean Prod* 2018;197:1619–36. <https://doi.org/10.1016/j.jclepro.2018.07.147>.
- [286] Hajer M, Versteeg W. Imagining the post-fossil city: why is it so difficult to think of new possible worlds? *Territ Polit Gov* 2019;7:122–34. <https://doi.org/10.1080/21622671.2018.1510339>.
- [287] Korhonen J, Nuur C, Feldmann A, Birkie SE. Circular economy as an essentially contested concept. *J Clean Prod* 2018;175:544–52. <https://doi.org/10.1016/j.jclepro.2017.12.111>.
- [288] Webster K. What might we say about a circular economy? Some temptations to avoid if possible. *World Futur J Gen Evol* 2013;69:542–54. <https://doi.org/10.1080/02604027.2013.835977>.

- [289] Korhonen J, Honkasalo A, Seppälä J. Circular Economy: The Concept and its Limitations. *Ecol Econ* 2018;143:37–46. <https://doi.org/10.1016/j.ecolecon.2017.06.041>.
- [290] Kelleher L, Henchion M, O'Neill E. Framing the Circular Bioeconomy in Ireland's Broadsheet Media, 2004–2019. *Environ Commun* 2021;0:1–21. <https://doi.org/10.1080/17524032.2021.1889632>.
- [291] Peltomaa J. Drumming the Barrels of Hope? Bioeconomy narratives in the media. *Sustain* 2018;10. <https://doi.org/10.3390/su10114278>.
- [292] Dewulf A, Craps M, Dercon G. How issues get framed and reframed when different communities meet: A multi-level analysis of a collaborative soil conservation initiative in the ecuadorian andes. *J Community Appl Soc Psychol* 2004;14:177–92. <https://doi.org/10.1002/casp.772>.
- [293] van Hulst M, Yanow D. From Policy “Frames” to “Framing”: Theorizing a More Dynamic, Political Approach. *Am Rev Public Adm* 2016;46:92–112. <https://doi.org/10.1177/0275074014533142>.
- [294] Dewulf A, Bouwen R. Issue Framing in Conversations for Change: Discursive Interaction Strategies for “Doing Differences.” *J Appl Behav Sci* 2012;48:168–93. <https://doi.org/https://doi.org/10.1177%2F0021886312438858>.
- [295] Rein M, Schon D. Problem Setting in Policy Research, using social research in public policy making. 1977.
- [296] Friese S. ATLAS.ti 8 Mac User Manual. ATLAS.ti Scientific Software Development; 2019.
- [297] Rijksen M. Recycling alleen verslaat plasticmonster niet. *De Volkskrant* 2019.
- [298] van den Hoff Harns J. Plastic soep. *Trouw* 2013.
- [299] Vink J. Bioplastic. *Trouw* 2016.
- [300] Kamsma M. Geen deksel meer op fruit: dat scheelt 300.000 kilo plastic. *NRC Handelsbl* 2018.
- [301] Romeo J. Plastics Engineering in 2019: The Technological Runway Ahead. *Plast Eng* 2019;1:42–7. <https://doi.org/https://doi.org/10.1002/peng.20058>.
- [302] Dobrucka R. Bioplastic packaging materials in circular economy. *LogForum* 2019;15:129–37. <https://doi.org/http://doi.org/10.17270/J.LOG.2019.322>.
- [303] Paço A, Jacinto J, da Costa JP, Santos PSM, Vitorino R, Duarte AC, et al. Biotechnological tools for the effective management of plastics in the environment. *Crit Rev Environ Sci Technol* 2019;49:410–41. <https://doi.org/https://doi.org/10.1080/10643389.2018.1548862>.
- [304] Linder M. Ripe for disruption: Reimagining the role of green chemistry in a circular economy. *Green Chem Lett Rev* 2017;10:428–35. <https://doi.org/https://doi.org/10.1080/17518253.2017.1392618>.
- [305] Kawashima N, Yagi T, Kojima K. How Do Bioplastics and Fossil-Based Plastics Play in a Circular Economy? *Macromol Mater Eng* 2019;304:1–14. <https://doi.org/https://doi.org/10.1002/mame.201900383>.
- [306] Laird K. Exploring plastics role in the future circular economy. *Plast Eng* 2017;6:12–9. <https://doi.org/10.1002/j.1941-9635.2017.tb01725.x>.
- [307] Speksnijder C. Alternatieven voor onze verslaving. *De Volkskrant* 2016.
- [308] Mohan Raj J. Picnic benches and the circular economy. *Reinf Plast* 2019;63:213–5. <https://doi.org/https://doi.org/10.1016/j.repl.2019.05.001>.
- [309] Aliotta L, Gigante V, Coltelli MB, Cinelli P, Lazzeri A. Evaluation of Mechanical and Interfacial Properties of Bio-Composites Based on Poly(Lactic Acid) with Natural Cellulose Fibers. *Int J Mol Sci* 2019;20. <https://doi.org/https://doi.org/10.3390/ijms20040960>.
- [310] Van Eygen E, Laner D, Fellner J. Circular economy of plastic packaging: Current practice and perspectives in Austria. *Waste Manag* 2018;72:55–64. <https://doi.org/https://doi.org/10.1016/j.wasman.2017.11.040>.
- [311] Ren H, Qiao F, Shi Y, Knutzen MW, Wang Z, Du H, et al. PlantBottle™ Packaging program is continuing its journey to pursue bio-mono-ethylene glycol using agricultural waste. *J Renew Sustain Energy* 2015;7:1–5. <https://doi.org/10.1063/1.4929336>.
- [312] Heidbreder LM, Bablok I, Drews S, Menzel C. Tackling the plastic problem: A review on perceptions,

- behaviors, and interventions. *Sci Total Environ* 2019;668:1077–93. <https://doi.org/10.1016/j.scitotenv.2019.02.437>.
- [313] Pahl S, Wyles KJ, Thompson RC. Channelling passion for the ocean towards plastic pollution. *Nat Hum Behav* 2017;1:697–9. <https://doi.org/10.1038/s41562-017-0204-4>.
- [314] Taufik D, Reinders MJ, Molenveld K, Onwezen MC. The paradox between the environmental appeal of bio-based plastic packaging for consumers and their disposal behaviour. *Sci Total Environ* 2020;705. <https://doi.org/10.1016/j.scitotenv.2019.135820>.
- [315] Beitzten-Heineke EF, Balta-Ozkan N, Reefke H. The prospects of zero-packaging grocery stores to improve the social and environmental impacts of the food supply chain. *J Clean Prod* 2017;140:1528–41. <https://doi.org/10.1016/j.jclepro.2016.09.227>.
- [316] Mohamed SAA, El-Sakhawy M, El-Sakhawy MAM. Polysaccharides, Protein and Lipid -Based Natural Edible Films in Food Packaging: A Review. *Carbohydr Polym* 2020;238:116178. <https://doi.org/10.1016/j.carbpol.2020.116178>.
- [317] Macnaghten P, Habets MGJL. Breaking the impasse: Towards a forward-looking governance framework for gene editing with plants. *Plants People Planet* 2020;2:353–65. <https://doi.org/10.1002/ppp3.10107>.
- [318] Selin C. The Sociology of the Future: Tracing Stories of Technology and Time. *Sociol Compass* 2008;2:1878–95. <https://doi.org/10.1111/j.1751-9020.2008.00147.x>.
- [319] Gironi F, Piemonte V. Bioplastics and petroleum-based plastics: Strengths and weaknesses. *Energy Sources, Part A Recover Util Environ Eff* 2011;33:1949–59. <https://doi.org/10.1080/15567030903436830>.
- [320] Sorichetti V, Hugouvieux V, Kob W. Structure and Dynamics of a Polymer-Nanoparticle Composite: Effect of Nanoparticle Size and Volume Fraction. *Macromolecules* 2018;51:5375–91. <https://doi.org/10.1021/acs.macromol.8b00840>.
- [321] Prasad AS, Wang Y, Li X, Iyer A, Chen W, Brinson LC, et al. Investigating the effect of surface modification on the dispersion process of polymer nanocomposites. *Nanocomposites* 2020;6:111–24. <https://doi.org/10.1080/20550324.2020.1809250>.
- [322] Jouault N, Dalmas F, Boué F, Jestin J. Multiscale characterization of filler dispersion and origins of mechanical reinforcement in model nanocomposites. *Polymer* 2012;53:761–75. <https://doi.org/10.1016/j.polymer.2011.12.001>.
- [323] Rubinstein M, Colby RH. *Polymer Physics*. New York: Oxford University Press; 2003.
- [324] Carsi M, Sanchis MJ, Gómez CM, Rodríguez S, Torres FG. Effect of chitin whiskers on the molecular dynamics of carrageenan-based nanocomposites. *Polymers* 2019;11:1–16. <https://doi.org/10.3390/POLYM11061083>.
- [325] Drelich JW. Contact angles: From past mistakes to new developments through liquid-solid adhesion measurements. *Adv Colloid Interface Sci* 2019;267:1–14. <https://doi.org/10.1016/j.cis.2019.02.002>.
- [326] Ruiz-Cabello FJM, Rodríguez-Valverde MA, Cabrerizo-Vilchez MA. Equilibrium contact angle or the most-stable contact angle? *Adv Colloid Interface Sci* 2014;206:320–7. <https://doi.org/10.1016/j.cis.2013.09.003>.
- [327] Kung CH, Sow PK, Zahiri B, Mérida W. Assessment and Interpretation of Surface Wettability Based on Sessile Droplet Contact Angle Measurement: Challenges and Opportunities. *Adv Mater Interfaces* 2019;6:1–27. <https://doi.org/10.1002/admi.201900839>.
- [328] Shrestha S, Wang B, Dutta P. Nanoparticle processing: Understanding and controlling aggregation. *Adv Colloid Interface Sci* 2020;279:102162. <https://doi.org/10.1016/j.cis.2020.102162>.
- [329] Trenkenschuh E, Friess W. Freeze-drying of nanoparticles: How to overcome colloidal instability by formulation and process optimization. *Eur J Pharm Biopharm* 2021;165:345–60. <https://doi.org/10.1016/j.ejpb.2021.05.024>.
- [330] Derjaguin B, Landau L. Theory of the stability of strongly charged lyophobic sols and of the adhesion of strongly charged particles in solutions of electrolytes. *Prog Surf Sci* 1993;43:30–59. [https://doi.org/10.1016/0079-6816\(93\)90013-L](https://doi.org/10.1016/0079-6816(93)90013-L).

- [331] Verwey EJW, Overbeek JTG. Theory of the stability of lyophobic colloids. *J Colloid Sci* 1955;10:224–5. [https://doi.org/10.1016/0095-8522\(55\)90030-1](https://doi.org/10.1016/0095-8522(55)90030-1).
- [332] Naguib YW, Cui Z. *Nanomedicine: The promise and challenges in cancer chemotherapy*. vol. 811. London: Springer; 2014. [https://doi.org/10.1007/978-94-017-8739-0\\_11](https://doi.org/10.1007/978-94-017-8739-0_11).
- [333] Lintingre E, Lequeux F, Talini L, Tsapis N. Control of particle morphology in the spray drying of colloidal suspensions. *Soft Matter* 2016;12:7435–44. <https://doi.org/10.1039/c6sm01314g>.
- [334] Geng S, Wei J, Aitomäki Y, Noël M, Oksman K. Well-dispersed cellulose nanocrystals in hydrophobic polymers by: In situ polymerization for synthesizing highly reinforced bio-nanocomposites. *Nanoscale* 2018;10:11797–807. <https://doi.org/10.1039/c7nr09080c>.
- [335] Carvalho AJF, Curvelo AAS, Gandini A. Surface chemical modification of thermoplastic starch: Reactions with isocyanates, epoxy functions and stearyl chloride. *Ind Crops Prod* 2005;21:331–6. <https://doi.org/10.1016/j.indcrop.2004.04.027>.
- [336] Uschanov P, Johansson LS, Maunu SL, Laine J. Heterogeneous modification of various celluloses with fatty acids. *Cellulose* 2011;18:393–404. <https://doi.org/10.1007/s10570-010-9478-7>.
- [337] Hamad WY. *Cellulose nanocrystals: Properties, production and applications*. Peachtree Corners: Tappi Press; 2017. <https://doi.org/10.1002/9781118675601>.
- [338] Ferreira F V., Dufresne A, Pinheiro IF, Souza DHS, Gouveia RF, Mei LHI, et al. How do cellulose nanocrystals affect the overall properties of biodegradable polymer nanocomposites: A comprehensive review. *Eur Polym J* 2018;108:274–85. <https://doi.org/10.1016/j.eurpolymj.2018.08.045>.
- [339] Miao C, Hamad WY. Critical insights into the reinforcement potential of cellulose nanocrystals in polymer nanocomposites. *Curr Opin Solid State Mater Sci* 2019;23:100761. <https://doi.org/10.1016/j.cossms.2019.06.005>.
- [340] Kamal MR, Khoshkava V. Effect of cellulose nanocrystals (CNC) on rheological and mechanical properties and crystallization behavior of PLA/CNC nanocomposites. *Carbohydr Polym* 2015;123:105–14. <https://doi.org/10.1016/j.carbpol.2015.01.012>.
- [341] Efros AL. *Physics and geometry of disorder : percolation theory*. Moscow: Imported Pubn; 1986.
- [342] Razavi R, Zare Y, Rhee KY. A model for tensile strength of polymer/carbon nanotubes nanocomposites assuming the percolation of interphase regions. *Colloids Surfaces A Physicochem Eng Asp* 2018;538:148–54. <https://doi.org/10.1016/j.colsurfa.2017.10.063>.
- [343] Irzhak VI. Percolation Threshold in Polymer Nanocomposites. *Colloid J* 2021;83:64–9. <https://doi.org/10.1134/S1061933X21010063>.
- [344] Moll J. *Polymer-Particle Nanocomposites : Size and Dispersion Effects*. Doctoral dissertation, Columbia University, 2012. <https://doi.org/10.7916/D8959QN5>.
- [345] Senses E, Darvishi S, Tyagi MS, Tyagi MS, Faraone A. Entangled Polymer Dynamics in Attractive Nanocomposite Melts. *Macromolecules* 2020;53:4982–9. <https://doi.org/10.1021/acs.macromol.9b02545>.
- [346] Dufresne A. Processing of Polymer Nanocomposites Reinforced with Polysaccharide Nanocrystals. *Molecules* 2010;4111–28. <https://doi.org/10.3390/molecules15064111>.
- [347] Mariano M, El Kissi N, Dufresne A. Cellulose nanocrystals and related nanocomposites: Review of some properties and challenges. *J Polym Sci Part B Polym Phys* 2014;52:791–806. <https://doi.org/10.1002/polb.23490>.
- [348] Pirani SI, Krishnamachari P, Hashaikeh R. Optimum loading level of nanoclay in PLA nanocomposites: Impact on the mechanical properties and glass transition temperature. *J Thermoplast Compos Mater* 2014;27:1461–78. <https://doi.org/10.1177/0892705712473627>.
- [349] Pal AK, Katiyar V. Nanoamphiphilic Chitosan Dispersed Poly(lactic acid) Bionanocomposite Films with Improved Thermal, Mechanical, and Gas Barrier Properties. *Biomacromolecules* 2016;17:2603–18. <https://doi.org/10.1021/acs.biomac.6b00619>.
- [350] Priestley RD, Cangialosi D, Napolitano S. On the equivalence between the thermodynamic and dynamic measurements of the glass transition in confined polymers. *J Non Cryst Solids* 2015;407:288–95. <https://doi.org/10.1016/j.jnoncrysol.2014.09.048>.

- [351] Cui Y, Kumar S, Rao Kona B, Van Houcke D. Gas barrier properties of polymer/clay nanocomposites. *RSC Adv* 2015;5:63669–90. <https://doi.org/10.1039/c5ra10333a>.
- [352] Wolf C, Angellier-Coussy H, Gontard N, Doghieri F, Guillard V. How the shape of fillers affects the barrier properties of polymer/non-porous particles nanocomposites: A review. *J Memb Sci* 2018;556:393–418. <https://doi.org/10.1016/j.memsci.2018.03.085>.
- [353] Kumar P, Sandeep KP, Alavi S, Truong VD. A Review of Experimental and Modeling Techniques to Determine Properties of Biopolymer-Based Nanocomposites 2011;76. <https://doi.org/10.1111/j.1750-3841.2010.01919.x>.
- [354] Pei A, Zhou Q, Berglund LA. Functionalized cellulose nanocrystals as biobased nucleation agents in poly(l-lactide) (PLLA) - Crystallization and mechanical property effects. *Compos Sci Technol* 2010;70:815–21. <https://doi.org/10.1016/j.compscitech.2010.01.018>.
- [355] Hu F, Lin N, Chang PR, Huang J. Reinforcement and nucleation of acetylated cellulose nanocrystals in foamed polyester composites. *Carbohydr Polym* 2015;129:208–15. <https://doi.org/10.1016/j.carbpol.2015.04.061>.
- [356] Papageorgiou GZ, Achilias DS, Bikiaris DN, Karayannidis GP. Crystallization kinetics and nucleation activity of filler in polypropylene/surface-treated SiO<sub>2</sub> nanocomposites. *Thermochim Acta* 2005;427:117–28. <https://doi.org/10.1016/j.tca.2004.09.001>.
- [357] Quaresimin M, Schulte K, Zappalorto M, Chandrasekaran S. Toughening mechanisms in polymer nanocomposites: From experiments to modelling. *Compos Sci Technol* 2016;123:187–204. <https://doi.org/10.1016/j.compscitech.2015.11.027>.
- [358] Yanat M, Colijn I, Schroen K. Chitin Nanocrystals Provide Antioxidant Activity to Polylactic. *Polymers* 2022;14. <https://doi.org/https://doi.org/10.3390/polym14142965>.
- [359] Aider M. Chitosan application for active bio-based films production and potential in the food industry: Review. *LWT - Food Sci Technol* 2010;43:837–42. <https://doi.org/10.1016/j.lwt.2010.01.021>.
- [360] Raafat D, Von Barga K, Haas A, Sahl HG. Insights into the mode of action of chitosan as an antibacterial compound. *Appl Environ Microbiol* 2008;74:3764–73. <https://doi.org/10.1128/AEM.00453-08>.
- [361] Jayakumar R, Prabakaran M, Sudheesh Kumar PT, Nair S V., Tamura H. Biomaterials based on chitin and chitosan in wound dressing applications. *Biotechnol Adv* 2011;29:322–37. <https://doi.org/10.1016/j.biotechadv.2011.01.005>.
- [362] Ing LY, Zin NM, Sarwar A, Katas H. Antifungal activity of chitosan nanoparticles and correlation with their physical properties. *Int J Biomater* 2012;2012. <https://doi.org/10.1155/2012/632698>.
- [363] Serhan M, Sprowls M, Jackemeyer D, Long M, Perez ID, Maret W, et al. Total iron measurement in human serum with a smartphone. *AICHE Annu Meet Conf Proc* 2019;2019-Novem. <https://doi.org/10.1039/x0xx00000x>.
- [364] Fischer ARH, Tobi H, Ronteltap A. When natural met social: A review of collaboration between the natural and social sciences. *Interdiscip Sci Rev* 2011;36:341–58. <https://doi.org/10.1179/030801811X13160755918688>.
- [365] Owen R, Macnaghten P, Stilgoe J. Responsible research and innovation: From science in society to science for society, with society. *Sci Public Policy* 2012;39:751–60. <https://doi.org/10.1093/scipol/scs093>.
- [366] Ellen MacArthur Foundation. The Global Commitment 2020 2020:76.
- [367] The Ellen MacArthur Foundation. a Vision of a Circular 2019:1–3.
- [368] Brizga J, Hubacek K, Feng K. II Perspective The Unintended Side Effects of Bioplastics : Carbon , Land , and Water Footprints. *One Earth* 2020;3:45–53. <https://doi.org/10.1016/j.oneear.2020.06.016>.
- [369] Coelho PM, Corona B, ten Klooster R, Worrell E. Sustainability of reusable packaging—Current situation and trends. *Resour Conserv Recycl X* 2020;6:100037. <https://doi.org/10.1016/j.rcrx.2020.100037>.
- [370] Holden NM, White EP, Lange MC, Oldfield TL. Review of the sustainability of food systems and transition using the Internet of Food. *Npj Sci Food* 2018;2. <https://doi.org/10.1038/s41538-018-0027-3>.



---

# Summary

The discovery of plastics has revolutionized the world we live in due to their astonishing properties including mouldability, durability, price, and strength in combination with light weight. In fact, the demand for plastic products is still increasing. However, our consumption pattern in combination with the (often) non-biodegradable/compostable nature of plastics is no longer compatible. A circular bio-economy offers an escape from our current reality in which fossil fuels negatively impact the environment, and plastic pollution affects life on the planet. There is a clear demand for plastic products as well as a desire to reduce the impact on the planet, and we need to ask ourselves what these novel materials should look like.

At present, much can be gained by recycling, reusing, or reducing traditional fossil-based plastics. In a polluted world where fossil sources are scarce and oil prices are heavily fluctuating, it is advisable to focus on biobased materials for the long(er) term. Biobased (biodegradable/compostable) plastics are particularly relevant because of their low footprint compared to their fossil-based counterparts. Today, the use of bioplastics is still a niche, mainly because their functionality does not compare favourably to their intended use.

The addition of nanoparticles to a biobased polymer has been shown to lead to nanocomposites with enhanced mechanical, thermal, and barrier properties, and has the potential to expand bioplastic use. In **Chapter 1** we outlined the concept of thermoplastic (bio)nanocomposites as novel materials that fit within the circular biobased economy. We highlighted that chitin nanocrystals are excellent candidates for plastic reinforcement as they are abundantly present in nature, are strong, and easy to modify. Furthermore, chitin based products possess antioxidant and antimicrobial activity, which may add functionality to the bioplastic beyond what is currently feasible with fossil-based plastics. Despite the potential to use nanoparticles in bioplastics, their application is greatly underexplored.

Within this thesis, we aimed to investigate and characterize the multiscale physical and chemical properties of nanoparticle reinforced plastics that fit within a circular economy.

It is the result of multidisciplinary research and divided into three parts:

- **Part I:** Model systems.
- **Part II:** Biobased systems.
- **Part III:** Plastic products and society.

Improved material properties are observed when nanoparticles are homogeneously dispersed in the polymer matrix. In practice however, nanoparticles tend to aggregate. The first part of this thesis is dedicated to model systems to investigate the effect of various design parameters on nanoparticle dispersion, and how the resultant nanocomposite structure affects material properties.

In practice, nanocomposite design often relies on trial-and-error approaches, despite the various theoretical frameworks available. In **Chapter 2** we reviewed these frameworks and summarized experimental techniques to measure fundamental properties. Nanoparticle dispersion is predominantly affected by thermodynamic factors; for optimal nanoparticle dispersion, the nanoparticle – polymer interaction forces need to be higher than the interaction forces between the nanoparticles themselves. This clearly illustrates we should look beyond the famous ‘like-dissolves-like theory’. From the review, it became clear that kinetic effects – such as shear forces – can bring nanoparticles to a new ‘equilibrium’, but these effects are of lesser importance in nanocomposite design.

In **Chapter 3** we used molecular dynamics simulations to investigate the effect of nanoparticle – polymer interactions on nanoparticle dispersion. Our results highlight that this affects nanoparticle dispersion, which is the key to the creation of enhanced material properties. In brief, increased polymer density at the nanoparticle interface, and thus increased interphasial layer thickness, leads to the formation of nanoparticle bridges, and an increased glass transition temperature that in turn correlates with more stable materials.

In **Chapter 4** we experimentally investigated the effect of nanoparticle – polymer interactions on dispersion, and local and bulk material dynamics. We showed that interphasial relaxation times were  $10^2 - 10^3$  times longer in nanocomposites than in neat polylactic acid (PLA). As such, nanoparticles essentially play the role of long-lived physical crosslinks. Nanoparticle dispersion highly affected nano- and bulk scale dynamics inside polymers. We

hypothesized that individual interphasial regions can affect each other which is enhanced by improved dispersion and higher nanoparticle loading. The nano- and bulk scale dynamics were practically independent of the enthalpic component, and that leads to thought-provoking indications that dispersion is more important than nanoparticle – polymer interactions, whereas the latter is generally considered most important.

In the second part of the thesis, we focussed on the development of fully biobased and compostable nanocomposites consisting of PLA and chitin nanocrystals. In **Chapter 5** we determined the critical sonication energy input required for chitin nanocrystal aggregate size reduction. These strong aggregates form upon drying, and we showed that ultrasound can easily deliver the critical energy input needed to break up chitin nanocrystal aggregates, whereas the energy input achieved during extrusion of polymer melts is expected to be too low for this. From this, we concluded that other methods than those classically used should be considered to achieve optimal chitin nanocrystal dispersion.

In **Chapter 6** we modified chitin nanocrystals with fatty acids differing in carbon chain length to facilitate their dispersion in polylactic acid. Particles modified with the longest fatty acid showed the highest hydrophobicity, and dispersibility. Generally, particle addition resulted in brown colour formation which was reduced when the particles were modified. This was likely the result of better dispersibility of modified chitin nanocrystals, and reduced reactivity. Overall, the addition of chitin nanocrystals improved barrier properties and provided high UV protection without this being at the expense of mechanical strength.

The last part of this thesis was dedicated to plastic materials in society. Plastics play an important role in the transition from a linear economy toward a circular one, but ideas about this role differ among actors. In **Chapter 7** we studied these ideas as a form of futurity framing of traditional media and international academic papers. Within the linear economy futurity frame, actors envision today's issues with plastics such as their non-biodegradability. Within the vision of a transition toward a circular economy, actors focus on the processes and steps required for change including consumer behaviour, social structures, and waste management systems. In both sources actors envision plastics as part of our future circular economy. Academic papers focus mainly on alternative forms of plastics, whereas newspapers mainly report on closing the loop for traditional forms of plastic. We observed a

missed opportunity to combine both visions to develop alternative biobased and biodegradable forms of plastics that can be recycled. The further development of this future vision of recyclable bioplastics and biodegradable plastics by industry, academics, governments, and NGOs, including citizens, may contribute to a more fully circular biobased plastics economy.

In **Chapter 8** we discussed how fundamental insights can be used to rationally design nanocomposite materials that fit within a circular economy. Enthalpic and entropic factors are important for interphasial and overall nanocomposite architecture, and collectively affect material dynamics. On the smallest scale, it seems important to maximize the polymer density near the nanoparticle surface to reduce interphasial dynamics. In order to get improved materials, interphasial properties need to be translated to the bulk, and we illustrated that the overall nanocomposite dispersion state plays a crucial role in this.

Aggregation reduces the polymer density at the interphasial region, while in well-dispersed systems interphasial layers interact with each other, potentially via overlapping interphasial zones, polymer bridges, or communicate via entanglements (if applicable). Eventually, a pseudo-percolation network is formed which reduces the dynamics of most of the material. From this, we concluded that nanoparticle dispersion is the key factor for nanocomposite design, and we discussed various thermodynamic and kinetic routes to facilitate that. This leads to altered mechanical, barrier, and thermal properties. Besides, the functionality of the nanoparticles can give optical, antioxidant, and antimicrobial features to the material.

Before novel materials - such as bio-nanocomposites - can successfully be introduced into society, other factors should be investigated as well including scalability, accessibility, end-of-life possibilities, sustainability, toxicology, and consumer acceptance and handling. This thesis clearly illustrates that the rational design of nanocomposites needs to be approached in a truly multifaceted way that combines various fields of science.





---

# Acknowledgements

Ironically, the PhD is considered training to become an independent researcher, but the work of this thesis is far from an individual effort. Throughout the last four years, I have met many great scientists and colleagues whose help, support, and contribution must not be underestimated. Thank you for joining my PhD journey.

**Karin Schroën**, bedankt dat jij mijn enige echte promotor was en wilde zijn! Veel dank voor je vertrouwen, en het bieden van een veilige haven wanneer het anders ging dan gepland. Ik waardeer het ontzettend dat je mij het rijke scala aan onderwerpen hebt laten ontdekken (ook degene die het boekje niet hebben gehaald), waarvoor we regelmatig op zoek gingen naar andere inspirerende onderzoek(st)ers. Waarschijnlijk had dit boekje meer focus gehad als je dit niet had toegestaan, maar ik weet zeker dat de ervaring minder leuk was geweest. Uiteraard ook dank voor alle praktische tips omtrent studenten begeleiden, presenteren en het schrijven van papers. Het zal vast niet altijd makkelijk zijn geweest om door al mijn stukken te lopen... ik gebruik nogal wat woorden..., maar de manuscripten zijn er zeker beter op geworden. Verder hoop ik dat je al je (academische) ambities waar zal maken, hoewel ik daar niet aan twijfel. Het beste gewenst en gegund in de toekomst.

**Murat Yanat**, my partner in crime, shrimp rider, and paranymph! I cannot imagine what my PhD experience would have looked like without you in the project. Your presence definitely made it more fun! Thank you for all the Subway lunches, walks, and fruit plates in the office. I'm grateful for your listening ear during my 'down' times, and for all the times you helped me or my students in the lab. Looking back, I am sure you would be proud of yourself if you could see how much you (/we) have grown. Good luck with the final stages of the PhD, and the next steps in the future. For now, I am a little bit (read: very much) afraid of the content of my stukje. Don't worry, payback time is approaching soon...

Dank aan de volgende mensen bij **FBR** voor alle hulp bij experimenten: **Wouter Teunissen**, **Frans Kappen**, **Herman de Beukelaer**, **Sharon Chu**, en **Guus Frissen**. Special thanks to **Carmen Boeriu**. I have always appreciated your chemical vision on the topic; I would never have been able to modify and characterize my particles without your help. I will always

remember your smile when I was entering your office. **Karin Molenveld**, ik heb de volgende zin meerdere malen uitgesproken “*Ik weet het niet, maar ik weet zeker dat Karin Molenveld het wel weet*”. Bedankt voor je praktische hulp, inhoudelijke feedback, en de gezellige Teamsmeetings.

**PAP**, thank you for the nice introduction to the social sciences. **Efrat Gommeh**, I really enjoyed our collaboration. You were a great social science mom to Fabrice and me. Good luck with the final stage of your PhD, and I am looking forward to reading your dissertation. **Tamara Metze-Burghouts**, bedankt voor alle hulp! Ik ben ontzettend blij dat de resultaten van Fabrice zijn gepubliceerd in een van mijn favoriete journals. Dit was nooit gelukt zonder jouw prikkelende en tegelijkertijd doelgerichte vragen waardoor we elke keer een stap dichterbij een manuscript kwamen. **Fabrice Fraiture**, dank voor het analyseren van de honderden artikelen, je harde werk, en je (welverdiende) co-auteurschap!

**PCC**, bedankt voor het zijn van onze goede burens, waar ik regelmatig te vinden was. **Hanne van der Kooij**, wat heb ik ontzettend veel van jou geleerd! Je hebt het werk (hierbij quote ik jou) “*tot een hoger, maar ook vooral lager (/kleiner) niveau*” gebracht. Heel erg bedankt voor al je hulp, betrokkenheid en oprechte interesse. Het was niet alleen inspirerend, maar ook hartstikke leuk en gezellig om met jou samen te werken. **Remko Fokkink**, bedankt voor de hulp tijdens het opzetten van de SALS en het oplossen van de vele LSI-/computerproblemen. Hopelijk heb ik ergens een beetje kunnen bijdragen aan de optimalisatie. **Raoul Fix**, bedankt dat je op het laatste moment nog hebt geholpen met de rheologiemetingen.

**Wouter van den Berg** en **Erik Bijleveld**, dank voor het industriële kijkje in jullie keuken, jullie input en accurate feedback en advies! Ik waardeer het ontzettend dat ik altijd welkom was bij dé **Compound Company**, waar het dagprogramma standaard afsloot met een goed gesprek, en een hapje & drankje.

**Sissi de Beer**, wat was het gezellig om met jou (en Qixin en Hanne) samen te werken. Bedankt voor je uitleg en input, en heel veel succes gewenst in de toekomst. **Leon Smook**, dank dat je op het einde nog aan wilde sluiten, wat nogal chaotisch was. Je hebt ontzettend goede ideeën en deze weet je op een goede manier over te brengen. Veel succes met de resterende jaren van je PhD.

All the (internship) students who contributed to the project, thank you for your motivation, enthusiasm, and critical questions. **Kieke de Boer**, wat heb ik geluk gehad dat jij mijn eerste student was. Heel veel succes met de resterende jaren van je PhD. **Marte Colijn, Pien van Streun, Iris Luiten**, jullie hebben allemaal bijgedragen aan het paper dat Murat en ik uiteindelijk hebben geschreven. Veel dank voor het uitvoeren van de eerste (maar vele) experimenten. **Janneke Schlatman**, dank voor het ontwikkelen van het uiteindelijke protocol voor de productie van onze nanodeeltjes. **Floris de Heer**, bedankt voor de gezellige gesprekken en je open blik. **Zoë Veldhuizen**, je nieuwsgierigheid werkt aanstekelijk; dank voor je oprechte interesse. **Geertje Terhardt** and **Wei-Yi Lu**, modifying nanoparticles was definitely not easy. I appreciate your determination and contribution to my thesis. **Davide Biella**, many thanks for our inspirational conversations and your honest care about the planet. **Shanjana Ashok Kumar** and **Xinyuan Cao**, I will always admire how both of you kept motivated during the pandemic. I'm grateful for your hard work, and I wish you all the best in the future. **Erik Postma**, je ging als een speer. Dank voor het uitvoeren van de LSI-experimenten en succes met je PhD. **Qixin He**, thank you for all the hard work and the preliminary simulation experiments. **Terry McCormick**, thank you being my last student who was so committed to the project.

Bedankt technicians van FPE: **Maurice Strubel, Jos Sewalt, Wouter de Groot, Jarno Gieteling**, en **Lyneth Duipmans**! Dank voor alle hulp en uitleg op het lab! Maar ook belangrijk, dank voor de vele koffies en de gezellige gesprekken. Extra dank voor Maurice en Jos voor het meedenken betreft de veiligheid van nanodeeltjes en chemicaliën. **Martin de Wit** dank voor het regelen van de financiën en voor de bezoeken langs mijn kantoor als ik weer een dief van mijn eigen portemonnee was. **Marjan de Lange, Iona Meurs**, en **Evelyn Schreuder**, bedankt voor alle administratie.

Everyone at the **Micro-team**, thank you for the great discussions: **Meinou Corstens, Sten ten Klooster, Lingfeng Wu, Herehau Balais, Jiarui Cao, Yhan Williams, Ruyuan Zhang, Asif Aslam, Fathinah Hasyati**. I'm looking forward to reading your future work. **Pina Fritz**, I have always appreciated your versatile look on the topic and tips-and-tricks in the lab. All the best in London.

Thank you **FPE-colleagues** for making my PhD not only about work, but also about having fun. I am extremely grateful that I was able to join the PhD-trip and create wonderful memories with each one of you. I would love to pass by the department and grab a cup of coffee. Invitations are welcome!

Thank you, **Katharina Muench** and **Boxin Deng** for sharing the first PhD experiences. I always enjoyed our 6-pack dinners (I am afraid they did not contribute to the ‘6-pack’ though...), drinks, and lunches. Thank you, **Zhaojun Wang**, **Birgit Dekkers**, **Zulhaj Rizki**, and **Anna Möller** for such a nice welcome to the office near the coffee corner. **Loes Hoppenreijns** and **Aaditya Venkatachalam**, thank you for our too many and too nice conversations in the office. I guess it is a good sign people get distracted by the noises coming from the nicest office of the department (according to my ‘humble’ opinion). Lieve **Anneloes van Boven** (ja lieve), vanaf de AID ben jij actief betrokken geweest bij mijn ‘studententijd’ en ik vind het ontzettend leuk dat je mij – als paranimf – bijstaat op moment suprême! Ik ben erg ‘benieuwd’ naar jouw bijdrage aan mijn stukje, en heb nu al zin in jouw verdediging.

Lieve **vrienden**, hoewel jullie niet direct betrokken waren bij mijn onderzoek, wil ik jullie juist bedanken voor alle momenten dat ik niet aan werk hoefde te denken. De gezellige afspraken, terrasjes, het samen sporten, en de lieve berichtjes hebben zeker geholpen!

Lieve (schoon)ouders bedankt voor de emotionele en praktische support. De combinatie PhD, Covid-19, en een klushuis is verre van optimaal. Zonder jullie hadden we niet zo een sterke basis kunnen bouwen (vrij letterlijk). **Sander** en **Sonja** (de Wit), bedankt voor alle hulp bij het klussen, het verzorgen van de katten, en de gezellige momenten samen. **Cor**(nelis Colijn) en **Elizabeth** (do Amaral Lins), ik mag van geluk spreken met ouders die mij onvoorwaardelijk steunen en volledig achter mijn keuzes staan. Beth, obrigada pela bandeira invisível que sempre está tremulando. Cor, dank voor de continue herinnering dat ik het “*toch gewoon kan proberen*”. Met en zonder woorden is jullie liefde voelbaar.

Lieve **Guido** (de Wit), dank voor je luisterende oor, het relativeren, de bodemloze hoeveelheid emotionele support, en het zijn van mijn steun en toeverlaat. Als ik elk bemoedigend woord van de afgelopen 4 jaar zou hebben opgeschreven, had dat geleid tot een boek duizend maal dikker dan het huidige. Je bent het beste dat mij ooit is overkomen ♥.





---

## About the author



Ivanna Lins Colijn was born on the 27<sup>th</sup> of March in 1994 (Utrecht, the Netherlands). She attended Brokledede, in Breukelen, where she obtained her VWO diploma in 2012, with a major in Nature and Health<sup>5</sup>.

In 2013, Ivanna started the bachelor Food Technology at Wageningen University with a minor in Micro and Bio Nano Technology. For her bachelor thesis, she used a microfluidic tool to study protein stabilized emulsions at the laboratory of Food Process Engineering. After obtaining her bachelor diploma, Ivanna continued with the master Food Technology with a specialization in Ingredient Functionality at Wageningen University. For her master thesis, she developed alginate micro beads coated with chitosan at the laboratory of Physics and Physical Chemistry of Foods. After that, she did her master internship at Nestlé Research Centre (Lausanne, Switzerland), where she investigated in-mouth emulsion behaviour *in vivo*.

After gaining her master diploma, Ivanna continued as a PhD candidate at the laboratory of Food Process Engineering at Wageningen University, under the supervision of prof. dr. ir. CGPH Schroën. During this research, she worked on the physical chemical characterization of plastic polymers reinforced with nanoparticles; of which the findings are discussed in this thesis.

---

<sup>5</sup> In Dutch: *Natuur en Gezondheid*



---

# Publications

## *This thesis*

**Ivanna Colijn**, and Karin Schroën. 2021. “Thermoplastic Bio-Nanocomposites: From Measurement of Fundamental Properties to Practical Application.” *Advances in Colloid and Interface Science* 292: 102419.

**Ivanna Colijn**, Remco Fokkink, Karin Schroën. 2021. “Quantification of Energy Input Required for Chitin Nanocrystal Aggregate Size Reduction through Ultrasound.” *Scientific Reports* 11 (1): 1–9.

**Ivanna Colijn**, Murat Yanat, Geertje Terhaerd, Karin Molenveld, Carmen G Boeriu, and Karin Schroën. 2022. “Chitin Nanocrystal Hydrophobicity Adjustment by Fatty Acid Esterification for Improved Polylactic Acid Nanocomposites” *Polymers* (13): 2619.

**Ivanna Colijn**, Fabrice Fraiture, Efrat Gommeh, Karin Schroën, Tamara Metz. 2022. “Science and Media Framing of the Future of Plastics in Relation to Transition to a Circular Economy.” *Journal of Cleaner Production* 370:133472.

**Ivanna Colijn**, Erik Postma, Raoul Fix, Hanne van der Kooij, Karin Schroën. “Particle dispersion governs nano to bulk dynamics for tailored nanocomposite design” (*submitted*).

## *Other*

Muijlwijk, Kelly, **Ivanna Colijn**, Herditya Harsono, Thomas Krebs, Claire Berton-Carabin, and Karin Schroën. 2017. “Coalescence of Protein-Stabilised Emulsions Studied with Microfluidics.” *Food Hydrocolloids* 70: 96–104.

**Ivanna Colijn**<sup>6</sup>, Anthony Ash<sup>6</sup>, Marie Dufauret, Melissa Lepage, Céline Loussert-Fonta, Martin E. Leser, Peter J. Wilde, and Tim J. Wooster. 2022. “Colloidal Dynamics of Emulsion Droplets in Mouth.” *Journal of Colloid and Interface Science* 620: 153–67.

Murat Yanat, **Ivanna Colijn**, and Karin Schroën. 2022. “Chitin Nanocrystals Provide Antioxidant Activity to Polylactic.” *Polymers* (14) 14:2965.

Murat Yanat<sup>6</sup>, **Ivanna Colijn**<sup>6</sup>, Kieke de Boer, Karin Schroën. “Comparison of the degree of acetylation of chitin nanocrystals measured by various analysis methods” (*submitted*)

---

<sup>6</sup> *Equal authorship*



---

# Overview of completed training activities

## *Discipline Specific Activities*

Summer school polymer science and advanced polymers in engineering and energy	Bayreuth Universität	2019
M2i conference <sup>7,8</sup>	M2i	2018 – 2021
Nucleation workshop	M2i	2020
Framing workshop	WUR - PAP	2020
Nimac <sup>8</sup>	Nimac	2021
EPNOE <sup>8</sup>	EPNOE	2021
Circul-a-bility <sup>8</sup>	European Union	2021
IUFOST <sup>8</sup>	IUFOST	2022

## *General Courses*

VLAG PhD week	VLAG	2019
Competence assessment	WGS	2018
Brain Training	WGS	2019
Searching and organising literature	WGS	2019
PhD Workshop Carousel	WGS	2019
Scientific Integrity	WGS	2019
Scientific Publishing	WGS	2019
Introduction to R	VLAG	2020
Scientific Writing	WGS	2020
Critical Thinking	WGS	2020
Adobe InDesign Essential Training	WGS	2021
Career Perspectives	WGS	2021

## *Other*

Preparation research proposal	WUR – FPE	2018
Weekly group meetings	WUR – FPE	2018 – 2022
PhD-trip Singapore	WUR – FPE	2022
WPS committee	WPC	2018
FPE-day	WUR – FPE	2019
Monthly FPE Micro-meetings	WUR – FPE	2021 - 2022

---

<sup>7</sup> Poster presentation

<sup>8</sup> Oral presentation



---

# About the cover

The circular (bio)economy offers an escape from our current reality, in which we are depleting Earth and plastic waste is negatively impacting human and animal's health. We took this as inspiration and explored the potential of (bio)nanocomposites as advanced materials within a future circular economy for plastics.

The background of the cover consists of a nanocomposite system, where polymers are illustrated as green and turquoise strings, and nanoparticles as blue beads (**Chapter 1, 2, 3, and 4**). One of the nanoparticles illustrates our planet (**Chapter 7 & 8**); it pictures a positive future where biobased materials are used as source and bioplastic packages can be composed after use. Within this thesis, we used the bioplastic polylactic acid (PLA) (**Chapter 4 & 6**), which is often made from corn. The shrimp in the ocean is a representation of our source chitin (**Chapter 5 & 6**), from which we made nanocrystals. Last but not least, the two people on the planet illustrate myself (on the leaf) and Murat Yanat (on the shrimp) (**Acknowledgements**).

This research was carried out under projectnumber A17020 in the framework of the Research program of the Materials innovation institute (M2i) ([www.m2i.nl](http://www.m2i.nl)) supported by the Dutch government.

Financial support from Wageningen University and M2i for printing this thesis is gratefully acknowledged.

Cover illustrated by Anastasia Khmelevska

Printed by ProefschriftMaken || [www.proefschriftmaken.nl](http://www.proefschriftmaken.nl)



